

CLIMATIC AND ENVIRONMENTAL CHANGE IN THE COLORADO ROCKY
MOUNTAINS DURING THE LATE QUATERNARY: A PALEOLIMNOLOGICAL
APPROACH

by

DANIELLE RENEE HASKETT

(Under the Direction of Marguerite Madden)

ABSTRACT

This dissertation explores the relationship between chironomid communities and the climatic and other environmental variables that are responsible for their distribution over modern, historical, and millennial time scales in the Front Range of the Colorado Rocky Mountains. This study found that surface water temperature, nitrate, boron, and carbon explained the most variance in the modern distribution of chironomids collected from nine alpine lakes. However, the relationship between surface water temperature (SWT) and nitrate was strongly and negatively correlated suggesting that glacial meltwater is the environmental variable that explains the most control over chironomid communities. Lakes receiving glacial meltwater were 2.62°C colder and contained 66% more nitrate. This is the first evidence that atmospheric deposition of nitrate is affecting benthic invertebrates in the Western United States. This is also the first time that a relationship between boron and chironomid communities has been documented. This finding further substantiates that anthropogenic land-use practices are shaping and influencing remote alpine ecosystems. A high-resolution thermal reconstruction was developed to study the climatic amelioration that occurred at the Pleistocene-Holocene transition. Progressive, three-step warming

of SWT was evident for a 3400-year record. Only one period of abrupt climatic amelioration was evident. A dramatic increase of 4.7°C occurred at 11,300 cal yr BP. However, a brief but significant cooling event occurred at 10,570 cal yr BP. These results were found using a chironomid-based SWT inference model ($r^2_{boot} = 0.38$, RMSEP = 2.74°C) that was developed using a lake training set incorporating 153 lakes from California, Utah, and Colorado. No chironomids were present in the sediment corresponding to the Younger Dryas. Reconstructed temperatures ranged from 7.8°C to 13.4°C. Chironomids were used to develop temperature reconstructions for mean July air temperature (MJAT) and SWT for the 20th and 21st centuries and compared to instrumental data for six alpine lakes. Glacial meltwater decoupled the signal between air temperature and water temperature and was evident between the relationships between the predicted MJAT and SWT for lakes receiving meltwater. Within-lake variability may account for discrepancies apparent between the six site locations. Study site selection is crucial for midge-based thermal reconstructions and basins that receive meltwater.

INDEX WORDS: Chironomid, glacial retreat, Colorado, paleoclimate, abrupt climate change, alpine, limnology, Diamesa, chironomid succession, study site selection

CLIMATIC AND ENVIRONMENTAL CHANGE IN THE COLORADO ROCKY
MOUNTAINS DURING THE LATE QUATERNARY: A PALEOLIMNOLOGICAL
APPROACH

by

DANIELLE RENEE HASKETT

BS, University of Georgia, 2004

MS, University of Georgia, 2013

A Dissertation Submitted to the Graduate Faculty of The University of Georgia in Partial
Fulfillment of the Requirements for the Degree

DOCTOR OF PHILOSOPHY

ATHENS, GEORGIA

2020

© 2020

Danielle Renee Haskett

All Rights Reserved

CLIMATIC AND ENVIRONMENTAL CHANGE IN THE COLORADO ROCKY
MOUNTAINS DURING THE LATE QUATERNARY: A PALEOLIMNOLOGICAL
APPROACH

by

DANIELLE RENEE HASKETT

Major Professor:	Marguerite Madden
Committee:	David S. Leigh
	Suzanne Pilaar Birch
	Sally Walker

Electronic Version Approved:

Ron Walcott
Interim Dean of the Graduate School
The University of Georgia
May 2020

DEDICATION

I am so lucky to have a fantastic support system that has been both bemused and concerned during this doctoral process. Thank you to my husband Kyle, who has supported me and encouraged me and who has been my anchor and rock. Additionally, I would also like to dedicate this to my parents (both sets), to Kristine (the most amazing sister and friend), Lucy and Jasper, Dr. Andrea Presotto, Dr. Kimberly Love (and Curly and Gemini), Dr. Gloria Howerton, Mr. Sean Cameron, and Dr. Gretchen Sneegas.

ACKNOWLEDGEMENTS

Thank you to my committee Marguerite Madden, Suzie Pilaar Birch, David Leigh, and Sally Walker, for their help in getting me to the finish line. I want to thank the many members and staff from Rocky Mountain National Park that assisted in fieldwork and planning that was necessary for the successful completion of this work. I was fortunate to work with amazing students that helped with work in the field and lab. I want to thank Uday Sachdeva, Stephen Cooper, Nicole Campbell, Gretchen Sneegas, Todd Emmenegger, Aileen Nicolas, Harrison Brock, Henry Miller, and Gloria Howerton for their dedication in helping to complete this work. Thank you to Gonzalo Jiménez-Moreno and R. Scott Anderson for allowing me to work on the sediment they collected from Kite Lake. David Porinchu is appreciated and acknowledged for the work he shared from his training set, for his assistance in the field, for the use of the Environmental Change Lab, and his advice in all things chironomids. Thank you to the entirety of the Geography Department. This department has felt like home for nine years, and that is due to your classes, open office doors, and professional development advice. Thank you to CAIS and especially Jeff Speakman, Emmy Deng, Carla Hadden, Alex Cherkinsky, and Tom Maddox. My gratitude for Marguerite Madden (again), Hilda Kurtz, Emily Duggar, Loretta Scott, Steve Holloway, Andy Grundstein, Sergio Bernardes, and David Cotton is endless. Funding for this work was provided by the Department of the Interior (P16AC00587), NSF DDRI (1633959, GSA, the Limnogeology specialty group (GSA), The Explorers Club, and the UGA Graduate School.

TABLE OF CONTENTS

	Page
ACKNOWLEDGEMENTS	v
LIST OF TABLES	viii
LIST OF FIGURES	ix
CHAPTER	
1 INTRODUCTION AND LITERATURE REVIEW	1
Thesis Objectives	7
2 IS GLACIAL RETREAT IMPACTING MODERN BENTHIC CHIRONOMID COMMUNITIES? A CASE STUDY FROM ROCKY MOUNTAIN NATIONAL PARK, COLORADO.....	9
Abstract.....	10
Introduction.....	11
Study Area	14
Methods.....	18
Results and Discussion	21
Conclusion	34
3 CHIRONOMID-BASED EVIDENCE OF GLACIAL RETREAT AND CORRESPONDING CHANGES IN SURFACE WATER TEMPERATURES DURING THE PLEISTOCENE-HOLOCENE TRANSITION FROM AN ALPINE LAKE IN COLORADO, USA	36

Abstract.....	37
Introduction.....	38
Study Area	40
Materials and Methods.....	44
Results	51
Discussion.....	59
Conclusion	64
4 WHICH LAKES SHOULD BE SAMPLED FOR PALEOENVIRONMENTAL CHIRONOMID WORK? A CASE STUDY APPROACH TO DETERMINE STUDY SITE SELECTION FOR PALEOCLIMATIC RESEARCH	65
Abstract.....	66
Introduction.....	67
Study Area and Methods.....	70
Results	83
Discussion and Conclusion.....	100
5 CONCLUSIONS.....	109
REFERENCES	117
APPENDICES	
A CODE FOR ALL ANALYSIS IN R	145
B ADDITIONAL MATERIALS.....	196

LIST OF TABLES

	Page
Table 2.1: Limnological variables sampled for nine alpine lakes in Rocky Mountain National Park, Colorado.	16
Table 2.2: Carlson’s Trophic Level Index	22
Table 2.3: Forward selection of variables with Monte Carlo permutations (n=999).....	30
Table 3.1: Western United States chironomid-based inference model for surface water temperature (°C)	48
Table 4.1: Environmental variables for sampled alpine lakes	71
Table 4.2: Chironomid taxa sorted for surface water temperature by individual weighted averaging optima and tolerances.....	79
Table 4.3: Statistics for inference models for both chironomid-inferred surface water temperature and chironomid-inferred mean July air temperature.....	82
Table 4.4: Temperature averages, ranges, and averages for sample-specific errors for midge-inferred temperatures	98

LIST OF FIGURES

	Page
Figure 1.1: The chironomid life cycle.....	5
Figure 2.1: Base map for study sites in Rocky Mountain National Park, Colorado	17
Figure 2.2: Relative abundance curves for the modern assemblages collected from nine alpine lakes in Rocky Mountain National Park, Colorado	24
Figure 2.3: Detrended correspondence analysis bi-plot indicating the relationship between taxa, or assemblages, and corresponding lakes	27
Figure 2.4: Redundancy analysis bi-plot depicting the relationship between surface water temperature (°C), carbon %, boron, and chironomid taxa from the study sites.....	28
Figure 3.1a: Colorado study site in context of the United States.....	40
Figure 3.1b: Extent of alpine glaciers in the Colorado Rocky Mountains during the last glacial maximum	41
Figure 3.1c: Map of Kite Lake study site	41
Figure 3.2: Age-depth diagram for the Kite Lake stratigraphy	45
Figure 3.3: Relative abundance curves for the Western United States training set.....	53
Figure 3.4 Relationship between observed mean July air temperature and midge-inferred mean July air temperature.....	54
Figure 3.5.: Derived chironomid zones based on constrained hierarchical cluster analysis.....	55
Figure 3.6: The Kite Lake relative abundance curve	56

Figure 3.7: Concentration and richness curves derived from subfossil chironomid assemblages present in Kite Lake	57
Figure 3.8: Chironomid-inferred surface water temperature reconstructions for the Kite Lake stratigraphy	60
Figure 3.9: Passive plotting of fossil assemblages against the training set assemblage in correspondence analysis ordination space	61
Figure 3.10: Significance test of the proportion of variance that surface water temperature explains	61
Figure 4.1a: Study sites in Rocky Mountain National Park, Colorado.....	72
Figure 4.1b: Study sites along the continental divide in Rocky Mountain National Park, Colorado.....	73
Figure 4.2: ²¹⁰ Pb chronologies and sedimentation rates	75
Figure 4.3: Trends in detrended correspondence analysis with changepoints	78
Figure 4.4: Passive plotting of fossil assemblages from six alpine lakes against the training set assemblage in correspondence analysis ordination space.....	80
Figure 4.5: Midge-based mean July air temperature (°C) and surface water temperature (°C) reconstructions plotted against PRISM-derived mean July air temperature (°C) for each lake	81
Figure 4.6: Deviations from averages for PRISM-based mean July air temperature, midge-based mean July air temperature, and midge-based surface water temperature	83
Figure 4.7: Bland-Altman plots are useful for comparing two datasets (midge-based surface water temperature and PRISM-based mean July air temperature)	84

Figure 4.8: Bland-Altman plots are useful for comparing two datasets (midge-based mean July air temperature and PRISM-based mean July air temperature)	85
Figure 4.9a: Cony Lake relative abundance organized by the weighted averaging optima of surface water temperature for taxa.....	88
Figure 4.9b: Pipit Lake relative abundance organized by the weighted averaging optima of surface water temperature for taxa.....	89
Figure 4.9c: Eagle Lake relative abundance organized by the weighted averaging optima of surface water temperature for taxa.....	93
Figure 4.9d: Box Lake relative abundance organized by the weighted averaging optima of surface water temperature for taxa.....	94
Figure 4.9e: Black Lake relative abundance organized by the weighted averaging optima of surface water temperature for taxa.....	96
Figure 4.9f: Thunder Lake relative abundance organized by the weighted averaging optima of surface water temperature for taxa.....	97
Figure 4.10: Chironomid-based temperature reconstructions for Kite Lake (surface water temperature and mean July air temperature).....	101
Figure 4.11: Deviations from the averages for midge-based surface water temperature and midge-based mean July air temperature based on Kite Lake stratigraphy	102

CHAPTER 1

INTRODUCTION AND LITERATURE REVIEW

The last century witnessed abrupt climatic and environmental changes that are pervasive over many parts of the globe (Stocker et al., 2013). Alpine and subalpine environments are particularly sensitive to these changes (Dahe et al., 2006; Chen et al., 2011; Elliot, 2012). Elevated temperatures alter the hydrological cycle by affecting the proportion of precipitation that falls as snow, the total amount of winter precipitation, and the timing of snowmelt (Haeberli and Beniston, 1998; Khamis et al., 2014). Increasing air temperature also creates conditions conducive for alpine glacial recession and an upslope movement of permafrost (Haeberli and Beniston, 1998; Chen et al., 2011; Mark and Fernández, 2017). The instability of soil surfaces created by melting permafrost promote mass wasting and increase sediment flux downstream (Haeberli and Beniston, 1998). Elevated temperatures and longer growing seasons affect alpine ecosystems by promoting changes in treeline ecotones by altering the spatiotemporal patterns of tree establishment at regional scales (Elliot et al., 2012) as well as promoting lake eutrophication (Catalan et al., 2013). The magnitude and rate of biophysical changes observed during recent decades in the montane environments of the western United States are at the extreme end of the range of variations seen historically (Barnett et al., 2008; Pederson et al., 2011, Van Mantgem et al., 2011). The current trajectories of climate change in the Rocky Mountain region suggest dramatic shifts in the extent of perennial ice in the immediate future (Hall and Fagre, 2003; Barnett et al., 2008). Higher temperatures, reduced snowpack and a persistent drying trend, will ultimately result in lengthier fire seasons and a corresponding increase in extreme fire weather. These factors will likely

continue to adversely impact alpine and subalpine ecosystems in the western United States in the future (Westerling et al., 2006). With the recognition that high-elevation regions are responsive and extremely sensitive to anthropogenic climate change, we must improve our understanding of how regional climate change will affect freshwater resources and aquatic ecosystems in alpine and subalpine environments. This is especially true given the heightened concern over the present and future water availability in mountainous environments, such as those that characterize much of the Intermountain West of the United States.

The remote lakes found at high elevations act as sentinels of change and are among the first bodies of water impacted by climate change (Heino et al., 2009; Dodds and Whiles, 2010). Despite their remoteness, mountain lakes and their aquatic ecosystems have been severely impacted by multiple anthropogenic stressors, including climate change. The structure, function, and composition of aquatic ecosystems in alpine and subalpine settings will be dramatically transformed as current warming trends continue (Schindler, 2009; Adrian et al., 2009). For example, recent studies suggest that the range of invasive fish species and invertebrates will expand due to their ability to move to higher elevation lakes via warmer creeks with stable environments (Khamis et al., 2014). This will impact the natural communities that exist in alpine lakes by altering food web and predator/prey dynamics (Khamis et al., 2014). Additionally, an increase in the supply of dissolved organic carbon (DOC) related to the upslope movement of the treeline will increase lake productivity and potentially the biological diversity of lake ecosystems in these sensitive environments (Messner et al., 2012).

One of the significant changes that high-elevation lakes in the western United States will experience in the coming decades relates to the retreat of the small alpine glaciers in response to altered temperature and precipitation regimes. Many of the alpine and subalpine lakes in the

western United States are fed by meltwater emanating from glaciers and climate models suggest that many of these glaciers will no longer exist by 2030 (Hall and Fagre, 2003). Other studies indicate that the cirque glaciers located in the Sierra Nevada, California, may be protected by their position concerning shading, aspect, and relief, and will disappear between 50 and 250 years from now (Basagic and Fountain, 2018). The importance of glaciers to montane environments and ecosystems cannot be overstated. Glaciers act as natural reservoirs by storing water and providing a constant and dependable source of cool fresh water. The influx of cold glacial meltwater helps to regulate stream and lake water temperatures and provides the only reliable source of base flow to alpine streams in late summer and during droughts. A reduction in glacial meltwater will ultimately result in elevated summer water temperatures, which in turn could negatively impact thermally sensitive aquatic invertebrates (Brown et al., 2007). The alteration of the structure and composition of the aquatic invertebrate community may affect threatened native Salmonid species (Keleher and Rahel, 1996). The influence of glacial meltwater on hydrology and the turbidity of high-elevation lacustrine ecosystems has been well documented (Thies et al., 2007). More recently, the contribution of glacial meltwater to the nutrient chemistry of alpine lakes has also been recognized (Saros et al., 2010; Slemmons et al., 2015). For example, Wolfe et al. (2001) used diatoms and sediment $\delta^{15}\text{N}$ to document that the composition of diatom communities responded to N-loading in the late 20th century and that the ecological shifts exceed the natural variability evident during last 14,000 years. Geochemical studies have also explored the role that recent atmospheric nitrogen deposition has played on lake trophic levels in the Front Range of the Colorado Rockies (Baron et al., 2005). However, little is understood about the response of insect communities in aquatic ecosystems to past and contemporary episodes of climate change-induced glacial ablation (Slemmons et al., 2013; Michelutti et al., 2015).

Lake sediment is a powerful archive that preserves physical, geochemical, and biotic proxies that may be used to develop high-resolution reconstructions of past environmental and climatic changes (Battarbee, 2000). Information extracted from lake sediment can be used to create baseline limnological information against which future changes may be compared (Smol and Douglas, 2007). Biological proxies extracted and analyzed from lake sediment cores include aquatic insects, such as chironomids (Insecta: Diptera). Chironomids, or midges, are one of the most abundant insects found in freshwater ecosystems. They are particularly sensitive to temperature and are used as a biological proxy to investigate changing thermal regimes (Walker, 1987). Battarbee (2000) states that chironomids are one of the most promising approaches to reconstructing past temperature change.

Aquatic insects belonging to the order Diptera are among the most abundant benthic insects present in lake sediment and make up 40% of all aquatic insects (Dodds and Whiles, 2010). The skeletal remains of larval chironomids are composed of chitin and are preserved in lake sediment, particularly those collected from Quaternary sediment (Cohen, 2003; Brooks et al., 2007). The fossilized remains are primarily head capsules that act as the teeth mechanism for the maggot-like midge. This head capsule is present during the larval stage of life, where the midge subsists at the sediment-water interface (Walker, 1987; Porinchu and MacDonald, 2003). This stage in the life cycle of larval midges goes through four progressive instars before the insect metamorphoses into pupae (Figure 1.1). The pupae phase is short-lived as it rises through the water column and emerges as a winged-adult fly (Walker, 1987). The adult midge then flies to their preferred environment until mating occurs, where male chironomids form swarms that females enter to mate (Porinchu and MacDonald, 2003). The female deposits an egg mass on the surface of lake water where it sinks through the water column and hatches to become larvae (Walker, 1987). The rate of

the egg mass development is primarily controlled by temperature, but other environmental factors such as pH, salinity, and oxygen concentration, may influence this phase of the chironomid life cycle (Pinder, 1995).

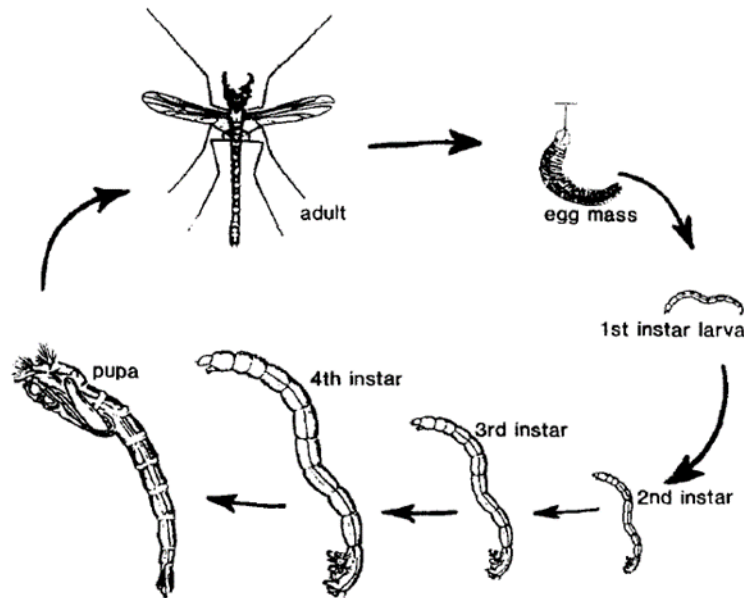


Figure 1.1: The chironomid life cycle (Walker, 1987).

Walker et al. (1991) were the first to use a transfer function to model the relationship between surface water temperatures and chironomid assemblages (Porinchu and MacDonald, 2003). Lotter et al. (1997) developed modeled air temperature using similar methods soon afterward (Porinchu and MacDonald, 2003). The quantitative reconstructions for air temperatures that have been developed typically have robust performance statistics (Velle et al., 2010). Researchers also suggest that air temperature has the most significant influence on the ecology of chironomid distribution (Eggermont and Heiri, 2012). It is argued that air temperature affects both adult and larval stages because of the covarying relationship between air and water temperatures that are typically evident (Livingstone et al., 1999; Lotter et al., 1999; Eggermont and Heiri, 2012).

Air temperature data are often available at high resolutions with records sometimes having daily or even hourly information that may be aggregated to provide more precise temperature records than the one temperature of water temperature that is recorded during sampling (Eggermont and Heiri, 2012). The water temperatures collected may be variable between the time of day or even time of year and is thus less trustworthy. Therefore, as air and water temperatures are highly correlated, it has been acceptable to model air temperature using the remains of chironomids (Livingstone et al., 1999; Eggermont and Heiri, 2012).

These claims are often spurious as the need for understanding the ecology of chironomids has been debated vigorously for three decades, and little work has endeavored to elucidate how environment affects chironomid communities (Walker and Mathewes, 1987; Warner and Hann, 1987; Walker and Mathewes, 1991; Velle et al., 2010, Brooks et al., 2012; Eggermont and Heiri, 2012; Velle et al., 2012a). It is clear that the distribution of the chironomid assemblages is strongly related to summer air and water temperatures for lakes in temperate and subarctic regions, and yet these relationships are poorly or not understood (Velle et al., 2010; Eggermont and Heiri, 2012). Many critics of the method point to other factors that may impact the distribution of chironomids including natural (Brodersen and Lindegaard, 1999; Brooks and Birks, 2001) and anthropogenic (Haskett, 2020a) nutrient loading (Landgon et al., 2010; Garzke et al., 2019), lake depth (Kurek and Cwynar, 2009; Velle et al., 2012b), oxygen levels (Little and Smol, 2001; Verbruggen et al., 2011), aquatic vegetation (Langdon et al., 2010), and glacial melt (Eggermont and Heiri, 2012). It has been argued that many of these relationships are ultimately controlled by temperature, and thus temperature is ultimately what is controlling the distribution of chironomid communities (Velle et al., 2010; Brooks et al., 2012; Eggermont and Heiri, 2012).

Eggermont and Heiri (2012) argue that “a major complicating factor for the use of chironomids for palaeoclimate reconstruction is that the exact nature of the mechanism responsible for the strong relationship between temperature and chironomid assemblages in lakes remains uncertain.” While adult chironomids are mobile and may travel to areas within their preferred climatic ranges, the juvenile stages of the chironomid lifecycle are spent as larvae that subsist at the sediment-water interface. The temperature of the water largely influences these larval chironomids by moderating physiological and geochemical processes such as growth and development (Porinchu and MacDonald, 2003; Eggermont and Heiri, 2012). Future research should endeavor to elucidate which temperature (air or water) is more appropriate for transfer function development as the ecology and forcing factors related to chironomid distribution is poorly understood (Eggermont and Heiri, 2012).

THESIS OBJECTIVES

This manuscript-style dissertation focuses on reconstructing recent (i.e., late 20th and early 21st centuries) and long-term (i.e., the Pleistocene-Holocene transition) climate and environmental variability in the Front Range of the Colorado Rocky Mountains by explicitly focusing on episodes of sustained and rapid warming during the late Quaternary. The proposed research is timely, given the very narrow window in which such studies may be conducted due to the rate of glacial ablation that is currently occurring in the western United States (Basagic and Fountain 2011; Slemmons et al., 2013). The first article will be submitted to *Oceanology and Limnology* in 2020 for peer-review and will determine if the response of chironomid communities in alpine lakes currently fed by glacial meltwater is de-coupled from observed increases in summer air temperature during the late 20th and early 21st centuries in Rocky Mountain National Park (RMNP), Colorado due to the increase influx of cold glacial meltwater. The second article will be submitted to *The Holocene* in

the fall of 2020 and will develop a quantitative paleotemperature reconstruction for a high elevation site in the Colorado Rockies spanning the Pleistocene-Holocene transition to determine the rates and magnitude of warming during the most recent episode of extended warmth. The third manuscript will be submitted to *Quaternary Science Reviews* in 2020 and will explore the relationships between midge-based surface water temperatures and mean July air temperatures and how they compare to instrumental data over the 20th and 21st centuries. These findings will lead to criteria for study site selection as well as aiding chironomid workers in identifying periods of extended meltwater using subfossil chironomid assemblages and reconstructions. The goals of this dissertation have three foci:

- 1) investigating the influence of glacial meltwater on the modern midge communities in alpine and subalpine lakes in RMNP;

- 2) developing a quantitative paleotemperature reconstruction spanning the Pleistocene-Holocene transition;

- 3) establishing methods to assess how historic midge-based reconstructions compare to instrumental data to establish criteria for study site selection.

Upon completion of this work, a clearer understanding of the modern ecology for chironomids in environments that receive glacial meltwater will be evident. These findings will aid paleoclimatologists that use chironomids as a biological proxy for temperature in refining paleoreconstructions over varying timescales.

CHAPTER 2

IS GLACIAL RETREAT IMPACTING MODERN BENTHIC CHIRONOMID
COMMUNITIES? A CASE STUDY FROM ROCKY MOUNTAIN NATIONAL PARK,
COLORADO.¹

¹ Haskett, D.R. To be submitted to *Limnology and Oceanography*

ABSTRACT

The aim of this study was to determine which environmental variables are responsible for modern benthic chironomid distributions in a glacial setting. The chironomid communities from nine alpine lakes were assessed and forty-three individual taxa were extracted and identified. Surface water temperature and nitrate were strongly and negatively correlated (-0.82 , $p=0.007$), suggesting that glacial meltwater (the driver that explains both surface water temperature (SWT) and nitrate ($\text{NO}_3+\text{NO}_2\text{-N}$) is the environmental variable that explains the most variance (15%). On average, lakes receiving glacial meltwater were 2.62°C colder and contained 66% more $\text{NO}_3+\text{NO}_2\text{-N}$ than lakes only receiving meltwater from snow. The presence of taxa from the tribe Diamesinae indicates very cold input from running water, and these taxa may be used as a qualitative indicator species for the existence of glacial meltwater within a lake catchment. The presence of boron and the percentage of carbon in bulk sediment (i.e., lake productivity) are also responsible for the distribution of modern chironomid communities in Rocky Mountain National Park, Colorado. *Heterotrissocladius*, *Diamesa* spp., and *Pseudodiamesa* were present in the coldest lakes. *Chironomus*, *Diplocladius*, and *Protanypus* were assemblages found in cold lakes affiliated with the littoral zone or alpine streams.

Keywords: Chironomid; Glacial Retreat; Meltwater; Nitrogen; Boron; Modern Distribution

INTRODUCTION

Globally, the remote lakes found at high elevations act as sentinels of change and are among the first bodies of water impacted by climate change (Heino et al., 2009; Dodds and Whiles, 2010; Catalan et al., 2013). As anthropogenic warming continues, the physical and chemical limnology of these lakes will change. As a result, the structure, function, and composition of aquatic ecosystems in sub-alpine and alpine settings will be significantly transformed (Rosenzweig et al., 2007; Schindler, 2009; Adrian et al., 2009). Recent studies suggest that the range of invasive fish species and invertebrates will expand due to their ability to move to higher elevation lakes via warmer creeks with stable environments (Khamis et al., 2014). This movement will impact natural communities that exist in alpine lakes by altering food web and predator/prey dynamics (Khamis et al., 2014). Increases in terrestrial vegetation related to the upslope movement of timberlines will supply higher amounts of dissolved organic carbon (DOC) to sub-alpine and alpine lakes, which will increase productivity and potentially affect the diversity of high lake ecosystems (Messner et al., 2012). Other lake-related changes include an increase in water acidification, long-range atmospheric pollution, and large ecological shifts (Catalan et al., 2013).

Many of the alpine lakes in the western United States receiving cold meltwater emanating from small cirque glaciers located in alpine environments are sensitive to regional climate. Hall and Fagre (2003) modeled glacial retreat for Glacier National Park and concluded that glaciers would disappear from the landscape by 2030. Recent work suggests that local topographic effects may buffer against regional warming and glacial extinction may be delayed. Basagic and Fountain (2018) suggest that if trends of glacial activity for small alpine glaciers maintain current rates of retreat, they will mostly likely disappear in the next 50 to 250 years. Many studies indicate that glacial meltwater affects alpine hydrology, chemistry, and the turbidity of high alpine lake water

(Slemmons et al., 2015). Temperatures in the western United States have steadily increased over the past few decades and have amplified the rate at which glaciers and permafrost are melting in alpine areas (Diaz and Eischeid, 2007; Mark and Fernández, 2017). The addition of this cold, silt-enriched water into alpine lakes will impact the timing of lake stratification (Hood and Berner, 2009), increase turbidity, decrease optical transparency (Moore et al., 2009), and alter the water chemistry (Mark and Fernández, 2017) of these alpine lakes. Studies indicate that lakes receiving glacial meltwater have up to 200x more nitrogen than those lakes that only receive snowmelt (Slemmons et al., 2015). Atmospheric nitrogen has been accumulating on the surface of glaciers for decades. This nitrate is then added to lake system with the onset of glacial retreat. The additional input of nitrogen to N-limited lakes promotes enhanced primary productivity, such as algal blooms (Fenn et al., 2003; Slemmons et al., 2013; Greaver et al., 2016). While many studies have endeavored to elucidate the physical and geochemical changes within these systems, little work has addressed how biotic communities in alpine lakes will respond to the increased flux of glacial meltwater in the short term (Slemmons et al., 2015). Limited studies have documented that diatom communities in many alpine lakes are shifting from large filamentous diatoms (i.e., *Aulacoseira* taxa) to *Cyclotella* spp. as a result of longer growing seasons, increased stratification, and decreased ice cover (Catalan et al., 2013).

Chironomids, or midges, are one of the most abundant insects found in freshwater ecosystems (Walker, 1987). They are considered both ubiquitous and cosmopolitan (Porinchu and MacDonald, 2003; Brooks et al., 2007; Ferrington, 2007), making them a useful insect to study changes in temperature, pollution, and dynamic system changes. Midges occupy several trophic levels in aquatic ecosystems and therefore play a vital ecological role in lakes (Walker, 1987;

Porinchu and MacDonald, 2003). However, the ecological understanding of chironomid distribution is poorly understood (Eggermont and Heiri, 2012).

The life cycle of a chironomid goes through several stages and begins as an egg mass deposited on the surface of the water by an adult chironomid. As the eggs hatch, chironomids erupt in their first larval state and mainly persist as benthos on the floor of the lake. In this state, the chironomid has a maggot-like form and a chitinous head capsule that is shed three more times as individuals grow (Walker, 1987; Porinchu and MacDonald, 2003). Eventually, the larval chironomid reaches the pupae stage and rises through the water column of the lake. This stage is abrupt and leads to metamorphosis from pupae to an adult fly that emerges from the lake (Walker, 1987; Porinchu and MacDonald, 2003). Thus, the survival of chironomid egg masses is largely controlled by surface water temperature (Schütz and Füreder, 2019), the larval stage is influenced by bottom water temperature, and adult flies exist in environments dominated by air temperature (Eggermont and Heiri, 2012). Chironomids have been used as a biological proxy to model both SWT (Walker et al., 1997; Brooks and Birks (2001); Porinchu et al. (2007) and air temperature (Lotter et al., 1997; Larocque et al., 2001; Heiri and Lotter, 2010; Haskett and Porinchu, 2014) based on the assumption that a strong relationship exists between surface water temperature and air temperature. Eggermont and Heiri (2012) caution that multiple factors (e.g. depth, thermal stratification, and glacial melt, i.e., an influx of cold water) may impact the relationship between air and surface water temperatures. Understanding the dichotomy between air and water temperatures in chironomid ecology is imperative for future chironomid-based paleoclimate studies.

To date, the studies that have assessed the response of midges to glacial melt in alpine settings focus on montane streams (Lods-Crozet, et al., 2001; Milner et al., 2001; Rossaro et al.,

2016; Lencioni, 2018). These studies indicate that chironomid communities are responsive to glacier meltwater input; however, there remains a paucity of studies documenting the response of midges to glacial melt in lacustrine settings. Information extracted from lake sediment can be used to develop baseline limnological information against which future changes can be compared (Smol and Douglas, 2007). This research is vital due to the very narrow window of time that is left for studies that examine glacial retreat due to the projected demise of alpine glaciers, especially those present in the western United States (Slemmons et al., 2013).

STUDY AREA

The Colorado Rocky Mountains possess the most southern-reaching alpine glaciers currently still active in the United States. While many areas present in the Northern and Central Rocky Mountains have shown pronounced ablation rates for alpine glaciers (Appenzeller, 2007; Munroe et al., 2012), the behavior of glaciers in the Southern Rocky Mountains is quite different. Studies documenting air temperature variability in the Front Range reveal that the alpine tundra (>3000 m above sea level) in this region is experiencing a progressively strong heat sink in the Colorado Rocky Mountains due to increased snow cover, decreased solar radiation input, and enhanced air movement over the surface (Pepin and Losleben, 2002). Rangwala and Miller (2010) found that minimum and maximum temperatures in San Juan Mountains are warming at similar rates (1°C/decade). However, greater differences were observed for minimum temperatures during the winter than those of maximum temperatures in the summer. Thus, the rate of glacial retreat is much slower in this region relative to regions to the north, such as Glacier National Park (Pepin and Losleben, 2002; Hoffman et al., 2007; Rangwala and Miller, 2010; Rangwala and Miller, 2012) and makes the Front Range a critical location for monitoring glacier change (Hoffman et al., 2007).

Rocky Mountain National Park (RMNP) is located in the northern portion of the Front Range and is home to 30 glaciers (Hoffman et al., 2007). The glaciers in RMNP straddle an elevational range that includes regional timberline (3500 m Above Sea Level or ASL) and lies between 3416 and 4068 m ASL. Most glaciers are found on the eastern side of the Continental Divide and occupy north- to east-facing cirques (Madole, 1976). Snow accumulation is frequently redistributed into these cirques by strong westerly winds and avalanching (Outcalt and MacPhail, 1965; Winstral et al., 2002; Hoffman et al., 2007). The local topographic shading evident on the eastern side of the Continental Divide also has strong control over ablation rates and may account for the highly irregular ablation-altitude gradients evident in the Front Range (Outcalt and Macphail, 1965; Hoffmann et al., 2007).

Comparing the chironomid assemblages found in lakes located in glaciated catchments to those found in lakes located in unglaciated catchments (with variations in elevation, geology, and vegetation controlled for) enabled an assessment of the relative role meltwater plays in shaping chironomid communities in alpine lakes in the Park. All lakes were found in areas that consisted of igneous proterozoic diorites and granites that intrude into ancestral metamorphic proterozoic biotite gneisses, migmatites and schists (Kellogg et al., 2004).

The collection of five pairs of short lacustrine sediment cores occurred during the late summers of 2015 and 2016 (Figure 2.1). Study sites and their corresponding pair were chosen to be at the approximate elevation with similar vegetation and geology. The only obvious differences between the paired lakes was the type of meltwater input that the lakes received. One lake received meltwater from a receding glacier, while the other only received meltwater from the annual accumulation of snow. Table 2.1 lists the following lakes and their abbreviations along with elevation, lake depth, and other variables. Cony (CNY) and Pipit (PIP) lakes were the highest

elevations and were sampled at 3509 and 3479 m ASL, respectively. These paired lakes were located in rocky cirques above timberline adjacent to the continental divide. Cony Lake receives

	Pipit Lake	Cony Lake	Box Lake	Eagle Lake	Thunder Lake	Black Lake	Falcon Lake	Hutcheson Lake	Odessa Lake
Lake Code	PIP	CNY	BOX	EGL	THD	BLK	FAL	HCH	ODS
Elevation (m asl)	3479	3509	3274	3298	3225	3237	3371	3413	3051
Depth (m)	10.4	16.8	11	10.15	7.05	21.2	8.1	3.1	5.95
Secchi Disk Depth (m)	3.6	3.5	2.2	7.4	2.2	6.4	3.5	2.3	33
Mean July Air Temperature (°C)	11.29	11.13	12.42	12.29	12.69	13.12	11.89	11.66	13.65
Surface Water Temperature (°C)	9.2	8.2	13.9	10.9	13.1	10.9	9.2	10	10.5
Bottom Water Temperature (°C)	8.1	5.1	6.2	6	8.5	4.2	8.2	9.3	9.1
Glacial Index (GI)	0.00	0.85	0.00	0.52	0.00	0.56	0.00	0.45	0.65
Glacial Coverage in Catchment (GCC) (%)	0	18.18	0	8.74	0	3.16	0	4.37	5.43
Distance (m)	0	0.5	0	1.34	0	1.31	0	1.74	1.74
pH	8.61	7.3	7.17	7.3	8.76	8.23	7.92	7.88	8.11
Specific Conductivity	0.011	0.017	0.011	0.01	0.014	0.009	0.01	0.02	0.012
Dissolved Oxygen (DO) (mg/L)	7.7	2.72	3.7	3.16	2.85	2.45	3.49	2.92	4.21
Dissolved Organic Carbon (DOC) (ppm)	2.578	1	1.52	0.92	1.04	1.08	1.07	2.04	0.93
Dissolved Inorganic Carbon (DIC) (ppm)	1.764	1.86	1.64	1.4	1.58	1.34	1.06	2.19	0.87
Total Phosphorous as PO ₄ -P (ppb)	8.99	46.81	20.19	19.09	52.08	43.85	21.73	17.85	29.2
NO ₃ + NO ₂ -N (ppm)	0.274	0.164	0.003	0.139	0.059	0.156	0.175	0.108	0.143
Active Chlorophyll- <i>a</i> (ug/L)	0.8	1.5	1.7	0.2	5.8	0.6	1.5	2.2	4
Boron (B) (ppm)	0	0.02	0	0.02	0.01	0.02	0.05	0	0
Calcium (Ca) (ppm)	1.152	1.382	0.948	1.055	1.093	0.787	1.217	1.963	1.051
Magnesium (Mg) (ppm)	0.153	0.09	0.13	0.12	0.11	0.06	0.08	0.17	0.13
Sodium (Na) (ppm)	0.429	0	0.2	0.6	0.3	0.2	0.2	0.2	0.5
Phosphorous (P) (ppm)	0.083	0.03	0.05	0.04	0	0	0	0.04	0.04
Silica (Si) (ppm)	1.274	0.533	0.967	1.735	1.046	0.671	1.191	1.054	1.673
Arsenic (As) (ppm)	0.024	0.002	0.013	0	0.008	0	0.01	0.012	0
Selenium (Se) (ppm)	0	0.018	0	0.019	0.011	0.021	0.004	0	0.033
Trophic Level	Oligotrophic	Mesotrophic	Mesotrophic	Mesotrophic	Eutrophic	Mesotrophic	Mesotrophic	Mesotrophic	Mesotrophic
Aluminum (Al) (ppm)	0	0	0	0	0	0	0	0	0
Barium (Ba) (ppm)	0	0	0	0	0	0	0	0	0
Cobalt (Co) (ppm)	0	0	0	0	0	0	0	0	0
Copper (Cu) (ppm)	0	0	0	0	0	0	0	0	0
Potassium (K) (ppm)	0	0	0	0	0	0	0	0	0
Manganese (Mn) (ppm)	0	0	0	0	0	0	0	0	0
Strontium (Sr) (ppm)	0	0	0	0	0	0	0	0	0
Cerium (Ce) (ppm)	0	0	0	0	0	0	0	0	0
Conductivity (µS/cm)	8.4	11.6	9	7	10.6	6.5	6.8	14.3	8.3
Dissolved oxygen (%)	99.3	35	43.4	41.8	39.4	32.2	45.9	39.1	53.4
Phosphate (PO ₄ -P) (ppb)	1.82	2.54	1.23	5.87	1.87	6.13	4.5	7.15	1.75
Total dissolved Phosphorous as PO ₄ -P (ppb)	12.18	27.06	24.33	26.19	24.04	17.99	17.56	35.12	25.79
Total Nitrogen as NO ₃ -N (ppm)	0.317	0.481	0.139	0.212	0.103	0.196	0.186	0.136	0.474
Nitrite (NO ₂ -N) (ppb)	n/a	1.48	0.58	1.31	1.29	0.62	1.32	2.58	1.49
Ammonium (NH ₄ -N) (ppb)	0	137.9	23.35	65.77	56.34	17.07	50.1	315.99	2.16

Table 2.1: Limnological variables sampled for nine alpine lakes in Rocky Mountain National Park, Colorado. Glacially-fed lakes are highlighted in gray. Variables with red print were not used in analysis.

glacial melt from an unnamed glacier, whereas Pipit only receives melt from annual snowfall. Hutcheson Lake (HCH) (3413 m ASL) receives glacial input from Cony Lake, which lies immediately above the catchment. Grasses that are typical of alpine tundra surround the lake. It is

paired with snowmelt-fed Falcon Lake (FAL), which lies at 3371 m ASL and is located in a small rocky cirque with small patches of krummholz. The paired Box (BOX) and Eagle (EGL) Lakes

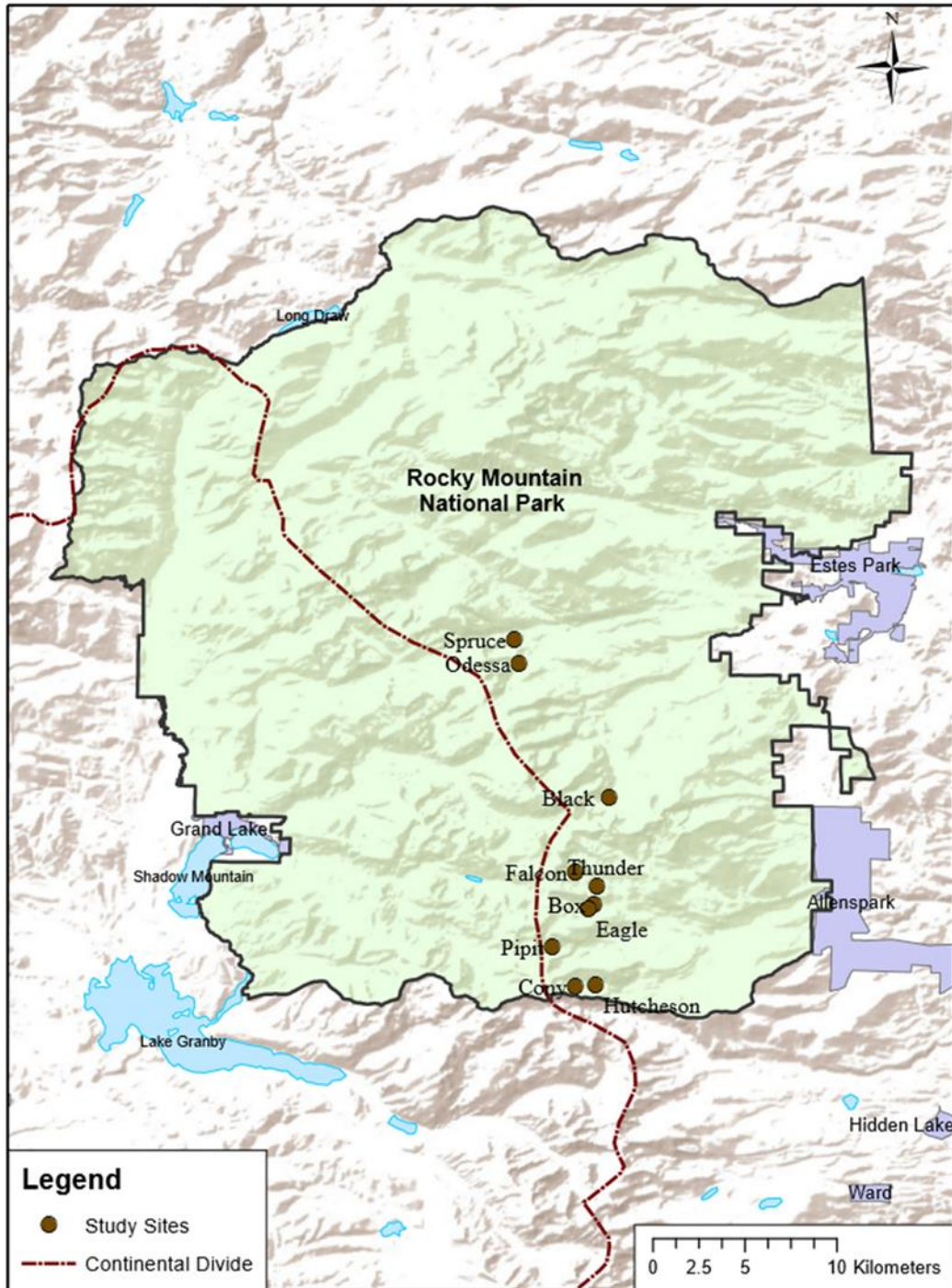


Figure 2.1: Base map for study sites in Rocky Mountain National Park, Colorado.

lie at 3274 and 3298 m ASL, respectively and are located at timberline. Eagle Lake receives glacial meltwater from Moomaw Glacier, whereas Box Lake only receives annual snowmelt.

The remaining lakes all lie below timberline and are located in subalpine forest predominately composed of *Pseudotsuga menziesii* (Douglas fir) and *Picea engelmannii* (Engelmann spruce). Black (BLK) Lake, located at 3237 m ASL is the deepest lake sampled at 21.2 m and receives glacial melt. BLK also has fairly steep scree slopes SSW and S of the lake. It is paired with Thunder (THD) Lake, which lies at 3225 m ASL and is on a much gentler slope than BLK. The lake is surrounded by forest almost to the edge of the lake. Odessa (ODS) and Spruce (SPR) Lakes were the final pair. ODS (3051 m ASL) receives glacial input from three unnamed glaciers located higher in the catchment. Spruce Lake (2947 m ASL) was unlike any other lake sampled. It was only 1-m deep and had tall grasses throughout the entire bed of the lake. It also contained no chironomid subfossil remains and thus was eliminated from the analysis.

METHODS

Field Methods

The sediment cores were collected from the approximate center of the study lakes using a gravity-corer, deployed from a small, two-person inflatable raft that allows recovery of lake surface sediment with minimum disturbance of the mud-water interface. The cores were typically 20-cm long and represented approximately 150 years of deposition. Observations regarding the stratigraphy and color of each core were recorded in a field notebook and then sectioned into 0.25-cm intervals and placed into Whirlpaks®. A Yellow Springs Instrument (YSI) Professional Plus was used to collect a suite of limnological variables, such as temperature, pH, and specific conductivity. Water samples were collected from the center of each lake and submitted to the Center for Applied Isotope Studies (CAIS) at the University of Georgia for analysis of analytes

for nitrogen and phosphorous, as well as nutrients (chloride, sulfate, and Chlorophyll α). The cores were transported to the Environmental Change Lab at the University of Georgia in coolers after the end of each field season. Total carbon (%) of dry bulk sediment was analyzed using EA-IRMS at CAIS. Distance (m) is the measured distance from the lake to the terminus of the glacier in the lake catchment. The glacial index (GI) is a measure of environmental harshness and is an index of glacial influence following Jacobsen and Dangles (2012). The GI was calculated as $GI = \frac{\sqrt{\text{area}}}{\text{distance} + \sqrt{\text{area}}}$ (for $\text{area} > 0$). The glacial coverage in the catchment (GCC) was also calculated (Jacobsen et al., 2012). The area of each catchment as well as those for each glacier was determined using the GLIMS Glacier Database in ArcGIS (Raup et al., 2007).

Laboratory

Chironomid extraction procedures followed the protocol established by Walker (2002). Bulk sediment samples were soaked in an 8% KOH solution and heated to 40°C for a minimum of 30 minutes. The solution was then sieved through a 95 μm -grade mesh screen using distilled water to eliminate any remaining KOH residue. The material remaining on the screen was transferred into a beaker with distilled water. The resulting residue was then poured into a Bogorov counting tray and sorted using a stereoscope at 40X. The sub-fossil chironomid head capsules extracted from the residue were permanently mounted on glass slides using Entellan®. This process was repeated until a minimum of 50 head capsules were recovered from each sample following the advice of Heiri and Lotter (2001). A Nikon Eclipse E100 (x100) microscope was used for taxonomic determination of the midge remains. The taxonomic keys by Brooks et al. (2007) and Andersen et al. (2013) were instrumental in the identification of midge taxa.

Data Analysis

All lakes produced a minimum of 49.5 chironomid head capsules for analysis in the upper 0.50 cm of sediment (Laroque, 2001). Spruce Lake contained zero chironomid remains and was removed from the analysis. Detrended canonical analysis (DCA) is an indirect ordination technique that is useful in the exploration of taxa data collected from the lacustrine sediment. Chironomid taxa possess the highest abundances in environments that maximize their preferred habitats. Abundances begin to decline or disappear as they become farther removed from their preferred environment. Due to these characteristics, ecological data typically possess “a modal relationship to their ecological gradients” (Holland, 2008). DCA assumes that the data have a unimodal distribution. The chironomid assemblage data followed a Poisson distribution and satisfied this assumption. The data were square-root transformed to shorten the distribution and to make the data homoscedastic. The effect of rare taxa was down-weighted to dampen their effects on the ordination. DCA is used to determine whether a linear, e.g., redundancy analysis (RDA) or unimodal, e.g., canonical correspondence analysis (CCA), model should be used to understand which environmental variables explain the most variance in the distribution of chironomid communities (Ter Braak and Verdonschot, 1995).

Redundancy analysis (RDA) was used to assess which environmental variable explains the most variance in species distribution (Van den Wollendberg, 1977; Zuur et al., 2007).

RDA is used to extract and summarise variation in the chironomid taxa data that can be explained by environmental variables (Zuur et al., 2007). A forward selection process was used to identify the environmental variables that most likely explained the distribution of modern chironomid communities. This method, combined with permutations, was used to determine the statistical significance ($p < 0.05$) of each environmental variable, as well as demonstrating the amount of

variance that each variable accounted for (Birks, 1998; ter Braak and Verdonschot, 1995). Forty environmental variables were collected. However, 26 elements collected from lake water were below detection and removed from the analysis. Variables that covaried, such as dissolved oxygen (%) and dissolved oxygen (mg/L) were examined, and only one representative variable was used. Twenty-five remaining environmental variables were assessed for linearity, and specific conductivity, lake depth, and Secchi disk depth were log-transformed to ensure that homoscedasticity assumptions were met (Table 2.1). All statistical analyses were performed using the open-source platform R (version 3.6.1) (R Development Core Team, 2019, <http://www.R-project.org>). DCA and RDA were implemented in the vegan package (Oksanen, 2015).

RESULTS AND DISCUSSION

Water Chemistry

The summary of environmental variables included in the analysis is provided in Table 2.1. In general, the lakes sampled were relatively deep, and all were over 5 m with the exception of Hutcheson Lake (3.1 m). Lake depths ranged from 3.1 m to 21.2 meters deep, with an average of 10.42 m. The surface temperature for lake water was variable and ranged from 8.2°C to 13.9°C. This wide range in surface water temperature (SWT) is of note as these lakes are not found on a particularly long elevational gradient (458 m). All lakes were open basins and received input from alpine streams as well as having outlet streams. The temperature profiles for the shallowest lakes that received glacial meltwater (i.e., Odessa and Hutcheson Lakes) showed no sign of thermal stratification and only varied by $\leq 1.4^{\circ}\text{C}$. Pipit and Falcon Lakes were deeper (10.4m and 8m, respectively) but only had temperature profiles that varied by 1°C from the surface water to the bottom of the lake. These lakes are fed only by annual snowmelt. Cony, Eagle, Box, Black, and

Thunder Lakes all possessed temperature profiles indicative of thermal stratification with an epilimnion thickness of 6 to 8 m.

The trophic class of each lake was evaluated following Carlson’s Trophic State Index (Carlson, 1977). The Carlson Index uses three independent variables of aquatic biomass that includes Secchi depth (SD), total phosphorus (TP) from the epilimnion, and chlorophyll α (Chl) (Table 2.2). However, Horne and Goldman (1994) warn that trophic classifications are idealized concepts and that real-world examples are more varied. For this study, lakes were classified if two of the three variables fell within range of a specific trophic level. The results indicate that only Pipit Lake may be considered oligotrophic (Table 2.1 and Table 2.2). Total P was below the upper threshold of 12.0 ppm at 8.8 ppm, and very little active Chl (0.8) was present in the sampled lake water. The only eutrophic lake sampled was Thunder Lake. TP was high at 52.08 ppm, and the SD was 2.2 m. The remaining seven lakes are classed as mesotrophic, which are typically lakes with an intermediate level of productivity (Horne and Goldman, 1994).

Chl	P	SD	Trophic Class
0.0 - 2.6	0.0 - 12.0	>8.0 - 4.0	Oligotrophic
2.6 - 20.0	12.0 - 24.0	4.0 - 2.0	Mesotrophic
20.0 - 56.0	24.0 - 96.0	2.0 - 0.5	Eutrophic
56.0 - 155.0+	96.0 - 384.0 +	0.5 - < 0.25	Hypereutrophic

Table 2.2: Carlson’s Trophic Level Index. (Chl = Chlorophyll- α , P = Phosphorous, SD = Secchi Disk depth (m)).

Chironomids

A total of 542.5 head capsules was collected and counted from the top 0.50 cm of sediment of each lake in order to assess the modern distribution of chironomid communities (mean=60.28,

maximum=88, minimum=43). Forty-three taxa were identified from the modern sediment. However, if less than 2% of a particular taxon was represented and they were present in fewer than 2 lakes, they were removed from statistical analyses following Quinlan and Smol (2001). Thus 30 taxa were used in analysis.

Chironomus spp. was the dominant taxa present and comprised 24.3% of the total chironomids recovered from all lakes (Figure 2.2). *Chironomus* is eurythermic and is known as a “blood worm” as it emits a red color due to the hemoglobin it produces (Pinder, 1986). It is mostly found in the profundal zone (i.e., the deepest zone) of lakes and can tolerate low levels of oxygen and or short periods of anoxia for this reason (Wilson et al., 2004; Brooks et al., 2007). It is opportunistic and is often found in lakes undergoing environmental change as it is an early colonizer (Brooks et al., 2007). *Corynocera oliveri*-type was the second most abundant taxa (10.9%). This taxon is typically found in the muddy substrate of cold lakes (Brooks et al., 2007; Andersen et al., 2013). Porinchu and Cwynar (2000) documented the presence of these insects with regard to timberline in Siberia. They found that *C. oliveri* was found typically in the colder lakes located above timberline. While this is true of the assemblages collected from Pipit, Hutcheson, Eagle, and Box Lakes, *C. oliveri* had higher relative abundances from lakes below timberline (Thunder Lake and Odessa Lake). *Heterotrissocladius* spp. (6.9%) is a very common taxon in all lakes collected and is typically found in the profundal of cold oligotrophic lakes that are well-oxygenated (Walker and Matthewes, 1988; Brooks et al., 2007; Anderson et al., 2013). *Procladius* (3.7%) was also one of the most prevalent taxa. However, the relative abundance of *Procladius* is very high in Pipit Lake and much lower in every other lake. *Procladius* is very common in lakes that are classified as mesotrophic and eutrophic and is typically associated with the profundal zone (Brooks et al., 2007). *Sergentia* (3.52%) is typically found in relatively deep,

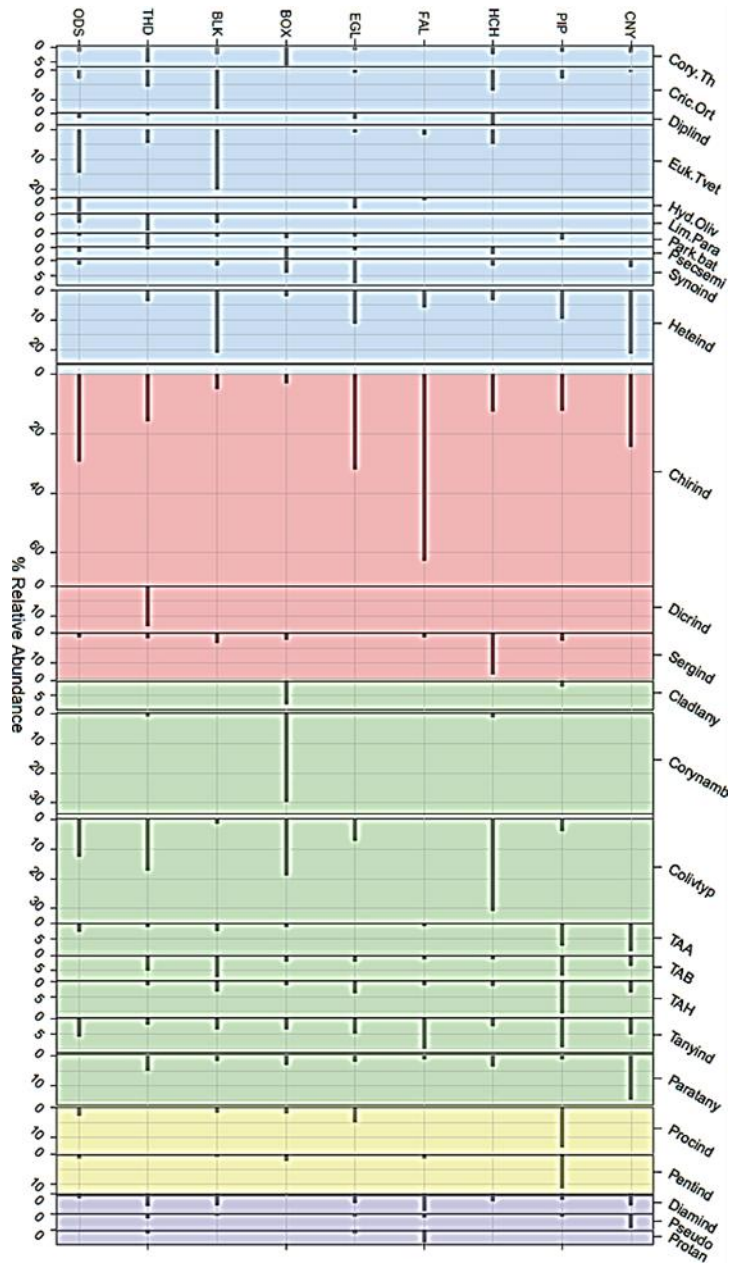


Figure 2.2: Relative abundance curves for the modern assemblages collected from nine alpine lakes in Rocky Mountain National Park, Colorado. The taxa are arranged by subfamilies: Blue: Orthocladinae; Red: Chironominae; Green: Subtribe Tanytarsini; Yellow: Tanypodinae; Purple: Diamesinae. They are arranged with the highest elevation lake at the top and the lowest elevation lake at the bottom of the y-axis. A key to taxa names is available in Appendix B.2.

mesotrophic lakes. This taxon is found in all sampled lakes except for Cony and Eagle Lakes. The presence of both *Chironomus* and *Sergentia* indicates early colonization is occurring, and a transition from an oligotrophic state to a mesotrophic trophic state is in progress.

The presence of taxa from the tribe Diamesinae (including *Diamesa* spp., *Pseudodiamesa*, and *Protanypus*) is of particular interest in that the remains of these taxa are extremely rare in lake sediment and poorly studied (Pinder, 1986; Walker, 1993; Brooks et al., 2007). Recent studies of chironomids in alpine streams find that the presence of Diamesinae increases with the closer proximity to the terminus of melting glaciers (Lencioni, 2018). Larocque et al. (2001) found that “*Pseudodiamesa* and *Diamesa* were most abundant in alpine-tundra lakes above timberline, characterized by cold climatic conditions and low sedimentary organic content” in Swedish lakes. *Protanypus* has also been found in high elevation lakes in Canada and is associated with deep and cold lakes (Walker and Mathewes, 1989; Larocque et al., 2001). However, these taxa have not been identified in previous work done on modern chironomid distribution in the continental Western United States (Porinchu et al., 2002; Porinchu et al., 2003, Porinchu et al., 2007; Haskett and Porinchu, 2014; Reinemann et al., 2014). Porinchu et al. (2003) did find *Pseudodiamesa* in sediment collected from California from the interval corresponding to ages between 14,800 cal yr BP and 13,700 cal yr BP. No modern assemblages were comparable at that time, and the authors suggested that the presence of *Pseudodiamesa* indicated that the glacial meltwater was responsible for their deposition (Porinchu et al., 2013). The presence and relative abundances of Diamesinae present in sediment collected from Rocky Mountain National Park suggest that this tribe may be used as a qualitative indicator of glacial meltwater and may assist historical reconstructions that use chironomids as a biological proxy for temperature.

The length of the first DCA axis was 2.48, and RDA was chosen as the appropriate model to assess the relationship between chironomids and environmental variables. DCA also showed a strong relationship between glacial lakes and lakes only receiving melt from annual snowfall (Figure 2.3). The first DCA axis possesses taxa associated with the colder lakes typical of glacial input in the negative range of DCA axis 1. Taxa affiliated with warmer temperatures are located to the right of the axis and are positive. DCA axis 2 represents the presence or absence of macrophytes in the system. Positive values are indicative of taxa typically affiliated with the presence of macrophytes (i.e., *Psectrocladius*, *Paratanytarsus*, *Cladotanytarsus*, and *Tanytarsus*). Negative values are affiliated with taxa that are typically found in the littoral zone of lakes or even small running streams such as *Eukiefferiella*, *Diplocladius*, *Limnophyes*, and *Cricotopus/Orthocladius*. The top left quadrant of Figure 2.3 contains some of the coldest stenotherms that have been noted in the literature. According to Brooks et al. (2007), *Abiskomyia* only occurs in the coldest lakes of the arctic. *Heterotrissocladius*, *Diamesa* spp., and *Pseudodiamesa* are also noted as the coldest stenotherms present in assemblages (Walker et al., 1997; Porinchu et al., 2003). Cony and Black Lakes are the only lakes that contain this assemblage. The taxa found in the bottom left quadrant are still indicative of cold water but are also affiliated with running water from streams or taxa more likely to be found in the littoral zone of lakes. *Diplocladius*, *Limnophyes*, *Eukiefferiella*, and *Smittia* are all uncommon in lake sediment and indicative of cold running water entering into the lake system. Surprisingly, two lakes that were thought to be only fed by year-of-snow, fall within this ordination space. Falcon Lake strongly falls within this zone. This lake was located in a rocky cirque and contained large snowfields that may mirror the action of glacially-fed lakes. Thunder Lake barely falls within this ordination space

and may be indicative of a transitional lake. However, it may also suggest that this lake is receiving cold meltwater from somewhere higher in its catchment.

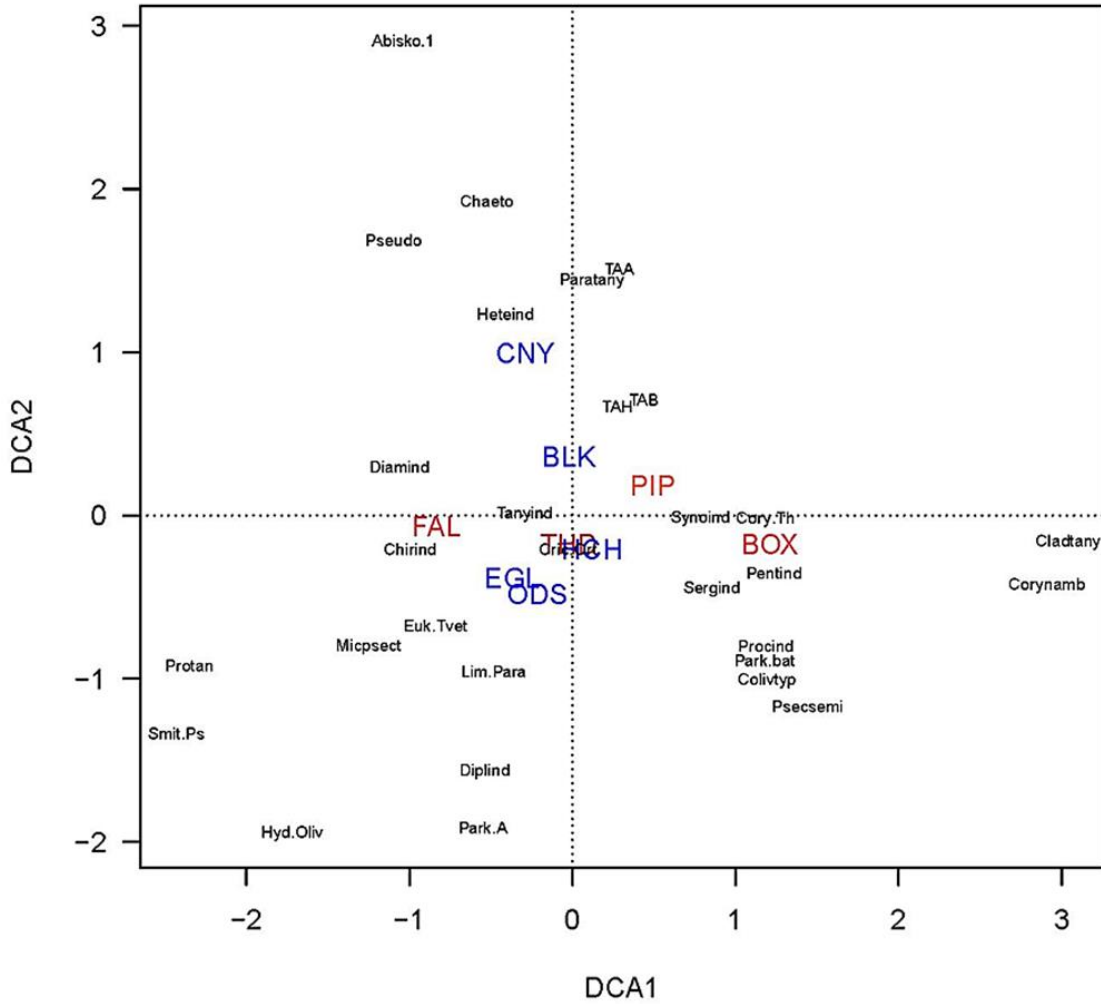


Figure 2.3: Detrended correspondence analysis bi-plot indicating the relationship between taxa, or assemblages, and corresponding lakes. Lakes in blue are fed by glacial meltwater. Lakes in red are fed by melt emanating from the annual accumulation of snow.

Relationship between environmental variables and chironomid communities

RDA was used to assess which environmental variable explains the most variance in species distribution (Ter Braak and Verdonschot, 1995). RDA models were developed using forward selection combined with Monte Carlo Permutation tests ($p < 0.05$, 999 permutations) (Table 2.3; Figure 2.4). Only 3 of the 26 environmental variables were statistically significant with a fourth being close; SWT ($p = 0.037$), $\text{NO}_3 + \text{NO}_2\text{-N}$ ($p = 0.049$), boron (B) ($p = 0.053$), and C % ($p = 0.057$). The first axis of the RDA, consisting of SWT, boron, and C%, were identified as statistically significant ($p = 0.022$). Surface water temperature explained the majority of the variance present within the data (7.5%), followed by $\text{NO}_3 + \text{NO}_2\text{-N}$ (7.5%), B (7.4%), and C% (7.1%). The first RDA axis explained 9.8% in the variation of the distribution of chironomid taxa and was the only axis that was statistically significant ($p = 0.019$).

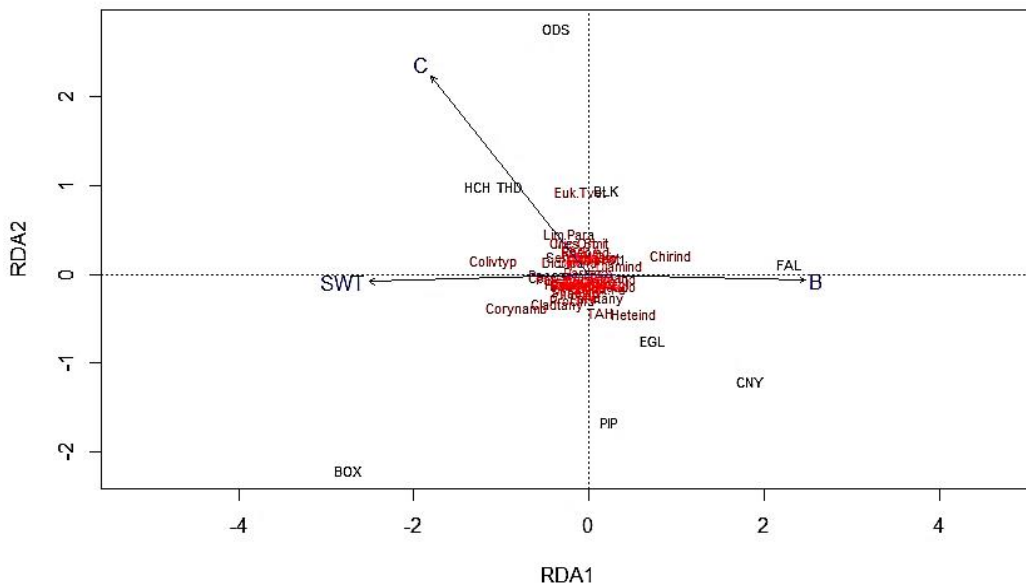


Figure 2.4: Redundancy analysis bi-plot depicting the relationship between surface water temperature ($^{\circ}\text{C}$), carbon %, boron, and chironomid taxa from the study sites.

Relationships between statistically significant variables were explored using Pearson's correlation coefficient. Only SWT and $\text{NO}_3+\text{NO}_2\text{-N}$ were strongly and negatively correlated ($r=-0.82$, $p=0.007$), and glacial meltwater is the driver that explains the relationship between the two variables. For this study, $\text{NO}_3+\text{NO}_2\text{-N}$ was removed from the analysis as the correlation is too strong. However, this trend is well-documented in the western United States (Slemmons et al., 2013). The atmospheric deposition of nitrogen has been collecting on stable glaciers for decades due to urbanization. Elevated air temperatures in the latter part of the 20th and into the 21st century have caused glaciers to recede, which has introduced nitrogen into these systems (Wolfe et al., 2003). Slemmons et al. (2017) found that glacially-fed lakes in the Rocky Mountains are 47 times higher in nitrogen than snow-fed lakes. The Loch Vale Watershed is a long-term research site in Rocky Mountain National Park. Regional data collected from the Loch Vale Watershed site indicate that nitrate concentrations in alpine streams have increased by 50% since 2000 (Baron et al., 2009). While SWT was the variable used in the analysis, this variable represents glacial meltwater contribution. The surface water temperatures of glacially-fed lakes were $\sim 2.62^\circ\text{C}$ colder than their paired lakes that only receive year-of-snow meltwater. The average difference in nitrogen was 66% higher in glacial lakes. While the relationship between atmospheric nitrogen deposition and algal communities is established (Slemmons et al., 2015; Slemmons et al., 2017), this is the first study to find a relationship between atmospherically-deposited nitrogen and chironomids.

The relationship between chironomid communities and temperature is well established but poorly understood. Brundin (1949) noted cold stenotherms such as *Heterotrissocladius* spp. and *Sergentia coracina* present in late glacial sediment (Brundin, 1949; Porinchu and MacDonald, 2003). Quantitative paleotemperature reconstruction of SWT were first performed by Walker et

	Df	variance	F	Pr(>F)
SWT + B + Carbon	3	18.51	1.52	0.022*
SWT	1	7.50	1.68	0.037*
NO3-N+NO2-N	1	7.45	1.67	0.049*
B	1	7.35	1.64	0.053*
Carbon (%)	1	7.12	1.58	0.057.
Depth	1	5.75	1.22	0.240
Elevation	1	5.63	1.19	0.242
Secchi	1	4.93	1.02	0.328
Mg	1	5.26	1.10	0.360
Distance	1	5.26	1.10	0.349
Chl	1	5.11	1.06	0.369
MJAT	1	5.23	1.09	0.372
Si	1	5.07	1.05	0.398
DIC (ppm)	1	4.70	0.97	0.467
BWT	1	4.75	0.98	0.483
P	1	4.66	0.96	0.525
Se	1	4.63	0.95	0.512
As	1	4.52	0.92	0.522
DOC (ppm)	1	4.41	0.90	0.557
pH	1	4.43	0.90	0.568
Total P as PO4 (ppb)	1	4.46	0.91	0.581
DO (mg/L)	1	4.33	0.88	0.583
GCC	1	4.16	0.84	0.640
GI	1	3.95	0.79	0.738
Na	1	3.90	0.78	0.750
Sp Cond	1	3.06	0.60	0.931

Table 2.3: Forward selection of variables with Monte Carlo permutations (n=999). Statistically significant variables are in bold font.

al. (1991) on sediment collected from eastern Canada in the early 1990's. Air temperature models followed soon after. Lotter et al., (1997) reconstructed air temperatures from a core collected from the Swiss Alps in the late 1990's. (Lotter et al., 1997). However, the findings from this study indicate that SWT (i.e., glacial melt) is the environmental variable most responsible for the distribution of modern chironomid communities, whereas Mean July Air Temperature (MJAT)

was not significant ($p=0.372$). This finding illustrates that applying inference models to find to solely model air temperature is inappropriate when developing temperature reconstructions for fossil records as SWT and air temperature don't always covary. A need for a more in-depth understanding of how different temperatures affect the different lifecycles of chironomids is necessary to address future chironomid work. The results of this study suggest that active glacial activity present within a catchment will directly influence the chironomid communities present on the benthos. Future studies should acknowledge if the lake under investigation is/or has ever been influenced by glacial meltwater. If the presence and/or absence is not known for the history of the lake, the presence of taxa from the tribe Diamesinae may act as qualitative indicator species downcore. Diamesinae may also indicate the presence of cold, flowing water into the system and would indicate that temperature reconstructions will produce colder conditions for SWT than were present for air temperature.

The presence of boron in lake water and its impacts on chironomid communities is poorly understood, and no studies currently exist that investigate this relationship. While boron may be a natural byproduct derived from weathering processes on sedimentary bedrock such as shales and coal deposits (Moss and Nagpal, 2003; Barber et al., 2006), the bedrock of all lakes sampled for this study are igneous diorites and granites interspersed with biotite gneisses and schists. However, boron may be used as an inorganic tracer of anthropogenic activity (Barber et al., 2006). Boron is known as an indicator of wastewater and is a byproduct of nonchlorine bleach. The third pathway of boron deposition may result from the fly ash particles created from coal-fired power plants (Moss and Nagpal, 2003; Barber et al., 2006). Due to the remoteness and elevation of the sample sites, this scenario is the most likely explanation for the presence of boron in high alpine lake water. The coal-fired Valmont Generating Station was located down the valley in the Boulder

Creek Watershed from 1924 to 2017 and may be a possible source for the boron present in these systems. Trace amounts of boron could potentially be uplifted into the mountains by winds controlled by the summer monsoon. Additionally, the dominant westerly winds could be carrying boron derived from fertilizers to the west of the study site. Further research is needed to resolve the source of boron in this area.

Initially, the relationship between boron and glacial activity was explored as a possible explanation for the distribution of boron in these lakes. However, the correlation between SWT and boron ($r=-0.36$, $p\text{-value}=0.345$) as well as $\text{NO}_3+\text{NO}_2\text{-N}$ and boron ($r=0.22$, $p\text{-value}=0.566$) were not statistically significant. Furthermore, two glacial lakes had boron levels below detection (Hutcheson and Odessa Lakes), and two snow-fed lakes have varying levels (Falcon Lake (0.05 ppm) and Thunder Lake (0.01 ppm)). The levels of boron are very low (0.00 – 0.05 ppm) and mirror minimum to median values for naturally occurring boron in surface water collected in British Columbia, Canada (0.01 ppm and 0.07 ppm, respectively) (Moss and Nagpal, 2003). On average, levels of boron in US freshwater are about 0.10 ppm (Butterwick et al., 1989). Maier and Knight (1991) investigated the role of toxicity of waterborne sodium tetraborate on *Chironomus decorus* and found that growth rates were affected at 20 mg B/L, and acute toxicity occurred after 48 hours at a level of 1376 mg B/L. However, the authors caution that aquatic macrophytes are much more susceptible to boron than macroinvertebrates and thus food dynamics for chironomids are more likely to be affected, which may explain the relationship between modern chironomid communities and the presence of boron in RMNP (Maier and Knight, 1991). Other studies indicate higher uptake of boron in filamentous algae than chironomids (Saiki et al., 1993). Future research is needed to address these relationships in a more in-depth manner.

Carbon (C %) collected from bulk sediment is often used to understand the organic matter content within a lake (Meyers and Ishiwatari, 1993). Higher levels of organic carbon indicate that the lake is more productive, and larger sources of available food for chironomid larvae (Francis, 2004). Many studies have found a strong statistical relationship between organic carbon and chironomids in Fennoscandia (Olander, 1999), Sweden (Larocque et al., 2001), northwestern Canada (Wilson and Gajewski, 2004), and New England of the United States (Francis, 2004). Wilson and Gajewski (2004) argue that the large gradient of organic carbon collected for these studies captures a wide array (3 to 87%) that partially explain the distribution of chironomid communities in northern British Columbia and southwestern Yukon. The authors argue that other chironomid workers, such as Walker et al. (1991), did not capture as full a gradient and were less likely to see this relationship. Our study only captures a gradient from 5.3% to 13.4%, and yet C (%) is an important environmental variable for understanding the modern distribution of chironomid communities in the alpine lakes of Rocky Mountain National Park. However, it should be noted that organic carbon content of bulk sediment is created from the interaction of primary productivity, wind and wave action, sediment availability, distance from shore, light penetration, and nutrient availability (McGarrigle, 1980; Wilson et al., 2004). For this reason, chironomid workers have been cautious in their interpretation of the relative importance of organic carbon as it is often highly correlated with depth and surface water temperature (Lotter et al., 1997; Olander et al., 1999; Wilson et al., 2004). The relationship between surface water temperature and C% is correlated in this study ($r=0.66$, $p=0.055$). However, this relationship is not strong enough to warrant removing it from analysis as the statistical probability that the relationship between SWT and C% occurred by chance is more likely than the relationship evident between SWT and $\text{NO}_3+\text{NO}_2\text{-N}$.

CONCLUSION

The findings of this study indicate that glacial retreat is impacting the chironomid communities in the high elevation lakes located along the continental divide of the Colorado Rocky Mountains. Surface water temperature and $\text{NO}_3+\text{NO}_2\text{-N}$ were extremely and strongly negatively correlated, indicating that glacial retreat is responsible for the greatest amount of explained variance (14.95%) from our model. Furthermore, limnological measures and the high presence of *Chironomus* and *Sergentia* suggest that early colonization of formerly oligotrophic to mesotrophic conditions is currently underway. However, cold stenotherms, such as *Heterotrissocladius*, are still present in high relative abundances suggesting these lakes are still affiliated with extremely cold conditions. The presence of taxa from the tribe Diamesinae (*Diamesa*, *Pseudodiamesa*, and *Protanypus*) are present in high numbers relative to the previous chironomid lacustrine studies and may indicate extremely cold and running water entering into the lakes. These taxa may be useful as qualitative indicators of meltwater and may be useful for downcore paleotemperature chironomid-based reconstructions.

The findings from this study indicate that the high elevation lakes located in the remote lands of Rocky Mountain National Park have been impacted by decades of land use practices and increasing temperatures. Almost all lakes in this study are no longer oligotrophic and are becoming more productive. The presence of boron in some lakes is also concerning as their presence indicates that anthropogenic activities are shaping these remote alpine ecosystems. This understanding will enable land managers for Rocky Mountain National Park to understand the current situation of water quality within the park.

The results from this study also inform our understanding of the processes that occur during the transition from glacial to interglacial stages in sediment. Many lakes that are studied for

paleoclimatology are often found in remote locations and were formed by glacial activity. This study indicates that future work should endeavor to understand the glacial history within the lake catchment in order to refine midge-based temperature reconstructions. The presence of Diamesinae may suggest that warmer air temperatures were occurring as SWTs were decreasing. Future research may also explore possibilities of combining reconstructions of SWT and air temperature as drivers change within the system.

CHAPTER 3

CHIRONOMID EVIDENCE OF GLACIAL RETREAT AND CORRESPONDING CHANGES IN SURFACE WATER TEMPERATURES DURING THE PLEISTOCENE-HOLOCENE TRANSITION FROM AN ALPINE LAKE IN COLORADO, USA.²

² Haskett, D.R., G. Jiménez-Moreno, and R.S. Anderson. To be submitted to *The Holocene*.

ABSTRACT

A high-resolution record for environmental change during the transition from the Pleistocene into the Holocene was developed using chironomid data for central Colorado. The chironomid-based surface water temperature (SWT) inference model ($r^2_{\text{boot}} = 0.38$, RMSEP = 2.74°C) incorporated 153 lakes from California, Utah, and Colorado. Three distinct zones were evident in the subfossil chironomid assemblages based upon constrained hierarchical clustering analysis. The oldest zone (12,659 - 11,901 cal yr BP) coincides with the Younger Dryas chron (c. 12.9-11.5 ka), and no chironomid remains were recovered until ~11,900 cal yr BP. The transition into the Holocene was captured in the second zone (11,901 - 10,033 cal yr BP). SWT temperatures were the lowest evident in the reconstruction until 11,334 cal yr BP and averaged 8.2°C. An increase of 4.7°C occurred after this period and led to a new stable period that fluctuated around an average SWT of 9.8°C. The indicator species, *Diamesa* spp., was found at the base of this zone, suggesting glacial meltwater from the Pinedale Glaciation continued to enter into Kite Lake until ~11,000 cal yr BP. Change-point analysis of faunal turnover suggests that *Chironomus* replaced *Diamesa*, a species affiliated climatic amelioration at 11,300 cal yr BP. The third zone (10,033 - 9,236 cal yr BP) represents the earliest stable Holocene. The presence of *Cladotanytarsus*, *Paratanytarsus*, and *Procladius* indicates a period of warmth and productivity. SWTs were the highest recorded and averaged 12.5°C.

Keywords: Pleistocene-Holocene Transition; Abrupt Climate Change; Chironomid; Glacial Retreat; Chironomid Succession; Colorado

INTRODUCTION

The Younger Dryas (YD) was first recognized in Allerød, Scandinavia, when scientists found pollen from the cold-loving arctic and alpine herb *Dryas Octapela* in a sandy layer overlying peaty sediment containing evidence of thermophilous trees (Anderson et al., 2013). Not only did this discovery define the transition from the warmer Bølling-Allerød to the much colder YD, but it also marked the breakthrough of one the most significant climatic deteriorations in recent geologic history. The Younger Dryas began 12,800 years ago and lasted until 11,600 y BP, a date that corresponds with the transition to the Holocene (Rasmussen et al., 2006; Anderson et al., 2013). Evidence from ice cores collected in Greenland indicates the onset of a prominent decade-long stepped cooling to near glacial conditions at ~12,850 (Alley et al., 1993). The cold phase lasted for approximately 1,200 years before the climate warmed by 7°C in less than 50 years in Greenland (Anderson et al., 2013).

Glacial, paleolimnological and paleobotanical evidence suggests that much of the Western United States were affected by the colder conditions that were evident during the Younger Dryas (Porinchu et al., 2003; Licciardi et al., 2004; MacDonald et al., 2008; Goebel et al., 2011). Dated records of moraines collected from the Colorado Front Range, the Wyoming Wind River Range, the Canadian Rockies, and the Cascades all indicate the readvancement of alpine glaciers during this chronozone (Licciardi et al., 2004). Diatoms, isotopes, and chironomids collected from two lakes in the east-central Sierra Nevada suggest cooler temperatures as well as a shift from dry to moist conditions with the onset of the YD (MacDonald et al., 2008). These findings are also evident with increases in lake levels of Lake Bonneville and the Lahontan Basin of the Great Basin (Goebel et al., 2011).

Paleoclimatic reconstructions from the Colorado Rocky Mountains indicate that the magnitude and extent of the YD in this area are less apparent. Reasoner and Jodry (2000) estimated that treeline in the Southern Rocky Mountains moved downslope by 60-120 m, indicating that the area was affected by the climatic cooling of the YD. Pollen records show an increase in the amount of *Artemisia* at the same time that *Pinus* and *Picea* decreased, which suggests a shift from subalpine forest to alpine tundra (Markgraff and Scott, 1981; Vierling, 1998; Briles et al., 2012). Monazite dissolution peaked at ~10.5 ka, and represents a major paleoweathering boundary in a sediment record collected from the Front Range, Colorado at the Pleistocene-Holocene transition (Price et al., 2017). However, some studies indicate asynchronous glacier maxima (Brugger et al., 2019). Some studies suggest that this trend is muted (Briles et al., 2012) or completely absent from some records collected from the area (Fall, 1997). Vierling (1998) suggests that the dynamic processes at work in mountainous environments could account for this trend.

Chironomids (Insecta: Diptera) have been extensively used to qualitatively and quantitatively (Battarbee, 2000; Porinchu and MacDonald, 2003; Smol, 2010) describe climatic and environmental change over variable timescales (Porinchu et al., 2010; Axford et al., 2011). Recent work indicates that chironomids are sensitive to glacial meltwater and may aid in the interpretation of downcore reconstructions of abrupt climatic change associated with deglaciation (Lencioni, 2018; Haskett, 2020a). This biological proxy, combined with pollen and magnetic susceptibility work done by Jiménez-Moreno and Anderson (2012), may refine our understanding of high alpine lake response to the transition from the cold conditions evident during the YD into the warmer, stable states of the early Holocene in central Colorado.

STUDY AREA

Kite Lake (39.33° , -106.13°) is located at 3665m asl and is located in the Pike Nation Forest, which is found in the Mosquito Range of the central Colorado Rocky Mountains (Chronic, 1964) (Figure 3.1a and Figure 3.1c). The lake basin is surrounded by four high mountain peaks (Mount Democrat 4314m; Mount Cameron 4340m; Mount Lincoln 4357m; Mount Bross 4322m) and lies in a cirque basin comprised of Precambrian granites, granodiorites, and monzonites. Outcrops of intrusive biotite gneiss, limestone, and sandstone are also present in the catchment (Stoeser et al., 2005).

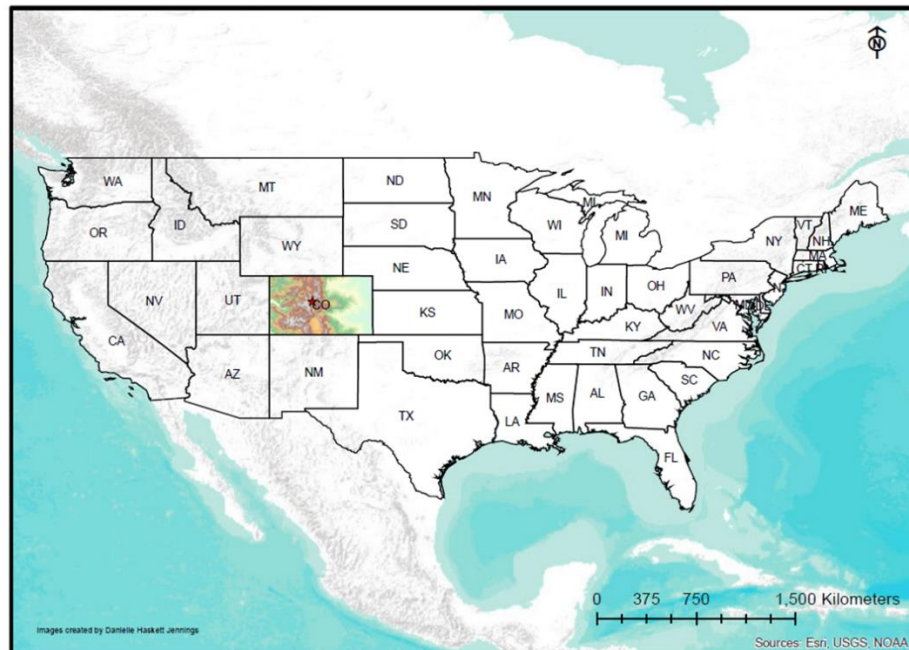


Fig. 1a: Colorado study site in context of the United States.

The climate of Colorado is influenced by its continental position within the United States. Air masses originating over the Gulf of Alaska and Baja, California, deliver moisture to the Colorado Rockies in the form of significant snowfall events from October to May (Carrara et al.,

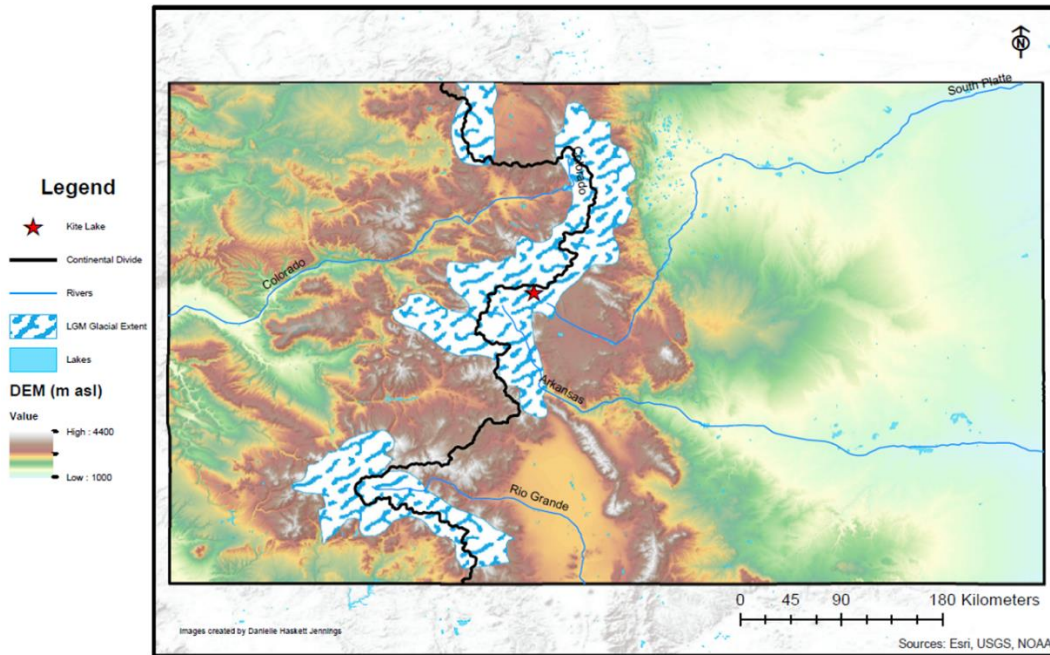


Figure 3.1b: Extent of mountain glaciers in the Colorado Rocky Mountains during the last glacial maximum

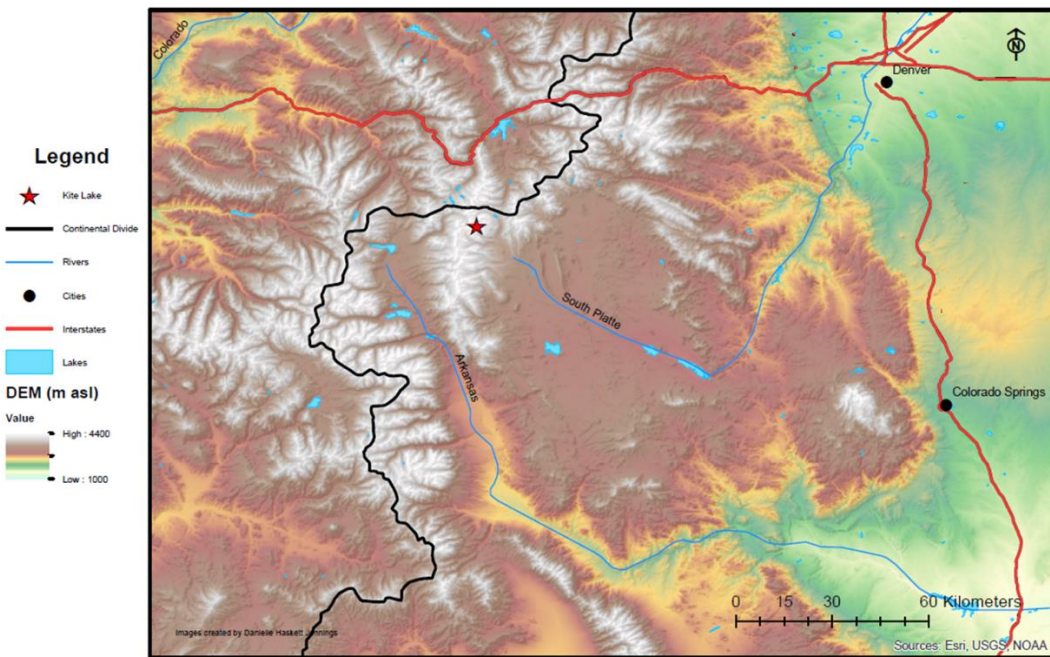


Figure 3.1c: Map of Kite Lake study site

1991). These events account for the majority of rainfall that the areas receive, particularly in higher elevations (Carrera et al., 1991). By July, the Arizona Monsoon sets up when warmer subtropical air masses form over the Gulf of California and the Gulf of Mexico. The deserts to the southwest of Colorado cause a thermal low to form, which then draws moisture-laden air up from the Gulf of California (Carrera et al., 1991). The air masses that developed over the Gulf of Mexico join them and cause enhanced circulation and heavy thunderstorms, which contribute 30-35% of the area's annual precipitation (Carrera et al., 1991). The active monsoon season creates a climate that is warm and moist. This situation allows for the expansion of forests if monsoonal activity prevails over extended periods of time. During colder periods, the monsoonal strength is limited, and therefore cooler temperatures and/or drier conditions inhibit plant growth and treeline, sub-alpine, and montane forests respond by moving downslope (Markgraff and Scott, 1981; Reasoner and Jodry, 2000). Jiménez-Moreno and Anderson (2012) describe the modern climate for Kite Lake based on climate data collected from the Western Regional Climate Center (WRCC). Annual average high and low temperatures for the Kite Lake site are 6.1°C and -7.3°C, respectively. The average summer high temperatures for June, July, and August are 16.6°C, and average winter low temperatures for December, January, and February are -16.3°C. The area receives 713 cm of snow and an annual average of 62.8 of precipitation (Jiménez-Moreno and Anderson, 2012)

The Colorado Rocky Mountains possesses a glacial history evident as diachronous changes that affected individual local environments differently (Richmond, 1960; Benedict, 1973; Benson et al., 2007). The Pinedale glaciation, which was concurrent with the last glacial maximum (LGM), occurred earlier than other environments around North America (Pierce, 2003; Leonard et al., 2017). Radiocarbon dating of organic materials collected from lake sediment support ages that range 22,000 to 25,700 years before the present before retreating to cirque basins (Rosenbaum and

Larson, 1983; Pierce 2003). Other studies have found dates that indicate a later onset of glacial retreat that began 17,000 years before present in the Mosquito Range (Ehlers et al., 2011; Leonard et al., 2017; Brugger et al., 2019) (Figure 3.1b). A small advance, known as The Satanta Peak, was concurrent with the Younger Dryas (Benedict, 1973; Benson et al., 2007). Holocene glacial advancements have primarily been restricted to cirques and were much smaller than those that moved downslope during the Pinedale Glacial (Benedict, 1973).

Elevational gradients control the vegetation located in central Colorado and broadly make up six different vertical zones: 1) the Upper Sonoran life zone found along the lowest elevations of eastern slopes. Pinyon-Juniper forests are typical and located on localized foothill communities with warmer aspects; 2) the montane forest lies below 2700 m and is composed primarily of ponderosa pine (*Pinus ponderosa*) savanna on the southern exposures. Northern slopes support Douglas fir (*Pseudotsuga menziesii*) and lodgepole pine (*Pinus contorta*) forests. Shrubland may exist on drier slopes and are dominated by communities composed of big sagebrush (*Artemisia tridentata*). 3) Aspen (*Populus tremuloides*) colonies demarcate the transition zone from montane forest to subalpine forest. 4) The subalpine zone lies between ~2700 m and ~3500 m and is characterized by spruce-fir forest with significant areas of lodgepole and limber pine (*Pinus contorta* and *Pinus flexilis*) as well as aspen; 5) the transition zone to alpine tundra is dominated by spruce-fir krummholz; 6) alpine tundra lies above ~3500 m and consists of grasses, sedges, and dwarf shrubland. The highest elevations of this region are typically free of vegetation and are comprised of bare rock, fell fields, snowbanks, and glaciers (RMNP, 2006). The vegetation surrounding Kite Lake consists of Engelmann Spruce (*Picea engelmannii*) krummholz and willow (*Salix*) (Jiménez-Moreno and Anderson, 2012).

MATERIALS AND METHODS

Two cores were collected from the approximate center of Kite Lake during the summer of 2007 (Jiménez-Moreno and Anderson, 2012). The first core (KL-07-01) was collected using a Livingstone corer and measured 830 cm in length. A second shorter core containing the uppermost flocculent sediment was also collected (KL-07-02). The purpose of this study was to assess environmental and climatic change from the transition from the Pleistocene into the Holocene; only the sediment collected from KL-07-01 was used as this core represented the oldest sediment collected.

The chronology developed by Jiménez-Moreno and Anderson (2012) was used in this study to aid in the comparison between chironomid and pollen data. Twelve AMS dates were analyzed using the remains of plant material as well as bulk sediment. Radiocarbon dates were calibrated using Calib version 5.0.2 (Jiménez-Moreno and Anderson, 2012; Stuiver et al., 1998). The median calibrated age was used for each sampled date. The chronology was then developed using linear interpolation between each adjacent date, following Jiménez-Moreno and Anderson (2012) in order to explore the relationships between chironomid communities and pollen assemblages (Figure 3.2). Please see Jiménez-Moreno and Anderson (2012) for more details regarding chronology development.

Chironomid Inference Model Development

A suite of limnological variables and corresponding chironomid counts from 153 lakes were used for the creation of a training set from the western United States (Haskett and Porinchu, 2014) and includes data from 51 lakes from the Uinta Mountains in Utah, 55 lakes from the Sierra Nevada

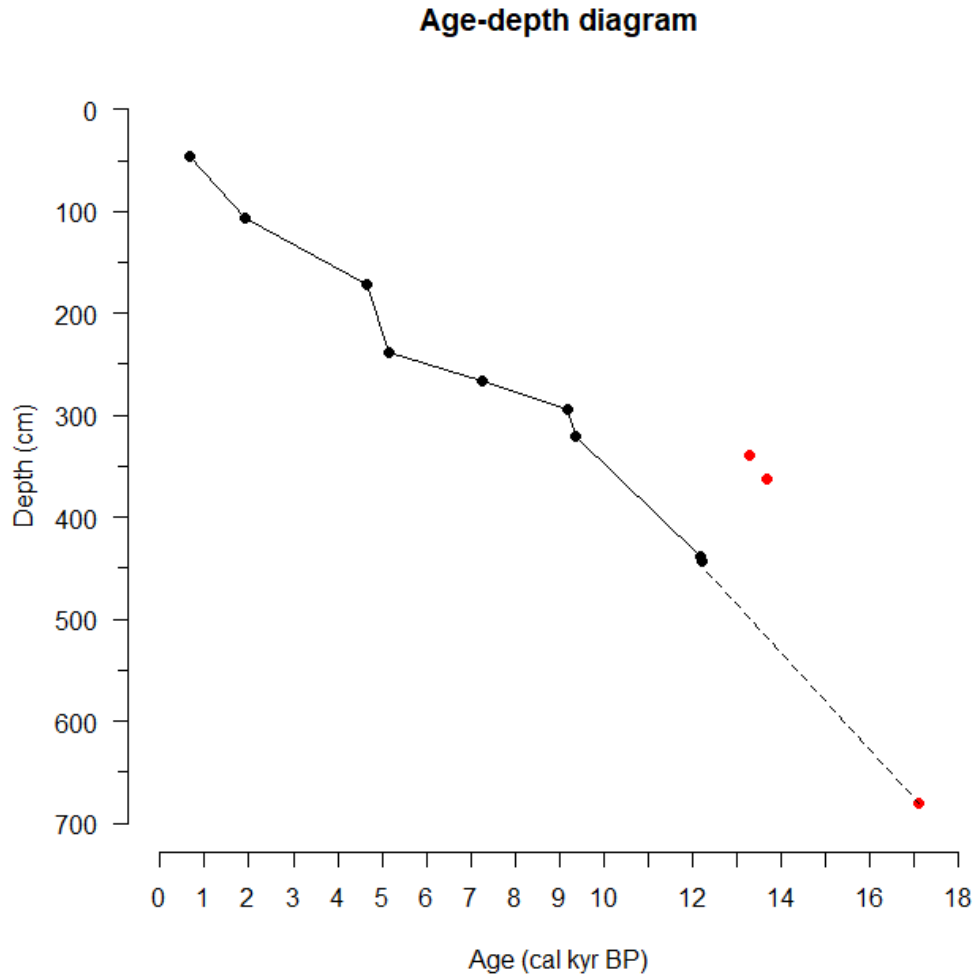


Figure 3.2: Age-depth diagram for the Kite Lake stratigraphy. The samples not used in model development are shown in red. The dashed line represents represents uncertainty between the two points as the the basal date was found to be too old. Data from Jiménez-Moreno and Anderson (2012).

in California, and 38 lakes from the Sawatch Range in Central Colorado. An additional nine lakes from the Front Range of Colorado were added (Haskett, 2020a). Dr. David Porinchu collected the lakes from California and Utah for his work in the Western United States (Porinchu et al., 2002; Porinchu et al., 2010). The lakes from CO were collected by Haskett and Porinchu (2014) and Haskett (2020). A suite of environmental variables captured by the training set represents large

gradients of natural variability with elevations lying between 2115 to 3893 m, surface water temperatures between 5.4-21.4°C, and air temperatures between 8.2-18.7°C (Appendix B.1).

Limnological variables were collected from the center of each lake. A Yellow Springs Instrument (YSI) professional probe was used to sample pH, surface water temperature in °C (SWT), dissolved oxygen (DO), and specific conductivity. A Secchi disk was used to find the depths at which the Secchi disk disappeared and reappeared, which provides a useful measure of optical transparency. The rope of the Secchi disk was demarcated at 1-meter intervals and was also used to measure maximum lake depth. Mean July air temperatures (MJAT) were extrapolated from the PRISM dataset provided by the PRISM Climate Group at Oregon State University (<http://www.prism.oregonstate.edu/>). Short sediment cores were collected from each lake using a DeGrand Corer. The uppermost 1.00 cm of sediment was processed for subfossil chironomid remains following the procedures outlined in Walker (2001). All statistical analysis was performed using the opensource platform R (Team, 2013).

Haskett and Porinchu (2014) developed a robust model for the Intermountain West (IMW) for mean July air temperature (MJAT) ($r^2_{\text{jack}}=0.61$, $\text{RMSEP}=0.97^\circ\text{C}$) that reconstructed MJAT for a site in central Colorado that spanned MIS 5 and MIS 6. In a recent study, Haskett (2020a) found that glacial meltwater influences modern chironomid communities in the Front Range of the Rocky Mountains. The study also found that SWTs and MJATs were decoupled, and SWT was the sole temperature that was statistically significant ($p=0.037$). The glacial history of the Mosquito Range (Brugger et al., 2019) combined with a bottom age of ~17,000 cal yr BP collected from Kite Lake (Jiménez-Moreno and Anderson, 2012) suggest that deglaciation initiated during the late Pleistocene for this site. Further evidence from the chironomid communities collected from Kite Lake's stratigraphy (to be discussed) suggests that glacial meltwater contributed to Kite

Lake's hydrology until ~11,000 cal yr BP (Haskett, 2020). For this reason, it was determined that SWT was the more likely environmental variable responsible for fossil chironomid distribution, and a new inference model for SWT was developed for this study, which will hereafter be referred to as the Western US (WUS) chironomid calibration set and SWT inference model. All 153 lakes were included in the creation of the model as no *a priori* details were available to determine if any lake or sample were outliers. To find outliers in training set data, some authors use an absolute residual (predicted-observed) greater than one standard deviation away from the modeled environmental variable (Jones and Juggins, 1995; Haskett and Porinchu, 2014). The author feels that this procedure inappropriately refines the model by using data that was unknown until model creation and thus provides robust performance statistics that may or may not represent reality as it artificially enhances the performance of the model. Salonen et al. (2013) studied how quantitative paleoclimatic reconstructions are impacted by calibration data set selection and found that while absolute temperatures were influenced by the training set used, the overall relative shapes of the reconstructed curve are robust. Other studies have found that that training set development does not affect transfer function development (Ginn et al., 2007)

The Rioja package (Juggins and Juggins, 2019) for the platform 'R' was used to develop the WUS chironomid-based inference model for surface water temperature (SWT). A minimum of 50 subfossil chironomid head capsules was extracted (Quinlan and Smol, 2001; Larocque, 2001) from sediment, and chironomid count data were square-root transformed to stabilize variances (Prentice, 1980). Weighted-averaging partial least squares (WA-PLS) up to five components and modern analog technique (MAT) were both used to develop chironomid-inference models for SWT (Table 3.1).

WUS Inference Model	WA-PLS		bootstrapping	n=10,000			
Components	RMSE	R2	Max Bias	RMSEP	R2	Max Bias X Val	Random t-test p-value
1*	2.5	0.47	4.34	2.8	0.38	5.52	0.001
2	2.2	0.58	4.51	2.9	0.38	6.08	0.591
3	2.1	0.63	3.54	3.1	0.35	6.65	0.977
4	2.0	0.65	3.59	3.3	0.32	7.11	0.993
5	2.0	0.67	3.43	3.5	0.30	7.29	0.999
WUS Inference Model	MAT						
Components	RMSE	R2	Max Bias	RMSEP	R2	Max Bias wm	
1*	3.5	0.18	6.86	3.5	0.18	6.86	
2	3.1	0.26	6.64	3.1	0.26	6.65	
3	3.0	0.27	7.03	3.0	0.27	6.98	
4	2.8	0.32	6.10	2.8	0.32	6.13	
5	2.8	0.33	6.52	2.8	0.33	6.49	

Table 3.1: Western United States chironomid-based inference model for surface water temperature (°C)

Weighted-averaging (WA) was not exclusively explored as the first component of WA-PLS is equivalent to WA (ter Braak et al., 1993). The model was cross-validated using bootstrapping (n=10,000). Bootstrap cross-validation is the more appropriate choice for cross-validation for more extensive training sets (Juggins and Birks, 2012). The performance of each cross-validated model was then evaluated by assessing different metrics for performance. The parameters included the 1) root mean square error of prediction (RMSEP); 2) the maximum bias, which is a measure of the maximum mean bias along the temperature gradient (ter Braak et al., 1993); 3) the correlation between the predicted SWTs and measured SWTs (r2) (Telford and Birks, 2011a); and 4) the number of components necessary for model development (Telford and Birks,

2011a). A randomization t-test of the cross-validated WA-PLS model was performed to aid in the selection of the appropriate number of components (van der Voet, 1994).

The Kite Lake chironomid-based SWT reconstruction was assessed for reliability. Reconstructions are considered to be reliable if 95% of the subfossil taxa collected from the long core are present in the modern calibration set (Birks, 1998). Correspondence analysis (CA) was used to establish the correspondence between species (species scores) and their corresponding site or location (sample scores) (Legendre and Legendre, 2012). The diagnostic statistics resulting from MAT were also useful in exploring how reliable the SWT reconstructions were. The distribution of dissimilarities based on square chord distances found the taxonomic distances from fossil assemblages to the most similar modern assemblage (Birks et al., 1990). Percentiles (5th and 10th) of the distribution of dissimilarities were used to define areas of “no close analogs” and “no-analogs,” respectively (Telford and Birks, 2011b). These analyses were performed in the R statistical package “Rioja” (Juggins and Juggins, 2019). Additional significance testing was performed by exploring whether the fossil data explained more variance than 95% from randomized reconstructions (Telford and Birks, 2011b) (Figure 3.10).

Stratigraphic chironomid analysis

Samples for chironomid extractions were taken every 2 cm throughout the core (Jiménez-Moreno and Anderson, 2012). Access to data was limited for sections 362-372 cm and 374-384 cm, and chironomid extraction was not possible for these samples.

Chironomid subfossil remains were extracted from the Kite Lake stratigraphy following methods found in Walker et al. (1991). Sediment was heated in an 8% potassium hydroxide (KOH) solution at 35°C until the sediment disaggregated. The remaining material was then rinsed with distilled water over a 95µm sieve to collect residual matter. Chironomid head capsules were removed from the solution using fine forceps under a stereomicroscope and permanently mounted on microscopic slides. A minimum of 50 identifiable head capsules was collected to satisfy statistical limits before moving to the next sample (Larocque et al., 2001). Several taxonomic keys were used to aid in the identification of extracted chironomids and include Brooks et al., (2007), Andersen et al., (2013), and Chiro Key (2020). Subfossil chironomid relative abundance data were square-root transformed and taxa were removed if they were present in less than two lakes and possessed 2% of the relative abundance of the sample. This deletion limits the influence of rare taxa on the SWT reconstruction (Quinlan and Smol, 2001).

The Rioja (Juggins and Juggins, 2019) and Vegan (Oksanen et al., 2013) R packages were used to identify naturally occurring zones in subfossil chironomid communities by using constrained hierarchical cluster analysis (Bennett, 1996; Birks, 2012a). The Vegan package (Oksanen et al., 2013) was used to analyze detrended correspondence analysis (DCA), a form of indirect gradient analysis. DCA is used to quantify faunal turnover (Smol and Douglas, 2007; Legendre and Birks, 2012a), represents a measure of “episodes of synchronous appearance and disappearance of species from a community” (Badgley and Gingerich, 1988). The rapid compositional change associated with faunal turnover often represents significant fluctuations in environmental conditions (Battarbee, 2000; Smol and Douglas, 2007). The changepoint analysis was performed on the results of the DCA to detect where changes occurred in the stratigraphy (Killick et al., 2012; Haynes et al., 2016). The package “changepoint.np” was used to locate these

areas of change (Haynes et al., 2017). Indicator species are organisms that reflect specific environmental conditions based on their abundance, presence, and/or absence in an assemblage (McDonough et al., 2012). Multi-level pattern analysis was implemented in the R package ‘indicspecies’ (De Cáceres and Jansen, 2019).

RESULTS

Modern Chironomid Assemblages

An additional nine lakes were collected from the Front Range of Colorado and added to the 144 existing training set lakes established by Porinchu et al. (2010) and Haskett and Porinchu (2014) (Figure 3.3). The addition of these lakes added new information regarding the distribution of the subfamily Diamesinae. Three species from this subfamily were added to the training set and included *Diamesa* spp., *Pseudodiamesa*, and *Protanypus*. Diamesinae is known for chironomid taxa that are cold stenotherms and have been well-documented in Southern Alps alpine streams where they are affiliated with glacial meltwater (Lencioni, 2018). However, they are poorly understood and underrepresented in lake sediment (Pinder, 1986; Walker, 1993; Brooks et al., 2007). A recent study (Haskett, *in prep*) found that this relatively obscure subfamily are present in lakes that are currently receiving glacial meltwater.

Diamesa was present in two additional lakes (MLA-CO and SVL-CA) in the training set. Silver Lake (SVL) (37.78, -119.12) is located in the Sierra Nevada in CA and lies directly south of Mono Lake. Upon closer examination using data from Fountain et al., (2007), two small and unnamed glacial bodies feed Silver Lake from the west. Maroon Lake-adjacent (MLA) (39.40, -106.52) is located in the Sawatch Range of the Colorado Rocky Mountains. No apparent ice bodies were evident using the data set from Fountain et al. (2007). After using Google Earth to explore the area, the lobe of a distinct rock glacier (Stumm et al., 2015) is reaching into the lake basin,

which could account for the presence of *Diamesa* in the chironomid assemblage collected from the basin. These findings further substantiate the relationship between glacial retreat and the presence of Diamesinae in lake sediment.

After assessing performance statistics, WA (or the first component from the WA-PLS model) was found to be the most robust model with an RMSEP=2.74°C and $r^2_{boot} = 0.38$ (Figure 3.4a). Kite lake has experienced significant changes in its history over time, which began with deglaciation from LGM, or the Pinedale Glaciation, and thus all 153 lakes were included to capture as much natural variability as possible. The performance of the new WUS inference model is not as robust as previous inference models of MJAT in the Intermountain West (Porinchu et al., 2010; Haskett and Porinchu, 2014). The presence of taxa from the subfamily Diamesinae downcore in the Kite Lake stratigraphy indicated that glacial retreat was present in the catchment. Thus, SWT was the more appropriate temperature to model.

Kite Lake Midge Stratigraphy

Constrained hierarchical cluster analysis indicates that three zones exist in the chironomid subfossil assemblage data (Figure 3.5). Kite Lake Zone 1 (KLZ1) represents the most recent sediment analyzed for chironomid remains (Figure 3.6). Cluster analysis indicates that this zone is comprised of sediment collected from 300 – 344 cm with ages ranging from 9,236 – 10,033 cal yr BP. Kite Lake Zone 2 (KLZ2) ranges from 344-418 cm in the stratigraphic record. This sediment corresponds to ~10,033 to 11,901 cal yr BP. The deepest sediment included in this analysis represents Kite Lake Zone 3 (KLZ3). KLZ3 makes up sediment from 428-466 cm and includes ages that range from 11,901 to 12,659 cal yr BP. The sediment of this entire section is composed of laminated clays that are light gray (Jiménez-Moreno and Anderson, 2012).

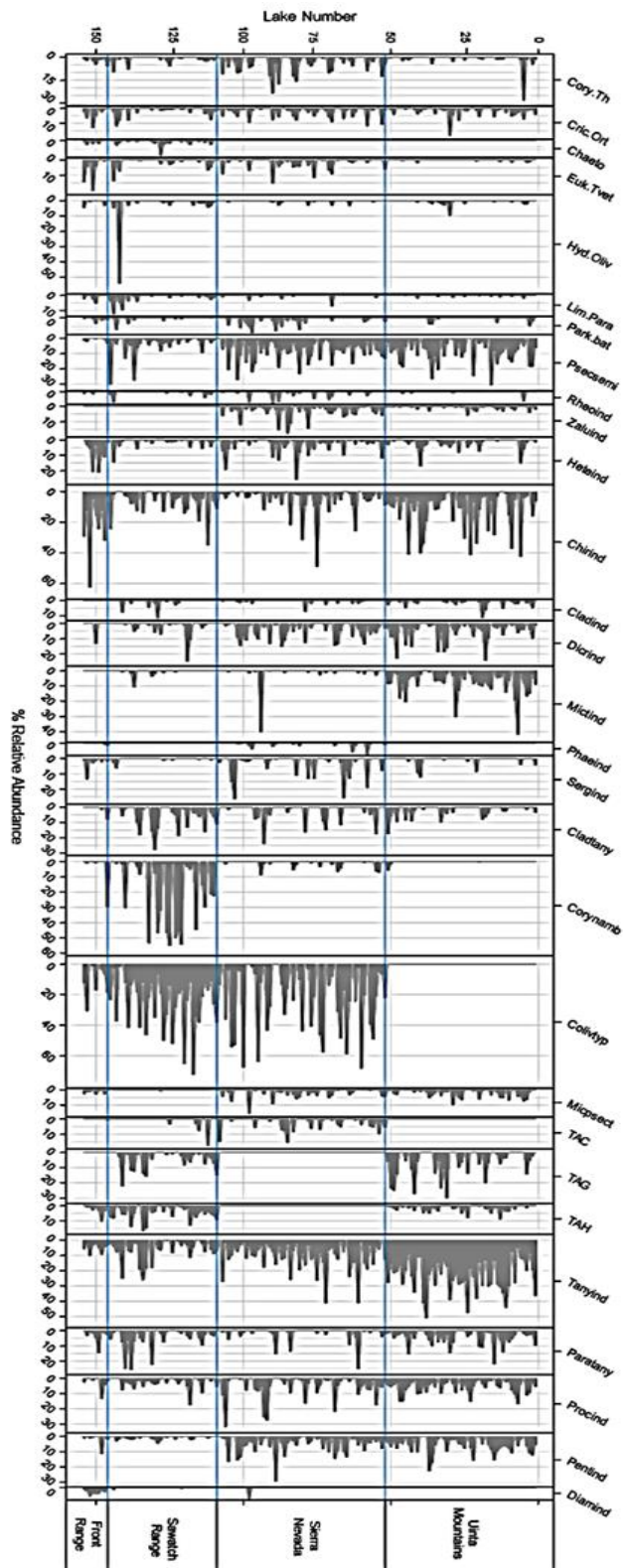


Figure 3.3: Relative abundance curve of the Western United States training set (Cory.Th = *Corynoneura/Thienemanniella*; Cric.Ort = *Cricotopus/Orthocladius*; Chaeto = *Chaetocladius*; Euk.Tvet = *Eukiefferiella/Tvetenia* ; Hyd.Oliv = *Hydrobaenus/Oliveridia*; Lim.Para = *Limnophyes/Paralimnophyes*; Park.bat = *Parakiefferiella bathophila*-type; Psecsemi = *Psectrocladius sordidellus*-type; Rheoind = *Rheocricotopus*; Zaluind = *Zalutschia*; Heteind = *Heterotrissocladius* ; Chirind = *Chironomus* ; Cladind= *Cladopelma*; Dicrind = *Dicrotendipes*; Micrind = *Microtendipes*; Phaenind = *Phaenopsectra*; Sergind = *Sergentia*; Cladtany = *Cladotanytarsus*; Corynamb = *Cornocera ambigua*-type; Colivtyp = *Corynocera oliveri*-type; Micpsect = *Micropsectra*; TAC = *Tanytarsus type C*; TAG = *Tanytarsus type G*; TAH = *Tanytarsus type H*; Tanyind = *Tanytarsus indeterminable* ; Paratany = *Paratanytarsus*; Procind = *Procladius*; Penind = *Pentaneurini*; Diamind = *Diamesa*).

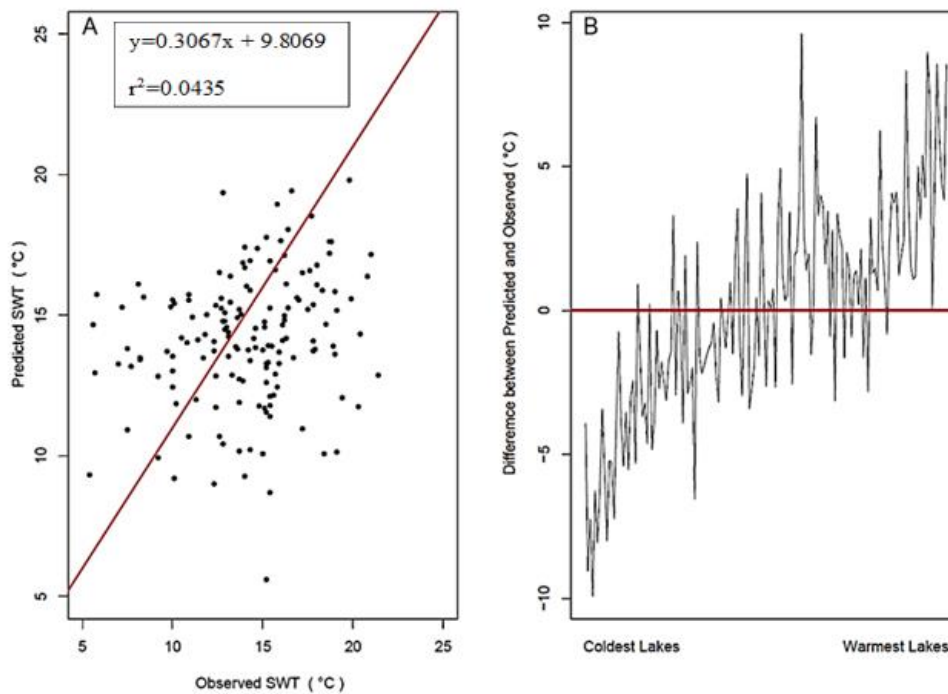


Figure 3.4: A) Relationship between recorded surface water temperatures and midge-based predicted surface water temperatures. The red line represents the 1:1 relationship; B) The difference between observed and predicted surface water temperatures (°C).

KLZ3 (466-428 cm; 12,659 - 11,901 cal yr BP): Younger Dryas

The deepest and oldest sections sampled for analysis contained no subfossil chironomid remains. The lack of head capsules did not satisfy the minimum 50 head capsule requirement and could not be analyzed.

KLZ2 (428-344 cm; 11,901 - 10,033 cal yr BP): Transition into the Holocene

Overall, the species richness (min=1; max=14; avg=8.4) sharply increases with the onset of KLZ2 and decreases by 11,500 cal yr BP. Sharp peaks exist in head capsule concentration (# head

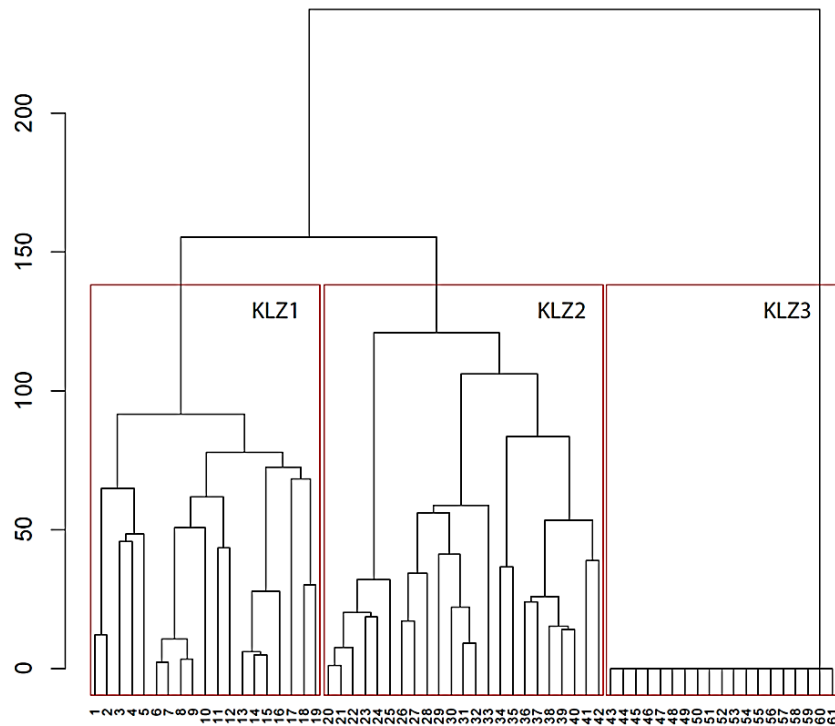


Figure 3.5: Derived chironomid zones based on constrained hierarchical cluster analysis

capsules/mL), richness, and SWT (4.7°C) at 11,293 cal yr BP (Figure 3.7). These observations coincide with a changepoint in DCA, which indicates that faunal turnover changed significantly at this time. Once SWTs increased at 11,293 cal yr BP, temperatures fluctuated around an average of 9.8°C. This trend is warmer than the midge-based SWT reconstructions before the changepoint. This period was characterized by cooler SWTs that averaged 8.2°C. Chironomid concentrations decreased to 2.5/mL at 372cm (10,577 cal yr BP), and analysis could not be performed for this section of the Kite Lake record. A second large peak in concentration (n=245.5) and richness occur with the onset of KLZ1 that corresponds with an increase in SWT to 11.8°C. Multi-level pattern analysis only found one indicator value that was statistically significant ($r=0.645$, $p=0.002$). This

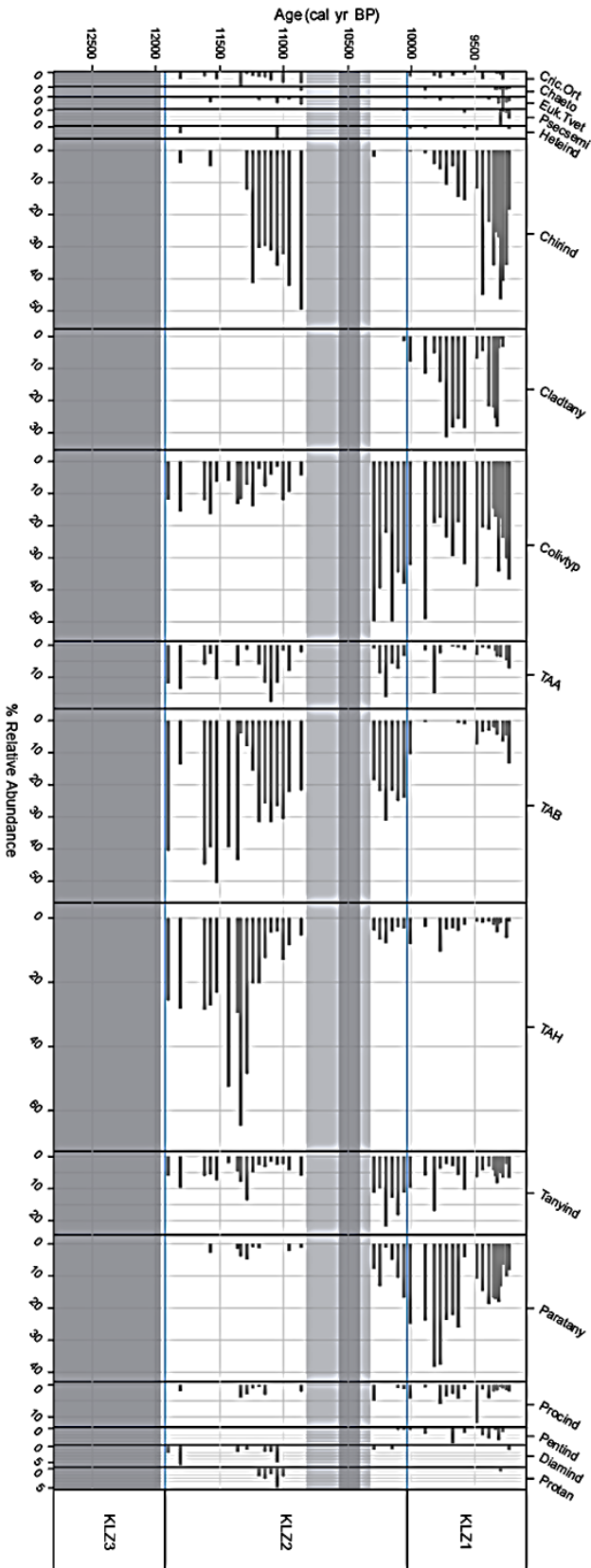


Figure 3.6: The Kite Lake relative abundance curve. Dark gray boxes indicate zones with no chironomid remains. Light gray boxes indicate no access to samples for analysis. (Cric.Ort = *Cricotopus/Orthocladius*; Chaeto = *Chaetocladius*; Euk.Tvet = *Eukiefferiella/Tvetenia*; Psecsemi = *Psectrocladius sordidellus*-type; Heteind = *Heterotrissocladius*; Chirind = *Chironomus*; Cladtany = *Cladotanytarsus*; Colivtyp = *Corynocera oliveri*-type; TAA = *Tanytarsus* type A; TAB = *Tanytarsus* type B; TAH = *Tanytarsus* type H; Tanyind = *Tanytarsus* indeterminable; Paratany = *Paratanytarsus*; Procind = *Procladius*; Pentind = *Pentaneurini*; Diamind = *Diamesa*; Protan = *Protanypus*).

value corresponds to the appearance of *Diamesa* at 11,900 cal yr Bp. Subfossil chironomid head capsules are not present in the sediment that corresponds to 10,150 cal yr BP. Sediment for chironomid extraction were not available for samples 384-374 cm (10,813-10,624 cal yr BP) and 372-32 cm (10,530-10,340 cal yr BP).

KLZ1 (344 – 300 cm; 10,033 - 9,236 cal yr BP): Stable Early Holocene

The most recent sediment analyzed for chironomid data suggests that the environment surrounding the Kite Lake basin stabilized during KLZ1. Concentrations declined during this zone overall (9.2-129.8; avg=62.3). However, richness became increasingly higher (min=7, max=15, avg=11.1) and peaks at the termination of the record at 9240 cal yr BP. Midge-based SWTs were also the highest and fluctuated around a stable average SWT of 12.5°C. The chironomid taxa that

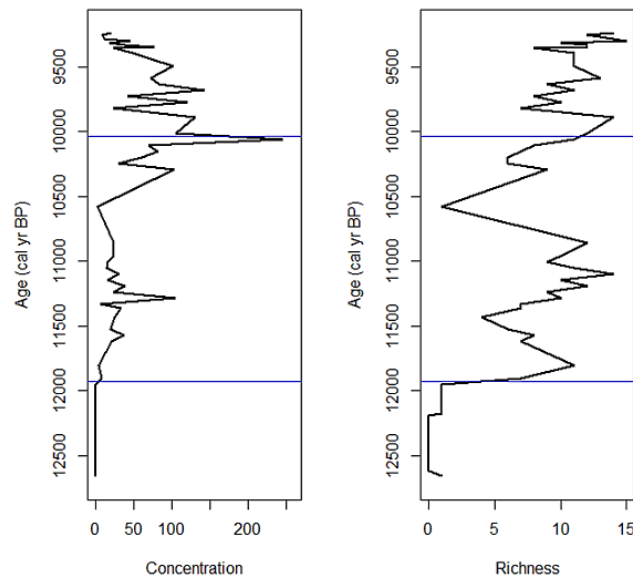


Figure 3.7: Concentration and richness curves derived from subfossil chironomid assemblages present in Kite Lake.

dominate the assemblage in this zone provide additional qualitative evidence of climatic amelioration during KLZ1. The chironomid assemblage is more diverse than any other zone and is dominated by *Chironomus* (46%), *Cladotanytarsus* (28%), *Paratanytarsus* (38%), and *Procladius* (12%). These taxa are affiliated with warm and productive conditions (Brooks et al., 2007; Andersen et al., 2013). Indicator species analysis found four statistically significant species. They are *Cladotanytarsus* ($r=0.965$, $p=0.001$), *Pentaneurini* ($r=0.680$, $p=0.001$), *Chaetocladius* ($r=0.525$, $p=0.023$), and *Corynocera ambigua*-type ($r=0.471$, $p=0.036$) (not shown). Both *Chaetocladius* and *C. ambigua* (not pictured) appear at the same time at ~9340 cal yr BP and are present through the upper extent of KLZ1. *Cladotanytarsus* and *Pentaneurini* both appear at the same time as well and appear at 10,050 cal yr BP.

Kite Lake SWT Reconstruction and Reliability

The chironomid-based SWT model for Kite Lake ranges from 7.2°C to 13.4°C. The sample-specific error estimates for each SWT estimate varied between 2.7°C and 3.0°C and are shown in Figure 3.8a. It is of note that a plot of observed SWT versus midge-inferred SWT indicates that the midge-based MJAT model appears to underestimate inferred temperatures at the low end and overestimate temperatures at the high end of the captured temperature range (Figure 3.4b).

All subfossil taxa are present in the training set, which indicates that the modern training set represents the subfossil chironomid assemblages. This finding is further substantiated by passively plotting subfossil taxa in ordination space over the training set ordination (Figure 3.9). The distribution of dissimilarities based on square chord distances derived from MAT suggests that the oldest samples before the changepoint at 11,293 cal yr BP possess no modern analog, and

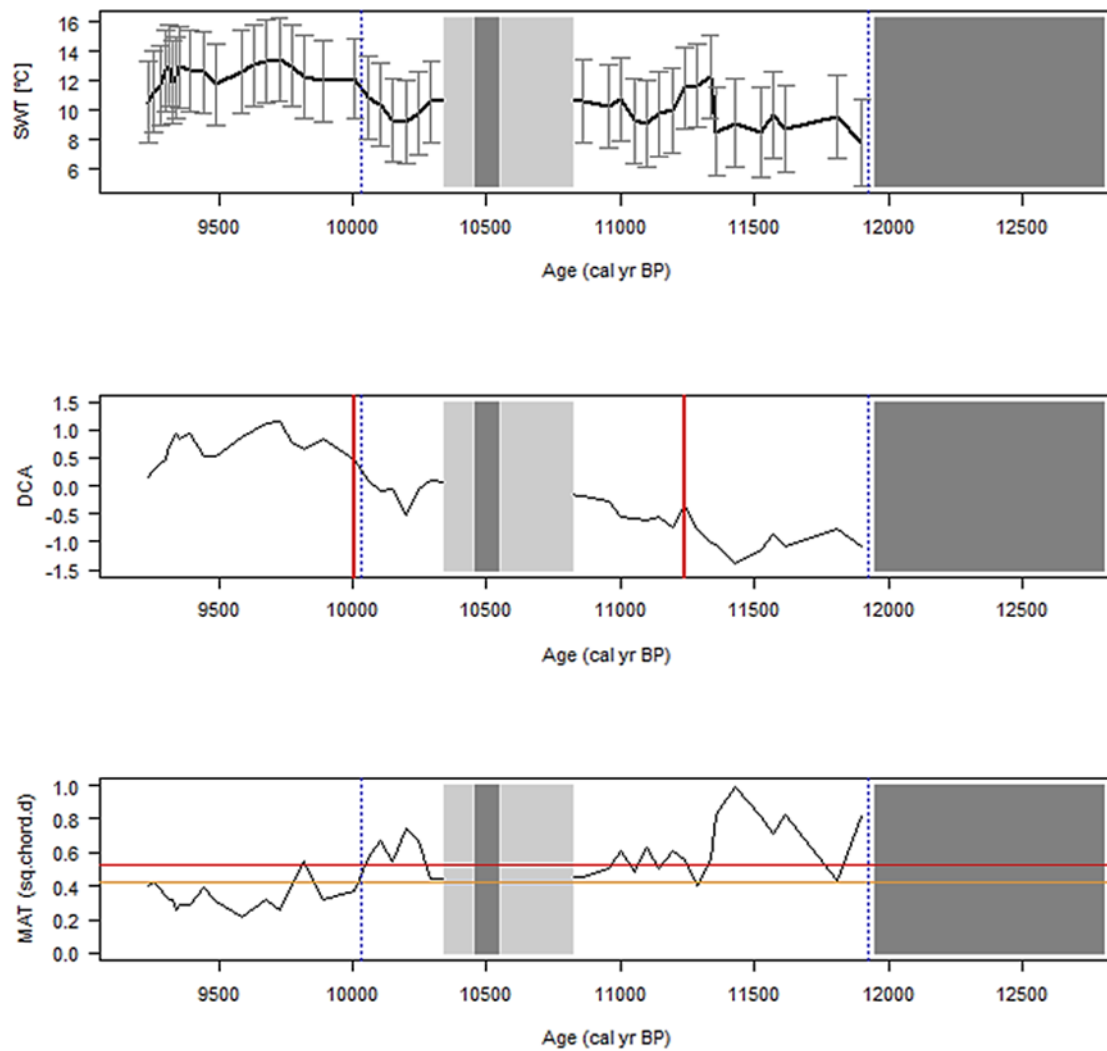


Figure 3.8: A) Chironomid-inferred surface water temperature reconstructions (thick black line) for Kite Lake stratigraphy plotted with sample specific error (gray lines with error bars) for chironomid zones; B) DCA axis 1 scores plotted with identified changepoints (red line) ; C) Squared chord dissimilarity distance (sq.chord.d) to nearest modern analog (MAT) from the WUS training set (orange line = 5th percentile, red line = 10th percentile).

no good fit exists in the modern training set. The samples from 11,293 to 10,033 cal yr BP are represented in the training set, but interpretation should be made with caution. KLZ1 is robust and mostly above the 0.05% cut off, suggesting good modern analogs exist. Significance testing indicates that the model is not statistically significant when compared to random variables (SWT = 0.40 variance explained, $p=0.214$) (Figure 3.10). Telford and Birks (2011b) suggest that if the environmental variable “is of uncertain ecological significance,” that results may not be statistically significant. This finding is expected due to the sensitivity of chironomids to environmental change. The successional changes that chironomid communities undergo in response to deglaciation certainly satisfy an unknown response that has not been established by prior research. These relationships require further examination to fully understand the extent to which chironomid communities are affected by these environmental mechanisms. Overall, the application and interpretation of the WUS midge-based SWT reconstruction should be analyzed with caution.

DISCUSSION

The subfossil chironomid stratigraphy developed for Kite Lake provides a record of environmental change for Central Colorado between 12,659 and 9,236 cal yr BP, a time that captures the climatic amelioration associated with the transition from the Pleistocene into the Holocene (Figure 3.8a). Changepoints evident in DCA located two discrete points in time that chironomid communities experienced faunal turnover (Figure 3.8b). The first interval is characterized by a shift in chironomid communities from an assemblage dominated by cold stenotherms associated with postglacial succession (*Tanytarsus*, *Diamesa*, *Protanypus*) (Saulnier-Talbot and Pienitz, 2010) to one composed primarily of *Chironomus*. The sudden appearance of *Chironomus* would suggest that a climatic amelioration occurred at ~11, 293 cal yr BP as this

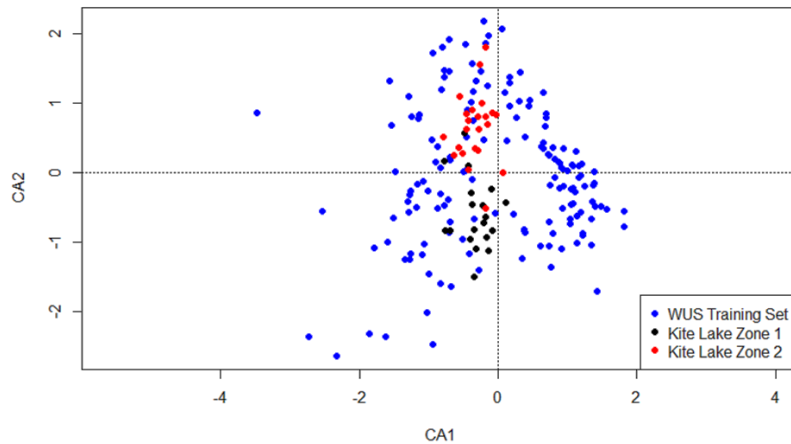


Figure 3.9: Passive plotting of fossil assemblages against the training set assemblage in correspondence analysis ordination space

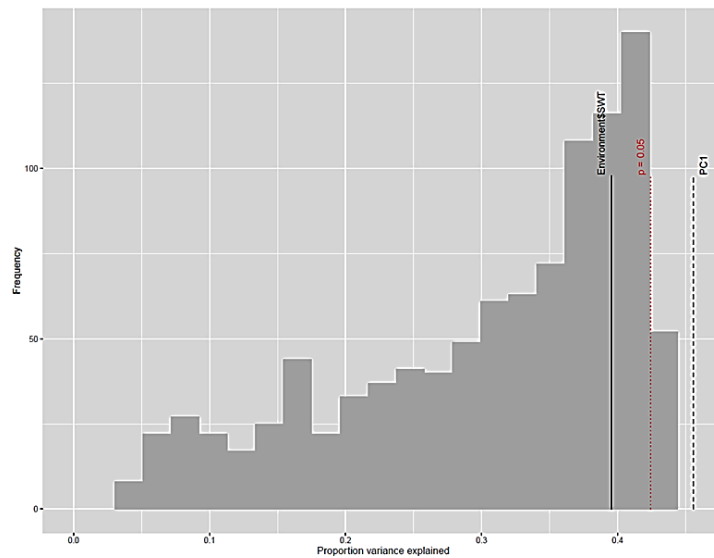


Figure 3.10: Significance test of the proportion of variance that surface water temperature explains. The proportion of variance that surface water temperature explains (black solid line, $n=999$, $p=0.214$) is found in the highest histograms that explains variance explained by random data. The red dashed line indicates the 95th confidence interval and the black, thick dashed line indicates the proportion explained by PCA1 (0.446).

taxon is often an early colonizer for lakes transitioning to a more productive environment (Brooks et al., 1997; Haskett, 2020). The most substantial increase of 4.7°C in the midge-based SWT reconstruction occurred at ~11,334 cal yr BP and provides further evidence of warming during this time. The absence of chironomid head capsules ~ 10,580 cal yr BP could reflect a period of stable cooling and glacier expansion. This hypothesis corresponds with evidence that glacial expansion and stable cooling occurred in the Front Range of Colorado between $11,010 \pm 120$ and $9,523 \pm 155$ cal yr BP (Menounos and Reasoner, 1997; Muhs et al., 1999). This period of cooling has been recognized in other studies and has been attributed to the Younger Dryas chron (Menounos and Reasoner, 1997; Muhs et al., 1999).

Corynocera oliveri was present during this entire interval but steadily increased in relative abundance over time. The presence of *Corynocer oliveri* and *Corynocera ambigua* have been linked to the location of the treeline (Porinchu and Cwynar, 2000). *C. oliveri* is primarily found in lakes basins that are found in tundra and lie above treeline. *C. ambigua* is not known to exist for extended periods (Brooks et al., 2007), and its presence may be used to assess the relocation of treeline (Porinchu and Cwynar, 2000). While the reconstructed SWTs for this zone fluctuate around an average of 12.5°C, the temperature does decrease at the uppermost sections that correspond with the arrival of *C. ambigua* and *Chaetocladius* around ~9340 cal yr BP. Thus, treeline appeared roughly at this time. This evidence substantiates the downslope displacement of subalpine vegetation several hundred meters during the Younger Dryas (Fall, 1997; Reasoner and Jodry, 2000). However, this finding contradicts Jiménez-Moreno and Anderson's (2012) evidence that a subalpine forest composed of *Picea*, *Abies*, and *Pinus aristate* surrounded Kite Lake by 12,200 cal yr. BP, suggesting that the treeline was much higher than its location today.

The second change point date coincides with the transition from KLZ2 to KLZ1 at 10,033 cal yr BP. The chironomid assemblage transitions from a community primarily composed of *Tanytarsus* and *C. oliveri*, to an assemblage dominated by *Cladotanytarsus*, *Paratanytarsus*, and *Procladius*. This shift is indicative of a change from cold, oligotrophic conditions to a warmer and more productive environment (Brooks et al., 2007; Andersen et al., 2013). Saulnier-Talbot and Pienitz (2010) found a very similar postglacial chironomid assemblage in the northernmost Ungava region of Nunavik, Canada. They concluded that the chironomid communities present at their site were explained by postglacial succession.

Very little research has explored successional trends in chironomid communities. Early work found that succession due to anthropogenic eutrophication was related to the availability of food materials (Warwick (1975; 1978; Saether, 1979). Walker and Mathewes (1990) initially explored chironomid postglacial succession and found cold stenotherms (*Heterotrissocladius*, *Parakiefferiella*, *Protanypus*, *Stictochironomus*, and *Pseudodiamesa*) were collected from sediment that corresponded with the timing of glacial retreat. While the authors caution that multiple environmental factors may contribute to the distribution of chironomids, including lake depth, links to terrestrial vegetation, climate, and lake trophic state, their seminal work established the work of quantitative midge studies. This debate continues today (Velle et al., 2010; Brooks et al., 2010; Velle et al., 2012; Eggermont and Heiri, 2012) and the modern exploration of chironomid ecology may help to address these questions and concerns.

The lack of recoverable chironomid head capsules for the entirety of KLZ3, as well as the sample corresponding to a depth of 372-374 cm (10,577 cal yr BP), is notable as chironomids are typically ubiquitous and present in large enough numbers for statistical analysis in lakes (Porinchu and MacDonald, 2003). Two long chironomid records have been developed on millennial

timescales representing time going back to ~140 ka and ~200 ka respectively (Axford et al., 2011; Haskett and Porinchu, 2014.) Both records possessed large sections of their respective cores that contained no recoverable head capsules that were explained by the presence of extensive ice cover that did not allow for the deposition of subfossil chironomids. The absence at ~10,577 cal yr BP in our record corresponds with considerable peaks in magnetic susceptibility (Jiménez-Moreno and Anderson, 2012). High sedimentation rates may have impeded larval chironomid survival.

CONCLUSION

The Kite Lake stratigraphy contains subfossil chironomid communities that are comprised of environmental specialists that suggest that chironomid communities experience postglacial succession. These conditions consist of; 1) the lack of recoverable chironomid head capsules indicates the presence of extensive ice cover into the growing season related to the advancement of glacial conditions. The presence of pollen indicates that passive deposition was possible during this time. However, chironomid egg masses may not have survived extensive ice cover. 2) the transitional period of glacial retreat is comprised of a *Tanytarsini*-rich assemblage and possess taxa from the subfamily Diamesinae. 3) early colonization occurs with the appearance of *Chironomus*. 4) *C. oliveri* represents an environment that exists in cold tundra conditions above treeline. 5) the appearance *C. ambiguus* demarcates the location of treeline. More research is needed from modern environments experiencing glacial retreat to build modern ecological foundations for this phenomenon in paleoenvironmental interpretations.

Future research is needed to establish mechanisms driving egg mass survival rates for lakes that experience prolonged periods of ice cover. The presence of pollen (Jiménez-Moreno and Anderson, 2012) in KLZ3 suggests that passive deposition was possible. Thus, Kite Lake experienced short periods of melting ice during the summer growing season, but timing and/or the

extent of ice cover inhibited the survival of chironomid egg masses during this period could be one explanation that could explain the absence of chironomid head capsules in KLZ3.

CHAPTER 4

WHICH LAKES SHOULD BE SAMPLED FOR PAELOENVIRONMENTAL CHIRONOMID WORK? A CASE STUDY APPROACH TO DETERMINE STUDY SITE SELECTION FOR PALEOCLIMATE RESEARCH³

³ Haskett, D.R. To be submitted to *Palaeogeography, Paleoclimatology, Palaeoecology*.

ABSTRACT

Chironomids are used to develop temperature reconstructions for mean July air temperature (MJAT) and surface water temperature (SWT) for the 20th and 21st centuries for six alpine lakes in Rocky Mountain National Park, Colorado. These results were compared to extrapolated mean July air temperatures from the PRISM dataset. Glacial meltwater decouples the signal between air temperature and water temperature and was evident between the relationships between the predicted MJAT and SWT for lakes receiving meltwater from glaciers or perennial snowfields. Periods of glacial retreat, or warming temperatures, occurred during the earliest part of the century to the mid-1950s and from the mid-1990s to present. Glaciers stabilized or expanded during the cooler period from the mid-1950s to the mid-1970s. Within-lake variability may account for discrepancies evident between site locations in downcore interpretation. These findings may provide a new method for chironomid interpretation. Overall, the deviations plotted from average SWTs performed better at predicting warming and cooling trends than the midge-based predicted values for MJAT and SWT. Study site selection is crucial for midge-based thermal reconstructions and basins that receive, or have received, meltwater should be avoided if modeling MJAT.

Keywords: Chironomid, Paleoenvironmental Reconstruction, Colorado, Glacial Meltwater, Study Site Selection, Instrumental Data, Centennial Time Scale

INTRODUCTION

The relationship between the chironomid family (Insecta: Diptera: Chironomidae) and their environment has been well established since the early work of Thienemann, which recognized the usefulness of using chironomid taxa as indicators for trophic level classification at the beginning of the 20th century (Porinchu and MacDonald, 2003). This logic expanded to how chironomid assemblages relate to temperature by recognizing that assemblages were composed of cold stenotherms or thermophilous taxa that corresponded with colder or warmer lakes respectively (Brundin, 1949; Porinchu and MacDonald, 2003). Andersen (1938) was the first to use chironomids to qualitatively describe the changes in climate during the Late Pleistocene in Europe (Walker, 1987). By the late 1980s, Walker and Mathewes (1987) hypothesized that climate (i.e., temperature) was the main driver for the distribution of chironomid communities. Walker et al. (1991) extended this work and created the first quantitative reconstruction of surface water temperature in Canada. It wasn't long after this seminal paper was published that chironomid workers began to model air temperatures (Lotter et al., 1997) with the justification that air temperature models have more robust statistics (Velle et al., 2010). Also, a strong correlation often exists between air temperature and surface water temperature that is strongly statistically significant (Lotter et al., 1997; Livingstone and Lotter, 1998; Velle et al., 2005). In the decades since these initial studies were published, chironomid thermal reconstructions cover multiple time scales that range from exploring historical data (Reinemann et al., 2014) to the changes that occurred over glacial-interglacial cycles (Axford et al., 2011; Haskett and Porinchu, 2014) and cover a geographic range that encompasses the entire globe (Rees et al., 2008; Eggermont et al., 2010; Heiri et al., 2011; Haskett and Porinchu, 2014; Wu et al., 2015; Zhang et al., 2017). Nicacio et al. (2015) performed a scientometric analysis of chironomid papers published between 1992 to

2012 and found that trends in bioassessment publications regarding chironomids grew steadily over the period that was studied. Paleolimnology (25%) and lake studies (33%) accounted for a vast majority of publications over the last three decades. They were only surpassed by diversity studies (35%) and studies focusing on rivers and streams (43%).

Multiple paleoecological studies indicate the power of chironomid paleoreconstructions that quantitatively model broad-scale climatic changes that are in agreement with multi-proxy approaches, such as data derived from ice cores from Greenland and Antarctica (Brooks and Birks, 2000; Velle et al., 2010; Axford et al., 2011). And yet other chironomid studies have reported variable results even between geographically close sites (Caseldine et al., 2003; Kurek et al., 2004; Velle et al., 2005; Reinemann et al., 2014) This disagreement has been evident in vigorous debate regarding the usefulness of chironomids as a proxy solely for temperature for over three decades (Walker and Mathewes, 1987; Warner and Hann, 1987; Walker and Mathewes, 1991; Velle et al., 2010, Brooks et al., 2012; Eggermont and Heiri, 2012; Velle et al., 2012a). Many critics of the method point to other environmental factors that may impact the distribution of chironomids including changes in natural (Brodersen and Lindegaard, 1999; Brooks and Birks, 2001) and anthropogenic (Haskett, 2020) trophic levels due to nutrient loading (Langdon et al., 2010; Garzke et al., 2019), lake depth (Kurek and Cwynar, 2009; Velle et al., 2012b), oxygen levels (Little and Smol, 2001; Verbruggen et al., 2011), aquatic vegetation (Langdon et al., 2010), and glacial retreat (Eggermont and Heiri, 2012; Haskett, 2020). The strength of temperature in previous research as the main driver for chironomid distribution may be due to statistical methods that artificially enhance the robustness of inference models. This is accomplished by the development of training sets that artificially improve the signal of air temperature by selectively sampling along an environmental gradient that enhances the air temperature signal (Birks, 1995; Birks, 1998; Velle

et al., 2010). Recent trends in chironomid work have been combining small regional training sets to create training sets that cover large geographical areas. These expanded training sets indicate that the relationship between midge communities and air temperature are statistically stronger and capture more variability in chironomid assemblages that limit the “no modern analog” problem for fossil communities downcore (Fortin et al., 2015; Kotrys et al., 2020; Porinchu et al., 2017).

In order to refine paleoenvironmental interpretations, it is imperative to expand our understanding of the modern relationships between chironomids and the many variables that may influence their distribution. Velle et al., (2010) suggest that conducting studies that compare midge-inferred temperatures to instrumental data may help to refine interpretations downcore with the logic that chironomid assemblages that accurately assess recent temperature change may provide more robust temperature reconstructions from the same lake over more extended periods. Surprisingly, only very few researchers have accepted this invitation (Battarbee et al., 2002; Larocque and Hall, 2003; Larocque et al., 2009; Reinemann et al., 2014; Larocque-Tobler et al., 2015; Luoto and Ojala, 2017). Studies that compare instrumental data to temperatures derived from chironomid communities may also help to address which temperature models (air vs. water) are more appropriate when these two variables no longer covary; i.e., when glacial meltwater cools lake water during elevated air temperatures as hypothesized by Velle et al. (2010) and Eggermont and Heiri (2012). A recent study validated these hypotheses and found that chironomid communities are responding to surface water temperature rather than the air temperature in regions where glaciers are retreating (Haskett, 2020). These relationships may have implications for the interpretation of downcore reconstructions as the remote lakes often studied for climate change are often formed during glacial retreat in alpine or high latitude environments. Depending on the periods of study, chironomid communities may be impacted by glacial meltwater and

interpretations of climate change based on models for midge-based air temperatures may be incorrect and lead to erroneous findings.

This paper builds on the findings from Haskett (2020) and follows the advice of Velle et al. (2010). Because glacial retreat alters temperature regimes for alpine lakes, this study examined both air and water temperatures derived from chironomid inference models and compared them to regional air temperatures collected from instrumental data for six lakes in an area receiving glacial meltwater during the 20th and 21st centuries. To the author's knowledge, no previous study has explored the differences and the similarities between reconstructions of surface water temperature and air temperature explicitly. These models are then applied to chironomid communities extracted from the stratigraphy of a long core that spans the Pleistocene-Holocene transition with a known alpine glacial history as a proof-of-concept for the findings found during the historical timescale presented in this paper.

STUDY AREA AND METHODS

Study Area

Short sediment cores were collected from six alpine lakes during the late summers of 2015 and 2016 (Table 4.1). All lakes are located along the eastern margin of the Continental Divide in Rocky Mountain National Park, which is located in the Front Range of the Rocky Mountains, Colorado (Figure 4.1). Lakes were paired to elucidate the influence of glacial meltwater on chironomid communities. All pairs are similar in elevation, vegetation, and geology with the only different variable being meltwater input. Cony Lake (3509m asl) and Pipit Lake (3479m asl) lie adjacent to the continental divide and are present in rocky cirques with no vegetation. An unnamed glacier lies directly above Cony Lake. Perennial snowfields were present in the catchment immediately surrounding Pipit Lake during sampling in August, 2015. Eagle (3298 m) and Box

Variables	Cony Lake (CNY)	Pipit Lake (PIP)	Eagle Lake (EGL)	Box Lake (BOX)	Black Lake (BLK)	Thunder Lake (THD)
Elevation (m)	3509	3479	3298	3274	3237	3225
Latitude (dd)	40.173	40.193	40.211	40.213	40.265	40.222
Longitude (dd)	-105.658	-105.669	-105.652	-105.649	-105.641	-105.647
Environment	Rocky Cirque	Rocky Cirque	Timberline	Timberline	Subalpine Forest	Subalpine Forest
Meltwater input type	Glacial	Snow	Glacial	Snow	Glacial	Snow
Fish	no	no	yes	yes	yes	yes
Lake depth (m)	16.8	10.4	10.15	11	21.2	7.05
Surface water temp. (°C)	8.2	9.2	10.9	13.9	10.9	13.1
Mean July air temp. (°C)	11.2	9.6	10.1	10.3	11.4	11.9
pH	7.3	8.61	7.3	7.17	8.23	8.76

Table 4.1: Environmental variables for the six sampled alpine lakes.

(3274 m asl) Lakes were found at timberline with fir, Engleman spruce (*Picea engelmannii*) and willow shrub (*Salix* spp.) present in each catchment. Eagle Lake currently receives glacial meltwater. Black Lake (3237m asl) is fed by meltwater emanating from Moomaw Glacier and is the deepest lake sampled with a depth of 21.2m. Thunder Lake (3225m asl) is the pair to Black Lake, is 7.05m deep, and receives annual snowmelt as meltwater contribution. A subalpine forest composed of subalpine fir and Engleman spruce surrounds both lakes. Long-term climate data is available from the Bear Lake SNOTEL site (40.32, -105.65; 2896m asl) and the study sites range from 5.75 km to 16.00 km away from the site. Averages for the 1981-2010 climate normal for mean January temperature (-6.7°C), mean July temperature (13.3°C), and annual precipitation (46.2cm) were calculated from daily data available on <https://wcc.sc.egov.usda.gov/nwcc/site?sitenum=322>.

Two different methods were explored to find the mean July air temperature (MJAT) for each study site. Daily data is available from the long-term ecological research site Niwot Ridge going back to 1952 from the D1 climate station (3739m asl) (Kittel et al., 2019). The initial exploratory analysis used this data combined with the environmental lapse rate of 5.5°C/km (Pepin

and Losleben, 2002). However, this data is collected from an environment that is not representative of the sampled lakes as mountain summits are not influenced by the surface complexities introduced by topography, such as relief and aspect (Pepin and Lundquist, 2008). Thus, the PRISM

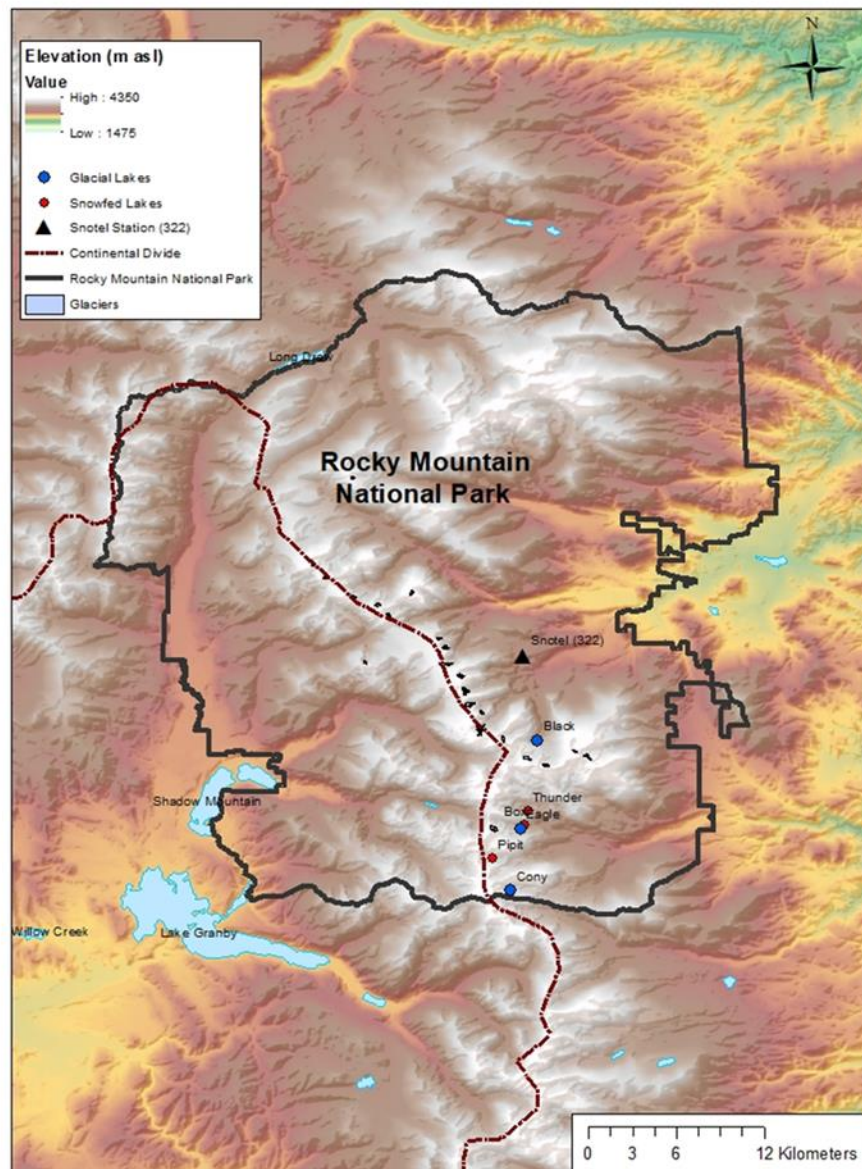


Figure 4.1a: Study sites in Rocky Mountain National Park, Colorado

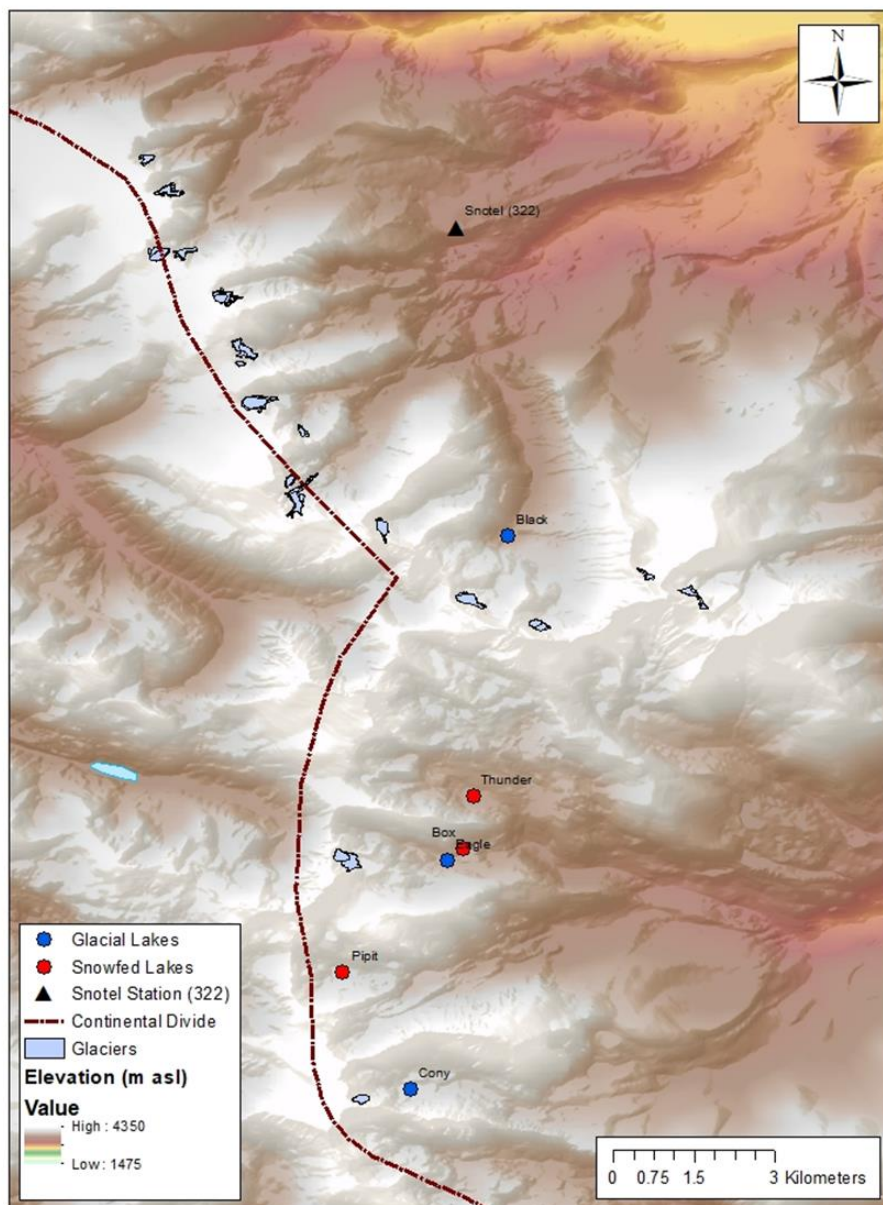


Figure 4.1b: Study sites along the continental divide in Rocky Mountain National Park, Colorado.

dataset was used in the analysis (Prism Climate Group, 2020). This dataset relies on 4 km gridded air temperature data and provides dates going back to 1895 for all lakes. Some authors suggest that

the interpretation of this data should be made with caution as observations are limited above 3000m and none exist above 3500m (Rangwala and Miller, 2012; Haskett and Porinchu, 2013).

Reconstructions of SWT and MJAT are performed for the Kite Lake stratigraphy for proof-of-concept. Information regarding the study site for this lake is found in Haskett et al. (2020).

Field Methods

Short sediment cores were recovered from the center of each lake using a modified DeGrand gravity corer from a small inflatable raft. Each core had no noticeable disturbance at the sediment/water interface and was considered undisturbed during sediment collection. Observations regarding color and stratigraphic characteristics were recorded in a field notebook. Each core was sectioned at 0.25cm intervals into Whirlpacks using a modified Glew extruding device for the uppermost 10cm of stratigraphy (Glew, 1998; Porinchu et al., 2017). Sediment below 10 cm was subsampled at a 0.50cm resolution. The sediment was then stored in portable coolers to keep them cool and dark during transportation to the Environmental Change Lab at the University of Georgia. Variables that capture the modern limnology for each lake were collected during core extraction and include water temperature profiles, lake depth, Secchi disk depth as a measure for optical transparency, pH, and specific conductivity.

Chronology Development

Twelve bulk sediment samples were subsampled along the length of each short core and sent to MyCore Scientific Incorporated (Chalk River, Canada) for ^{210}Pb dating. Constant rate of supply (CRS) was used to calculate ^{210}Pb ages and sedimentation rates ($\text{g cm}^{-2} \text{ yr}^{-1}$) for each lake stratigraphy (Appleby and Oldfield, 1978). Cony, Eagle, Black, and Thunder Lakes contained

enough supported ^{210}Pb to extend chronologies into the very late 19th century. The age-depth models for Pipit and Box Lakes could only be developed into the 1930s. Chronologies were developed between dated samples using locally weighted scatterplot smoothing (LOESS) regression with smoothing curves (span=0.25) for each lake (Cleveland et al., 1996) (Figure 4.2).

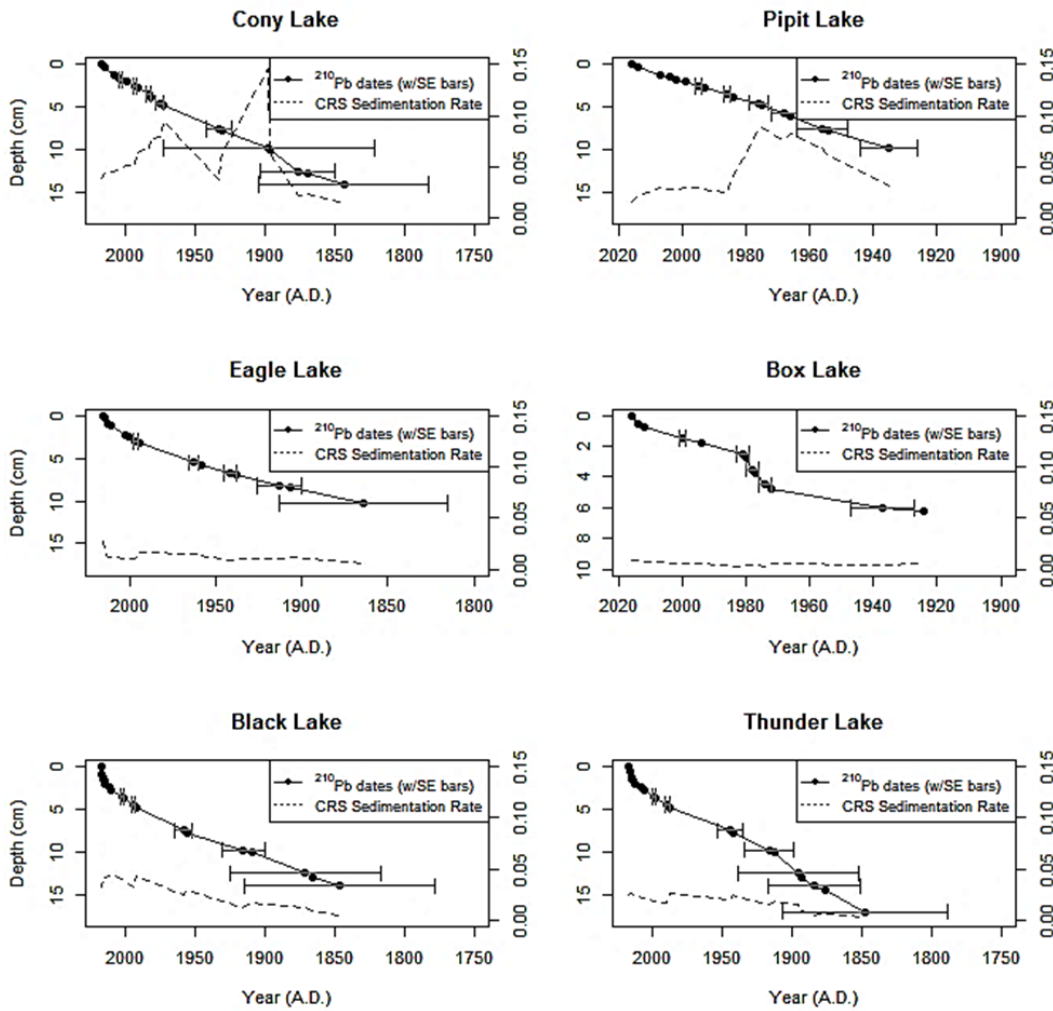


Figure 4.2: ^{210}Pb chronologies and sedimentation rates

Chironomid Analysis

Chironomid extraction followed the protocol established by Walker (2001). Samples for chironomid collection were prepared using every other sample. The altering sediment was used for geochemical analysis of the sediment and was limited for chironomid work (not presented). Sediment was heated in an 8% KOH solution at 30°C until the colloidal matter was broken down and remnant materials could be rinsed through a 95 µm mesh sieve. The remaining residue was rinsed with distilled water back into a beaker and then poured into a Bogorov counting tray. Fine-tipped forceps were used to extract chironomid head capsules under a dissection stereomicroscope at 40x magnification. The head capsules were then placed in a water droplet on a coverslip for microscopic slide creation. Once the water evaporated from the coverslip, the chironomids were permanently mounted to the glass slide with Entellan[®]. Some studies indicate that a minimum of 50 head capsules (HCs) should be used in chironomid quantitative analysis (Larocque, 2001). Other work has found that between 40 and 50 HCs are sufficient (Quinlan and Smol, 2001; Porinchi et al., 2007; Reinemann et al., 2014). Efforts during chironomid extractions were made to reach a minimum of 50 HCs but for very few samples, sediment availability was exhausted before attaining this number. All samples from Cony, Box, and Thunder Lakes possessed more than 50 head capsules. Eagle Lake had one sample comprised of 49.5 HCs, while Pipit and Black had two (42 and 48.5 HCs) and three samples (40, 42, and 46.5 HCs) respectively. A Nikon Eclipse E100 (up to 100x magnification) microscope was used for chironomid identification. Taxonomic keys by Brooks et al. (2007), Andersen et al. (2013), and the website Chiro Key (2020) were used to identify subfossil chironomid remains. Three taxa belonging to the subfamily Diamesinae could not be identified and were grouped as *Diamesa* spp.

Statistical Analysis

All statistical methods were performed on the open-source platform R (R Development Core Team, 2020). Chironomid data were square-root transformed to stabilize the variance inherent in count data (Prentice, 1980). Individual taxa were considered rare and removed from analysis if they were present in two or fewer samples and contained 2% or less of the total relative abundance (Quinlan and Smol, 2001). The ecological optimum for SWT and the tolerance for each taxon present in the calibration set was found using the weighted averaging (WA) method using the package “analogue” (ter Braak and Barendregt, 1986; Cristóbal et al., 2014; Simpson et al., 2019) (Table 4.2) (Appendix B.3).

Detrended correspondence analysis (DCA) is often used as a means to establish periods of compositional turnover in ecological communities (Hill and Gauch, 1980; Smol and Douglas, 2007; Birks and Birks, 2012). This analysis was performed in the R package “Vegan” (Oksanen, 2015). The R package “changepoint.np” was used to perform changepoint analysis on the results of the DCA analysis to determine the years at which these transitions occurred (Killick et al., 2012; Haynes et al., 2016; Haynes et al., 2017) (Figure 4.3). Chironomid zones were created for each lake using these data. The relative abundance curves for each lake were plotted using the “stratplot” function in the “analogue” package in R (Simpson and Oksanen, 2013; R Development Core Team, 2020). The taxa present in relative abundance curves were arranged by the lowest optimal WA Optima for SWT to the left of the plots with progressively thermophilous taxa becoming more dominant to the right of the plot. Chironomid-based inference models were developed for both mean July air temperature (MJAT) and surface water temperature (SWT) using the package “Rioja” (Juggins and Juggins, 2019). Both inference models are based on the 153 lakes and 77 midge taxa from the Western United States (WUS) training set (Haskett et al., 2020).

Both inference models were developed using the weighted averaging-partial least squares (WA-PLS) approach (ter Braak et al., 1993; Juggins and Birks, 2012). In order to determine the appropriate number of components to be used for each model, a randomization t-test of the

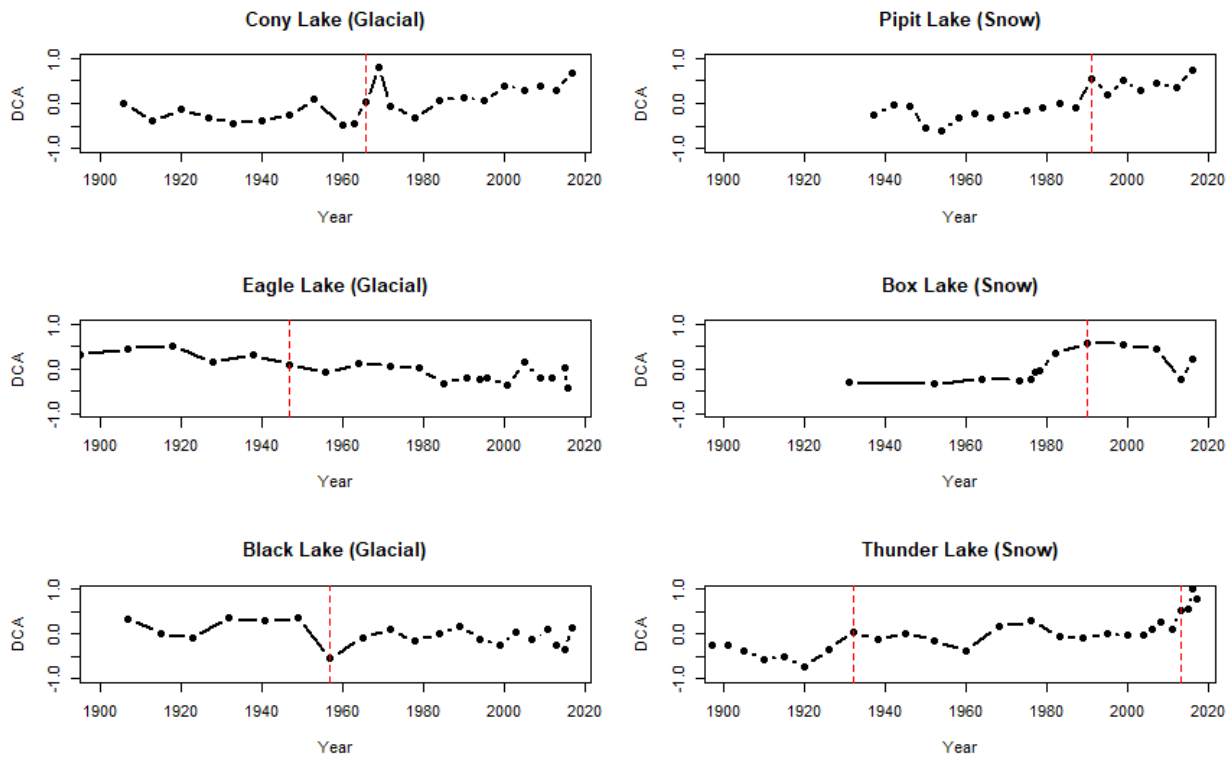


Figure 4.3: Trends in detrended correspondence analysis with changepoints.

cross-validated WA-PLS model was performed (van der Voet, 1994). The performance statistics for the SWT inference model indicated that the one-component WA-PLS or the weighted average (WA) inference model was the most appropriate with an $r^2_{boot} = 0.38$, root-mean-square-error of

Chironomid Taxon	WA Optima (°C)	Tolerance (°C)	Chironomid Taxon	WA Optima (°C)	Tolerance (°C)
Diplind	7.8	3.7	TAG	14.0	2.6
Brillia	8.1	NA	Cory.Th	14.0	3.2
Abisko.1	9.2	1.6	TAC	14.1	3.0
Paraind	9.4	4.3	Cladtany	14.2	3.7
Pseudo	9.9	2.3	Apedind	14.2	2.4
Park.A	10.4	0.4	Paratany	14.4	3.5
Mes.Smit	10.5	NA	Tribind	14.7	3.7
Hyd.Oliv	10.5	4.1	Dicrind	14.7	3.0
Protan	10.6	2.4	Psecsept	14.8	3.1
Chaeto	10.8	3.2	Tanyind	14.8	3.2
TAA	11.1	3.1	Procind	14.9	3.4
Smit.Ps	11.4	2.8	Zaluind	15.0	2.9
Diamind	11.4	2.7	Park.bat	15.0	4.1
TAB	11.5	2.1	Micpsect	15.1	2.8
Metrio	11.6	1.7	unknown1	15.1	NA
Stilo	11.8	2.2	Pentind	15.3	2.9
Monoind	12.1	3.0	Cladind	15.5	3.1
Sympind	12.2	2.2	TAE	15.5	1.7
Sergind	12.2	3.0	StZvgrp	15.6	0.4
Heteind	12.3	2.7	Psecsemi	15.6	3.1
Parorth	12.3	2.0	Psecmono	15.6	3.4
unk.ortho.egl	12.3	2.0	Nanoind	15.8	2.9
Euk.Tvet	12.6	2.8	Mictind	15.9	2.7
Georth	12.6	NA	unk.orth.MLC	15.9	NA
Pod.Ziegler	12.6	NA	Tany.chi	15.9	NA
Colivtyp	12.7	3.4	Psecall	16.0	2.9
Synoind	12.8	2.5	TAK	16.1	2.0
Lim.Para	12.9	3.9	Phaeind	16.3	2.6
Endoch	13.0	2.9	Glypind	16.5	2.3
Einfel	13.1	3.5	PsecWalk	16.6	3.0
Doi.Pseu	13.2	2.6	Pagaind	16.7	3.3
Cric.Ort	13.3	3.5	Polyind	16.9	2.6
Stemind	13.4	3.6	Labrind	17.7	3.5
Triss	13.5	0.8	Tany.A.C	17.7	2.5
Rheoind	13.6	3.1	Pseuchi	17.8	NA
Corynamb	13.7	2.8	Sticind	18.4	2.2
Chirind	13.7	3.5	TAD	19.2	1.7
TAH	13.8	3.6			
Chphgrp	13.9	3.2			

Table 4.2: Chironomid taxa sorted for surface water temperature by individual weighted average optima and tolerances. Taxa are listed in gray boxes.

prediction (RMSEP) = 2.75°C, a maximum bias of 4.34°C, and a p-value for the t-test of 0.001 (Table 4.3). The midge-based MJAT model was developed using the two-component WA-PLS inference model and had an $r^2_{\text{boot}} = 0.36$, root-RMSEP = 1.48°C, a maximum bias of 5.39°C, and a p-value for the t-test of 0.011. To assess how representative the training set is of the stratigraphic subfossil chironomid assemblages, the fossil assemblages from the six sampled lakes were passively plotted over the calibration (or training) set in canonical analysis (CA) ordination space (Anderson and Willis, 2003) (Figure 4.4).

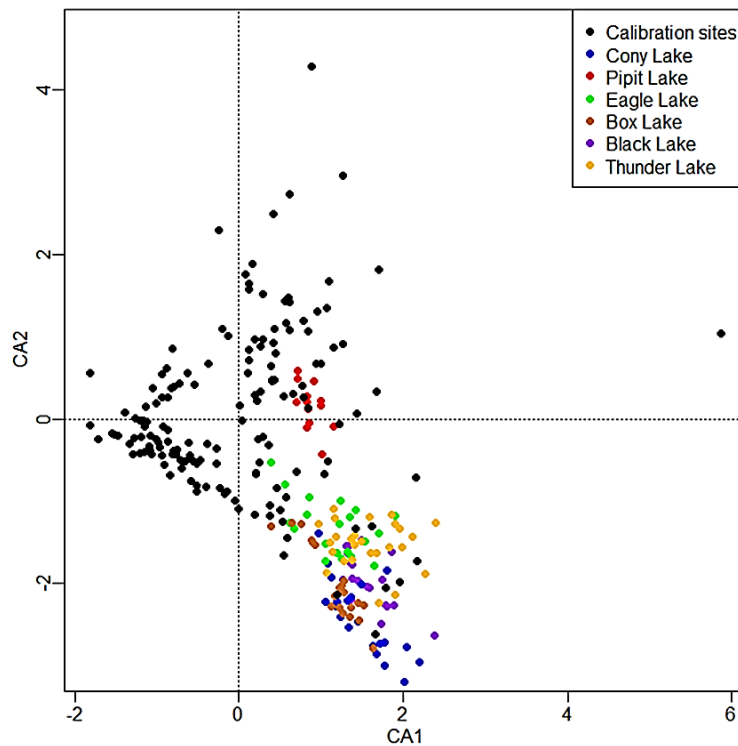


Figure 4.4: Passive plotting of fossil assemblages from six alpine lakes against the training set assemblage in correspondence analysis ordination space.

The predicted MJAT and SWT derived from the developed midge-based inference models were compared to the MJAT estimates extrapolated from the PRISM data for each study site (PRISM Climate Group, 2020) (Figure 4.5). The averages for the midge-based MJAT, midge-

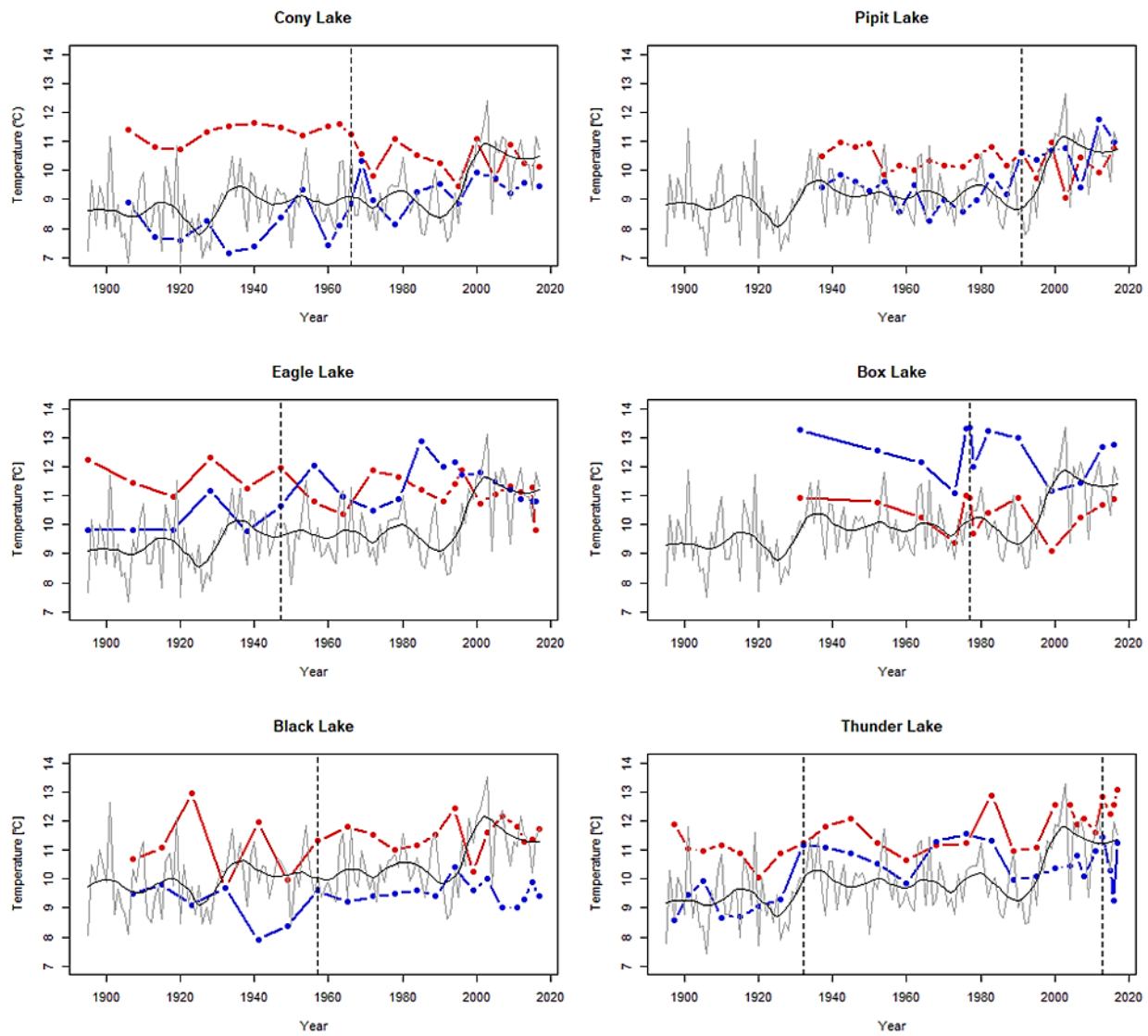


Figure 4.5: Midge-based mean July air temperature (MJAT) (°C) and surface water temperature (SWT) (°C) reconstructions plotted against PRISM-derived mean July air temperature for each lake. (Blue: SWT; Red: MJAT; Gray:PRISM-derived MJAT. Loess line =0.20)

based SWT, and PRISM-based MJAT were calculated, and the deviations from the mean for each stratigraphic sample was calculated (Figure 4.6). Bland-Altman Plots were plotted to assess how robust both midge-based predicted temperatures performed compared to PRISM data (Figs. 4.7 and 4.8). This method is used in biomedical research to evaluate the agreement between two variables measured by different instruments by plotting differences between the two variables against the mean of the two variables. (Bland and Altman, 1986; Giavarina, 2015). The 95th confidence interval bands constrain the values. Outliers will fall outside of the 95th confidence interval bands (Bland and Altman, 1986; Giavarina, 2015).

Environmental Variable	Inference Model	Apparent RMSE (°C)	r^2	Cross Validation RMSEP (°C)	r^2_{boot}	Maximum Bias (°C)	p value
SWT	WA	2.49	0.47	2.75	0.38	4.34	0.001
MJAT	WA-PLS 2 Component	1.12	0.58	1.48	0.36	5.39	0.011

Table 4.3: Statistics for inference models for both chironomid-inferred surface water temperature and chironomid-inferred mean July air temperature.

Chironomid counts collected from a long core collected from Kite Lake were used to model chironomid-based SWT and MJAT to apply the findings from the modern/historical relationships explored from the six lakes from Rocky Mountain National Park to stratigraphy that spans the Pleistocene-Holocene Transition where no instrumental data exists (Haskett et al., 2020).

RESULTS

Chronology Development

Sedimentation rates are higher in the highest elevation lakes. Cony Lake experienced pulses of increased sedimentation with the highest peak occurring ~ A.D. 1900. The rates fall and begin to climb again in the late A.D. 1970s. Pipit Lake has a lower sedimentation rate than Cony

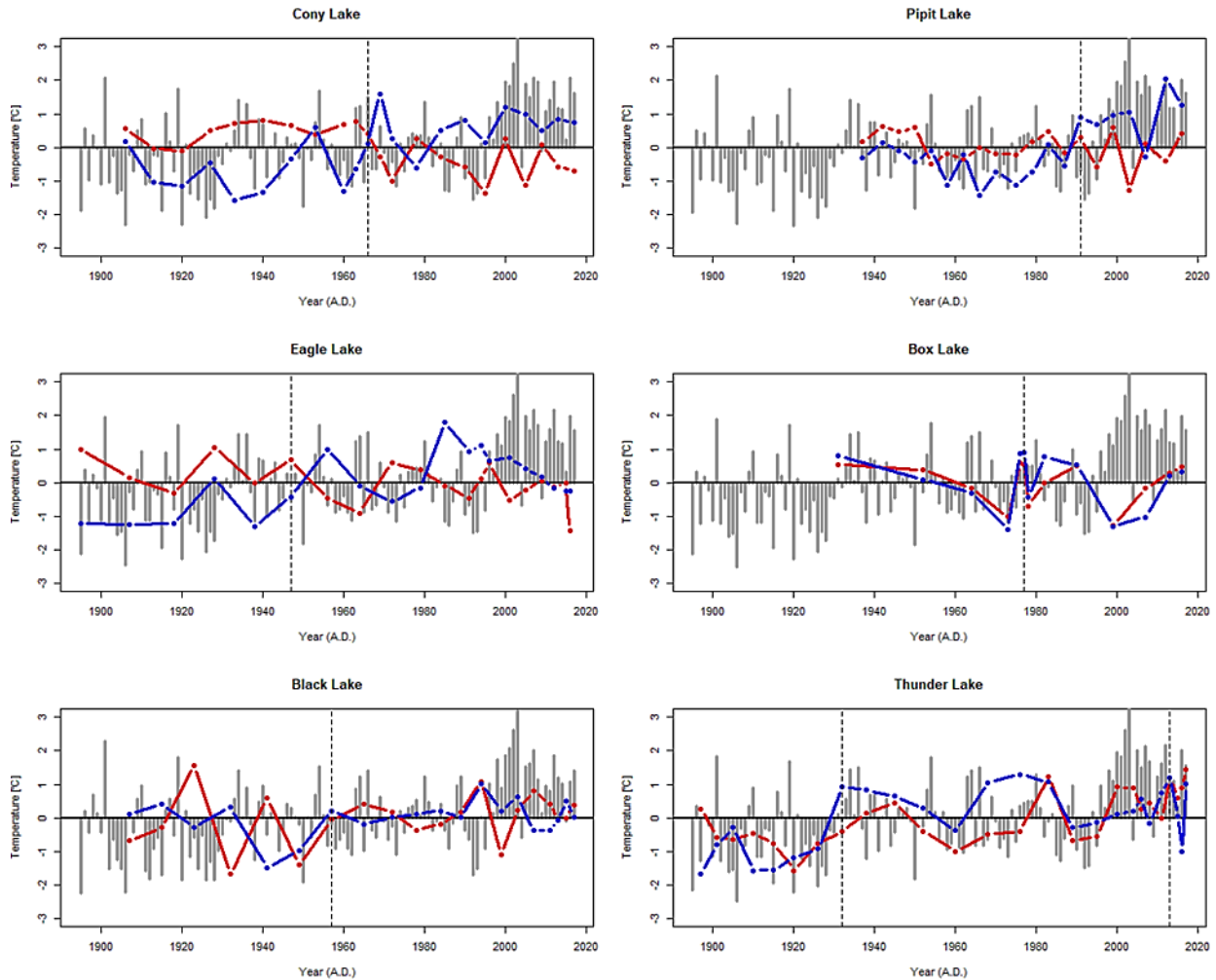


Figure 4.6: Deviations from averages for PRISM-based mean July air temperature (gray bars), midge-based mean July air temperature (red dashed line), and midge-based surface water temperature (blue dashed line).

Lake and peaks during the late A.D. 1970s. Both lakes experience a continual decrease in the 21st century. The lakes found at timberline have experienced the lowest sedimentation rates of all lakes examined and only Eagle lake experiences a slight increase in A.D. 2015. Black and Thunder Lakes had a gradual increase in sedimentation rates over the 20th and 21st centuries with Black Lake having slightly higher rates. Overall, the error associated with ²¹⁰Pb ages is 0 for the surface sediments and increases with increasing depth. The error is most significant for Cony Lake with

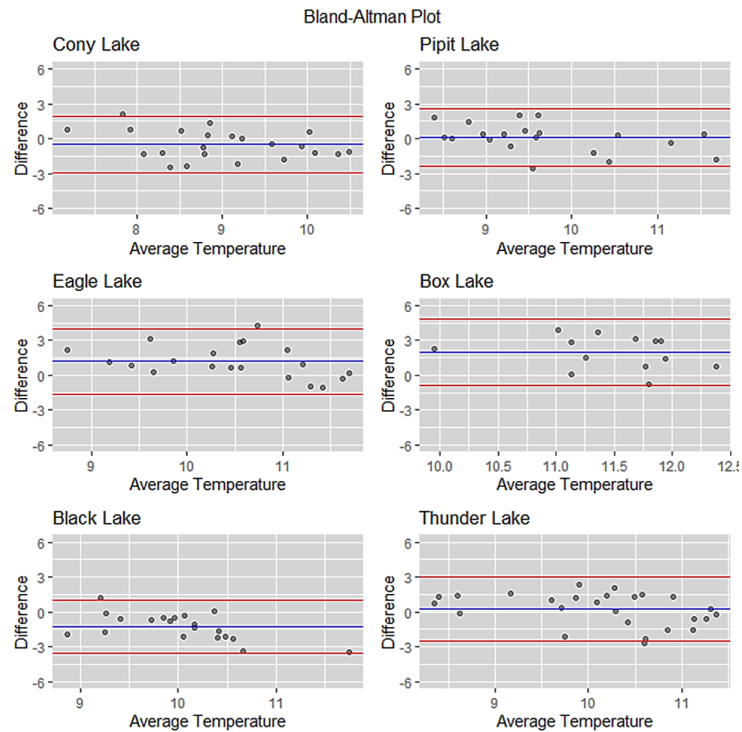


Figure 4.7: Bland-Altman plots are useful for comparing two datasets (midge-based surface water temperature and PRISM-based mean July air temperature). The blue line represents the average between differences in surface water temperature and mean July air temperature. The red lines represent the 95th confidence interval.

an error of 76 years but the error associated with the deepest dated sediment for the other lakes ranges from 9 years (Pipit Lake) to 68 years (Black Lake). The amount of sediment required to

reach the minimum head capsule (HC) count of 50 required processing between 2mL to 3mL of sediment. However, HCs were plentiful in Thunder Lake and only needed 1mL of sediment to reach the necessary HC counts for most samples. The amount of sediment preparation was more extensive for sediment collected from Eagle Lake and required an average of 5mL of sediment for HC recovery. The top two samples for both Eagle and Black Lakes were combined to achieve the minimum head capsules needed for analysis. The sediment required to reach these numbers required 18mL and 19mL respectively. The chronologies developed for sub-fossil chironomid analysis provide a sub-decadal scale resolution.

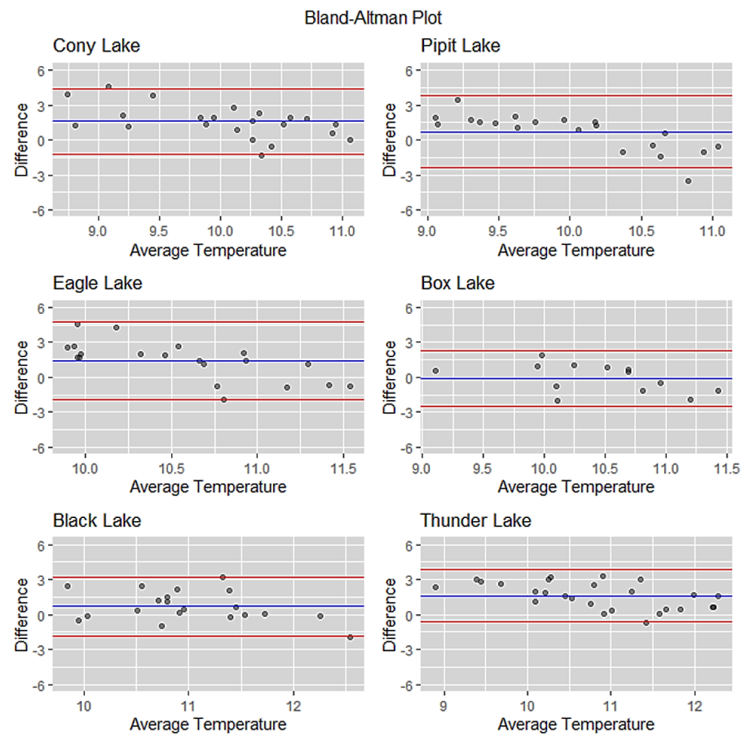


Figure 4.8: Bland-Altman plot to assess the strength of midge-based mean July air temperature and PRISM-based mean July air temperature. The blue line represents the average between differences in predicted mean July air temperature and PRISM-mean July air temperature. The red lines represent the 95th confidence interval.

3.2 Statistical Analysis

The results of DCA analysis indicate that changes in compositional turnover for each lake have changed over the 20th and into the onset of the 21st century. The changes evident for compositional turnover had a similar trajectory for Cony, Pipit, and Thunder Lakes. A shift in composition occurred in A.D. 1966 and A.D. 1991 for Cony and Pipit Lakes, respectively. Thunder Lake experienced two changepoints in faunal turnover. The change in A.D. 1932 increased slightly compared to the change that occurred in A.D. 2013, where the DCA trend rises dramatically. The decreasing direction for Eagle Lake's DCA was the opposite of those seen in other lakes and could be contributed to instability over the latter 20th century into the 21st century within the lake basin. Species richness, or the number of individual taxa present, fluctuated greatly during this time suggesting that within-lake variability for this lake basin changed during this time. Two taxa dominated the stratigraphic chironomid assemblages of Eagle Lake and could explain the overall decreasing trend in DCA for this lake. The changepoint analysis found a shift in compositional turnover during A.D. 1947 for Eagle Lake. Box Lake also witnessed dramatic changes to chironomid composition over this period. The early 20th century was stable until a changepoint was found at A.D. 1977. Iron nodules were collected in sediment during chironomid extraction and correspond to depths between 5.00cm and 7.5cm (i.e., 1964- beyond chronological control). The chemical composition of the iron nodules was confirmed using XRF at the Center for Applied Isotope Studies at the University of Georgia (Yu et al., 2015). They are 99% iron with trace amounts of potassium. The presence of iron nodules suggests that Box Lake has experienced periods of fluctuating levels of oxygen over the last 100 years and that within-lake variability is more likely to influence the distribution of chironomid communities within the lake basin, rather

than regional climatic signals (Davison, 1993). Any interpretation of chironomid-based temperatures for this lake should be undertaken with the utmost caution. Black Lake, the deepest lake sampled, experienced a decrease in DCA during A.D. 1957. Overall, Black Lake was relatively stable over the entire period of study and suggested that the longer residence time of the lake water may have moderated the overall climate signals. This lake was also dominated by one taxon (*Heterotrissocladius* -30 – 50%) which may account for the small amount of change in DCA over the 20th and beginning of the 21st century. Overall, the CA-biplot indicates that the majority of subfossil chironomid communities are located within the ordination space of the WUS calibration set (Figure 4.5). Some fossil assemblages from Cony and Black Lakes are not represented in the modern training set data.

Chironomid Relative Abundance Diagrams

Stratigraphic change in chironomid composition is provided in Figures 4.9a-4.9f. (Not all taxa are shown due to space constraints).

Cony Lake

A total of 21 taxa were identified in sediment collected from Cony Lake. Change-point analysis of faunal turnover divides the stratigraphy into two zones (Cony-2 and Cony-1). Cony-2 spans A.D. 1906 to A.D. 1966, and Cony-1 spans A.D. 1966 to 2016. The results from WA Optima and tolerances were used to organize the taxa on the relative abundance plots. Cold stenotherms are located to the left of the plot and become increasingly affiliated with warmer taxa as they approach the right of the diagram. The shift from Cony-2 to Cony-1 demarcates a zone dominated by cold-loving taxa such as *Pseudodiamesa*, *Diamesa* spp., and *Tanytarsus* type-A in the early

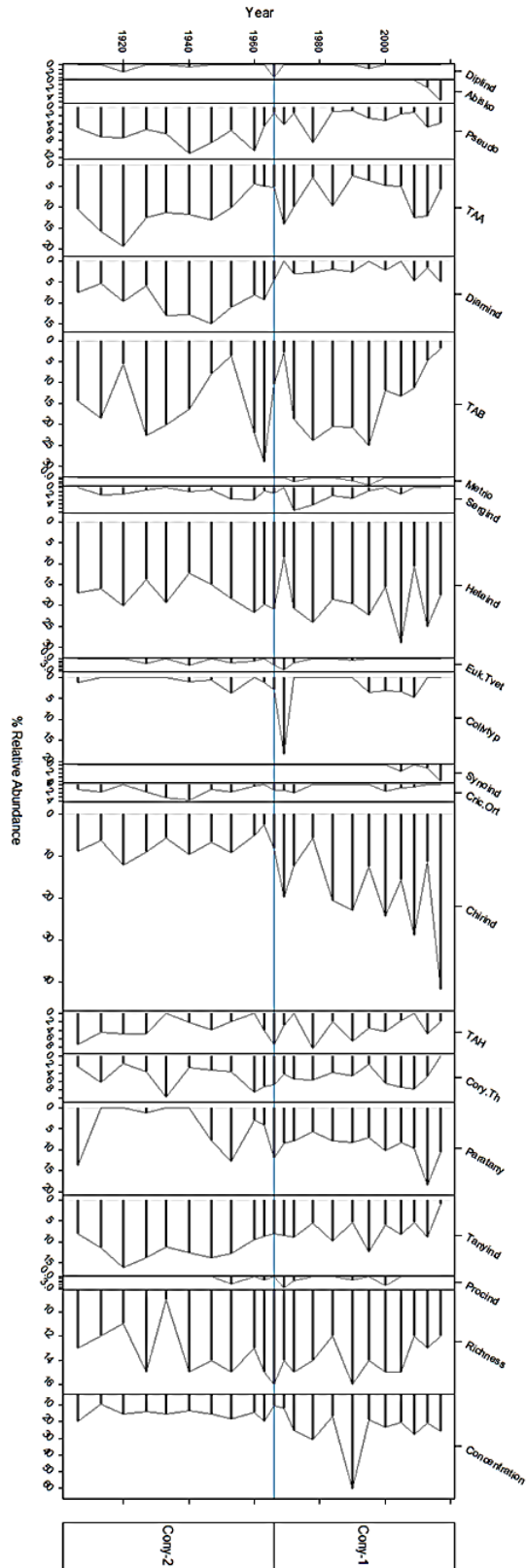


Figure 4.9a: Cony Lake relative abundance organized by the weighted averaging optima of surface water temperature for taxa. Coldest taxa appear at the top and become increasingly warm-loving moving down the chart. Zones based on changepoint analysis of detrended correspondence analysis results at 1966 (blue line).

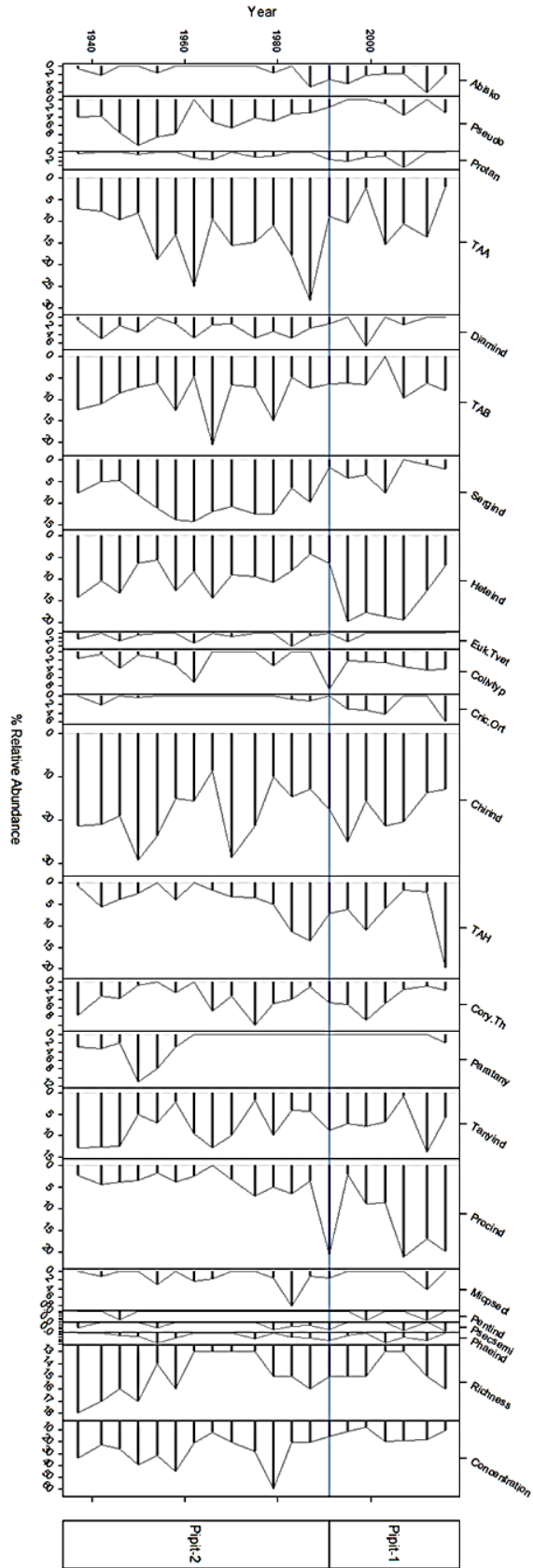


Figure 4.9b: Pipit Lake relative abundance organized by the weighted averaging optima of surface water temperature for taxa. Coldest taxa appear at the top and become increasingly warm-loving moving down the chart. Zones based on changepoint analysis of detrended correspondence analysis results at 1991 (blue line).

part of the 20th century to an assemblage increasingly dominated by *Chironomus*, which reaches 42% by A.D. 2016. The concentration of head capsules varied little throughout the record with an average of 20 HC per mL. The exception occurred in A.D. 1990 when the HC concentration increased to 60 HC per mL.

Pipit Lake

Pipit Lake sediment yielded a total of 21 taxa. A.D. 1991 demarcates the transition from Pipit-2 to Pipit-1. Thus, Pipit-2 spans from A.D. 1937 to 1991, and Pipit-1 represents sediment from A.D. 1991 to A.D. 2016. The assemblage present in zone Pipit-2 is comprised of the cold stenotherms *Pseudodiamesa*, *Tanytarsus* Type A, *Sergentia*, and *Paratanytarsus*. The transition to Pipit-1 has these taxa decreasing and witnesses an increase of *Abiskomyia*, *Protanypus*, and *Heterotrissocladius*. This assemblage possesses some of the taxa with the coldest WA temperature optima. This finding initially would suggest that temperatures decreased during Pipit-1. This finding is further substantiated by the decrease in HC concentrations from Pipit-2 to Pipit-1. However, this zone also sees an increase in *Procladius*, *Tanytarsus* type H, *Cricotopus/Orthocladius*, and *Phaenopsectra* which are all affiliated with more productive environments (Brooks et al., 2007).

Eagle Lake

A total of 26 taxa were identified in sediment collected from Eagle Lake. Changepoint analysis of faunal turnover divides the stratigraphy into two zones (Eagle-2 and Eagle-1). Eagle-2 spans A.D. 1895 to A.D. 1947, and Eagle-1 spans A.D. 1947 to 2016. The entire subfossil chironomid stratigraphy is dominated by two taxa: *Chironomus* and *Heterotrissocladius*. The

change point at A.D. 1947 coincides with an increase in *Chironomus* and a decline in *Heterotrissocladius*. Cold stenotherms located to the left of the plot (such as *Diplocladius*, *Pseudodiamesa*, and *Diamesa*) appear and disappear in pulses throughout the entire length of the studied core, rather than being normally distributed. *Synorthocladius* begins to increase after A.D. 1947 and is noteworthy as its presence denotes moving water entering into the lake as it occurs in streams and the littoral zone of lakes (Brooks et al., 2007). Taxa affiliated with warmer and more productive lakes, such as *Procladius*, *Psectrocladius sordidellus*-type, and *Phaenopsectra*, increase in relative abundance or appear after A.D. 1980. Richness indicates that Eagle-2 was more diverse and have an average of 18 taxa in each sample. The stability of the chironomid fluctuates and experiences sharp decreases (n=12) and increases (n=20) in richness.

Box Lake

Box Lake sediment yielded a total of 25 taxa. A.D. 1977 demarcates the transition from Box-2 to Box-1. Thus, Box-2 spans from A.D. 1931 to 1977, and Box-1 represents sediment from A.D. 1977 to A.D. 2016. The iron nodules identified during chironomid extraction are present in Box-2. The record for Box Lake is composed of few but very dominant taxa. *Corynocera oliveri*-type, *Corynocera ambigua*-type, *Chironomus*, and *Psectrocladius sordidellus*-type. An average of 19 taxa is present in zone Box -2 and stable before A.D. 1977. This trend is comparable to head capsule concentrations that yielded high numbers per mL of sediment (avg=45). An extreme event occurred at the transition zone as all taxa have a sharp decrease (i.e., *Heterotrissocladius*, and *Tanytarsus* type B) or increase (*Cornyonocera oliveri*-type and *Phaenopsectra*) in relative abundances. Concentrations also fall significantly with an average of only 16 head capsules per mL of sediment. The chironomid communities don't recover until A.D. 2013.

Black Lake

A total of 23 taxa were identified in sediment collected from Black Lake. Changepoint analysis of faunal turnover divides the stratigraphy into two zones (Black-2 and Black-1). Black-2 spans A.D. 1907 to A.D. 1957, and Black-1 spans A.D. 1957 to 2017. The subfossil chironomid stratigraphy is consistent for the majority of taxa. *Heterotrissocladius* is the dominant taxa with and averages 32% of the total relative abundance and peaks at 49% in A.D. 2013. The transition at A.D. 1957 corresponds with a decrease from 20% to 8% in *Eukiefferiella/Tvetenia* and an increase from 0% to 16% in *Corynocera oliveri*-type. The lowest richness also occurs at this interval with only 11 taxa present in the sample. The coldest taxa based on WA optima suggests pulses of cold water throughout the entire record (*Diplocladius*, *Pseudodiamesa*, and *Protanypus*). *Diamesa* is present throughout the record as well but decreases after A.D. 1957. The uppermost samples (A.D. 2015 - A.D. 2017) witnessed a sharp decrease in *Heterotrissocladius* from 49% to 21%. This decline corresponds to a reduction in concentration from 28 HCs per mL to 5 HCs per mL of sediment. This sample is composed of the sediment from the upper two sediment samples as chironomid extraction was not enough for enumeration.

Thunder Lake

Thunder Lake was the most diverse lake and possessed a total of 35 taxa. Three zones were identified. Thunder-3 spans A.D. 1895 to A.D. 1932. Thunder-2 spans 1932-2013, and Thunder-1 represents the most modern sediment that spans from 2013-2017. Thunder-3 contains an

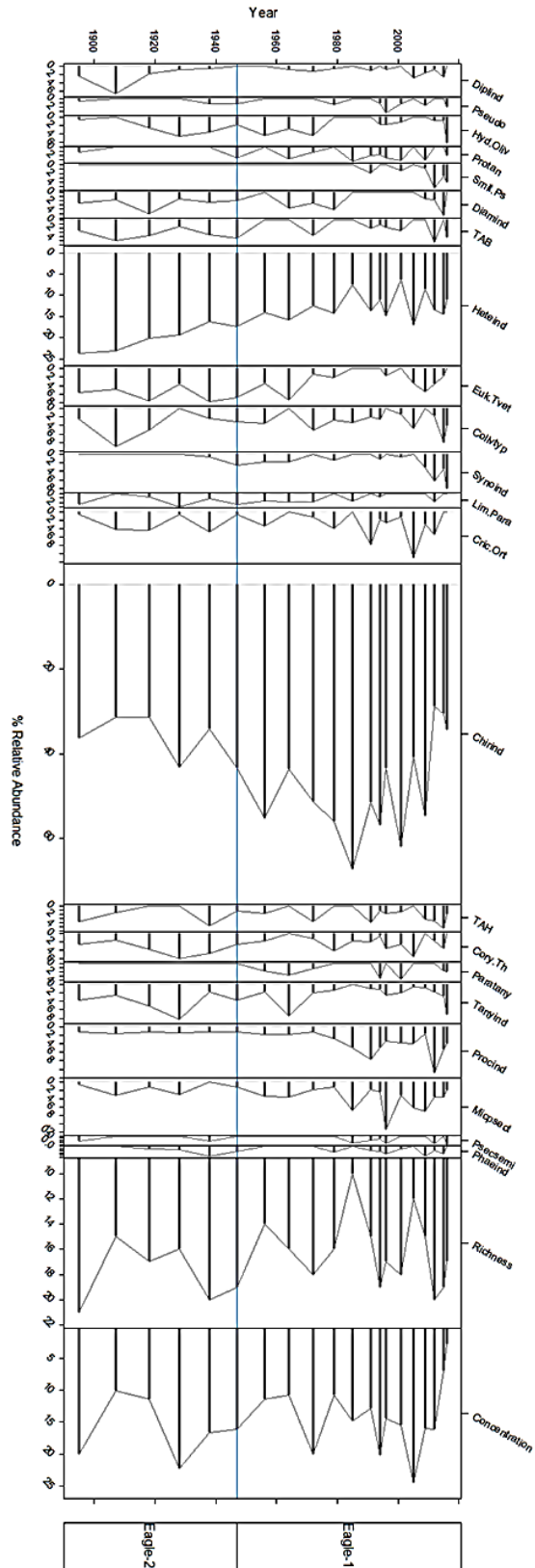


Figure 4.9c: Eagle Lake relative abundance organized by the weighted averaging optima of surface water temperature for taxa. Coldest taxa appear at the top and become increasingly warm-loving moving down the chart. Zones based on changepoint analysis of detrended correspondence analysis results at 1947 (blue line).

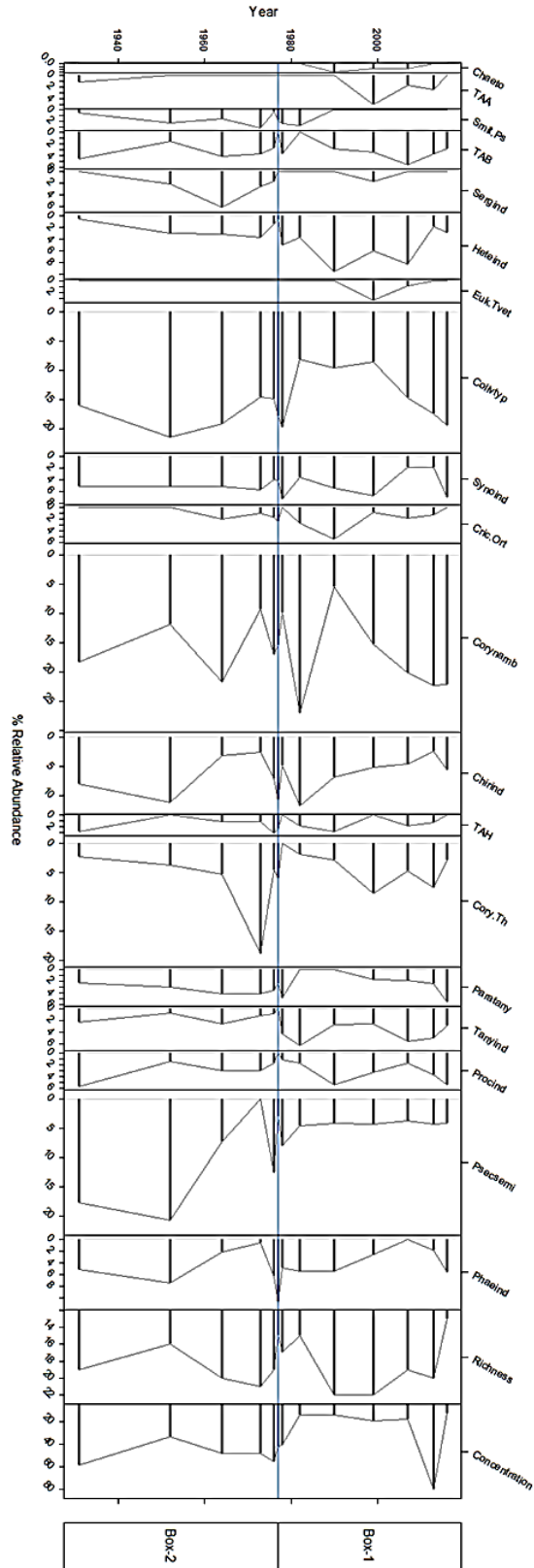


Figure 4.9d: Box Lake relative abundance organized by the weighted averaging optima of surface water temperature for taxa. Coldest taxa appear at the top and become increasingly warm-loving moving down the chart. Zones based on changepoint analysis of detrended correspondence analysis results at 1977 (blue line).

assemblage of *Tanytarsus* type A, *Tanytarsus* type B, and *Heterotrissocladius*. The dominant taxa in Thunder-2 transition to increases in *Corynocera oliveri*-type, *Chironomus*, and *Paratanytarsus*. The appearance of *Diamesa* and *Limnophyes/Paralimnophyes* marks the transition to Thunder-1 at A.D. 2013. This transition is all marked by sharp decreases in *Heterotrissocladius*, *Eukiefferiella/Tvetenia*, and *Corynocera oliveri*-type.

Chironomid-based Reconstructions

Overall, taxa present in the subfossil samples are well-represented by the WUS training set and indicate that the reconstructions may be considered reliable following Birks (1998) (Haskett, 2020b). While the taxa are all accounted for, the overall assemblages for Cony and Black were not as well represented by the training set in ordination space, suggesting that interpretation of reconstructions from these lakes should be made with caution. In training set formation, lakes with considerable depth, or even those that receive glacial meltwater, are considered outliers and are often avoided in data sampling and may account for the sparse representation for these lakes in the training set (Velle et al., 2010; Eggermont and Heiri, 2012).

Chironomid-based SWTs and MJATs are plotted for each lake with the PRISM-based MJAT for each lake (Figure 4.6). Reconstructions for MJAT overestimate PRISM-based air temperature for almost all lakes, with the exception of Box Lake. The reconstructed temperatures have opposite trends for the relationship between reconstructed MJAT and SWT, with SWT overestimating PRISM-based MJAT. The midge-inferred SWTs align closer to extrapolated air temperatures.

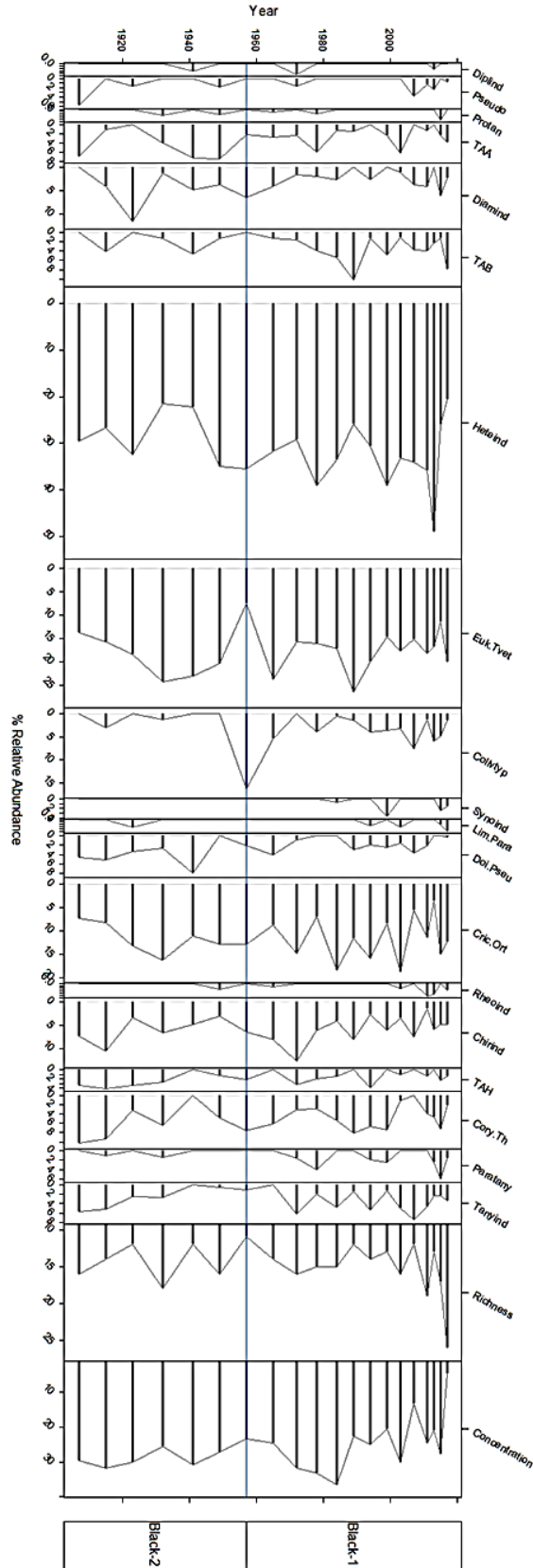


Figure 4.9e: Black Lake relative abundance organized by the weighted averaging optima of surface water temperature for taxa. Coldest taxa appear at the top and become increasingly warm-loving moving down the chart. Zones based on changepoint analysis of detrended correspondence analysis results at 1957 (blue line).

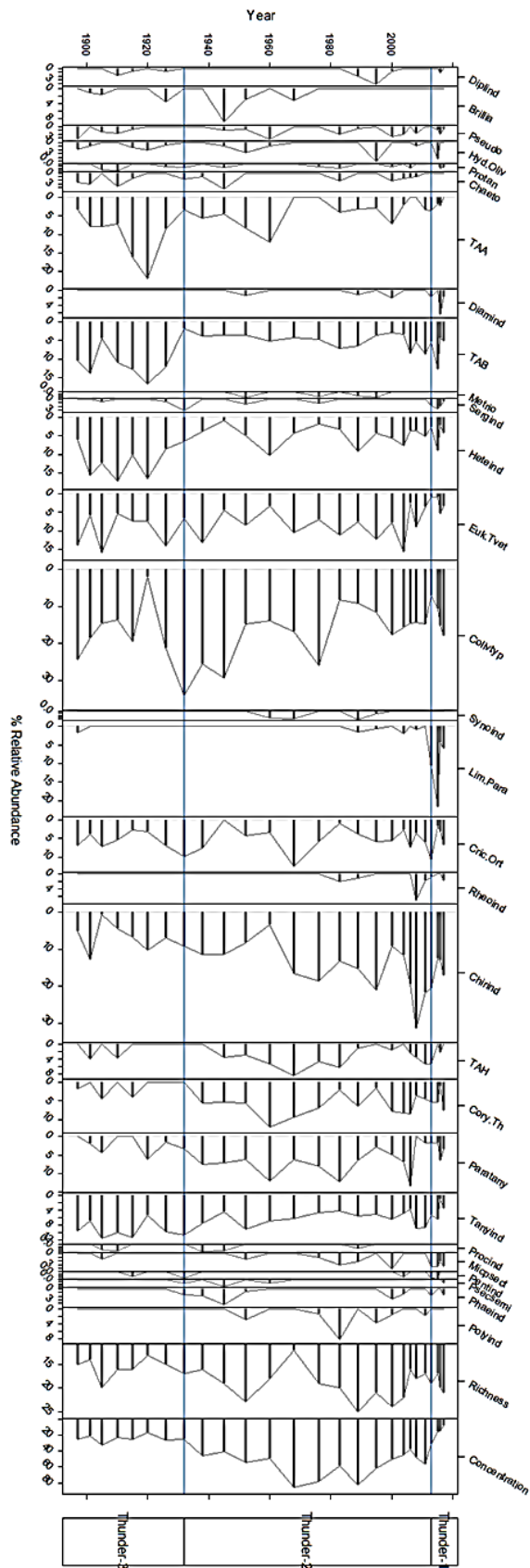


Figure 4.9f: Thunder Lake relative abundance organized by the weighted averaging optima of surface water temperature for taxa. Coldest taxa appear at the top and become increasingly warm-loving moving down the chart. Zones based on changepoint analysis of detrended correspondence analysis results at 1932 and 2013 (blue lines).

The relationships between the two midge-based temperatures show interesting trends that may be useful in paleotemperature reconstruction interpretation. All three glacial lakes have MJATs and SWTs that are inversely related to one another, except for the period from the 1970s until ~ A.D. 2000. After this date, the signals become decoupled and are inversely related. Eagle Lake does exhibit a similar trend but during differing periods. Before A.D. 1947, or over the interval for zone Eagle-2, the overall trends are parallel and mirror one another. After A.D. 1947, the reconstructed temperatures become inversely related. The relationships between midge-derived MJAT and SWT for the lakes receiving year-of-snow as meltwater input (Pipit, Box, and Thunder Lakes) possess temperatures that mirror one another. Pipit Lake does have an inverse relationship between A.D. 1954 to A.D. 1970. After A.D. 2000, Pipit Lake experiences a lag between when reconstructed MJAT decreases and SWT decreases by an offset of 4 years. The most recent samples do seem to possess the inverse relationship evident in the glacial lakes. This lag could be a byproduct of the sample size limiting the amount of time captured by the chronology, a limit based on the last collection occurring in 2016 with no more recent samples to extend the relationship, or it could be a byproduct of perennial snowmelt entering the lake's hydrological system. The averages for reconstructions of SWT and MJAT, PRISM-based MJAT, and associated ranges are presented in Table 4.4. The means for sample-specific errors for each lake are also included as these data limited the overall interpretation when plotted.

The deviations from the averages of reconstructed MJAT, reconstructed SWT, and PRISM-based MJAT were plotted together to examine the “warming” or “cooling” evident and how these trends agreed with PRISM-based MJAT (Figure 4.8). The inverse relationships visible in Figure

Variables	Cony Lake	Pipit Lake	Eagle Lake	Box Lake	Black Lake	Thunder Lake
Average SWT (°C)	8.7	9.7	11.1	12.5	9.4	10.3
SWT range (°C)	3.2	3.5	3.1	2.3	2.5	3.0
SWT SSE Error average (°C)	2.9	2.8	2.7	2.7	2.8	2.8
Average MJAT (°C)	10.8	10.3	11.3	10.4	11.4	11.6
MJAT range (°C)	2.2	1.9	2.5	1.9	3.3	3.0
MJAT SSE Error average (°C)	1.6	1.5	1.5	1.5	1.5	1.5
Average PRISM-based MJAT (°C)	9.1	9.3	9.8	10.0	10.3	9.9
PRISM range (°C)	4.3	5.1	4.3	3.3	4.9	4.2

Table 4.4: Temperature averages, ranges and averages for sample specific errors for midge-inferred temperatures. (MJAT = Mean July Air Temperature, SWT= Surface Water Temperature)

4.6 for Cony, Eagle, and Black Lakes are more apparent when plotted as deviations from their respective averages. The deviation from SWT performs better at estimating changes in instrumental MJAT data than those of chironomid-based MJAT. Black Lake does not follow deviations based on PRISM MJAT but instead seem to fluctuate around the averages. This relationship may be in response to the longer residence times associated with deep lakes. Both reconstructed temperatures follow the deviations evident for MJAT in zone Box-2. After the transition at A.D. 1997, Box Lake reconstructed temperatures no longer follow the deviations visible for MJAT during the latter part of the 20th and into the 21st centuries. Thunder Lake possesses the only midge-based MJAT deviation curve that mirrors deviations evident in PRISM-based MJAT.

“When comparing two sets of measurements for the same variable made by different instruments, it is often required to determine whether the instruments are in agreement or not” (Walsh, 2017). To assess the agreement between chironomid-based reconstructed temperatures and PRISM derived-MJAT, the data visualization technique, known as the Bland-Altman plot, were plotted and explored (Bland and Altman, 1986). Both midge-based MJAT (Figure 4.7) and midge-based SWT (Figure 4.8) were compared to the PRISM datasets for each lake. SWT was

examined as the temperatures seemed closer to PRISM-derived temperatures based on visual inspection of reconstructions (Figure 4.5) and the deviations from averages (Figure 4.6). Overall, the majority of samples fell within the 95th confidence interval for both SWT and MJAT. The only lake that contained no outliers were those from the SWT for Box Lake. Every other plot included one sample that fell on or just outside of the confidence interval band, which is consistent with normally distributed data (Bland and Altman, 1986; Giavarina, 2015).

Chironomid counts from the stratigraphy of Kite Lake were used to develop models for both MJAT and SWT to elucidate the relationships between these temperatures for a period spanning the transition from the latest Pleistocene into the Holocene (Haskett et al., 2020b) (Figure 4.10). The deviations from the averages were also plotted to explore the relationships that exist between the two reconstructions (Figure 4.11).

DISCUSSION AND CONCLUSION

Chironomid-based inference models are powerful tools that are used to explore changes in temperatures for periods that cannot provide instrumental data, such as periods from the Pleistocene. The magnitude of change is often greater during the Pleistocene and chironomids have been used extensively to model these changes (Walker et al., 1991; Axford et al., 2011; Ilyashuk et al., 2019). These significant shifts in temperature are often larger than RMSEP from the model and the error affiliated for each predicted temperature derived (Reinemann et al., 2014). However, temperature changes during the Holocene are more muted and vary only between 2 to 2.5°C for all sites that could be sampled (Wanner et al., 2008; Velle et al., 2010). Furthermore, studies indicate that within-lake variability is more likely to shape chironomid communities during periods of small climatic shifts, such as those that occurred during the Holocene (Engels et al., 2019), which will continue the debate between the proponents of temperature driving chironomid

distribution versus those that contend that chironomids are influenced by the complex relationships between multiple factors that are prevalent in lake systems. The work that compares midge-derived temperatures to instrumental data over historical periods has shown that the sensitivity of chironomids to muted temperature is present over recent decades (Larocque and Hall, 2003; Reinemann et al., 2014; Luoto and Ojala, 2017).

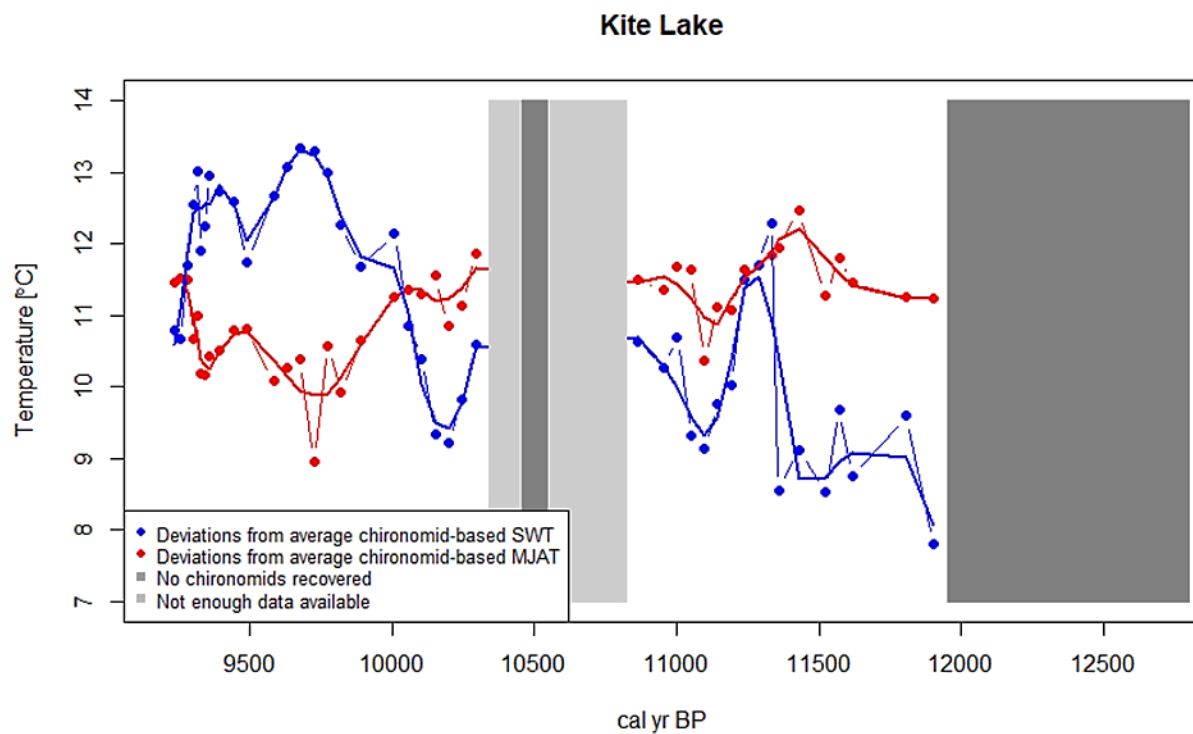


Figure 4.10: Chironomid-based temperature reconstructions for Kite Lake. The thin blue line with dots represents the predicted SWT values. The thick blue line represents the LOESS smoothed line (span=0.20). The thin red line with dots represents the predicted MJAT values. The thick red line represents the LOESS smoothed line (span=0.20). Chironomid recovery at the based contained no capsules and dark gray rectangles represent periods of time with no head capsule recovery. The light gray rectangles are indicative of a lack of data and inferences could not be made. The specific error for SWT

is between 2.7°C and 3.0°C and for MJAT is between 1.5°C and 2.0°C.

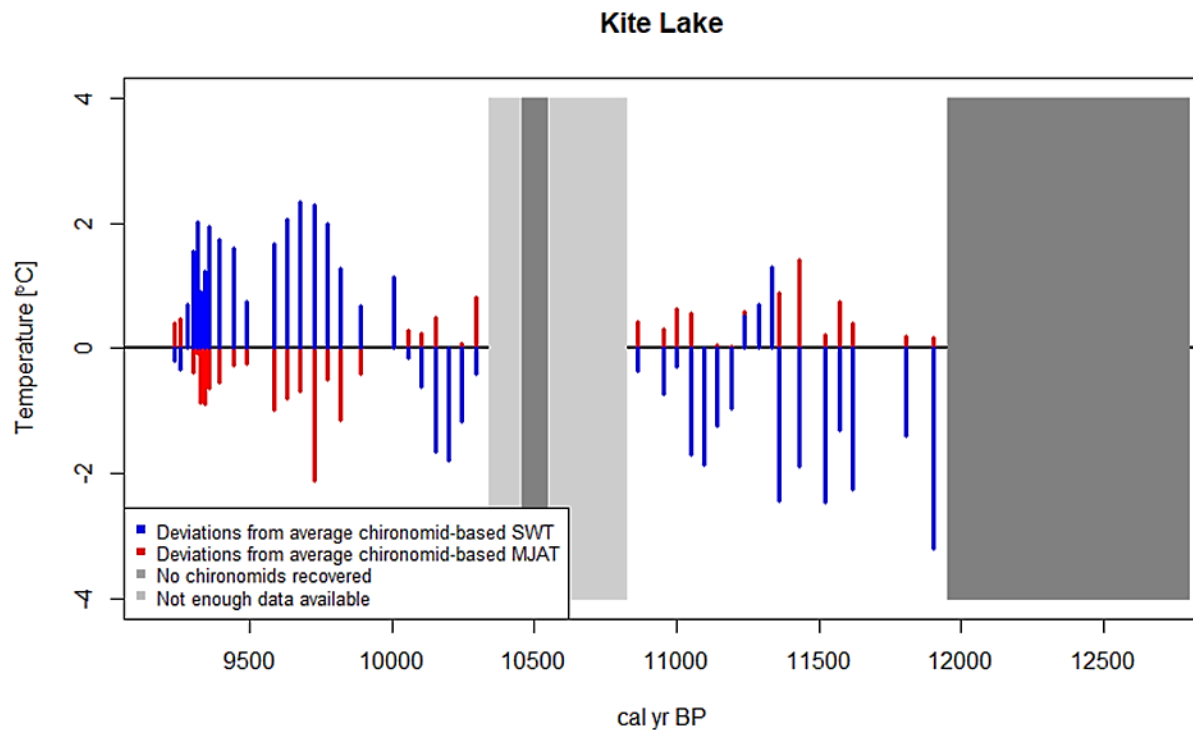


Figure 4.11: Kite Lake deviations from the averages for midge-based SWT (blue bars) and midge-based MJAT (red bars). Chironomid recovery at the based contained no capsules and dark gray rectangles represent periods of time with no head capsule recovery. The light gray rectangles are indicative of a lack of data and inferences could not be made.

In this study, I present both SWT and MJAT derived from chironomid inference models to instrumental data from six lakes in Rocky Mountain National Park in Colorado, with three lakes receiving glacial meltwater and three lakes only receiving meltwater from year-of-snow accumulation. The changes in air temperature evident in the mountains of Colorado over the 20th century had periods of warming and cooling. In general, the period between 1910 and 1930 was cooler followed by a period of warming from 1935 to 1955 (Rangwala and Miller, 2010; Rangwala and Miller, 2012). The period between 1955 and 1975 experienced a cold period with an average

drop of 1°C. Rapid warming of 1°C occurred between 1995 to 2005 (Rangwala and Miller, 2010; Rangwala and Miller, 2012). These findings agree with data collected from SNOTEL sites as well as the PRISM-derived temperatures presented here (Diaz and Eischeid, 2007; Daly et al., 2008; Rangwala and Miller, 2012.) Overall, the only lakes that follow these patterns of change are the reconstructed SWTs from Pipit Lake and both reconstructed temperatures from Thunder Lake, with very different magnitudes of change. Most of Pipit Lake's SWT follow the trends collected from instrumental data, but the chironomid-derived temperatures increased by 2°C during the latest part of the 20th and into the 21st centuries, rather than 1°C. The glacially-fed Cony and Black Lakes also follow a similar pattern for air temperatures as derived by chironomid-based SWT with the exception that includes the latter part of the 20th century and the beginning of the 21st century where SWT decreased by ~1°C. Eagle Lake was stable until A.D. 1920 but gradually increased over 3°C before an overall decrease of ~1°C from the mid-1990s through the aughts of the 21st century. Overall, midge-based MJATs over-estimate temperatures for all lakes, except Box Lake. However, the use of the Bland-Altman plots indicates that both sets of temperatures compared favorably to the PRISM data, and all predicted temperatures for all lakes could be considered reliable. And yet the disagreement between changes evident in faunal turnover differs from the lake to lake, suggesting that within-lake variability is more responsible for chironomid community dynamics rather than the temperature changes that occurred over the 20th century in Colorado. This difference within-lake variability is particularly evident in Box Lake, where the disappearance of iron nodules corresponds with a changepoint and temperature reconstructions that no longer align with temperatures derived from instrumental data after this point in time.

Studies of glacial retreat in the Rocky Mountains are limited during the earliest part of the 20th century. However, Hoffman et al. (2007) compared historical maps and photographs (aerial

and ground-based) to assess changes in the areas of cirque glaciers in Rocky Mountain National Park over the 20th century. Overall, they found that the earliest part of the 20th century decreased in size but grew larger during the 1950s through the 1970s where they then began to decline in area. The dimensions of glaciers started to decrease at an increasing rate during the 1990s, a trend that continues today. The relationship between area change and temperature change mostly agrees (Hoffman et al., 2007; Rangwala and Miller, 2012) with the exception of the earliest 20th century. The period between 1910 and 1930 was cooler, and glaciers should have grown larger in area, rather than shrinking. The discrepancy could be due to imperfect measurements of glacier area and limited air temperatures being available for Colorado during this time. In addition, it is possible that this period, while colder, may not have had significant contribution to annual snowpack during this time. Periods of disagreement occur between the two reconstructed temperatures that result in inverse relationships between chironomid-based temperature curves that correspond to periods of warming from 1935-1955 for Cony, Eagle, and Pipit Lake as well as the warming evident for the period 1995 to the present (2017) for the same lakes plus Black Lake. The addition of Black Lake during this period may be related to changes within the catchment. It is important to note that a change in faunal turnover occurred in A.D. 1957, that may have allowed these trends to become evident during the latter part of the 20th century. While Pipit Lake is not glacially fed, perennial snowfields were present in the immediate catchment surrounding the lake during sampling. The snowmelt emanating from these fields may mirror glacial melt activity as this lake has no vegetation to moderate the influence of meltwater. All lakes sampled, except for Eagle Lake, agreed with overall changes in temperature trends from A.D. 1970 to A.D. 2000, which coincides with a period of cooling and glacial expansion.

The presence of *Diamesa* in the Kite Lake stratigraphy indicated that glacial retreat affected the chironomid communities during the earliest Holocene (Haskett, 2020a; Haskett et al., 2020b). These findings were further substantiated by much colder surface water temperatures close to the Pleistocene-Holocene transition that became increasingly warmer over the Holocene (Haskett et al., 2020b). The inverse relationships visible in the historical reconstructions also exists over much more extended periods in the Kite Lake reconstruction (Figs. 4.11 and 4.12). From ~11,900 to ~11,360 cal yr BP, the reconstructions are inversely related and deviations from the average indicate disagreement between a warming or cooling trend. The relationships are less clear between ~11,900 and ~9,900 cal yr BP as chironomid HCs were missing from some samples and chironomid extraction wasn't possible for others. But the samples bounding this zone indicate that temperature curves become parallel and that overall agreement occurs for the deviations for both SWT and MJAT. This period could reflect a period of stable cooling and glacier expansion. This hypothesis corresponds with evidence that glacial expansion occurred in the Front Range of Colorado between $11,010 \pm 120$ and $9,523 \pm 155$ cal yr BP (Menounos and Reasoner, 1997; Muhs et al., 1999). The relationship between air and water temperature inverts again at ~9,820 cal yr BP and continues for the rest of the record to ~9,230 cal yr BP and may suggest another period of warming and glacial retreat. It should be noted that if the MJAT inference model had been selected, the overall interpretation would have been that air temperatures would continuously decrease following the Younger Dryas. This trend in MJAT temperature change is in disagreement with most paleoenvironmental studies from this area in Colorado (Carrara et al., 1991; Fall, 1997; Reasoner and Jodry, 2000; Jiménez-Moreno and Anderson, 2012).

The relationship between the presence of *Diamesa* and glacial retreat was identified in a recent modern chironomid distribution study (Haskett, 2020). *Diamesa* was only present in lakes

receiving glacial meltwater. This study is unusual in that all lakes with the exception of Box Lake, had subfossil remains of *Diamesa* present in stratigraphical samples. The presence of *Diamesa* was only expected in all three glacially-fed lakes. The presence of this taxon was unexpected in Thunder Lake and Pipit Lake. The relative abundances of *Diamesa* are sporadic and very low in Thunder Lake (~1-2%), but are present in almost every sample and are slightly higher in their relative abundance (1-7%) from Pipit Lake. This relationship substantiates the hypothesis that meltwater emanating from perennial snowfields may mirror glacial retreat in downcore reconstructions. More work is necessary to understand the relationship between species that belong to the subtribe Diamesinae and environmental forces that drive their distribution. To date, the studies that have assessed the response of midges to glacial melt in alpine settings focus on streams (Lods-Crozet, et al., 2001; Milner et al., 2001). More recent studies have found that *Diamesa steinboeckii*, *Diamesa goetghebuerei*, and *Diamesa zernyi* are indicator species for glaciality in alpine streams (Lencioni, 2018). These studies indicate that chironomid communities are responsive to glacier meltwater input; however, there remains a paucity of studies documenting the response of midges to glacial melt in lacustrine settings. This work attempts to contribute to this absence.

The characteristics evident in each of the six lakes presented in this study suggest that within-lake variability, primarily glacial meltwater, may have overridden regional climatic signals. Lake depth, the presence of iron nodules, and the poor-fit between Cony and Black fossil assemblages and modern assemblages from the training set may have also contributed to disagreement between climatic reconstructions. Velle et al. (2005) found a similar problem with the agreement between six cores collected from southern Scandinavia and explored among-site comparisons, the consensus of temperatures, dispersal constraints, productivity changes, and even

chronological uncertainties to address the differences between their sites. Future research in understanding the ecology of chironomids is vital in chironomid work to discuss and refine chironomid reconstructions. Until these relationships are explored further, careful study site selection for paleoclimate research is needed. Unfortunately, this area of study is also limited. “Since chironomids may respond to multiple environmental variables and these may co-vary with the variable of interest, it is important to choose sites where the environmental variables other than the one of interest is likely to have been stable” (Velle et al., 2010). Thunder Lake, a lake that does not receive glacial melt and is well below timberline, was the only lake from this study that showed agreement between the midge-based MJAT, chironomid-based SWT, and PRISM-derived temperatures and followed the description for study selection proposed by Velle et al., 2010.

Of all of the methods to assess agreement between modeled values based on instrumental data and midge-based predicted temperatures, the plotted deviations from averages performed the best and provided clearer visualization of agreement and disagreement between different lake reconstructions. The deviations plotted in Figure 4.8 very clearly indicate periods of discrepancy as well as showing that the deviations from the average SWT align with deviations in PRISM data. These relationships are compelling and should be used in chironomid work in conjunction with temperature reconstructions as they may indicate periods of warming and cooling, rather than stating specific quantitative temperatures that are prone to error. If inverted relationships are evident in the deviations plot, midge-based SWT reconstructions should be used instead of the MJAT inference model even though the performance statistics for SWT are often not as robust. This study is limited and has a small sample size ($n=6$). Future work should not only explore the relationships between chironomid communities and distance away from melting glaciers, but efforts should also include expanding along a longitudinal gradient as well as along an elevational

gradient. Training set creation should endeavor to include lakes receiving meltwater as these assemblages may provide modern analogues for fossil assemblages that often have no modern analogue downcore. This will also refine studies that explore using chironomids as a proxy for the identification of periods of active meltwater input.

CHAPTER 5

CONCLUSIONS

Modern distribution of chironomids in Rocky Mountain National Park, Colorado

Major Findings

The findings from Chapter 2 indicate that the high elevation lakes located in the remote lakes of Rocky Mountain National Park have been impacted by decades of land-use practices and increasing temperatures. Almost all high elevation lakes in this study are no longer oligotrophic and are becoming more productive. Forty-three chironomid taxa were identified from the surface sediment from nine alpine lakes. Redundancy analysis (RDA) found that the distribution of modern chironomid communities was influenced by surface water temperature (SWT), nitrate ($\text{NO}_3+\text{NO}_2\text{-N}$), boron (B), and carbon (C%). However, the relationship between SWT and $\text{NO}_3+\text{NO}_2\text{-N}$ was strongly and negatively correlated (-0.82 , $p=0.007$) and indicates that glacial meltwater is the environmental variable that explains the most variance (15%). Nitrate was not included in the analysis as the presence of both SWT and $\text{NO}_3+\text{NO}_2\text{-N}$, with B and C%, was no longer statistically significant. Surface water temperature was used as it had a higher p-value ($p=0.037$) and explained more variance (7.50%) than $\text{NO}_3+\text{NO}_2\text{-N}$ ($p=0.049$; 7.45%). On average, lakes receiving glacial meltwater were 2.62°C colder and contained 66% more $\text{NO}_3+\text{NO}_2\text{-N}$ than lakes only receiving meltwater from snow. This is the first time that a relationship between boron and chironomid communities was found to the author's knowledge. It is also the first evidence that nitrate is affecting benthic invertebrates in the alpine lakes located in Rocky Mountain National

Park. This finding further substantiates that anthropogenic land-use practices are shaping and influencing remote alpine ecosystems.

The presence of taxa from the subfamily Diamesinae indicates that the lakes in Rocky Mountain National Park are receiving very cold input from running water. These taxa may be useful as qualitative indicator species for the presence of glacial meltwater or melt derived perennial snowfields within a lake catchment. Caution should be used when interpreting temperature paleoreconstructions from stratigraphic subfossil chironomid remains if these taxa are present.

This study contributes to the debate that has raged between chironomid workers over three decades. Many studies have modeled air temperature using transfer functions derived from the relationship between modern air temperatures and chironomid assemblages as surface water temperature and air temperature often covary. This study illustrates that air temperatures can decouple from surface water temperatures and suggests that glacial retreat over varying timescales is likely to influence chironomid communities. Even though inference models of air temperature are often more statistically robust, they may be providing erroneous results.

Uncertainties

This study sampled ten lakes and thus is the only representative of a small sample size. These relationships need to be explored more fully by incorporating lakes along a longitudinal and elevational gradient in the region as well as in other environments that are experiencing glacial retreat. To this end, all sampled lakes lie within proximity to one another as well as being similar in elevation. This limits the influence of air temperature on the assemblages for each lake

as air temperatures were similar. This could explain why the mean July air temperature didn't explain the variance evident in the modern distribution of chironomid communities.

While work in alpine streams has found evidence that Diamesinae is an indicator species of glacial retreat (Lencioni, 2018), little work has explored these taxa in lake sediment. The high presence of Diamesinae in the deposits collected from Rocky Mountain National Park, compared to those found in the WUS calibration set, may indicate that these species are specialists that are endemic to the Front Range. Unfortunately, the taxa could not be identified down to the species level and suggest that these taxa may be newly identified species. Future work will unravel this mystery.

Kite Lake reconstruction

Major Findings

The third chapter explored the transition from the terminal Pleistocene into the Holocene in an alpine lake in the Mosquito Range, Colorado. The climatic amelioration that occurred at this transition was marked by progressive, three-step warming during the entirety of the 3,400-year record of surface water changes, with a brief but significant cooling event at 10,570 cal yr BP. This finding is in sharp contrast to results collected from the Greenland ice sheets that show a dramatic increase of 7°C over five decades (Anderson et al., 2013) and indicate that the response of chironomid response to climatic change is not instantaneous. These results were found using a chironomid-based surface water temperature (SWT) inference model ($r^2_{boot} = 0.38$, RMSEP = 2.74°C) that was developed using a lake training set incorporating 153 lakes from California, Utah, and Colorado. The zone that corresponds to the Younger Dryas chron had no chironomid remains. The beginning of the second zone contained the lowest temperatures from the record ($\bar{x} = 8.2^\circ\text{C}$)

and dramatically increased by 4.7°C at ~11,334 cal yr BP occurred after this period and led to a new stable period that fluctuated around an average SWT of 9.8°C. The indicator species *Diamesa* was found at the base of this zone, suggesting glacial meltwater from the Pinedale Glaciation continued to enter into Kite Lake until ~11,000 cal yr BP. The third zone represents the earliest stable Holocene. The presence of *Cladotanytarsus*, *Paratanytarsus*, and *Procladius* indicates a period of warmth and productivity. SWTs were the highest recorded and averaged 12.5°C.

The Kite Lake stratigraphy contains subfossil chironomid communities that are comprised of environmental specialists that suggest that chironomid communities experience postglacial succession. These conditions consist of a lack of recoverable chironomid head capsules that may indicate the presence of extensive ice cover related to the advancement of glacial conditions. The arrival of a *Tanytarsini*-rich assemblage that also contains Diamesinae may suggest a transitional period of glacial retreat. *Chironomus* begins to appear and to colonize following this assemblage. *C. oliveri* represents an environment that exists in cold tundra conditions above treeline and suggests that climate began to stabilize, but cold temperatures persisted. The appearance *C. ambigua* demarcates the location of the treeline. More research is needed from modern environments experiencing glacial retreat to build modern ecological foundations for this phenomenon in paleoenvironmental interpretations.

Uncertainties

The lack of chironomid head capsules in the oldest sediment suggests that future research is needed to establish mechanisms driving egg mass survival rates for lakes that experience prolonged periods of ice cover. Earlier studies that capture glacial/interglacial cycles have also

demonstrated the lack of subfossil chironomid remains during glacial periods (Axford et al., 2011; Haskett and Porinchu, 2014). The presence of pollen (Jiménez-Moreno and Anderson, 2012) denotes that passive deposition was possible. Thus, Kite Lake experienced short periods of melting ice during the summer growing season, but timing and the extent of ice cover inhibited the survival of chironomid egg masses during this period may be one explanation that could explain the absence of chironomid head capsules during this interval.

The chronology development followed Jiménez-Moreno and Anderson (2012) in order to aid in the comparison between the two proxies chironomids and pollen. This chronology relied on the linear regression between radiocarbon-dated samples. However, sedimentation rates are very rarely linear in deposition and could unduly influence the chronology of this reconstruction.

The model development for surface water temperature is not as statistically robust as previously published models for the western United States (Haskett and Porinchu). Both the root-mean-square error of prediction (RMSEP) and sample-specific errors (SSE) were high at 2.8°C compared to the overall predicted temperatures that had a range of only 5.6°C. However, the magnitude of temperature change was larger than both RMSEP and SSE, suggesting that the reconstruction performs well (Reinemann et al., 2014). The use of the model for surface water temperature (SWT) resulted in higher errors, but this decision was made intentionally as there was evidence that glacial retreat was present during the time-examined, and it was determined that the SWT was the more appropriate temperature to model. Errors were higher as lakes that are often considered “outliers” were left in the calibration set. It is standard in chironomid work to develop the inference model first before identifying outliers. To find outliers in training set data, some authors use an absolute residual (predicted-observed) greater than one standard deviation away from the modeled environmental variable (Jones and Juggins, 1995; Haskett and Porinchu, 2014).

The inclusion of the Front Range lakes may not be appropriate as these systems may not represent natural environments that would have been present during the Pleistocene and early Holocene. Anthropogenic input of atmospheric nitrogen from farming and boron from coal-fired plants are influencing modern chironomid communities. However, SWT was found to be the most statistically significant that explained the most variance in modern chironomid distributions (Chapter 2).

While no chironomids were present in the sediment that corresponded to 10,577 cal yr BP, no work could be completed on the sediment that bounded this sample due to no access to laboratory space for sediment preparation. Thus, the period between 10,340 to 10,813 cal yr BP is poorly resolved. However, future work will remedy this gap and refinement of this portion of the record is expected in the fall of 2020.

Study site selection

Major Findings

For the fourth chapter, chironomids were used to develop temperature reconstructions for mean July air temperature (MJAT) and surface water temperature (SWT) for the 20th and 21st centuries for six alpine lakes in Rocky Mountain National Park, Colorado. These results were compared to extrapolated mean July air temperatures from the PRISM dataset. Glacial meltwater decoupled the signal between air temperature and water temperature and was evident between the relationships between the predicted MJAT and SWT for lakes receiving meltwater from glaciers or perennial snowfields. If inverted relationships between the two temperature reconstructions are apparent, midge-based SWT reconstructions should be used instead of the MJAT. These inverse relationships may also act as a proxy for active meltwater input and may help refine these periods

in reconstructions that cover more extended periods, such as those relationships found in the reconstructions for Kite Lake. The deviations plotted from average SWTs performed better at predicting warming and cooling trends than the midge-based predicted values for MJAT and SWT. However, it should be noted that both midge-based SWT and MJAT performed well when using Bland-Altman Plots. Within-lake variability may account for discrepancies evident between site locations in downcore interpretation. Study site selection is crucial for midge-based thermal reconstructions and basins that receive or have received meltwater should be avoided if modeling MJAT is the objective of the study.

Uncertainties

This study is limited and has a small sample size (n=6). Future work should not only explore the relationships between chironomid communities and distance away from melting glaciers, but efforts should also include expanding along a longitudinal gradient as well as along an elevational gradient. Training set creation should endeavor to include lakes receiving meltwater as these assemblages may provide modern analogs for fossil assemblages that often have no modern analog downcore. This will also refine studies that explore using chironomids as a proxy for the identification of periods of active meltwater input.

This study is the first to explore both MJAT and SWT when compared to instrumental data and may contribute to the debate within the chironomid research community. However, the relationship between recent chironomid communities and their environments is poorly understood and does not satisfy the principle of Uniformitarianism which states that “the present is the key to the past.” Until work establishes and refines the modern relationships between chironomid communities and the multiple factors that may influence their distribution, it is inappropriate to

model temperatures over periods that possess no instrumental data without extreme caution. Work in the statistical refinement of training sets and inference models has significantly expanded over previous decades (Birks, 2012b, Juggins and Birks, 2012), but little effort has been made to satisfy whether their use is appropriate in paleoreconstruction work. Future research in chironomid studies should endeavor to refine the relationship between instrumental data and midge-based reconstructed temperatures.

Long instrumental records are limited for the Rocky Mountains of Colorado. An attempt was made to use data from the Niwot Ridge long-term ecological research site. Unfortunately, the instrument collecting air temperatures is present on a ridge and does not represent lower elevation sites that are influenced by complex topographic relationships. PRISM-derived temperatures were used instead. Unfortunately, very few places have instrumental data above 3000 m asl in this area. No sites currently contribute to the PRISM dataset above 3500m asl (Rangwala et al., 2012). The paucity of these sites may unduly influence air temperatures derived from PRISM (Daly et al., 2008). However, no other instrumental data is available for this area that extends into the earliest 20th century.

Of the six study sites that were examined, no good agreement was evident between any of them and suggests that within-lake variability is influencing chironomid communities. Differing responses were expected and controlled for between paired lakes (i.e., glacial meltwater vs. annual snowmelt), and differences between these lakes were expected. However, differences between placement on the landscape concerning treeline may also have affected chironomid communities. The highest lakes were adjacent to the continental divide and were characterized by harsh environments composed of rock falls, glaciers, and perennial snowfields. Iron nodules were collected from Box Lake stratigraphy during chironomid extraction and indicates that the earliest

period studied underwent changes in oxygen levels. These findings suggest that study site selection is imperative in chironomid work.

REFERENCES

- Adrian, R., O'Reilly, C. M., Zagarese, H., Baines, S. B., Hessen, D. O., Keller, W., ... & Winder, M., 2009. Lakes as sentinels of climate change. *Limnology and Oceanography*, 54(6part2), 2283-2297.
- Alley, R. B., Meese, D. A., Shuman, C. A., & and 8 others., 1993. *Abrupt increase in Greenland snow accumulation at the end of Younger Dryas event.*
- Altman, D.G. and Bland, J.M., 1983. Measurement in medicine: the analysis of method comparison studies. *Journal of the Royal Statistical Society: Series D (The Statistician)*, 32(3), pp.307-317.
- Andersen, F.S., 1938. Spätglaciale Chironomiden. *Medd. Dan. Geol. Foren*, 9, pp.320-326.
- Andersen, T., Cranston, P.S., & Epler, J.H. (Sci. eds), 2013: The larvae of Chironomidae (Diptera) of the Holarctic Region – Keys and diagnoses. – *Insect Systematics & Evolution*, Suppl. 66: 1-571
- Anderson, M.J. and Willis, T.J., 2003. Canonical analysis of principal coordinates: a useful method of constrained ordination for ecology. *Ecology*, 84(2), pp.511-525.
- Appenzeller, T. (2007). The big thaw. *National Geographic*, 211(6), 56-71.
- Appleby, P.G. and Oldfield, F., 1978. The calculation of lead-210 dates assuming a constant rate of supply of unsupported ^{210}Pb to the sediment. *Catena*, 5(1), pp.1-8.
- Axford, Y., Briner, J.P., Francis, D.R., Miller, G.H., Walker, I.R. and Wolfe, A. P., 2011. Chironomids Record terrestrial temperature changes throughout Arctic interglacials of the past 200,000 yr. *GSA Bulletin*, 123: 1275 – 1287.

- Badgley, C. and Gingerich, P.D., 1988. Sampling and faunal turnover in early Eocene mammals. *Palaeogeography, Palaeoclimatology, Palaeoecology*, 63(1-3), pp.141-157.
- Barber, L.B., Murphy, S.F., Verplanck, P.L., Sandstrom, M.W., Taylor, H.E. and Furlong, E.T., 2006. Chemical loading into surface water along a hydrological, biogeochemical, and land use gradient: A holistic watershed approach. *Environmental science & technology*, 40(2), pp.475-486.
- Barko, J.W., Adams, M.S. and Clesceri, N.L., 1986. Environmental factors and their consideration in the management of submersed aquatic vegetation: a review. *Journal of Aquatic Plant Management*, 24(1), pp.1-10.
- Barnett, T. P., Pierce, D. W., Hidalgo, H. G., Bonfils, C., Santer, B. D., Das, T., ... & Dettinger, M. D., 2008. Human-induced changes in the hydrology of the western United States. *Science*, 319(5866), 1080-1083.
- Baron, J. S., Nydick, K. R., Rueth, H. M., Lafrancois, B. M., & Wolfe, A. P., 2005. High elevation ecosystem responses to atmospheric deposition of nitrogen in the Colorado Rocky Mountains, USA. In *Global Change and Mountain Regions* (pp. 429-436). Springer Netherlands.
- Baron, J.S., Schmidt, T.M. and Hartman, M.D., (2009). Climate-induced changes in high elevation stream nitrate dynamics. *Global Change Biology*, 15(7), pp.1777-1789.
- Basagic, H.J. and Fountain, A.G., 2011. Quantifying 20th century glacier change in the Sierra Nevada, California. *Arctic, Antarctic, and Alpine Research*, 43(3), pp.317-330.
- Battarbee, R.W., 2000. Palaeolimnological approaches to climate, with special regard to the biological record. *Quaternary Science Reviews*, 19: 107 – 124.

- Battarbee, R.W., Grytnes, J.A., Thompson, R., Appleby, P.G., Catalan, J., Korhola, A., Birks, H.J.B., Heegaard, E. and Lami, A., 2002. Comparing palaeolimnological and instrumental evidence of climate change for remote mountain lakes over the last 200 years. *Journal of Paleolimnology*, 28(1), pp.161-179.
- Bennett, K.D., 1996. Determination of the number of zones in a biostratigraphical sequence. *New Phytologist*, 132(1), pp.155-170.
- Benson, L., Madole, R., Kubik, P., McDonald, R., 2007. Surface-exposure ages of Front Range moraines that may have formed during the Younger Dryas, 8.2 cal ka, and Little Ice Age events. *Quaternary Science Reviews*, 26: 1638 – 1649.
- Birks, H.J.B., Braak, C.T., Line, J.M., Juggins, S. and Stevenson, A.C., 1990. Diatoms and pH reconstruction. *Philosophical transactions of the royal society of London. B, Biological Sciences*, 327(1240), pp.263-278.
- Birks, H.J.B., 1995. Quantitative palaeoenvironmental reconstructions. *Statistical modelling of quaternary science data. Technical guide*, 5, pp.161-254.
- Birks, H. J. B., 1998. DG Frey and ES Deevey Review 1: Numerical tools in palaeolimnology—Progress, potentialities, and problems. *Journal of Paleolimnology*, 20(4): 307-332.
- Birks, H.J.B., 2012a. Analysis of stratigraphical data. In *Tracking environmental change using lake sediments* (pp. 355-378). Springer, Dordrecht.
- Birks, H.J.B., 2012b. Overview of numerical methods in palaeolimnology. In *Tracking environmental change using lake sediments* (pp. 19-92). Springer, Dordrecht.
- Bland, J.M. and Altman, D., 1986. Statistical methods for assessing agreement between two methods of clinical measurement. *The lancet*, 327(8476), pp.307-310.

- Briles, C. E., Whitlock, C., & Meltzer, D. J. (2012). Last glacial–interglacial environments in the southern Rocky Mountains, USA and implications for Younger Dryas-age human occupation. *Quaternary Research*, 77(1), 96-103.
- Brodersen, K.P. and Lindegaard, C., 1999. Classification, assessment and trophic reconstruction of Danish lakes using chironomids. *Freshwater Biology*, 42(1), pp.143-157.
- Brooks, S.J., Lowe, J.J. and Mayle, F.E., 1997. The Late Devensian Lateglacial palaeoenvironmental record from Whitrig Bog, SE Scotland. 2. Chironomidae (Insecta: Diptera). *Boreas*, 26(4), pp.297-308.
- Brooks, S.J. and Birks, H.J.B., 2000. Chironomid-inferred Late-glacial air temperatures at Whitrig Bog, southeast Scotland. *Journal of Quaternary Science: Published for the Quaternary Research Association*, 15(8), pp.759-764.
- Brooks, S. J., & Birks, H. J. B., 2001. Chironomid-inferred air temperatures from Lateglacial and Holocene sites in north-west Europe: progress and problems. *Quaternary Science Reviews*, 20(16), 1723-1741.
- Brooks, S.J., Bennion, H. and Birks, H.J.B., 2001. Tracing lake trophic history with a chironomid–total phosphorus inference model. *Freshwater Biology*, 46(4), pp.513-533.
- Brooks, S., Langdon P.G., and Heiri, O., 2007. The identification and use of Palaeartic Chironomidae larvae in palaeoecology. QRA Technical Guide No. 10, Quaternary Research Association, London. 276 pp.
- Brooks, S.J., Axford, Y., Heiri, O., Langdon, P.G. and Larocque-Tobler, I., 2012. Chironomids can be reliable proxies for Holocene temperatures. A comment on Velle et al.(2010). *The Holocene*, 22(12), pp.1495-1500.

- Brown, L.E., Hannah, D.M. and Milner, A.M., 2007. Vulnerability of alpine stream biodiversity to shrinking glaciers and snowpacks. *Global Change Biology*, 13(5), pp.958-966.
- Brugger, K.A., Laabs, B., Reimers, A. and Bensen, N., 2019. Late Pleistocene glaciation in the Mosquito Range, Colorado, USA: chronology and climate. *Journal of Quaternary Science*, 34(3), pp.187-202.
- Brundin, L., 1949. Chironomiden und ander Bodentiere de sudschwedischen Urgebirgseen. Ein Beitrag zur Kenntnis der bodenfaunistischen Charakterzuge shwedischer oligotropher Seen. *Report of the Insitute of Freshwater Research, Drottningholm*, 30, pp.1-914.
- Cáceres, M.D. and Legendre, P., 2009. Associations between species and groups of sites: indices and statistical inference. *Ecology*, 90(12), pp.3566-3574.
- Carrara, P.E., D.A. Trimble, and M. Rubin., 1991. Holocene treeline fluctuations in the northern San Juan Mountains, Colorado, U.S.A., as indicated by radiocarbon-dated conifer wood. *Arctic and Alpine Research*, 23 (3): 233-246.
- Carlson, R.E., 1977. A trophic state index for lakes 1. *Limnology and oceanography*, 22(2), pp.361-369.
- Caseldine, C., Geirsdóttir, Á. and Langdon, P., 2003. Efstadalsvatn—a multi-proxy study of a Holocene lacustrine sequence from NW Iceland. *Journal of Paleolimnology*, 30(1), pp.55-73.
- Catalan, J., Pla-Rabés, S., Wolfe, A. P., Smol, J. P., Rühland, K. M., Anderson, N. J., ... & Renberg, I., 2013. Global change revealed by palaeolimnological records from remote lakes: a review. *Journal of paleolimnology*, 49(3), 513-535.

- Chen, I., J.K. Hill, Ohlemuller, R., Roy, D.B., Thomas, C.D., 2011. Rapid range shifts of species associated with high levels of climate warming. *Science*, 333(6045): 1024-1026.
- Chiro Key 2020, viewed 6 February 2020, <http://chirokey.skullisland.info/>
- Chronic, J., 1964. Geology of the Southern Mosquito Range, Colorado. *The Mountain Geologist*.
- Cleveland, W.S. and Loader, C., 1996. Smoothing by local regression: Principles and methods. In *Statistical theory and computational aspects of smoothing* (pp. 10-49). Physica-Verlag HD.
- Cohen, A. S., 2003. *Paleolimnology: the history and evolution of lake systems*. Oxford University Press, USA. pp 85-95; 318-322
- Cristóbal, E., Ayuso, S.V., Justel, A. and Toro, M., 2014. Robust optima and tolerance ranges of biological indicators: a new method to identify sentinels of global warming. *Ecological research*, 29(1), pp.55-68.
- Dahe, Q., Shiyin, L., & Peiji, L., 2006. Snow cover distribution, variability, and response to climate change in western China. *Journal of climate*, 19(9), 1820-1833.
- Daly, C., Halbleib, M., Smith, J.I., Gibson, W.P., Doggett, M.K., Taylor, G.H., Curtis, J. and Pasteris, P.P., 2008. Physiographically sensitive mapping of climatological temperature and precipitation across the conterminous United States. *International Journal of Climatology: a Journal of the Royal Meteorological Society*, 28(15), pp.2031-2064.
- Davison, W., 1993. Iron and manganese in lakes. *Earth-Science Reviews*, 34(2), pp.119-163.
- De Cáceres, M., Legendre, P. and Moretti, M., 2010. Improving indicator species analysis by combining groups of sites. *Oikos*, 119(10), pp.1674-1684.
- Diaz, H. F., & Eischeid, J. K., 2007. Disappearing “alpine tundra” Köppen climatic type in the western United States. *Geophysical Research Letters*, 34(18).

- Dodds, W. and M. Whiles. 2010. Freshwater Ecology: concepts & environmental applications of limnology. *Academic Press*, 1 – 17.
- Dühnforth, M., & Anderson, R. S., 2011. Reconstructing the glacial history of green lakes valley, North Boulder Creek, Colorado front range. *Arctic, Antarctic, and Alpine Research*, 43(4), 527-542.
- Eggermont, H., Heiri, O., Russell, J., Vuille, M., Audenaert, L. and Verschuren, D., 2010. Paleotemperature reconstruction in tropical Africa using fossil Chironomidae (Insecta: Diptera). *Journal of Paleolimnology*, 43(3), pp.413-435.
- Eggermont, H., & Heiri, O., 2012. The chironomid-temperature relationship: expression in nature and palaeoenvironmental implications. *Biological Reviews*, 87(2): 430-456.
- Ehlers, J., Ehlers, J., Gibbard, P.L. and Hughes, P.D. eds., 2011. *Quaternary glaciations-extent and chronology: a closer look* (Vol. 15). Elsevier.
- Elliott, G.P, 2012. Extrinsic regime shifts drive abrupt changes in regeneration dynamics at upper treeline in the Rocky Mountains, USA. *Ecology*, 93 (7): 1614 – 1625.
- Engels, S., Medeiros, A.S., Axford, Y., Brooks, S.J., Heiri, O., Luoto, T.P., Nazarova, L., Porinchu, D.F., Quinlan, R. and Self, A.E., 2019. Temperature change as a driver of spatial patterns and long-term trends in chironomid (Insecta: Diptera) diversity. *Global change biology*.
- Fall, P. L., 1997. Timberline fluctuations and late Quaternary paleoclimates in the Southern Rocky Mountains, Colorado. *Geological Society of America Bulletin*, 109(10), 1306-1320.

- Fenn, M.E., Haeuber, R., Tonnesen, G.S., Baron, J.S., Grossman-Clarke, S., Hope, D., Jaffe, D.A., Copeland, S., Geiser, L., Rueth, H.M. and Sickman, J.O., 2003. Nitrogen emissions, deposition, and monitoring in the western United States. *BioScience*, 53(4), pp.391-403.
- Ferrington, L.C., 2007. Global diversity of non-biting midges (Chironomidae; Insecta-Diptera) in freshwater. In *Freshwater animal diversity assessment* (pp. 447-455). Springer, Dordrecht.
- Fountain, A.G., Hoffman, M., Jackson, K., Basagic, H., Nysten, T. and Percy, D., 2007. *Digital outlines and topography of the glaciers of the American West* (No. 2006-1340). US Geological Survey.
- Fortin, M.C., Medeiros, A.S., Gajewski, K., Barley, E.M., Larocque-Tobler, I., Porinchu, D.F. and Wilson, S.E., 2015. Chironomid-environment relations in northern North America. *Journal of paleolimnology*, 54(2-3), pp.223-237.
- Francis, D.R., 2004. Distribution of midge remains (Diptera: Chironomidae) in surficial lake sediments in New England. *Northeastern Naturalist*, 11(4), pp.459-479.
- Frouz, J. and Kindlmann, P., 2001. The role of sink to source re-colonisation in the population dynamics of insects living in unstable habitats: an example of terrestrial chironomids. *Oikos*, 93(1), pp.50-58.
- Garzke, J., Connor, S.J., Sommer, U. and O'Connor, M.I., 2019. Trophic interactions modify the temperature dependence of community biomass and ecosystem function. *PLoS biology*, 17(6), p.e2006806.
- Giavarina, D., 2015. Understanding bland altman analysis. *Biochimica medica: Biochimica medica*, 25(2), pp.141-151.

- Ginn, B.K., Cumming, B.F. and Smol, J.P., 2007. Diatom-based environmental inferences and model comparison from 494 Northeastern North American lakes. *Journal of Phycology*, 43(4), pp.647-661.
- Glew, J.R., 1988. A portable extruding device for close interval sectioning of unconsolidated core samples. *Journal of Paleolimnology*, 1(3), pp.235-239.
- Goebel, T., Hockett, B., Adams, K. D., Rhode, D., & Graf, K., 2011. Climate, environment, and humans in North America's Great Basin during the Younger Dryas, 12,900–11,600 calendar years ago. *Quaternary International*, 242(2), 479-501.
- Greaver, T.L., Clark, C.M., Compton, J.E., Vallano, D., Talhelm, A.F., Weaver, C.P., Band, L.E., Baron, J.S., Davidson, E.A., Tague, C.L. and Felker-Quinn, E., (2016). Key ecological responses to nitrogen are altered by climate change. *Nature Climate Change*, 6(9), p.836.
- Haeblerli, W., & Beniston, M., 1998. Climate change and its impacts on glaciers and permafrost in the Alps. *Ambio*, 258-265.
- Hall, M. H., & Fagre, D. B., 2003. Modeled climate-induced glacier change in Glacier National Park, 1850–2100. *BioScience*, 53(2), 131-140.
- Haskett, D.R. and Porinchu, D.F., 2013. *A quantitative midge-based reconstruction of thermal conditions in central Colorado during marine isotope stage 5* (Doctoral dissertation, University of Georgia).
- Haskett, D. R., & Porinchu, D. F., 2014. A quantitative midge-based reconstruction of mean July air temperature from a high-elevation site in central Colorado, USA, for MIS 6 and 5. *Quaternary Research*, 82(3), 580-591.

- Haskett, D.R., 2020. Is Glacial Retreat Impacting Modern Benthic Chironomid Communities? A Case Study from Rocky Mountain National Park, Colorado. In prep for *Oceanography and Limnology (In prep)*.
- Haskett, D.R., Jiménez-Moreno, G., and Anderson, R.S., 2020. Chironomid evidence of glacial retreat and corresponding changes in surface water temperatures during the Pleistocene-Holocene transition from an alpine lake in Colorado, USA. In prep for *The Holocene. (In Prep)*.
- Haynes, K., Fearnhead, P. and Eckley, I.A., 2016. changepoint. np: Methods for nonparametric changepoint detection. R package version 0.0, 2.
- Haynes, K., Fearnhead, P. and Eckley, I.A., 2017. A computationally efficient nonparametric approach for changepoint detection. *Statistics and Computing*, 27(5), pp.1293-1305.
- Heino, L. O., R. Virkkala and H. Toivonen, 2009. Climate change and freshwater biodiversity detected patterns, future trends and adaptations in northern regions. *Biological Reviews* 84: 39 – 54.
- Heiri, O., & Lotter, A. F., 2001. Effect of low count sums on quantitative environmental reconstructions: an example using subfossil chironomids. *Journal of Paleolimnology*, 26(3), 343-350.
- Heiri, O., Brooks, S.J., Birks, H.J.B. and Lotter, A.F., 2011. A 274-lake calibration data-set and inference model for chironomid-based summer air temperature reconstruction in Europe. *Quaternary Science Reviews*, 30(23-24), pp.3445-3456.
- Hill, M.O. and Gauch, H.G., 1980. Detrended correspondence analysis: an improved ordination technique. In *Classification and ordination* (pp. 47-58). Springer, Dordrecht.

- Hoffman, M. J., Fountain, A. G., & Achuff, J. M., 2007. 20th-century variations in area of cirque glaciers and glacierets, Rocky Mountain National Park, Rocky Mountains, Colorado, USA. *Annals of Glaciology*, 46(1), 349-354.
- Holland, S.M., 2008. Detrended Correspondence Analysis (DCA).
<http://strata.uga.edu/software/pdf/dcaTutorial.pdf>
- Hood, E., & Berner, L., 2009. Effects of changing glacial coverage on the physical and biogeochemical properties of coastal streams in southeastern Alaska. *Journal of Geophysical Research: Biogeosciences (2005–2012)*, 114(G3).
- Horne, A.J. and Goldman, C.R., 1994. Limnology (Vol. 2). New York: McGraw-Hill.
- Ilyashuk, B., Gobet, E., Heiri, O., Lotter, A.F., van Leeuwen, J.F., van der Knaap, W.O., Ilyashuk, E., Oberli, F. and Ammann, B., 2009. Lateglacial environmental and climatic changes at the Maloja Pass, Central Swiss Alps, as recorded by chironomids and pollen. *Quaternary Science Reviews*, 28(13-14), pp.1340-1353.
- Ilyashuk, E.A., Ilyashuk, B.P., Tylmann, W., Koinig, K.A. and Psenner, R., 2015. Biodiversity dynamics of chironomid midges in high-altitude lakes of the Alps over the past two millennia. *Insect Conservation and Diversity*, 8(6), pp.547-561.
- Ilyashuk, E.A., Ilyashuk, B.P., Heiri, O., Starnberger, R. and Spötl, C., 2019. The second Early Wurmian Interstadial recorded in palaeolake sediments from the Alp (Austria): Chironomid-based summer temperature inferences. *International Multidisciplinary Scientific GeoConference: SGEM*, 19(1.1), pp.663-668.
- Jiménez-Moreno, G., & Anderson, R. S., 2012. Pollen and macrofossil evidence of Late Pleistocene and Holocene treeline fluctuations from an alpine lake in Colorado, USA. *The Holocene*, 0959683612450199.

- Jones, V.J. and Juggins, S., 1995. The construction of a diatom-based chlorophyll a transfer function and its application at three lakes on Signy Island (maritime Antarctic) subject to differing degrees of nutrient enrichment. *Freshwater biology*, 34(3), pp.433-445.
- Juggins, S., & Birks, H. J. B., 2012. Quantitative environmental reconstructions from biological data. In *Tracking environmental change using lake sediments* (pp. 431-494). Springer Netherlands.
- Juggins, S. and Juggins, M.S., 2019. Package 'rioja'.
- Keleher, C.J. and Rahel, F.J., 1996. Thermal limits to salmonid distributions in the Rocky Mountain region and potential habitat loss due to global warming: a geographic information system (GIS) approach. *Transactions of the American Fisheries society*, 125(1), pp.1-13.
- Kellogg, K. S., Bryant, B., & Reed, J. C., 2004. The Colorado Front Range—Anatomy of a Laramide uplift. *Field Guides*, 5, 89-108.
- Khamis, K., Hannah, D. M., Clarvis, M. H., Brown, L. E., Castella, E., & Milner, A. M., 2014. Alpine aquatic ecosystem conservation policy in a changing climate. *Environmental Science & Policy*, 43, 39-55.
- Killick, R., Fearnhead, P. and Eckley, I.A., 2012. Optimal detection of changepoints with a linear computational cost. *Journal of the American Statistical Association*, 107(500), pp.1590-1598.
- Kittel, T., White, C., Hartman, M., Chowanski, K., Ackerman, T., Williams, M. and Losleben, M., 2019. Infilled air temperature data for D1 chart recorder, 1952-2018, daily.
- Kotrys, B., Płóciennik, M., Sydor, P. and Brooks, S.J., 2020. Expanding the Swiss-Norwegian chironomid training set with Polish data. *Boreas*, 49(1), pp.89-107.

- Kurek, J., Cwynar, L.C. and Spear, R.W., 2004. The 8200 cal yr BP cooling event in eastern North America and the utility of midge analysis for Holocene temperature reconstructions. *Quaternary Science Reviews*, 23(5-6), pp.627-639.
- Kurek, J. and Cwynar, L.C., 2009. Effects of within-lake gradients on the distribution of fossil chironomids from maar lakes in western Alaska: implications for environmental reconstructions. *Hydrobiologia*, 623(1), pp.37-52.
- Langdon, P.G., Ruiz, Z.O.E., Wynne, S., Sayer, C.D. and Davidson, T.A., 2010. Ecological influences on larval chironomid communities in shallow lakes: implications for palaeolimnological interpretations. *Freshwater Biology*, 55(3), pp.531-545.
- Larocque, I., 2001. How many chironomid head capsules are enough? A statistical approach to determine sample size for palaeoclimatic reconstructions. *Palaeogeography, Palaeoclimatology, Palaeoecology*, 172(1), 133-142.
- Larocque, I., Hall, R.I. and Grahn, E., 2001. Chironomids as indicators of climate change: a 100-lake training set from a subarctic region of northern Sweden (Lapland). *Journal of Paleolimnology*, 26(3), pp.307-322.
- Larocque, I. and Hall, R.I., 2003. Chironomids as quantitative indicators of mean July air temperature: validation by comparison with century-long meteorological records from northern Sweden. *Journal of Paleolimnology*, 29(4), pp.475-493.
- Larocque, I., Grosjean, M., Heiri, O., Bigler, C. and Blass, A., 2009. Comparison between chironomid-inferred July temperatures and meteorological data AD 1850–2001 from varved Lake Silvaplana, Switzerland. *Journal of Paleolimnology*, 41(2), pp.329-342.

- Larocque-Tobler, I., Filipiak, J., Tylmann, W., Bonk, A. and Grosjean, M., 2015. Comparison between chironomid-inferred mean-August temperature from varved Lake Żabińskie (Poland) and instrumental data since 1896 AD. *Quaternary Science Reviews*, 111, pp.35-50.
- Lehnert, B. and Lehnert, M.B., 2015. Package “BlandAltmanLeh.”. CRAN. Available online: <https://cran.r-project.org/web/packages/BlandAltmanLeh/BlandAltmanLeh.pdf> (accessed on 15 October 2016).
- Legendre, P. and Birks, H.J.B., 2012. From classical to canonical ordination. In Tracking environmental change using lake sediments (pp. 201-248). Springer, Dordrecht.
- Legendre, P. and Legendre, L., 2012. Numerical ecology. 3rd English ed. *Developments in environmental modelling*, 24.
- Lehnert, B. and Lehnert, M.B., 2015. Package “BlandAltmanLeh.”. CRAN. Available online: <https://cran.r-project.org/web/packages/BlandAltmanLeh/BlandAltmanLeh.pdf> (accessed on 15 October 2016).
- Lencioni, V., 2018. Glacial influence and stream macroinvertebrate biodiversity under climate change: Lessons from the Southern Alps. *Science of the Total Environment*, 622, pp.563-575.
- Leonard, E.M., Laabs, B.J.B., Schweinsberg, A.D., Russell, C.M., Briner, J.P. and Young, N.E., 2017. Deglaciation of the Colorado Rocky Mountains following the Last Glacial Maximum. *Cuadernos de Investigación Geográfica*, 43(2), pp.497-526.
- Levesque, A.J., Cwynar, L.C. and Walker, I.R., 1996. Richness, diversity and succession of late-glacial chironomid assemblages in New Brunswick, Canada. *Journal of Paleolimnology*, 16(3), pp.257-274.

- Licciardi, J. M., Clark, P. U., Brook, E. J., Elmore, D., & Sharma, P., 2004. Variable responses of western US glaciers during the last deglaciation. *Geology*, 32(1), 81-84.
- Little, J.L. and Smol, J.P., 2001. A chironomid-based model for inferring late-summer hypolimnetic oxygen in southeastern Ontario lakes. *Journal of Paleolimnology*, 26(3), pp.259-270.
- Livingstone, D.M., Lotter, A.F. and Walkery, I.R., 1999. The decrease in summer surface water temperature with altitude in Swiss Alpine lakes: a comparison with air temperature lapse rates. *Arctic, Antarctic, and Alpine Research*, 31(4), pp.341-352.
- Lods-Crozet, B., Castella, E., Cambin, D., Ilg, C., Knispel, S., & Mayor-Simeant, H., 2001. Macroinvertebrate community structure in relation to environmental variables in a Swiss glacial stream. *Freshwater Biology*, 46(12), 1641-1661.
- Lotter, A. F., Birks, H. J. B., Hofmann, W., & Marchetto, A., 1997. Modern diatom, cladocera, chironomid, and chrysophyte cyst assemblages as quantitative indicators for the reconstruction of past environmental conditions in the Alps. I. Climate. *Journal of Paleolimnology*, 18(4), 395-420.
- Lotter, A.F., Walker, I.R., Brooks, S.J. and Hofmann, W., 1999. An intercontinental comparison of chironomid palaeotemperature inference models: Europe vs North America. *Quaternary Science Reviews*, 18(6), pp.717-735.
- Luoto, T.P. and Ojala, A.E., 2017. Meteorological validation of chironomids as a paleotemperature proxy using varved lake sediments. *The Holocene*, 27(6), pp.870-878.

- MacDonald, G. M., Moser, K. A., Bloom, A. M., Porinchu, D. F., Potito, A. P., Wolfe, B. B., ... & Orme, A. J., 2008. Evidence of temperature depression and hydrological variations in the eastern Sierra Nevada during the Younger Dryas stade. *Quaternary Research*, 70(2), 131-140.
- Madole, R. F. (1976). Glacial geology of the front range, Colorado. *Quaternary Stratigraphy of North America*, 297-318.
- Maier, K.J. and Knight, A.W., 1991. The toxicity of waterborne boron to *Daphnia magna* and *Chironomus decorus* and the effects of water hardness and sulfate on boron toxicity. *Archives of environmental contamination and toxicology*, 20(2), pp.282-287.
- Mark, B.G. and Fernández, A., 2017. The significance of mountain glaciers as sentinels of climate and environmental change. *Geography Compass*, 11(6), p.e12318.
- Markgraf, V., & Scott, L., 1981. Lower timberline in central Colorado during the past 15,000 yr. *Geology*, 9(5), 231-234.
- McDonough, Jaffe, D., and Watzin, M., 2012. "Indicator species". In: *Encyclopedia of Earth*. Eds. Cutler J. Cleveland (Washington, D.C.: Environmental Information Coalition, National Council for Science and the Environment). [First published in the *Encyclopedia of Earth* December 18, 2009; Last revised Date June 11, 2012; Retrieved September 28, 2012 <http://www.eoearth.org/article/Indicator_species?topic=58074>
- McGarrigle, M.L., 1980. The distribution of chironomid communities and controlling sediment parameters in L. Derravaragh, Ireland. In *Chironomidae* (pp. 275-282). Pergamon.
- Menounos, B. and Reasoner, M.A., 1997. Evidence for cirque glaciation in the Colorado Front Range during the Younger Dryas chronozone. *Quaternary Research*, 48(1), pp.38-47.

- Messner, J. S., Maclennan, M. M., & Vinebrooke, R. D., 2013. Higher temperatures enhance the effects of invasive sportfish on mountain zooplankton communities. *Freshwater Biology*, 58(2), 354-364.
- Meyers, P.A. and Ishiwatari, R., 1993. Lacustrine organic geochemistry—an overview of indicators of organic matter sources and diagenesis in lake sediments. *Organic geochemistry*, 20(7), pp.867-900.
- Michelutti, N., Wolfe, A. P., Cooke, C. A., Hobbs, W. O., Vuille, M., & Smol, J. P., 2015. Climate change forces new ecological states in tropical Andean lakes. *PloS one*, 10(2), e0115338.
- Milner, A. M., Brittain, J. E., Castella, E., & Petts, G. E., 2001. Trends of macroinvertebrate community structure in glacier-fed rivers in relation to environmental conditions: a synthesis. *Freshwater Biology*, 46(12), 1833-1847.
- Moore, R. D., Fleming, S. W., Menounos, B., Wheate, R., Fountain, A., Stahl, K., ... & Jakob, M., 2009. Glacier change in western North America: influences on hydrology, geomorphic hazards and water quality. *Hydrological Processes*, 23(1), 42.
- Moss, S.A. and Nagpal, N.K., 2003. *Ambient water quality guidelines for boron*. Water Protection Section, Ministry of Water, Land and Air Protection.
- Muhs, D.R., Aleinikoff, J.N., Stafford Jr, T.W., Kihl, R., Been, J., Mahan, S.A. and Cowherd, S., 1999. Late Quaternary loess in northeastern Colorado: Part I—Age and paleoclimatic significance. *Geological Society of America Bulletin*, 111(12), pp.1861-1875.
- Munroe, J. S., Crocker, T. A., Giesche, A. M., Rahlson, L. E., Duran, L. T., Bigl, M. F., & Laabs, B. J., 2012. A lacustrine-based Neoglacial record for Glacier National Park, Montana, USA. *Quaternary Science Reviews*, 53, 39-54.

- Nicacio, G. and Juen, L., 2015. Chironomids as indicators in freshwater ecosystems: an assessment of the literature. *Insect Conservation and Diversity*, 8(5), pp.393-403.
- Oksanen, J., Blanchet, F.G., Kindt, R., Legendre, P., Minchin, P.R., O'Hara, R.B., Simpson, G.L., Solymos, P., Henry, M., Stevens, H. and Wagner, H., 2014. Package 'vegan'. *Community Ecology Package, R Package Version*, 2(2).
- Oksanen, J., 2015. Vegan: an introduction to ordination. URL <http://cran.r-project.org/web/packages/vegan/vignettes/introvegan.pdf>, 8, p.19.
- Olander, H., H. J. B. Birks, A. Korhola and T. Blom, 1999. An expanded calibration model for inferring lakewater and air temperatures from fossil chironomid assemblages in northern Fennoscandia. *The Holocene*, 9(3): 279 – 294.
- Outcalt, S. I., & MacPhail, D. D., 1965. *A survey of Neoglaciation in the Front Range of Colorado*. Boulder: University of Colorado Press.
- Oviatt, C.G., 1997. Lake Bonneville fluctuations and global climate change. *Geology*, 25(2), pp.155-158.
- Pederson, G. T., Gray, S. T., Woodhouse, C. A., Betancourt, J. L., Fagre, D. B., Littell, J. S., ... & Graumlich, L. J., 2011. The unusual nature of recent snowpack declines in the North American Cordillera. *Science*, 333(6040), 332-335.
- Pepin, N., & Losleben, M., 2002. Climate change in the Colorado Rocky Mountains: free air versus surface temperature trends. *International journal of climatology*, 22(3), 311-329.
- Pepin, N.C. and Lundquist, J.D., 2008. Temperature trends at high elevations: patterns across the globe. *Geophysical Research Letters*, 35(14).
- Pinder, L.C.V., 1986. Biology of freshwater Chironomidae. *Annual review of entomology*, 31(1), pp.1-23.

- Pinder, L.C.V., 1995. The habitats of chironomid larvae. In *The Chironomidae* (pp. 107-135). Springer, Dordrecht.
- Porinchu, D.F. and Cwynar, L.C., 2000. The Distribution of Freshwater Chironomidae (Insecto: Diptera) across Treeline near the Lower Lena River, Northeast Siberia, Russia. *Arctic, Antarctic, and Alpine Research*, 32(4), pp.429-437.
- Porinchu, D.F., MacDonald, G.M., Bloom, A.M. and Moser, K.A., 2002. The modern distribution of chironomid sub-fossils (Insecta: Diptera) in the Sierra Nevada, California: potential for paleoclimatic reconstructions. *Journal of Paleolimnology*, 28(3), pp.355-375.
- Porinchu, D. F., MacDonald, G. M., Bloom, A. M., & Moser, K. A., 2003. Late Pleistocene and early Holocene climate and limnological changes in the Sierra Nevada, California, USA inferred from midges (Insecta: Diptera: Chironomidae). *Palaeogeography, Palaeoclimatology, Palaeoecology*, 198(3), 403-422.
- Porinchu, D.F. and MacDonald, G.M., 2003. The use and application of freshwater midges (Chironomidae: Insecta: Diptera) in geographical research. *Progress in Physical Geography*, 27(3), pp.378-422.
- Porinchu, D.F., Moser, K.A., and Munroe, J.S., 2007. Development of a midge-based summer surface water temperature inference model for the Great Basin of the Western United States. *Arctic, Antarctic and Alpine Research* 39, 4: 566 – 577.
- Porinchu, D. F., Reinemann, S., Mark, B.G., Box, J.E., and Rolland, N., 2010. Application of a midge-based inference model for air temperature reveals evidence of late-20th century warming in sub-alpine lakes in the central Great Basin, United States. *Quaternary International* 215, 1-2: 15 – 26.

- Porinchu, D.F., Haskett, D.R. and Reinemann, S.A., 2017. Biostratigraphic evidence of human modification of high elevation aquatic ecosystems in the Intermountain West of the United States. *Anthropocene*, 20, pp.37-47.
- Prentice, I.C., 1980. Multidimensional scaling as a research tool in Quaternary palynology: a review of theory and methods, *Review of Palaeobotany and Palynology* 31, 71-104.
- PRISM Climate Group, Oregon State University, <http://prism.oregonstate.edu>, Accessed 20, January, 2020.
- Quinlan, R., & Smol, J. P., 2001. Setting minimum head capsule abundance and taxa deletion criteria in chironomid-based inference models. *Journal of Paleolimnology*, 26(3), 327-342.
- R Development Core Team, 2020. <http://www.R-project.org>, Accessed 6 February, 2020.
- Rangwala, I. and Miller, J.R., 2010. Twentieth century temperature trends in Colorado's San Juan Mountains. *Arctic, Antarctic, and Alpine Research*, 42(1), pp.89-97.
- Rangwala, I. and Miller, J.R., 2012. Climate change in mountains: a review of elevation-dependent warming and its possible causes. *Climatic Change*, 114(3-4), pp.527-547.
- Rasmussen, S. O., Andersen, K. K., Svensson, A. M., Steffensen, J. P., Vinther, B. M., Clausen, H. B., ... & Ruth, U., 2006. A new Greenland ice core chronology for the last glacial termination. *Journal of Geophysical Research: Atmospheres (1984–2012)*, 111(D6).
- Reasoner, M. A., & Jodry, M. A., 2000. Rapid response of alpine timberline vegetation to the Younger Dryas climate oscillation in the Colorado Rocky Mountains, USA. *Geology*, 28(1), 51-54.

- Rees, A.B., Cwynar, L.C. and Cranston, P.S., 2008. Midges (Chironomidae, Ceratopogonidae, Chaoboridae) as a temperature proxy: a training set from Tasmania, Australia. *Journal of Paleolimnology*, 40(4), pp.1159-1178.
- RMNP, 2006. Vegetation restoration management plan version 2:
http://www.nps.gov/romo/learn/management/upload/vegetation_restoration_management_plan_ver2.pdf
- Rosenzweig, C., Casassa, G., Karoly, D. J., Imeson, A., Liu, C., Menzel, A., ... & Hanson, C. E., 2007. Assessment of observed changes and responses in natural and managed systems. *Climate change*, 79-131.
- Rossaro, B., Montagna, M. and Lencioni, V., 2016. Environmental traits affect chironomid communities in glacial areas of the Southern Alps: evidence from a long-lasting case study. *Insect Conservation and Diversity*, 9(3), pp.192-201.
- Saether, O.A., 1979. Chironomid communities as water quality indicators. *Ecography*, 2(2), pp.65-74.
- Saiki, M.K., Jennings, M.R. and Brumbaugh, W.G., 1993. Boron, molybdenum, and selenium in aquatic food chains from the lower San Joaquin River and its tributaries, California. *Archives of environmental contamination and toxicology*, 24(3), pp.307-319.
- Salonen, J.S., Ilvonen, L., Seppä, H., Holmström, L., Telford, R.J., Gaidamavičius, A., Stančikaitė, M. and Subetto, D., 2012. Comparing different calibration methods (WA/WA-PLS regression and Bayesian modelling) and different-sized calibration sets in pollen-based quantitative climate reconstruction. *The Holocene*, 22(4), pp.413-424.

- Saros, J. E., Clow, D. W., Blett, T., & Wolfe, A. P., 2011. Critical nitrogen deposition loads in high-elevation lakes of the western US inferred from paleolimnological records. *Water, Air, & Soil Pollution*, 216(1-4), 193-202.
- Saulnier-Talbot, É. and Pienitz, R., 2010. Postglacial chironomid assemblage succession in northernmost Ungava Peninsula, Canada. *Journal of Quaternary Science*, 25(2), pp.203-213.
- Schindler, D. W. 2009. Lakes as sentinels and integrators for the effects of climate change on watersheds, airsheds, and landscapes. *Limnology and Oceanography*, 54(6part2), 2349-2358.
- Schütz, S.A. and Füreder, L., 2019. Egg development and hatching success in alpine chironomids. *Freshwater biology*, 64(4), pp.685-696.
- Simpson, G.L. and Oksanen, J., 2013. analogue: analogue matching and Modern Analogue Technique transfer function models (R package version 0.12–0).
- Simpson, G.L., Oksanen, J. and Simpson, M.G.L., 2019. Package ‘analogue’.
- Slemmons, K. E., Saros, J. E., & Simon, K., 2013. The influence of glacial meltwater on alpine aquatic ecosystems: a review. *Environmental Science: Processes & Impacts*, 15(10), 1794-1806.
- Slemmons, K. E., Saros, J. E., Stone, J. R., McGowan, S., Hess, C. T., & Cahl, D., 2015. Effects of glacier meltwater on the algal sedimentary record of an alpine lake in the central US Rocky Mountains throughout the late Holocene. *Journal of Paleolimnology*, 53(4), 385-399.

- Slemmons, K.E., Rodgers, M.L., Stone, J.R. and Saros, J.E., 2017. Nitrogen subsidies in glacial meltwaters have altered planktonic diatom communities in lakes of the US Rocky Mountains for at least a century. *Hydrobiologia*, 800(1), pp.129-144.
- Smol, J. P., & Douglas, M. S., 2007. From controversy to consensus: making the case for recent climate change in the Arctic using lake sediments. *Frontiers in Ecology and the Environment*, 5(9), 466-474.
- Smol, J.P., 2010. The power of the past: using sediments to track the effects of multiple stressors on lake ecosystems. *Freshwater Biology*, 55, pp.43-59.
- Stocker, T. F., Qin, D., Plattner, G. K., Tignor, M., Allen, S. K., & Boschung, J., 2013. Climate Change 2013: The Physical Science Basis. Working Group 1 (WG1) Contribution to the Intergovernmental Panel on Climate Change (IPCC) 5th Assessment Report (AR5). Cambridge, United Kingdom and New York, NY.
- Stoeser, D.B., Green, G.N., Morath, L.C., Heran, W.D., Wilson, A.B., Moore, D.W. and Gosen, B.S.V., 2005. Preliminary integrated geologic map databases for the United States. *US Geological Survey, Open-File Report, 2005-1351*.
- Stuiver, M., Reimer, P.J., Bard, E., Beck, J.W., Burr, G.S., Hughen, K.A., Kromer, B., McCormac, G., Van Der Plicht, J. and Spurk, M., 1998. INTCAL98 radiocarbon age calibration, 24,000–0 cal BP. *Radiocarbon*, 40(3), pp.1041-1083.
- Stumm, D., SCHMID, M., Gruber, S., Baral, P., Shahi, S., Shrestha, T. and Wester, P., 2015. Manual for Mapping Rock Glaciers in Google Earth. *Kathmandu: International Centre For Integrated Mountain Development (ICIMOD)*.
- Swarzenski, P.W., 2014. 210Pb dating. *Encyclopedia of Scientific Dating Methods*; Rink, WJ, Thompson, JW, Eds, pp.626-631.

- Team, R.C., 2013. R: A language and environment for statistical computing.
- Telford, R.J. and Birks, H.J.B., 2011a. Effect of uneven sampling along an environmental gradient on transfer-function performance. *Journal of Paleolimnology*, 46(1), p.99.
- Telford, R.J. and Birks, H.J.B., 2011b. A novel method for assessing the statistical significance of quantitative reconstructions inferred from biotic assemblages. *Quaternary Science Reviews*, 30(9-10), pp.1272-1278.
- Telford, R., Trachsel, M. and Telford, M.R., 2019. Package 'palaeoSig'.
- ter Braak, C.J. and Barendregt, L.G., 1986. Weighted averaging of species indicator values: its efficiency in environmental calibration. *Mathematical Biosciences*, 78, pp.57-72.
- ter Braak, C.J.F., Juggins, S., Birks, H.J.B. and Van der Voet, H., 1993. Weighted averaging partial least squares regression (WA-PLS): definition and comparison with other methods for species-environment calibration. In *Multivariate environmental statistics* (No. 6, pp. 525-560). Elsevier.
- ter Braak, C.J. and Barendregt, L.G., 1986. Weighted averaging of species indicator values: its efficiency in environmental calibration. *Mathematical Biosciences*, 78, pp.57-72.
- ter Braak, C. J., and Juggins, S., 1993. Weighted averaging partial least squares regression (WA-PLS): an improved method for reconstructing environmental variables from species assemblages. *Hydrobiologia*, 269(1), 485-502.
- ter Braak, C.J. and Verdonschot, P.F., 1995. Canonical correspondence analysis and related multivariate methods in aquatic ecology. *Aquatic sciences*, 57(3), pp.255-289.
- Thies, H., Nickus, U., Mair, V., Tessadri, R., Tait, D., Thaler, B., & Psenner, R., 2007. Unexpected response of high alpine lake waters to climate warming. *Environmental science & technology*, 41(21), 7424-7429.

- Turner, L.J. and Delorme, L.D., 1996. Assessment of ²¹⁰Pb data from Canadian lakes using the CIC and CRS models. *Environmental Geology*, 28(2), pp.78-87.
- Van Den Wollenberg, A.L., 1977. Redundancy analysis an alternative for canonical correlation analysis. *Psychometrika*, 42(2), pp.207-219.
- van der Voet, H., 1994. Comparing the predictive accuracy of models using a simple randomization test. *Chemometrics and intelligent laboratory systems*, 25(2), pp.313-323.
- van Mantgem, P. J., Stephenson, N. L., Knapp, E., Battles, J., & Keeley, J. E., 2011. Long-term effects of prescribed fire on mixed conifer forest structure in the Sierra Nevada, California. *Forest Ecology and Management*, 261(6), 989-994.
- Velle, G., Brooks, S.J., Birks, H.J.B. and Willassen, E., 2005. Chironomids as a tool for inferring Holocene climate: an assessment based on six sites in southern Scandinavia. *Quaternary Science Reviews*, 24(12-13), pp.1429-1462.
- Velle, G., Brodersen, K.P., Birks, H.J.B. and Willassen, E., 2010. Midges as quantitative temperature indicator species: Lessons for palaeoecology. *The Holocene*, 20(6), pp.989-1002.
- Velle, G., Brodersen, K.P., Birks, H.J.B. and Willassen, E., 2012a. Inconsistent results should not be overlooked: A reply to Brooks et al.(2012). *The Holocene*, 22(12), pp.1501-1508.
- Velle, G., Telford, R.J., Heiri, O., Kurek, J. and Birks, H.J.B., 2012b. Testing intra-site transfer functions: an example using chironomids and water depth. *Journal of paleolimnology*, 48(3), pp.545-558.
- Verbruggen, F., Heiri, O., Meriläinen, J.J. and Lotter, A.F., 2011. Subfossil chironomid assemblages in deep, stratified European lakes: relationships with temperature, trophic state and oxygen. *Freshwater Biology*, 56(3), pp.407-423.

- Vierling, L. A., 1998. Palynological evidence for late-and postglacial environmental change in central Colorado. *Quaternary Research*, 49(2), 222-232.
- Walker, I. R., 1987. Chironomidae (diptera) in paleoecology. *Quaternary Science Review*, 6: 29 – 40.
- Walker, I.R. and Mathewes, R.W., 1987. Chironomids, lake trophic status, and climate. *Quaternary Research*, 28(3), pp.431-437.
- Walker, I.R. and Mathewes, R.W., 1988. Late-Quaternary Fossil Chironomidae (Diptera) from Hippa Lake, Queen Charlotte Islands, British Columbia, with Special Reference to *Corynocera* Zett. *The Canadian Entomologist*, 120(8-9), pp.739-751.
- Walker, I.R. and Mathewes, R.W., 1990. Early postglacial chironomid succession in southwestern British Columbia, Canada, and its paleoenvironmental significance. *In Paleolimnology and the Reconstruction of Ancient Environments* (pp. 147-160). Springer, Dordrecht.
- Walker, I. R., Smol, J. P., Engstrom, D. R., & Birks, H. J. B., 1991. An assessment of Chironomidae as quantitative indicators of past climatic change. *Canadian Journal of Fisheries and Aquatic Sciences*, 48(6), 975-987.
- Walker, I.R., 1993. Paleolimnological biomonitoring using freshwater benthic macroinvertebrates. *Freshwater biomonitoring and benthic macroinvertebrates*, pp.306-343.
- Walker, I.R., Levesque, A.J., Cwynar, L.C. and Lotter, A.F., 1997. An expanded surface-water palaeotemperature inference model for use with fossil midges from eastern Canada. *Journal of Paleolimnology*, 18(2), pp.165-178.

- Walker, I.R., 2001. Midges: Chironomidae and related diptera. In Tracking environmental change using lake sediments (pp. 43-66). Springer, Dordrecht.
- Walker, I.R., Levesque, A., Pienitz, R. and Smol, J.P., 2003. Freshwater midges of the Yukon and adjacent Northwest Territories: a new tool for reconstructing Beringian paleoenvironments?. *Journal of the North American Benthological Society*, 22(2), pp.323-337.
- Walsh, S., 2017. Bland-Altman/Tukey Mean-Difference Plots using ggplot2. Environmental Science and Data Analytics with R: Posts on environmental science and general R-based data analysis, viewed 8 February 2020, <https://sw23993.wordpress.com/2017/05/31/bland-altmantukey-mean-difference-plots-using-ggplot2/>
- Wanner, H., Beer, J., Bütikofer, J., Crowley, T.J., Cubasch, U., Flückiger, J., Goosse, H., Grosjean, M., Joos, F., Kaplan, J.O. and Küttel, M., 2008. Mid-to Late Holocene climate change: an overview. *Quaternary Science Reviews*, 27(19-20), pp.1791-1828.
- Warner, B.G. and Hann, B.J., 1987. Aquatic invertebrates as paleoclimatic indicators?. *Quaternary research*, 28(3), pp.427-430.
- Warwick, W.F., 1975. The impact of man on the Bay of Quinte, Lake Ontario, as shown by the subfossil chironomid succession (Chironomidae, Diptera) With 7 figures in the text. *Internationale Vereinigung für theoretische und angewandte Limnologie: Verhandlungen*, 19(4), pp.3134-3141.
- Warwick, W.F., 1978. Man and the Bay of Quinte, Lake Ontario: 2800 years of cultural influence, with special reference to the Chironomidae (Diptera), sedimentation and eutrophication.

- Westerling, A. L., Hidalgo, H. G., Cayan, D. R., & Swetnam, T. W., 2006. Warming and earlier spring increase western US forest wildfire activity. *Science*, 313(5789), 940-943.
- Wilson, S.E. and Gajewski, K., 2004. Modern chironomid assemblages and their relationship to physical and chemical variables in southwest Yukon and northern British Columbia lakes. *Arctic, Antarctic, and Alpine Research*, 36(4), pp.446-455.
- Winstral, A., & Marks, D., 2002. Simulating wind fields and snow redistribution using terrain-based parameters to model snow accumulation and melt over a semi-arid mountain catchment. *Hydrological Processes*, 16(18), 3585-3603.
- Wolfe, A. P., Baron, J. S., & Cornett, R. J., 2001. Anthropogenic nitrogen deposition induces rapid ecological changes in alpine lakes of the Colorado Front Range (USA). *Journal of Paleolimnology*, 25(1), 1-7.
- Wolfe, A.P., Van Gorp, A.C. and Baron, J.S., 2003. Recent ecological and biogeochemical changes in alpine lakes of Rocky Mountain National Park (Colorado, USA): a response to anthropogenic nitrogen deposition. *Geobiology*, 1(2), pp.153-168.
- Wu, J., Porinchu, D.F., Horn, S.P. and Haberyan, K.A., 2015. The modern distribution of chironomid sub-fossils (Insecta: Diptera) in Costa Rica and the development of a regional chironomid-based temperature inference model. *Hydrobiologia*, 742(1), pp.107-127.
- Zhang, E., Chang, J., Cao, Y., Tang, H., Langdon, P., Shulmeister, J., Wang, R., Yang, X. and Shen, J., 2017. A chironomid-based mean July temperature inference model from the south-east margin of the Tibetan Plateau, China. *Climate of the Past*.
- Zuur, A., Ieno, E.N. and Smith, G.M., 2007. Analyzing ecological data. Springer Science & Business Media.

APPENDIX A

CODE FOR ALL ANALYSIS IN R

```
#####  
#####Chapter 2 #####
```

```
library(rioja)  
library (vegan)
```

```
#####Set Working Directory#####  
dir<-'C:\\Users\\Danielle\\Desktop\\Analysis Chapter 1'  
setwd(dir)
```

```
##### Data #####  
data <- read.table('taxaandvariables8.csv', header=TRUE, row.names = 1, sep=',')  
head(data)  
variables <- data [ ,1:29]  
transformed.variables = transform(variables,Depth = log(variables$Depth))  
transformed.variables1 = transform(transformed.variables,Secchi =  
log(transformed.variables$Secchi))  
transformed.variables2 = transform(transformed.variables1,Sp.Cond =  
log(transformed.variables1$Sp.Cond))  
transformed.variables3 = transform(transformed.variables2,DO.mg.L =  
log(transformed.variables2$DO.mg.L))  
transformed.variables4 = transform(transformed.variables3,DOC..ppm. =  
log(transformed.variables3$DOC..ppm.))  
transformed.variables5 = transform(transformed.variables3>Total.P.as.PO4.P..ppb. =  
log(transformed.variables3$Total.P.as.PO4.P..ppb.))  
transformed.variables6 = transform(transformed.variables5,Active.Chla.ug.L =  
log(transformed.variables5$Active.Chla.ug.L))
```

```
#Exploring distribution of data:  
summary(variables)
```

```
#Depth:  
windows()  
qqnorm(variables$Depth, main="Depth", las=1, pch=19)  
qqline(variables$Depth, col="red")
```

```

windows()
boxplot(variables$Depth, main="Depth", las=1)
windows()
hist(variables$Depth, main="", xlab="Depth (m)", las=1)

#Transformed Depth
windows()
qqnorm(transformed.variables$Depth, main="Depth", las=1, pch=19)
qqline(transformed.variables$Depth, col="red")
windows()
boxplot(transformed.variables$Depth, main="Depth", las=1)
windows()
hist(transformed.variables$Depth, main="", xlab="Depth (m)", las=1)

#Secchi
windows()
qqnorm(transformed.variables$Secchi, main="Log of Secchi Depth (m)", las=1, pch=19)
qqline(transformed.variables$Secchi, col="red")
windows()
hist(transformed.variables2$Secchi, main="", xlab="Secchi Depth (m)", las=1)
windows()
boxplot(transformed.variables2$Secchi, main="Secchi Depth", las=1)

#Transformed Secchi
windows()
qqnorm(transformed.variables1$Secchi, main="Log of Secchi Depth (m)", las=1, pch=19)
qqline(transformed.variables1$Secchi, col="red")
windows()
hist(transformed.variables1$Secchi, main="", xlab="Secchi Depth (m)", las=1)
windows()
boxplot(transformed.variables1$Secchi, main="Secchi Depth", las=1)

#Water Temp Surface
windows()
qqnorm(transformed.variables1$Water.Temp.surface, main="SWT (°C)", las=1, pch=19)
qqline(transformed.variables1$Water.Temp.surface, col="red")
windows()
boxplot(transformed.variables1$Water.Temp.surface, main="SWT (°C)", las=1)
windows()
hist(transformed.variables1$Water.Temp.surface, main="", xlab="SWT (°C)", las=1)

#Water Bottom Temp
windows()
qqnorm(transformed.variables1$Water.Temp.bottom, main="BWT (°C)", las=1, pch=19)
qqline(transformed.variables1$Water.Temp.bottom, col="red")
windows()

```

```

boxplot(transformed.variables1$Water.Temp.bottom, main="BWT (°C)", las=1)
windows()
hist(transformed.variables1$Water.Temp.bottom, main="", xlab="BWT (°C)", las=1)

#Specific Conductivity
windows()
qqnorm(transformed.variables1$Sp.Cond, main="Log of Specific Conductivity (µS•cm-1)",
las=1, pch=19)
qqline(transformed.variables1$Sp.Cond, col="red")
windows()
hist(transformed.variables1$Sp.Cond, main="", xlab="Specific Conductivity (µS•cm-1)", las=1)
windows()
boxplot(transformed.variables1$Sp.Cond, main="Specific Conductivity (µS•cm-1)", las=1)

#Transformed Specific Conductivity
windows()
qqnorm(transformed.variables2$Sp.Cond, main="Log of Specific Conductivity (µS•cm-1)",
las=1, pch=19)
qqline(transformed.variables2$Sp.Cond, col="red")
windows()
hist(transformed.variables2$Sp.Cond, main="", xlab="Specific Conductivity (µS•cm-1)", las=1)
windows()
boxplot(transformed.variables2$Sp.Cond, main="Specific Conductivity (µS•cm-1)", las=1)

#DO.mg.L
windows()
qqnorm(transformed.variables2$DO.mg.L, main="Dissolved Oxygen (mg/L)", las=1, pch=19)
qqline(transformed.variables2$DO.mg.L, col="red")
windows()
boxplot(transformed.variables2$DO.mg.L, main="Dissolved Oxygen (mg/L)", las=1)
windows()
hist(transformed.variables2$DO.mg.L, main="", xlab="Dissolved Oxygen (mg/L)", las=1)

#Transformed DO.mg.L
windows()
qqnorm(transformed.variables3$DO.mg.L, main="Dissolved Oxygen (mg/L)", las=1, pch=19)
qqline(transformed.variables3$DO.mg.L, col="red")
windows()
boxplot(transformed.variables3$DO.mg.L, main="Dissolved Oxygen (mg/L)", las=1)
windows()
hist(transformed.variables3$DO.mg.L, main="", xlab="Dissolved Oxygen (mg/L)", las=1)

#Prism.ELR
windows()

```

```

qqnorm(transformed.variables3$Prism.ELR, main="Mean July Air Temperature (°C)", las=1,
pch=19)
qqline(transformed.variables3$Prism.ELR, col="red")
windows()
boxplot(transformed.variables3$Prism.ELR, main="Mean July Air Temperature (°C)", las=1)
windows()
hist(transformed.variables3$Prism.ELR, main="", xlab="MJAT (°C)", las=1)

```

```

#pH
windows()
qqnorm(transformed.variables3$pH, main="pH", las=1, pch=19)
qqline(transformed.variables3$pH, col="red")
windows()
boxplot(transformed.variables3$pH, main="pH", las=1)
windows()
hist(transformed.variables3$pH, main="", xlab="pH", las=1)

```

```

#DOC (ppm)
windows()
qqnorm(transformed.variables3$DOC..ppm, main="DOC (ppm)", las=1, pch=19)
qqline(transformed.variables3$DOC..ppm, col="red")
windows()
boxplot(transformed.variables3$DOC..ppm, main="DOC (ppm)", las=1)
windows()
hist(transformed.variables3$DOC..ppm, main="", xlab="DOC (ppm)", las=1)

```

```

#Transformed DOC
windows()
qqnorm(transformed.variables4$DOC..ppm, main="DOC (ppm)", las=1, pch=19)
qqline(transformed.variables4$DOC..ppm, col="red")
windows()
boxplot(transformed.variables4$DOC..ppm, main="DOC (ppm)", las=1)
windows()
hist(transformed.variables4$DOC..ppm, main="", xlab="DOC (ppm)", las=1)

```

```

#DIC
windows()
qqnorm(transformed.variables3$DIC..ppm, main="DIC", las=1, pch=19)
qqline(transformed.variables3$DIC..ppm, col="red")
windows()
boxplot(transformed.variables3$DIC..ppm, main="DIC", las=1)
windows()
hist(transformed.variables3$DIC..ppm, main="", xlab="DIC", las=1)

```

```

#Total.P
windows()

```

```

qqnorm(transformed.variables$Total.P.as.PO4.P..ppb., main="Total P", las=1, pch=19)
qqline(transformed.variables$Total.P.as.PO4.P..ppb., col="red")
windows()
boxplot(transformed.variables$Total.P.as.PO4.P..ppb., main="Total P", las=1)
windows()
hist(transformed.variables$Total.P.as.PO4.P..ppb., main="", xlab="Total P", las=1)

```

```

transformed.variables3 = transform(transformed.variables2,Total.P =
log(transformed.variables$Total.P))

```

```

#Tranformed Total.P

```

```

windows()
qqnorm(transformed.variables5$Total.P.as.PO4.P..ppb., main="Total P", las=1, pch=19)
qqline(transformed.variables5$Total.P.as.PO4.P..ppb., col="red")
windows()
boxplot(transformed.variables5$Total.P.as.PO4.P..ppb., main="Total P", las=1)
windows()
hist(transformed.variables5$Total.P.as.PO4.P..ppb., main="", xlab="Total P", las=1)

```

```

# NO3.N

```

```

windows()
qqnorm(transformed.variables5$NO3.N...NO2.N.ppm., main="NO3", las=1, pch=19)
qqline(transformed.variables5$NO3.N...NO2.N.ppm., col="red")
windows()
boxplot(transformed.variables5$NO3.N...NO2.N.ppm., main="NO3", las=1)
windows()
hist(transformed.variables5$NO3.N...NO2.N.ppm., main="", xlab="NO3", las=1)

```

```

#Chl.a

```

```

windows()
qqnorm(transformed.variables5$Active.Chla.ug.L, main="Chl A", las=1, pch=19)
qqline(transformed.variables5$Active.Chla.ug.L, col="red")
windows()
boxplot(transformed.variables5$Active.Chla.ug.L, main="Chl A", las=1)
windows()
hist(transformed.variables5$Active.Chla.ug.L, main="", xlab="Chl A", las=1)

```

```

#transformed Chl.a

```

```

windows()
qqnorm(transformed.variables6$Active.Chla.ug.L, main="Chl A", las=1, pch=19)
qqline(transformed.variables6$Active.Chla.ug.L, col="red")
windows()
boxplot(transformed.variables6$Active.Chla.ug.L, main="Chl A", las=1)
windows()
hist(transformed.variables6$Active.Chla.ug.L, main="", xlab="Chl A", las=1)

```

```

#####PCA of environmental variables #####

transformed.variables7 <- transformed.variables6 [,-14:-29 ]

variables.pca <- prcomp(transformed.variables7, center=TRUE, scale.=TRUE)
sd <- variables.pca$sdev
loadings <- variables.pca$rotation
rownames(loadings) <- colnames(transformed.variables7)
scores <- variables.pca$x
biplot(variables.pca, scale=0)

variance <- sd^2
var.percent <- variance/sum(variance) * 100

#proportion of variance explained:
prop_varex <- variance/sum(variance)

#scree plot
plot(prop_varex, xlab = "Principal Component",
ylab = "Proportion of Variance Explained", type = "b")

#cumulative scree plot
plot(cumsum(prop_varex), xlab = "Principal Component",
ylab = "Cumulative Proportion of Variance Explained",
type = "b")

####PCA TUTORIAL FROM MISSOURI:
http://faculty.missouri.edu/huangf/data/mvnotes/pca\_in\_r\_2.html#####

R<-cor(transformed.variables7)
#saving the correlation matrix

e<-eigen(R)
#solving for the eigenvalues and eigenvectors from the correlation matrix
str(e)
L<-e$values

e$eigenvectors
#these are the eigenvectors-- these are the standardized regression weights

####Determine how many PCAs to use)###
library(hornpa)
hornpa(k=24,size=9, reps=500,seed=1234)
#k = # of variables, size = #sample size, reps =#of reps to run, seed =#optional seed

```

L #this will give the values to compare to hornpa results. Anything higher than the 95% is kept

```
dev.new()
barplot(var.percent, xlab="PC", ylab="Percent Variance", names.arg=1:length(var.percent),
las=1, ylim=c(0,max(var.percent)), col="gray")
abline(h=1/ncol(transformed.variables8)*100, col="red")
```

```
#Kaisers rule, retains Eiganvalues >1
plot(L,main="Scree Plot",ylab="Eigenvalues",xlab="Component number",type='b')
abline(h=1, lty=2)
```

```
var.percent[1:6]
sum(var.percent[1:6])
```

```
loadings
sqrt(1/ncol(transformed.variables7))
```

```
dev.new(height=7, width=7)
plot(scores[,1], scores[,2], xlab="PCA 1", ylab="PCA 2", type="n", asp=1, las=1)
scaling <- 3.5
textNudge <- 1.05
arrows(0, 0, loadings[,1]* scaling, loadings[,2]* scaling, length=0.1, angle=20, col="red")
text(loadings[,1]*scaling*textNudge, loadings[,2]*scaling*textNudge, rownames(loadings),
col="red", cex=0.7)
text(scores[,1], scores[,2], rownames(scores), col="blue", cex=0.7)
```

```
dev.new(height=7, width=7)
```

```
Glacial <- transformed.variables8$Water.Temp.surface >9.9 &
transformed.variables8$Water.Temp.surface < 10.91
Glacial1 <- transformed.variables8$Water.Temp.surface >8.1 &
transformed.variables8$Water.Temp.surface < 8.3
Snow <- transformed.variables8$Water.Temp.surface > 13
Snow1 <- transformed.variables8$Water.Temp.surface >9.1 &
transformed.variables8$Water.Temp.surface < 9.3
plot(scores[,1], scores[,2], xlab="PCA 1", ylab="PCA 2", type="n", asp=1, las=1)
points(scores[Glacial,1], scores[Glacial,2], pch=16, cex=0.7, col="blue")
points(scores[Glacial1,1], scores[Glacial1,2], pch=16, cex=0.7, col="blue")
points(scores[Snow,1], scores[Snow,2], pch=16, cex=0.7, col="red")
points(scores[Snow1,1], scores[Snow1,2], pch=16, cex=0.7, col="red")
```

```
text(0.5, -1.3, "Glacial", col="blue")
text(-0.5, 1.8, "Snow",col="red")
```

```

text(-0.5, 2.1, "warm", pos=3, col="gray")
text(-0.5, -2.2, "cold", pos=3, col="gray")
text(1.5, -0.2, "less productive", pos=3, col="gray")
text(-2.5, -0.2, "more productive", pos=3, col="gray")

##### DCA for taxa #####

library(vegan)
data <- read.table('taxaandvariables2.csv', header=TRUE, row.names = 1, sep=',')
head(data)
taxa <- data[,30:72]
taxa <- taxa[-7:-10,]
sqrt.taxa <- sqrt(taxa)
####transformation necessary because response is modal and not linear

#transformations to correct for differences in sample size and abundances
mydata.t1 <- decostand(sqrt.taxa, "total")
mydata.t2 <- decostand(mydata.t1, "max")
mydata.t2.dca <- decorana(mydata.t2)

mydata.t2.dca.DW <- decorana(mydata.t2, iweigh=1)

DCA <- summary(mydata.t2.dca)
write.csv(DCA, file="DCA results.csv")

#Plot scores
dev.new(height=8, width=8)
DCA <- plot(mydata.t2.dca)
pdf("C:/Users/Danielle/Desktop/Analysis Chapter 1/DCA.pdf")
plot(DCA)
dev.off()

#####RDA#####

library(vegan)
data <- read.table('taxaandvariables7.csv', header=TRUE, row.names = 1, sep=',')
head(data)
taxa <- data[,46:89]
taxa <- taxa[-7:-10,]
sqrt.taxa <- sqrt(taxa)

rda <- rda(sqrt.taxa~transformed.variables6$Depth)
anova(rda)

```

```

rda1 <- rda(sqrt.taxa~transformed.variables6$Prism.ELR)
anova(rda1)

rda2 <- rda(sqrt.taxa~transformed.variables6$Water.Temp.surface)
anova(rda2)

rda3 <- rda(sqrt.taxa~transformed.variables6$Water.Temp.bottom)
anova(rda3)

rda4 <- rda(sqrt.taxa~transformed.variables6$Sp.Cond)
anova(rda4)

rda5 <- rda(sqrt.taxa~transformed.variables6$Secchi)
anova(rda5)

rda6 <- rda(sqrt.taxa~transformed.variables6$DO.mg.L)
anova(rda6)

rda7 <- rda(sqrt.taxa~transformed.variables6$DOC..ppm.)
anova(rda7)

rda8 <- rda(sqrt.taxa~transformed.variables6$DIC..ppm.)
anova(rda8)

rda9 <- rda(sqrt.taxa~transformed.variables6$Total.P.as.PO4.P..ppb.)
anova(rda9)

rda10 <- rda(sqrt.taxa~transformed.variables6$NO3.N...NO2.N.ppm.)
anova(rda10)

rda11 <- rda(sqrt.taxa~transformed.variables6$Active.Chla.ug.L)
anova(rda11)

rda12 <- rda(sqrt.taxa~transformed.variables6$NO3.N...NO2.N.ppm. +
transformed.variables6$Water.Temp.surface)
anova(rda12)

#####Pearsons Correlation#####
cor.test(transformed.variables6$NO3.N...NO2.N.ppm.,transformed.variables6$Water.Temp.surf
ace)

```

```
#####  
#####Chapter 3 code #####
```

```
#####Reads in R Packages needed for Code#####
```

```
library(rioja)  
library(BlandAltmanLeh)  
library(tidyr)
```

```
#####Set Working Directory#####
```

```
dir<-'C:\\Users\\Danielle\\Desktop\\Analysis Chapter 2\\Kyle cleaned up files'  
setwd(dir)
```

```
#####
```

```
#####Choose which Lake you want to Work With#####
```

```
#####
```

```
#Lake<-'Black Counts Age Depth.csv'  
#Lake<-'Black N2 under 5 removed.csv'  
#Lake<-'Box Loess Counts.csv'  
#Lake<-'Box N2 under 5 removed.csv'  
#Lake<-'Cony Counts Age Depth.csv'  
#Lake<-'Cony N2 under 5 removed.csv'  
#Lake<-'Eagle Counts Age Depth.csv'  
#Lake<-'Eagle N2 under 5 removed.csv'  
#Lake<-'Pipit Counts Age Depth.csv'  
#Lake<-'Pipit N2 under 5 removed.csv'  
#Lake<-'Thunder Counts Age Depth.csv'  
#Lake<-'Thunder N2 under 5 removed.csv'  
#Lake<-'Training Set Data SWT.csv'  
#Lake<-'Training Set Data MJAT.csv'  
Lake<-'Kite Counts.csv'
```

```
#####Reads in Data for which lake above was selected#####
```

```
Lake_Data<-read.csv(Lake, header=TRUE) ###Reading In Lake Data  
rel_num<-grep('Abisko',colnames(Lake_Data))  
Lake_Rel_Abun<-Lake_Data[,-c(1:rel_num[1])] ###Removing all columns that are not part of  
Relative Abundance Data  
Lake_Rel_Abun[is.na(Lake_Rel_Abun)]<-0 ###Converts Missing Data NAs to 0
```

```
#####Reads in Training Set Relative Abundance
```

```
Training_Set<-read.csv("Training Set Data.csv", header=TRUE)
```

```
#####Reads in Training Set Environment Data
```

```
Environment<-read.csv("Training set with temperatures.csv", header=TRUE)
```

```

#####Matches Training Set Data Frames and removes those that aren't in both sets
test<-merge(Training_Set, Environment)

Environment<-data.frame(cbind(test$CodeNum, test$FullName, test$MJAT, test$SWT))
colnames(Environment)<-c('CodeNum','FullName','MJAT', 'SWT')

Training_Set<-test[, c(4:76)]
Training_Set[is.na(Training_Set)]<-0
Training_Set<-Training_Set[,-c(18,39,42,50)]

#####Reads in Historical Data and Formats it
Historic_temps<-read.csv('All Lakes Prism Interpolation on.csv', header=TRUE)
Historic_temps<-na.omit(Historic_temps)
Historic_temps$C_temp<-((as.numeric(Historic_temps$tmean..degrees.F.)-32)*(5/9))
Historic_temps<-Historic_temps[,-c(2:4,6)]

Historic_temps_wide<-spread(Historic_temps, Date, C_temp)

names(Historic_temps_wide)<-gsub("\\|-07", "", names(Historic_temps_wide))
rnames<-Historic_temps_wide$Name

names.use<-names(Historic_temps_wide)[(names(Historic_temps_wide) %in%
Lake_Data$Year)]
Historic_temps_wide<-Historic_temps_wide[,names.use]
row.names(Historic_temps_wide)<-rnames

Lake<-strsplit(Lake, " ")[[1]][1]

rm(rel_num, rnames, test)

new_dir<-paste0(Lake, "_Output")
dir.create(paste0(Lake, "_Output"))
setwd(paste0(dir,new_dir))

#####
#####Fits WAPLS Data for Training Set Using 5 Comp#####
#####

fit<-WAPLS(Training_Set,Environment$SWT, npls=5)
fit

##### cross-validate model
fit.cv <- crossval(fit, cv.method="bootstrap",nboot=10000)
fit.cv

```

```

##### How many components to use?
rand.t.test(fit.cv)
jpeg(paste0('ScreePlot_',Lake, '.jpeg'))
screepplot(fit.cv)
dev.off()

#####
##### Predicts the Values for the interested Lake#####
#####

pred <- predict(fit, Lake_Rel_Abun, npls=1)
pred

#####Writes Predicted Values to CSV
write.csv(pred, paste0('Predicted_',Lake, '.csv'))

#####plot predictions - depths are in rownames
Year <- as.numeric(Lake_Data$Year)

jpeg(paste0('Depth_Plot_', Lake, '.jpeg'))
plot(pred$fit[, 1],Year, type="b", xlab="Predicted Temperature", ylab='Year',
      main ='Reconstructed Mean July Air Temperature (Celsius) Over Time',las=1,
      xlim=c(10.5,12), ylim=rev(c(9000, 13000)))
fittedcurve <- loess(pred$fit[, 1]~Year, span=0.75)
lines(x=fittedcurve$fitted, y=Year, col=2, lwd=2)
dev.off()

Year <- as.numeric(Lake_Data$Year)

jpeg(paste0('Depth_Plot_', Lake, '.jpeg'))
plot(Year,pred$fit[, 1], type="b", xlab='Year', ylab="Predicted Temperature",
      main ='Reconstructed Mean July Air Temperature (Celsius) Over Time',las=1,
      xlim=rev(c(9000, 13000), ylim=c(10.5,12)))
fittedcurve <- loess(pred$fit[, 1]~Year, span=0.75)
lines(x=fittedcurve$fitted, y=Year, col=2, lwd=2)
dev.off()

# predictions with sample specific errors
## Not run:
#pred <- predict(fit, Black_Rel_Abun, npls=1, sse=TRUE, nboot=1000)
#pred

#####Plots Bland Altman Plot and outputs to a Jpeg
jpeg(paste0('Bland_Altman_Plot_',Lake, '.jpeg'))
bland.altman.plot(pred$fit[,1], as.numeric(Historic_temps_wide[Lake,]),

```

```
main=paste0(Lake, " Lake Bland Altman Plot"), xlab="Means", ylab="Differences")
dev.off()
```

```
##### Kite Relative Abundance #####
```

```
# Commands from Analogue:
```

```
#Stratiplot(x, y, type = "l", ylab = NULL, xlab = "", pages = 1, rev = TRUE,
# ylim, sort = c("none", "wa", "var"), svar = NULL, rev.sort = FALSE, strip = FALSE,
# topPad =6, varTypes = "relative", absoluteSize = 0.5, zoneNames = NULL, drawLegend =
TRUE,
# na.action = "na.omit", labelAt = NULL, labelRot = 60, yticks, ...)
```

```
#####Reads in R Packages needed for Code#####
```

```
library(analogue)
library(palaeoSig)
```

```
#####Set Working Directory#####
```

```
dir<-'C:\\Users\\Danielle\\Desktop\\Analysis Chapter 2\\Kyle cleaned up files'
setwd(dir)
```

```
#####Kite Lake#####
```

```
radioncarbon <- read.csv("Chronology without errors.csv", header=TRUE, sep=",")
erroneous <- read.csv("erroneous dates.csv", header=TRUE, sep=",")
fit8 <- read.csv("fit8.csv", header=TRUE, sep=",")
```

```
# Figure for Kite Chronology
```

```
dev.new(height=8, width=10)
```

```
age <-plot(radioncarbon$Cal.kyr.BP, radioncarbon$Depth, main="Age-depth diagram",
xlab="Age (cal kyr BP)",
ylab= "Depth (cm)", type="n", axes=FALSE, xlim=(c(0, 18)), ylim=(rev(c(0,700))))
```

```
#plot points of dated samples. Radiocarbon were used in the model. Erroneous weren't used
points(radioncarbon$Cal.kyr.BP, radioncarbon$Depth, type="p", pch=19)
points(erroneous$Cal.kyr.BP, erroneous$Depth, type="p", pch=19, col="red")
```

```
#plot axes
```

```
axis(1, at=seq(0,18,by=1),
labels=c("0","1","2","3","4","5","6","7","8","9","10","11","12","13","14","15","16","17","18"))
axis(2, at=seq(0,700,by=50), labels=FALSE, tcl=-0.3)
axis(2, at=seq(0,700,by=100), labels=
c('0','100','200','300','400','500','600','700'), las=1)
```

```

#adding lines
lines(radioncarbon$Cal.kyr.BP, radioncarbon$Depth,col="black")
lines(fit8$Cal.kyr.BP, fit8$Depth, col="black", lty="dashed")

## Relative Abundance Diagram

Kite <- read.csv(file="Kite Counts.csv", header=TRUE, sep=",")
attach(Kite)
#Zones <- c(12328,11712,10671,9489)          ### VEG zones
#zone.labs <- c("Ki-1a","Ki-1b","Ki-1c","Ki-1d", "KI-2")      ### VEG zones

Zones <- c(10033,11925 )
zone.labs <- c("KLZ3","KLZ2","KLZ1")
#WA Optima plot 12.19.19

pdf(file="Kite Lake Relative Abundance.pdf", height=7, width=12)

dev.new(height=8, width=10)
par(mfrow=c(1,1))

(plt <- Stratiplot(Year ~ Cric.Ort + Chaeto + Euk.Tvet + Psecsemi +
  Heteind + Chirind + Cladtany + Corynamb + Colivtyp + TAA + TAB +
  TAH + Tanyind + Paratany + Procind + Pentind +
  Diamind + Protan, data = Kite,
  rev = TRUE, type = c("h","g"), zones = Zones, zoneNames = zone.labs,
  xlab = "% Relative Abundance", varTypes = "relative", col="gray48", pages = 1))

# Richness and Concentration

dev.new(height=7, width=5)
par(mfrow=c(1,2))

#Concentration
Kite.Concentration <- read.csv(file="Kite Concentration.csv", header=TRUE, sep=",")
attach(Kite.Concentration)

pdf(file="Kite_Concentration.pdf", height=7, width=2)
plot(Concentration, Year, type='l', pch=20, xlim = c(0,260),lwd=2, ylim = rev(c(9200,12700)),
xlab='Concentration', ylab="Age (cal yr BP)")
abline(h=11925, col="blue")
abline(h=10033, col="blue")

#Species Richness

```

```

plot(Richness, Year, type='l', pch=20, xlim = c(0,15), lwd=2, ylim = rev(c(9200,12700)),
xlab='Richness', ylab="Age (cal yr BP)")
abline(h=11925, col="blue")
abline(h=10033, col="blue")
dev.off()

```

```
#####Training Set#####
```

```

# Commands from Analogue:
#Stratplot(x, y, type = "l", ylab = NULL, xlab = "", pages = 1, rev = TRUE,
# ylim, sort = c("none", "wa", "var"), svar = NULL, rev.sort = FALSE, strip = FALSE,
# topPad =6, varTypes = "relative", absoluteSize = 0.5, zoneNames = NULL, drawLegend =
TRUE,
# na.action = "na.omit", labelAt = NULL, labelRot = 60, yticks, ...)

```

```
#####Reads in R Packages needed for Code#####
```

```
library(analogue)
```

```
#####Set Working Directory#####
```

```

dir<-'C:\\Users\\Danielle\\Desktop\\Analysis Chapter 2\\Kyle cleaned up files'
setwd(dir)

```

```
#####Bringing in the data
```

```

TrainingSet <- read.csv(file="Training Set Data.csv", header=TRUE, sep=",")
attach(TrainingSet)
Zones <- c(52,109, 146)
zone.labs <- c("Front Range", "Sawatch Range", "Sierra Nevada", "Uintas")

```

```
#Plot by tribes
```

```
pdf(file="Training Set Relative Abundance.pdf", height=7, width=12)
```

```
dev.new(height=8, width=10)
```

```
par(mfrow=c(1,1))
```

```

(plt <- Stratplot(Number ~ Cory.Th + Cric.Ort + Chaeto + Euk.Tvet +
Hyd.Oliv + Lim.Para + Park.bat + Psecsemi + Rheoind +
Zaluind + Heteind + Chirind + Cladind + Dicrind + Mictind +
Phaeind + Sergind + Cladtany + Corynamb + Colivtyp + Micpsect +
TAC + TAG + TAH + Tanyind + Paratany + Procind + Pentind +

```

```

    Diamind, data = TrainingSet, rev = TRUE, type = c("h", "l", "g"), zones = Zones,
    zoneNames = zone.labs,
    xlab = "% Relative Abundance", ylab = "Lake Number", varTypes = "relative",
    col="gray48", pages = 1))
dev.off()

```

```

#####
#####CHAPTER 4#####

```

```

library(rioja)
library(tidyr)
library(ggplot2)

```

```

#Load data for NIWOT comparison
#Black <- read.csv("Black Data1.csv", header=TRUE, sep=",")
#Box <- read.csv("Box Data1.csv", header=TRUE, sep=",")
#Cony <- read.csv("Cony Data1.csv", header=TRUE, sep=",")
#Eagle <- read.csv("Eagle Data1.csv", header=TRUE, sep=",")
#Pipit <- read.csv("Pipit Data1.csv", header=TRUE, sep=",")
#Thunder <- read.csv("Thunder Data1.csv", header=TRUE, sep=",")
#NiwoT <- read.csv("NiwoT_July_Temps.csv", header=TRUE, sep=",")
#Dates <- read.csv("Dates.csv", header=TRUE, sep=",")
#Dates1 <- read.csv("Dates1.csv", header=TRUE, sep=",")
#Kite <- read.csv("Kite Counts1.csv", header=TRUE, sep=",")

```

```

#Load data for Prism comparison
Black <- read.csv("Black Data.csv", header=TRUE, sep=",")
Box <- read.csv("Box Data.csv", header=TRUE, sep=",")
Cony <- read.csv("Cony Data.csv", header=TRUE, sep=",")
Eagle <- read.csv("Eagle Data.csv", header=TRUE, sep=",")
Pipit <- read.csv("Pipit Data.csv", header=TRUE, sep=",")
Thunder <- read.csv("Thunder Data.csv", header=TRUE, sep=",")
Dates <- read.csv("Dates.csv", header=TRUE, sep=",")
Dates1 <- read.csv("Dates1.csv", header=TRUE, sep=",")
Prism <- read.csv("Prism.csv", header=TRUE, sep=",")
Kite <- read.csv("Kite Data.csv", header=TRUE, sep=",")
Blackbugs <- read.csv("Black Counts Age Depth.csv", header=TRUE, sep=",")
Boxbugs <- read.csv("Box Loess Counts.csv", header=TRUE, sep=",")
Conybugs <- read.csv("Cony Counts Age Depth.csv", header=TRUE, sep=",")
Eaglebugs <- read.csv("Eagle Counts Age Depth.csv", header=TRUE, sep=",")
Pipitbugs <- read.csv("Pipit Counts Age Depth.csv", header=TRUE, sep=",")
Thunderbugs <- read.csv("Thunder Counts Age Depth.csv", header=TRUE, sep=",")
mylist <- split(Prism, Prism$Name)
mylist

```

```
#####  
#####Choose which Lake you want to Work With#####  
#####
```

```
Lake<-'Black Counts Age Depth.csv'  
#Lake<-'Box Loess Counts.csv'  
#Lake<-'Cory Counts Age Depth.csv'  
#Lake<-'Eagle Counts Age Depth.csv'  
#Lake<-'Pipit Counts Age Depth.csv'  
#Lake<-'Thunder Counts Age Depth.csv'  
#Lake<-'Training Set Data SWT.csv'  
#Lake<-'Training Set Data MJAT.csv'
```

```
#####Reads in Data for which lake above was selected#####  
Lake_Data<-read.csv(Lake, header=TRUE) ###Reading In Lake Data  
rel_num<-grep('Cory.Th',colnames(Lake_Data))  
Lake_Rel_Abun<-Lake_Data[,-c(1:rel_num[1])] ###Removing all columns that are not part of  
Relative Abundance Data  
Lake_Rel_Abun[is.na(Lake_Rel_Abun)]<-0 ###Converts Missing Data NAs to 0
```

```
#####Reads in Training Set Relative Abundance  
Training_Set<-read.csv('Training Set Data.csv', header=TRUE)
```

```
#####Reads in Training Set Environment Data  
Environment<-read.csv('Training set with temperatures.csv', header=TRUE)
```

```
#####Matches Training Set Data Frames and removes those that aren't in both sets  
test<-merge(Training_Set, Environment)
```

```
Environment<-data.frame(cbind(test$CodeNum, test$FullName, test$MJAT, test$SWT))  
colnames(Environment)<-c('CodeNum','FullName','MJAT', 'SWT')
```

```
Training_Set<-test[, c(4:76)]  
Training_Set[is.na(Training_Set)]<-0  
Training_Set<-Training_Set[,-c(18,39,42,50)]
```

```
#####  
#####Fits WAPLS Data for Training Set Using 5 Comp#####  
#####
```

```
fit<-WAPLS(sqrt(Training_Set),Environment$SWT, npls=5)  
fit
```

```

##### cross-validate model
fit.cv <- crossval(fit, cv.method="bootstrap",nboot=10000)
fit.cv

##### How many components to use?
rand.t.test(fit.cv)
jpeg(paste0('ScreePlot_',Lake, '.jpeg'))
screplot(fit.cv)
dev.off()

##### Predicts the Values for the interested Lake#####

pred <- predict(fit, sqrt(Lake_Rel_Abun), npls=5)
pred

####Writes Predicted Values to CSV
write.csv(pred, paste0('Predicted_',Lake, '.csv'))

##### Predicts the sampled specific error for the interested Lake
#####

pred1 <- predict(fit, sqrt(Lake_Rel_Abun), npls=1, sse=TRUE)
pred1

####Writes Predicted Values to CSV
write.csv(pred1$SEP.boot, paste0('SSE_',Lake, '.csv'))

#####DCA#####
library(vegan)
vare.dca <- decorana(Lake_Rel_Abun)
vare.dca
summary(vare.dca)

#####Changepoint analysis for SWT, MJAT, DCA_SWT, and DCA_MJAT #####

library(changepoint)
library(changepoint.np)

ts.plot(Black$SWT)

```

```

out <- cpt.np(Black$SWT, method="PELT",minseglen=2, nquantiles
=4*log(length(Black$SWT)))
cpts(out)
##no changes

ts.plot(Black$MJAT)
out1 <- cpt.np(Black$MJAT, method="PELT",minseglen=2, nquantiles
=4*log(length(Black$MJAT)))
cpts(out1)
##no changes

ts.plot(Black$DCA)
out2 <- cpt.np(Black$DCA, method="PELT",minseglen=2, nquantiles
=4*log(length(Black$DCA)))
cpts(out2)
#14 = 1957

ts.plot(Box$SWT)
out3 <- cpt.np(Box$SWT, method="PELT",minseglen=2, nquantiles
=4*log(length(Box$SWT)))
cpts(out3)
#none

ts.plot(Box$MJAT)
out4 <- cpt.np(Box$MJAT, method="PELT",minseglen=2, nquantiles
=4*log(length(Box$MJAT)))
cpts(out4)
#none

ts.plot(Box$DCA)
out5 <- cpt.np(Box$DCA, method="PELT",minseglen=2, nquantiles
=4*log(length(Box$DCA)))
cpts(out5)
#8 = 1977

ts.plot(Cony$SWT)
out6 <- cpt.np(Cony$SWT, method="PELT",minseglen=2, nquantiles
=4*log(length(Cony$SWT)))
cpts(out6)
#11 = 1969

ts.plot(Cony$MJAT)
out7 <- cpt.np(Cony$MJAT, method="PELT",minseglen=2, nquantiles
=4*log(length(Cony$MJAT)))
cpts(out7)
#11 = 1969

```

```
ts.plot(Cony$DCA)
out8 <- cpt.np(Cony$DCA, method="PELT",minseglen=2, nquantiles
=4*log(length(Cony$DCA)))
cpts(out8)
#12 = 1966
```

```
ts.plot(Eagle$SWT)
out9 <- cpt.np(Eagle$SWT, method="PELT",minseglen=2, nquantiles
=4*log(length(Eagle$SWT)))
cpts(out9)
#14 = 1956
```

```
ts.plot(Eagle$MJAT)
out10 <- cpt.np(Eagle$MJAT, method="PELT",minseglen=2, nquantiles
=4*log(length(Eagle$MJAT)))
cpts(out10)
#14 = 1956
```

```
ts.plot(Eagle$DCA)
out11 <- cpt.np(Eagle$DCA, method="PELT",minseglen=2, nquantiles
=4*log(length(Eagle$DCA)))
cpts(out11)
#15 = 1947
```

```
ts.plot(Pipit$SWT)
out12 <- cpt.np(Pipit$SWT, method="PELT",minseglen=2, nquantiles
=4*log(length(Pipit$SWT)))
cpts(out12)
#7 = 1991
```

```
ts.plot(Pipit$MJAT)
out13 <- cpt.np(Pipit$MJAT, method="PELT",minseglen=2, nquantiles
=4*log(length(Pipit$MJAT)))
cpts(out13)
#16 = 1954
```

```
ts.plot(Pipit$DCA)
out14 <- cpt.np(Pipit$DCA, method="PELT",minseglen=2, nquantiles
=4*log(length(Pipit$DCA)))
cpts(out14)
#7 = 1991
```

```
ts.plot(Thunder$SWT)
out15 <- cpt.np(Thunder$SWT, method="PELT",minseglen=2, nquantiles
=4*log(length(Thunder$SWT)))
```

```
cpts(out15)
#19 = 1932
```

```
ts.plot(Thunder$MJAT)
out16 <- cpt.np(Thunder$MJAT, method="PELT",minseglen=2, nquantiles
=4*log(length(Thunder$MJAT)))
cpts(out16)
#12 = 1983
```

```
ts.plot(Thunder$DCA)
out17 <- cpt.np(Thunder$DCA, method="PELT",minseglen=2, nquantiles
=4*log(length(Thunder$DCA)))
cpts(out17)
#4 = 2013
#19 = 1932
```

```
ts.plot(Niwot$max)
out18 <- cpt.np(Niwot$max, method="PELT",minseglen=2, nquantiles
=4*log(length(Niwot$max)))
cpts(out18)
#27 = 1979
#34 = 1986
#59 = 2011
```

```
ts.plot(Niwot$min)
out19 <- cpt.np(Niwot$min, method="PELT",minseglen=2, nquantiles
=4*log(length(Niwot$min)))
cpts(out19)
#27 = 1979
#32 = 1984
#45 = 1997
#59 = 2011
```

```
ts.plot(Niwot$avg)
out20 <- cpt.np(Niwot$avg, method="PELT",minseglen=2, nquantiles
=4*log(length(Niwot$avg)))
cpts(out20)
#27 = 1979
#34 = 1986
#49 = 2001
#59 = 2011
```

```
#####
##### Plots of MJAT, and SWT with PRISM #####
mylist <- split(Prism, Prism$Name)
mylist
```

```
dev.new(height=8, width=10)
par(mfrow=(c(3, 2)))
```

```
##CNY
```

```
plot(Cony$Year, Cony$MJAT, main='Cony Lake', xlab='Year',
     ylab=expression(paste("Temperature (",degree,"C)")),
     type='n', xlim=(c(1895, 2017)), ylim=(c(7,14)))
```

```
points(Cony$Year, Cony$MJAT, type='b', pch=16, lwd=2, col="red")
#arrows(Black$Year, ((Black$SWT)-(Black$SWT_SSE)), Black$Year,
        ((Black$SWT)+(Black$SWT_SSE)), length=0.05, angle=90, code=3, col=gray(0.45))
points(Cony$Year, Cony$SWT, type='b', pch=16, lwd=2, col="blue")
points(mylist$Cony$Date, mylist$Cony$X, type='l', lwd=1, col="gray")
fittedcurve <- loess(mylist$Cony$X~mylist$Cony$Date, span=0.20)
smoothed20 <- predict(fittedcurve)
lines(smoothed20, x=mylist$Cony$Date, col="black", lwd=1)
```

```
#axis(side = 4)
```

```
#mtext(side = 4, line = 3, ")
```

```
#legend("bottomright",
```

```
#legend=c(expression(paste("Midge-inferred MJAT (",degree,"C)")), expression(paste("Midge-
inferred SWT (",degree,"C)")),
```

```
#lty=c(1,1), col=c("red", "blue"))
```

```
#PIPIT
```

```
plot(Pipit$Year, Pipit$MJAT, main='Pipit Lake', xlab='Year',
     ylab=expression(paste("Temperature (",degree,"C)")),
     type='n', xlim=(c(1895, 2017)), ylim=(c(7,14)))
```

```
points(Pipit$Year, Pipit$MJAT, type='b', pch=16, lwd=2, col="red")
#arrows(Black$Year, ((Black$SWT)-(Black$SWT_SSE)), Black$Year,
        ((Black$SWT)+(Black$SWT_SSE)), length=0.05, angle=90, code=3, col=gray(0.45))
points(Pipit$Year, Pipit$SWT, type='b', pch=16, lwd=2, col="blue")
points(mylist$Pipit$Date, mylist$Pipit$X, type='l', lwd=1, col="gray")
fittedcurve <- loess(mylist$Pipit$X~mylist$Pipit$Date, span=0.20)
smoothed20 <- predict(fittedcurve)
lines(smoothed20, x=mylist$Pipit$Date, col="black", lwd=1)
```

```
#Eagle
```

```
plot(Eagle$Year, Eagle$MJAT, main='Eagle Lake', xlab='Year',
```

```
ylab=expression(paste("Temperature [",degree,"C]")),
type='n', xlim=(c(1895, 2017)), ylim=(c(7,14)))
```

```
points(Eagle$Year, Eagle$MJAT, type='b', pch=16, lwd=2, col="red")
#arrows(Black$Year, ((Black$SWT)-(Black$SWT_SSE)), Black$Year,
((Black$SWT)+(Black$SWT_SSE)), length=0.05, angle=90, code=3, col=gray(0.45))
points(Eagle$Year, Eagle$SWT, type='b', pch=16, lwd=2, col="blue")
points(mylist$Eagle$Date, mylist$Eagle$X, type='l', lwd=1, col="gray")
fittedcurve <- loess(mylist$Eagle$X~mylist$Eagle$Date, span=0.20)
smoothed20 <- predict(fittedcurve)
lines(smoothed20, x=mylist$Eagle$Date, col="black", lwd=1)
```

```
#Box
```

```
plot(Box$Year, Box$MJAT, main='Box Lake', xlab='Year',
ylab=expression(paste("Temperature [",degree,"C]")),
type='n', xlim=(c(1895, 2017)), ylim=(c(7,14)))
```

```
points(Box$Year, Box$MJAT, type='b', pch=16, lwd=2, col="red")
#arrows(Black$Year, ((Black$SWT)-(Black$SWT_SSE)), Black$Year,
((Black$SWT)+(Black$SWT_SSE)), length=0.05, angle=90, code=3, col=gray(0.45))
points(Box$Year, Box$SWT, type='b', pch=16, lwd=2, col="blue")
points(mylist$Box$Date, mylist$Box$X, type='l', lwd=1, col="gray")
fittedcurve <- loess(mylist$Box$X~mylist$Box$Date, span=0.20)
smoothed20 <- predict(fittedcurve)
lines(smoothed20, x=mylist$Box$Date, col="black", lwd=1)
```

```
##Black
```

```
plot(Black$Year, Black$MJAT, main='Black Lake', xlab='Year',
ylab=expression(paste("Temperature [",degree,"C]")),
type='n', xlim=(c(1895, 2017)), ylim=(c(7,14)))
```

```
points(Black$Year, Black$MJAT, type='b', pch=16, lwd=2, col="red")
#arrows(Black$Year, ((Black$SWT)-(Black$SWT_SSE)), Black$Year,
((Black$SWT)+(Black$SWT_SSE)), length=0.05, angle=90, code=3, col=gray(0.45))
points(Black$Year, Black$SWT, type='b', pch=16, lwd=2, col="blue")
points(mylist$Black$Date, mylist$Black$X, type='l', lwd=1, col="gray")
fittedcurve <- loess(mylist$Black$X~mylist$Black$Date, span=0.20)
smoothed20 <- predict(fittedcurve)
lines(smoothed20, x=mylist$Black$Date, col="black", lwd=1)
```

```
##Thunder
```

```
plot(Thunder$Year, Thunder$MJAT, main='Thunder Lake', xlab='Year',  
     ylab=expression(paste("Temperature [",degree,"C]")),  
     type='n', xlim=(c(1895, 2017)), ylim=(c(7,14)))
```

```
points(Thunder$Year, Thunder$MJAT, type='b', pch=16, lwd=2, col="red")  
#arrows(Black$Year, ((Black$SWT)-(Black$SWT_SSE)), Black$Year,  
        ((Black$SWT)+(Black$SWT_SSE)), length=0.05, angle=90, code=3, col=gray(0.45))  
points(Thunder$Year, Thunder$SWT, type='b', pch=16, lwd=2, col="blue")  
points(mylist$Thunder$Date, mylist$Thunder$X, type='l', lwd=1, col="gray")  
fittedcurve <- loess(mylist$Thunder$X~mylist$Thunder$Date, span=0.20)  
smoothed20 <- predict(fittedcurve)  
lines(smoothed20, x=mylist$Thunder$Date, col="black", lwd=1)
```

```
#####Kite Lake
```

```
dev.new(height=8, width=10)  
par(mfrow=(c(1, 1)))
```

```
plot(Kite$Year, Kite$MJAT, main='Kite Lake', xlab='cal yr BP',  
     ylab=expression(paste("Temperature [",degree,"C]")),  
     type='n', xlim=rev(c(12700, 9200)), ylim=(c(7,14)))
```

```
points(Kite$Year, Kite$MJAT, type='b', pch=16, lwd=1, col="red")  
#arrows(Black$Year, ((Black$SWT)-(Black$SWT_SSE)), Black$Year,  
        ((Black$SWT)+(Black$SWT_SSE)), length=0.05, angle=90, code=3, col=gray(0.45))  
points(Kite$Year, Kite$SWT, type='b', pch=16, lwd=1, col="blue")  
fittedcurve <- loess(Kite$MJAT~Kite$Year, span=0.20)  
smoothed20 <- predict(fittedcurve)  
lines(smoothed20, x=Kite$Year, col="red", lwd=2)
```

```
fittedcurve1 <- loess(Kite$SWT~Kite$Year, span=0.20)  
smoothed20a <- predict(fittedcurve1)  
lines(smoothed20a, x=Kite$Year, col="blue", lwd=2)
```

```
rect(11950, 7, 12800, 14, col=gray(0.50), border=gray(0.50))  
rect(10450, 7, 10550, 14, col=gray(0.50), border=gray(0.50))
```

```
#adding dark rectangles to represent no chironomid data available  
rect(10340, 7, 10450, 14, col=gray(0.90), border=gray(0.90))  
rect(10550, 7, 10820, 14, col=gray(0.90), border=gray(0.90))
```

```
#Legend
```

```
legend("bottomleft",
```

```

legend=c("Deviations from average chironomid-based SWT", "Deviations from average
chironomid-based MJAT", "No chironomids recovered", "Not enough data available"),
pch=c(16,16,15,15), cex=0.8, col=c("blue", "red", "dark gray", "light gray"))

```

```

#Legend
#legend("bottomleft",
#legend=c("Chironomid-based SWT", "Chironomid-based MJAT"), lty=c(1,1),
pch=c(16,16), cex=0.8, col=c("blue", "red"))

```

```

#####
##### DCA Plots #####

```

```

dev.new(height=8, width=10)
par(mfrow=(c(3, 2)))

```

```

##CNY

```

```

plot(Cony$Year, Cony$DCA, main='Cony Lake', xlab='Year',
ylab= "DCA",
type='n', xlim=(c(1895, 2017)), ylim=(c(-1,1)))
points(Cony$Year, Cony$DCA, type='b', pch=16, lwd=2, col="black")
abline(v=(1966), col="red", lty="dashed")

```

```

#PIPIT

```

```

plot(Pipit$Year, Pipit$DCA, main='Pipit Lake', xlab='Year',
ylab="DCA",
type='n', xlim=(c(1895, 2017)), ylim=(c(-1,1)))
points(Pipit$Year, Pipit$DCA, type='b', pch=16, lwd=2, col="black")
abline(v=(1991), col="red", lty="dashed")

```

```

#Eagle

```

```

plot(Eagle$Year, Eagle$DCA, main='Eagle Lake', xlab='Year',
ylab="DCA",
type='n', xlim=(c(1895, 2017)), ylim=(c(-1,1)))
points(Eagle$Year, Eagle$DCA, type='b', pch=16, lwd=2, col="black")
abline(v=(1947), col="red", lty="dashed")

```

```
#Box
```

```
plot(Box$Year, Box$DCA, main='Box Lake', xlab='Year',  
      ylab="DCA",  
      type='n', xlim=(c(1895, 2017)), ylim=(c(-1,1)))  
points(Box$Year, Box$DCA, type='b', pch=16, lwd=2, col="black")  
abline(v=(1977), col="red", lty="dashed")
```

```
##Black
```

```
plot(Black$Year, Black$DCA, main='Black Lake', xlab='Year',  
      ylab="DCA",  
      type='n', xlim=(c(1895, 2017)), ylim=(c(-1,1)))  
points(Black$Year, Black$DCA, type='b', pch=16, lwd=2, col="black")  
abline(v=(1957), col="red", lty="dashed")
```

```
###Thunder
```

```
plot(Thunder$Year, Thunder$DCA, main='Thunder Lake', xlab='Year',  
      ylab="DCA",  
      type='n', xlim=(c(1895, 2017)), ylim=(c(-1,1)))  
points(Thunder$Year, Thunder$DCA, type='b', pch=16, lwd=2, col="black")  
abline(v=c(2013,1932), col="red", lty="dashed")
```

```
#####  
#####Passive Ordination Plots with Training set #####
```

```
library(rioja)  
library(analogue)
```

```
SWAP <- Training_Set#SWAP training set data  
RLGH <- Blackbugs [,5:27] #Core data Black Lake over the 20th and 21st century, selected taxa  
only are in brackets  
RLGH1 <- Boxbugs [,6:30] #Core data Box Lake over the 20th and 21st century, selected taxa  
only are in brackets  
RLGH2 <- Conybugs [,5:25] #Core data Cony Lake over the 20th and 21st century, selected taxa  
only are in brackets  
RLGH3 <- Eaglebugs [,5:30] #Core data Eagle Lake over the 20th and 21st century, selected  
taxa only are in brackets
```

```
RLGH4 <- Pipitbugs [,4:23] #Core data Pipit Lake over the 20th and 21st century, selected taxa only are in brackets
```

```
RLGH5 <- Thunderbugs [,5:24] #Core data Pipit Lake over the 20th and 21st century, selected taxa only are in brackets
```

```
all spp <- Merge(SWAP, RLGH, split=T)
all spp1 <- Merge(SWAP, RLGH1, split=T)
all spp2 <- Merge(SWAP, RLGH2, split=T)
all spp3 <- Merge(SWAP, RLGH3, split=T)
all spp4 <- Merge(SWAP, RLGH4, split=T)
all spp5 <- Merge(SWAP, RLGH5, split=T)
```

```
CA <- cca(sqrt(all spp$SWAP))
CA1 <- cca(sqrt(all spp1$SWAP))
CA2 <- cca(sqrt(all spp2$SWAP))
CA3 <- cca(sqrt(all spp3$SWAP))
CA4 <- cca(sqrt(all spp4$SWAP))
CA5 <- cca(sqrt(all spp5$SWAP))
```

```
pred <- predict(CA, newdata=sqrt(all spp$RLGH), type="wa")
pred1 <- predict(CA, newdata=sqrt(all spp1$RLGH), type="wa")
pred2 <- predict(CA, newdata=sqrt(all spp2$RLGH), type="wa")
pred3 <- predict(CA, newdata=sqrt(all spp3$RLGH), type="wa")
pred4 <- predict(CA, newdata=sqrt(all spp4$RLGH), type="wa")
pred5 <- predict(CA, newdata=sqrt(all spp5$RLGH), type="wa")
```

```
x11()
par(mar=c(3,3,1,1), mgp=c(1.5,.5,0))
plot(CA, type="n", display="sites")
points(CA, display="sites", pch=19, col="black")
points(pred[,1:2], type="p", pch=19, col="purple")
points(pred1[,1:2], type="p", pch=19, col="red")
points(pred2[,1:2], type="p", pch=19, col="blue")
points(pred3[,1:2], type="p", pch=19, col="green")
points(pred4[,1:2], type="p", pch=19, col="chocolate3")
points(pred5[,1:2], type="p", pch=19, col="darkgoldenrod1")
points(CA, display="sites", pch=19, col="black")
legend("topright", legend=c("Calibration sites", "Cony Lake", "Pipit Lake", "Eagle Lake", "Box Lake", "Black Lake", "Thunder Lake"),
      col=c("black", "blue", "red", "green", "chocolate3", "purple",
"darkgoldenrod1"),
      pch=c(19,19,19,19,19,19,19))
```

```
#####
##### Chronology Plot#####

mylist <- split(Dates, Dates$Lake)
mylist

myerror <- split(Dates1, Dates1$Lake)
myerror

dev.new(height=8, width=10)
par(mfrow=(c(3, 2)))

##CNY

age <-plot(mylist$CNY$Age, mylist$CNY$Depth, main='Cony Lake', xlab='Year (A.D.)',
  ylab= "Depth (cm)",
  type='n', xlim=rev(c(1750, 2017)), ylim=(rev(c(0,18))))

#Lowess Curve code
#Predict Loess
# get smoothed output
fittedcurve <- loess(mylist$CNY$Depth~mylist$CNY$Age, span=0.25)
smoothed50 <- predict(fittedcurve)
lines(smoothed50, x=mylist$CNY$Age, col="black", lwd=1)
points(mylist$CNY$Age, mylist$CNY$Depth, pch=16, col="black")

#adding error bars
points(myerror$CNY$Age, myerror$CNY$Depth, pch=16, col="black")
arrows((myerror$CNY$Age-myerror$CNY$Error), myerror$CNY$Depth,
(myerror$CNY$Age+myerror$CNY$Error),
  myerror$CNY$Depth, length=0.05, angle=90, code=3, col=gray(0.45))

par(new = T)
with(age, plot(mylist$CNY$Age, mylist$CNY$CRS.Sedimentation.Rate, type="l",
lty="dashed", axes=F, xlab=NA, ylab=NA,
  xlim=rev(c(1750, 2017)), ylim=(c(0,0.15)), cex=1.2))
axis(side = 4)
legend("topright",
  legend=c(expression(text="^210*'Pb dates (w/SE bars)'), expression(text= 'CRS
Sedimentation Rate')),
  lty=c(1,3), pch=c(16, NA), cex=0.9 , col=c("black", "black"))

#PIPIT
```

```

age <-plot(mylist$PIP$Age, mylist$PIP$Depth, main='Pipit Lake', xlab='Year (A.D.)',
          ylab= "",
          type='n', xlim=rev(c(1900, 2017)), ylim=(rev(c(0,18))))

#Lowess Curve code
#Predict Loess
# get smoothed output
fittedcurve <- loess(mylist$PIP$Depth~mylist$PIP$Age, span=0.25)
smoothed50 <- predict(fittedcurve)
lines(smoothed50, x=mylist$PIP$Age, col="black", lwd=1)
points(mylist$PIP$Age, mylist$PIP$Depth, pch=16, col="black")

#adding error bars
points(myerror$PIP$Age, myerror$PIP$Depth, pch=16, col="black")
arrows((myerror$PIP$Age-myerror$PIP$Error), myerror$PIP$Depth,
(myerror$PIP$Age+myerror$PIP$Error),
      myerror$PIP$Depth, length=0.05, angle=90, code=3, col=gray(0.45))

par(new = T)
with(age, plot(mylist$PIP$Age, mylist$PIP$CRS.Sedimentation.Rate, type="l", lty="dashed",
axes=F, xlab=NA, ylab=NA,
            xlim=rev(c(1900, 2017)), ylim=(c(0,0.15)), cex=1.2))
axis(side = 4)
legend("topright",
      legend=c(expression(text="^210*Pb dates (w/SE bars)'), expression(text= 'CRS
Sedimentation Rate')),
      lty=c(1,3), pch=c(16, NA),cex=0.9, col=c("black", "black"))

#Eagle

age <-plot(mylist$EGL$Age, mylist$EGL$Depth, main='Eagle Lake', xlab='Year (A.D.)',
          ylab= "Depth (cm)",
          type='n', xlim=rev(c(1800, 2017)), ylim=(rev(c(0,18))))

#Lowess Curve code
#Predict Loess
# get smoothed output
fittedcurve <- loess(mylist$EGL$Depth~mylist$EGL$Age, span=0.25)
smoothed50 <- predict(fittedcurve)
lines(smoothed50, x=mylist$EGL$Age, col="black", lwd=1)
points(mylist$EGL$Age, mylist$EGL$Depth, pch=16, col="black")

#adding error bars

```

```

points(myerror$EGL$Age, myerror$EGL$Depth, pch=16, col="black")
arrows((myerror$EGL$Age-myerror$EGL$Error), myerror$EGL$Depth,
(myerror$EGL$Age+myerror$EGL$Error),
  myerror$EGL$Depth, length=0.05, angle=90, code=3, col=gray(0.45))

par(new = T)
with(age, plot(mylist$EGL$Age, mylist$EGL$CRS.Sedimentation.Rate, type="l", lty="dashed",
axes=F, xlab=NA, ylab=NA,
  xlim=rev(c(1800, 2017)), ylim=(c(0,0.15)), cex=1.2))
axis(side = 4)
legend("topright",
  legend=c(expression(text="^210*'Pb dates (w/SE bars)'), expression(text= 'CRS
Sedimentation Rate')),
  lty=c(1,3), pch=c(16, NA), cex=0.9, col=c("black", "black"))

#Box main='Box Lake (3274 m asl)

age <-plot(mylist$BOX$Age, mylist$BOX$Depth, main='Box Lake', xlab='Year (A.D.)',
  ylab= "",
  type='n', xlim=rev(c(1900, 2017)), ylim=(rev(c(0,10))))

#Lowess Curve code
#Predict Loess
# get smoothed output
fittedcurve <- loess(mylist$BOX$Depth~mylist$BOX$Age, span=0.25)
smoothed50 <- predict(fittedcurve)
lines(smoothed50, x=mylist$BOX$Age, col="black", lwd=1)
points(mylist$BOX$Age, mylist$BOX$Depth, pch=16, col="black")

#adding error bars
points(myerror$BOX$Age, myerror$BOX$Depth, pch=16, col="black")
arrows((myerror$BOX$Age-myerror$BOX$Error), myerror$BOX$Depth,
(myerror$BOX$Age+myerror$BOX$Error),
  myerror$BOX$Depth, length=0.05, angle=90, code=3, col=gray(0.45))

par(new = T)
with(age, plot(mylist$BOX$Age, mylist$BOX$CRS.Sedimentation.Rate, type="l",
lty="dashed", axes=F, xlab=NA, ylab=NA,
  xlim=rev(c(1900, 2017)), ylim=(c(0,0.15)), cex=1.2))
axis(side = 4)
legend("topright",
  legend=c(expression(text="^210*'Pb dates (w/SE bars)'), expression(text= 'CRS
Sedimentation Rate')),
  lty=c(1,3), pch=c(16, NA), cex=0.9, col=c("black", "black"))

```

```

##Black main='Black Lake (3237 m asl)

age <-plot(mylist$BLK$Age, mylist$BLK$Depth, main='Black Lake', xlab='Year (A.D.)',
          ylab= "Depth (cm)",
          type='n', xlim=rev(c(1750, 2017)), ylim=(rev(c(0,18))))

#Lowess Curve code
#Predict Loess
# get smoothed output
fittedcurve <- loess(mylist$BLK$Depth~mylist$BLK$Age, span=0.25)
smoothed50 <- predict(fittedcurve)
lines(smoothed50, x=mylist$BLK$Age, col="black", lwd=1)
points(mylist$BLK$Age, mylist$BLK$Depth, pch=16, col="black")

#adding error bars
points(myerror$BLK$Age, myerror$BLK$Depth, pch=16, col="black")
arrows((myerror$BLK$Age-myerror$BLK$Error), myerror$BLK$Depth,
(myerror$BLK$Age+myerror$BLK$Error),
      myerror$BLK$Depth, length=0.05, angle=90, code=3, col=gray(0.45))

par(new = T)
with(age, plot(mylist$BLK$Age, mylist$BLK$CRS.Sedimentation.Rate, type="l", lty="dashed",
axes=F, xlab=NA, ylab=NA,
          xlim=rev(c(1750, 2017)), ylim=(c(0,0.15)), cex=1.2))
axis(side = 4)
legend("topright",
      legend=c(expression(text="^210*Pb dates (w/SE bars)'), expression(text= 'CRS
Sedimentation Rate')),
      lty=c(1,3), pch=c(16, NA), cex=0.9, col=c("black", "black"))

##Thunder

age <-plot(mylist$THD$Age, mylist$THD$Depth, main='Thunder Lake', xlab='Year (A.D.)',
          ylab= "",
          type='n', xlim=rev(c(1750, 2017)), ylim=(rev(c(0,18))))

#Lowess Curve code
#Predict Loess
# get smoothed output
fittedcurve <- loess(mylist$THD$Depth~mylist$THD$Age, span=0.25)
smoothed50 <- predict(fittedcurve)
lines(smoothed50, x=mylist$THD$Age, col="black", lwd=1)
points(mylist$THD$Age, mylist$THD$Depth, pch=16, col="black")

```

```

#adding error bars
points(myerror$THD$Age, myerror$THD$Depth, pch=16, col="black")
arrows((myerror$THD$Age-myerror$THD$Error), myerror$THD$Depth,
(myerror$THD$Age+myerror$THD$Error),
      myerror$THD$Depth, length=0.05, angle=90, code=3, col=gray(0.45))

par(new = T)
with(age, plot(mylist$THD$Age, mylist$THD$CRS.Sedimentation.Rate, type="l",
lty="dashed", axes=F, xlab=NA, ylab=NA,
      xlim=rev(c(1750, 2017)), ylim=(c(0,0.15)), cex=1.2))
axis(side = 4)
legend("topright",
      legend=c(expression(text="^210*'Pb dates (w/SE bars)'), expression(text= 'CRS
Sedimentation Rate')),
      lty=c(1,3), pch=c(16, NA), cex=0.9, col=c("black", "black"))

#####Constrained heirarchical clustering#####
library(olsrr)
library(vegan)
library(palaeoSig)

dev.new(height=8, width=10)
par(mfrow=c(1,1))

#Finding distance measures
dud.dist1 <- dist(sqrt(Lake_Rel_Abun))
dud.clust1 <- chclust(dud.dist1)
plot(dud.clust1,hang=-1)
plot(dud.clust1,hang=-1, horiz=TRUE ,x.rev=TRUE)
plot(dud.clust1,hang=-1, horiz=TRUE ,x.rev=TRUE,cex=.6,main="Cluster Analysis of Thunder
Lake")

#With the function rect.hclust (vegan) is it possible to visualize them:
plot(dud.clust1,hang=-1,cex=.6,main="Cluster Analysis of Thunder Lake")
rect.hclust(dud.clust1,3)

#Let's try a different distance metric:
dud.dist2 <- vegdist(sqrt(Lake_Rel_Abun))
dud.clust2 <- chclust(dud.dist2)
par(mfrow=c(1,1))
plot(dud.clust1,hang=-1,cex=.6) #cex specify here the size of the sample labels
plot(dud.clust2,hang=-1,cex=.6)

```

```
#we can than compare the correlation of the graphical output with the originally distances between the samples:
```

```
cor(dud.dist1, cophenetic(dud.clust1))
```

```
# 0.6072662
```

```
cor(dud.dist2, cophenetic(dud.clust2))
```

```
#0.0.6648711
```

```
#As we have distinguished two groups we can create a vector enfold the information of the membership to this 12 groups, by numbers 1,2
```

```
grp <- cutree(dud.clust1, 2)
```

```
#Now we can run a multivariable analysis of the core data:
```

```
mod<-cca(sqrt(Lake_Rel_Abun))
```

```
plot(mod,type="n")
```

```
text(mod,display="sites",col=grp)
```

```
#Before applying a transfer function to the core data, it has to be checked, whether the core data are
```

```
#well represented by the used training
```

```
library (analogue)
```

```
data <- join(Training_Set, Lake_Rel_Abun, verbose = TRUE)
```

```
# both data sets need to have the same columns, alternative function: join in package analogue or the function merge().
```

```
dev.new(height=8, width=10)
```

```
names(data)
```

```
mod<-cca(downweight(sqrt(data$Training_Set))) # normal CA
```

```
fit<-predict(mod,newdata=sqrt(data$Lake_Rel_Abun),type="wa") # prediction of the core data using the CA model
```

```
plot(mod,type="n")
```

```
points(mod,dis="sites",pch=19,col=4)
```

```
points(fit,col=grp,pch=19)
```

```
legend("bottomright",c("WUS Training Set","KLZ1","KLZ2"),pch=19,col=c(4,1,2,3))
```

```
#####
```

```
##### Deviations SWT and MJAT WITH PRISM MJAT #####
```

```
dev.new(height=8, width=10)
```

```
par(mfrow=(c(3, 2)))
```

```
##CNY
```

```

Dev <-plot(Cony$Year, Cony$Difference, main='Cony Lake', xlab='Year (A.D.)',
          ylab= expression(paste("Temperature [",degree,"C]")),
          type='n', xlim=(c(1895, 2017)), ylim=((c(-3,3))))

##Plotted SWT and LOWESS of PRISM

#PRism temp with midge-Based SWT and lowess of PRISM
#points(mylist$Cony$Date, mylist$Cony$X, type="l", lwd=1, col="dark gray")
#fittedcurve <- loess(mylist$Cony$X~mylist$Cony$Date, span=0.20)
#smoothed20 <- predict(fittedcurve)
#lines(smoothed20, x=mylist$Cony$Date, col="black", lwd=2)
#points(Cony$Year, Cony$SWT, type="b", lwd=2, pch=16, col="blue")

#adding error bars
#arrows(Cony$Year, (Cony$SWT-Cony$SWT_SSE), Cony$Year,
        (Cony$SWT+Cony$SWT_SSE),
        # length=0.05, angle=90, code=3, col="blue")

#Deviation of Prism-based MJAT with deviation of midge inferred MJAT
points(mylist$Cony$Date, mylist$Cony$dev, type="h", lwd=3, col="darkgray")
abline(h=0, col="black", lwd=2 )
points(Cony$Year, Cony$dev.avg.MJAT, type="b", lwd=3, pch=16, col="red")
points(Cony$Year, Cony$dev.SWT.SWT, type="b", lwd=3, pch=16, col="blue")
#points(Cony$Year, Cony$dev.SWT.Prism, type="l", lwd=2, pch=16, col="forestgreen")
#points(Cony$Year, Cony$Inverse.dev.SWT, type="l", lwd=2, pch=16, col="darkorange1")

#Legend
#legend("bottomright",
        #legend=c("Deviation of PRISM-based MJAT", "Deviation of chironomid-inferred MJAT",
        "Deviation of chironomid-inferred SWT"),
        #lty=c(NA,1,1), pch=c(15,16,16), cex=0.5, col=c("dark gray", "red", "blue"))

#####PIPIT#####
#####
dev.new(height=8, width=10)
par(mfrow=(c(1, 1)))

####Pipit###

Dev <-plot(Eagle$Year, Pipit$Difference, main='Pipit Lake', xlab='Year (A.D.)',
          ylab= expression(paste("Temperature [",degree,"C]")),
          type='n', xlim=(c(1895, 2017)), ylim=((c(-3,3))))

```

```

#PRism temp with midge-Based SWT and lowess of PRISM
#points(mylist$Pipit$Date, mylist$Pipit$X, type="l", lwd=1, col="dark gray")
#fittedcurve <- loess(mylist$Pipit$X~mylist$Pipit$Date, span=0.20)
#smoothed20 <- predict(fittedcurve)
#lines(smoothed20, x=mylist$Pipit$Date, col="black", lwd=2)
#points(Pipit$Year, Pipit$SWT, type="b", lwd=2, pch=16, col="blue")

#adding error bars
#arrows(Pipit$Year, (Pipit$SWT-Pipit$SWT_SSE), Pipit$Year, (Pipit$SWT+Pipit$SWT_SSE),
#length=0.05, angle=90, code=3, col="blue")

#Deviation of Prism-based MJAT with deviation of midge inferred MJAT
points(mylist$Pipit$Date, mylist$Pipit$dev, type="h", lwd=3, col="dark gray")
abline(h=0, col="black", lwd=2 )
points(Pipit$Year, Pipit$dev.avg.MJAT, type="b", lwd=3, pch=16, col="red")
points(Pipit$Year, Pipit$dev.SWT.SWT, type="b", lwd=3, pch=16, col="blue")

#Legend
legend("bottomright",
      legend=c("Deviation of PRISM-based MJAT", "Deviation of chironomid-inferred MJAT",
"Deviation of chironomid-inferred SWT"),
      lty=c(NA,1,1), pch=c(15,16,16), cex=0.8, col=c("dark gray", "red", "blue"))

#####
#####Eagle#####

dev.new(height=8, width=10)
par(mfrow=(c(1, 1)))

Dev <-plot(Eagle$Year, Eagle$Difference, main='Eagle Lake', xlab='Year (A.D.)',
      ylab= expression(paste("Temperature [",degree,"C]")),
      type='n', xlim=(c(1895, 2017)), ylim=((c(-3,3))))

#PRism temp with midge-Based SWT and lowess of PRISM
#points(mylist$Eagle$Date, mylist$Eagle$X, type="l", lwd=1, col="dark gray")
#fittedcurve <- loess(mylist$Eagle$X~mylist$Eagle$Date, span=0.20)
#smoothed20 <- predict(fittedcurve)
#lines(smoothed20, x=mylist$Eagle$Date, col="black", lwd=2)
#points(Eagle$Year, Eagle$SWT, type="b", lwd=2, pch=16, col="blue")

#adding error bars
#arrows(Eagle$Year, (Eagle$SWT-Eagle$SWT_SSE), Eagle$Year,
(Eagle$SWT+Eagle$SWT_SSE),
      #length=0.05, angle=90, code=3, col="blue")

```

```

#Deviation of Prism-based MJAT with deviation of midge inferred MJAT
points(mylist$Eagle$Date, mylist$Eagle$dev, type="h", lwd=3, col="dark gray")
abline(h=0, col="black", lwd=2 )

points(Eagle$Year, Eagle$dev.avg.MJAT, type="b", lwd=3, pch=16, col="red")
points(Eagle$Year, Eagle$dev.SWT.SWT, type="b", lwd=3, pch=16, col="blue")

#Legend
legend("bottomright",
      legend=c("Deviation of PRISM-based MJAT", "Deviation of chironomid-inferred MJAT",
              "Deviation of chironomid-inferred SWT"),
      lty=c(NA,1,1), pch=c(15,16,16), cex=0.8, col=c("dark gray", "red", "blue"))

#####
#####Box#####
dev.new(height=8, width=10)
par(mfrow=(c(1, 1)))

Dev <-plot(Box$Year, Box$Difference, main='Box Lake', xlab='Year (A.D.)',
          ylab= expression(paste("Temperature [",degree,"C]")),
          type='n', xlim=(c(1895, 2017)), ylim=((c(-3,3))))

#PRism temp with midge-Based SWT and lowess of PRISM
#points(mylist$Box$Date, mylist$Box$X, type="l", lwd=1, col="dark gray")
#fittedcurve <- loess(mylist$Box$X~mylist$Box$Date, span=0.20)
#smoothed20 <- predict(fittedcurve)
#lines(smoothed20, x=mylist$Box$Date, col="black", lwd=2)
#points(Box$Year, Box$SWT, type="b", lwd=2, pch=16, col="blue")

#adding error bars
#arrows(Box$Year, (Box$SWT-Box$SWT_SSE), Box$Year, (Box$SWT+Box$SWT_SSE),
        #length=0.05, angle=90, code=3, col="blue")

#Deviation of Prism-based MJAT with deviation of midge inferred MJAT
points(mylist$Box$Date, mylist$Box$dev, type="h", lwd=3, col="dark gray")
abline(h=0, col="black", lwd=2 )
points(Box$Year, Box$dev.avg.MJAT, type="b", lwd=3, pch=16, col="red")
points(Box$Year, Box$dev.SWT.SWT, type="b", lwd=3, pch=16, col="blue")

#Legend
legend("bottomright",
      legend=c("Deviation of PRISM-based MJAT", "Deviation of chironomid-inferred MJAT",
              "Deviation of chironomid-inferred SWT"),

```

```

lty=c(NA,1,1), pch=c(15,16,16), cex=0.8, col=c("dark gray", "red", "blue"))

#####
#####Black#####
dev.new(height=8, width=10)
par(mfrow=c(1, 1)))

Dev <-plot(Black$Year, Black$Difference, main='Black Lake', xlab='Year (A.D.)',
          ylab= expression(paste("Temperature [",degree,"C]")),
          type='n', xlim=c(1895, 2017)), ylim=((c(-3,3))))

#PRism temp with midge-Based SWT and lowess of PRISM
#points(mylist$Black$Date, mylist$Black$X, type="l", lwd=1, col="dark gray")
#fittedcurve <- loess(mylist$Black$X~mylist$Black$Date, span=0.20)
#smoothed20 <- predict(fittedcurve)
#lines(smoothed20, x=mylist$Black$Date, col="black", lwd=2)
#points(Black$Year, Black$SWT, type="b", lwd=2, pch=16, col="blue")

#adding error bars
#arrows(Black$Year, (Black$SWT-Black$SWT_SSE), Black$Year,
        (Black$SWT+Black$SWT_SSE),
        #length=0.05, angle=90, code=3, col="blue")

#Deviation of Prism-based MJAT with deviation of midge inferred MJAT
points(mylist$Black$Date, mylist$Black$dev, type="h", lwd=3, col="dark gray")
abline(h=0, col="black", lwd=2 )
points(Black$Year, Black$dev.avg.MJAT, type="b", lwd=3, pch=16, col="red")
points(Black$Year, Black$dev.SWT.SWT, type="b", lwd=3, pch=16, col="blue")

#Legend
legend("bottomright",
      legend=c("Deviation of PRISM-based MJAT", "Deviation of chironomid-inferred MJAT",
              "Deviation of chironomid-inferred SWT"),
      lty=c(NA,1,1), pch=c(15,16,16), cex=0.8, col=c("dark gray", "red", "blue"))

#####
#####Thunder#####

dev.new(height=8, width=10)
par(mfrow=c(1, 1)))

Dev <-plot(Thunder$Year, Thunder$Difference, main='Thunder Lake', xlab='Year (A.D.)',
          ylab= expression(paste("Temperature [",degree,"C]")),
          type='n', xlim=c(1895, 2017)), ylim=((c(-3,3))))

```

```

#PRism temp with midge-Based SWT and lowess of PRISM
#points(mylist$Thunder$Date, mylist$Thunder$X, type="l", lwd=1, col="dark gray")
#fittedcurve <- loess(mylist$Thunder$X~mylist$Thunder$Date, span=0.20)
#smoothed20 <- predict(fittedcurve)
#lines(smoothed20, x=mylist$Thunder$Date, col="black", lwd=2)
#points(Thunder$Year, Thunder$SWT, type="b", lwd=2, pch=16, col="blue")

#adding error bars
#arrows(Thunder$Year, (Thunder$SWT-Thunder$SWT_SSE), Thunder$Year,
(Thunder$SWT+Thunder$SWT_SSE),
  #length=0.05, angle=90, code=3, col="blue")

#Deviation of Prism-based MJAT with deviation of midge inferred MJAT
points(mylist$Thunder$Date, mylist$Thunder$dev, type="h", lwd=3, col="dark gray")
abline(h=0, col="black", lwd=2 )
points(Thunder$Year, Thunder$dev.avg.MJAT, type="b", lwd=3, pch=16, col="red")
points(Thunder$Year, Thunder$dev.SWT.SWT, type="b", lwd=3, pch=16, col="blue")

#Legend
legend("bottomright",
  legend=c("Deviation of PRISM-based MJAT", "Deviation of chironomid-inferred MJAT",
"Deviation of chironomid-inferred SWT"),
  lty=c(NA,1,1), pch=c(15,16,16), cex=0.8, col=c("dark gray", "red", "blue"))

#####KITE DEVIATIONS#####
dev.new(height=8, width=10)
par(mfrow=(c(1, 1)))

plot(Kite$Year, Kite$MJAT, main='Kite Lake', xlab='cal yr BP',
  ylab=expression(paste("Temperature [",degree,"C]")),
  type='n', xlim=rev(c(12700, 9200)), ylim=(c(-4,4)))

abline(h=0, col="black", lwd=2 )
points(Kite$Year, Kite$dev.avg.MJAT, type="h", lwd=3, col="red")
points(Kite$Year, Kite$dev.SWT.SWT, type="h", lwd=3, col="blue")
#points(Kite$Year, Kite$dev.avg.MJAT, type="b", lwd=3, pch=16, col="red")
#points(Kite$Year, Kite$dev.SWT.SWT, type="b", lwd=3, pch=16, col="blue")
#adding dark rectangles to represent 0-5 chironomids present
rect(11950, 4, 12800, -4, col=gray(0.50), border=gray(0.50))
rect(10450, 4, 10550, -4, col=gray(0.50), border=gray(0.50))

#adding dark rectangles to represent no chironomid data available
rect(10340, 4, 10450, -4, col=gray(0.90), border=gray(0.90))
rect(10550, 4, 10820, -4, col=gray(0.90), border=gray(0.90))

```

```

#Legend
legend("bottomleft",
  legend=c("Deviations from average chironomid-based SWT", "Deviations from average
chironomid-based MJAT", "No chironomids recovered", "Not enough data available"),
  pch=c(15,15,15,15), cex=0.8, col=c("blue", "red", "dark gray", "light gray"))

#####
##### Bland Altman Plots #####

library(gridExtra)
dev.new(height=8, width=10)
#https://www.r-bloggers.com/bland-altmantukey-mean-difference-plots-using-ggplot2/

#Cony

#Each row in the dataframe consists of a pair of measurements. The Bland-Altman plot has the
average of the
#two measures in a pair on the x-axis. The y-axis contains the difference between the two
measures in each pair.
#Add the averages and differences data to the dataframe.

ConyAvg <- (Cony$SWT + Cony$PRISM.MJAT) / 2
ConyDif <- Cony$SWT - Cony$PRISM.MJAT

#Finally, code the plot and add the mean difference (blue line) and a 95% confidence interval
(red lines)
#for predictions of a mean difference. This prediction interval gives the level of agreement (1.96
* SD).

Conypl <-ggplot(Cony, aes(x = ConyAvg, y = ConyDif)) +
  geom_point(alpha = 0.5) +
  geom_hline(yintercept = mean(ConyDif), colour = "blue", size = 0.5) +
  geom_hline(yintercept = mean(ConyDif) - (1.96 * sd(ConyDif)), colour = "red", size = 0.5)
+
  geom_hline(yintercept = mean(ConyDif) + (1.96 * sd(ConyDif)), colour = "red", size = 0.5)
+
  ylab("Difference") +
  xlab("Average Temperature") + ggtitle("Cony Lake") + coord_cartesian(ylim = c(-6, 6))

#Pipit
PipitAvg <- (Pipit$SWT + Pipit$PRISM.MJAT) / 2

```

```
PipitDif <- Pipit$SWT - Pipit$PRISM.MJAT
```

```
#Finally, code the plot and add the mean difference (blue line) and a 95% confidence interval (red lines)
```

```
#for predictions of a mean difference. This prediction interval gives the level of agreement (1.96 * SD).
```

```
Pipitpl <-ggplot(Pipit, aes(x = PipitAvg, y = PipitDif)) +  
  geom_point(alpha = 0.5) +  
  geom_hline(yintercept = mean(PipitDif), colour = "blue", size = 0.5) +  
  geom_hline(yintercept = mean(PipitDif) - (1.96 * sd(PipitDif)), colour = "red", size = 0.5) +  
  geom_hline(yintercept = mean(PipitDif) + (1.96 * sd(PipitDif)), colour = "red", size = 0.5)  
+  
  ylab("Difference") +  
  xlab("Average Temperature") + ggtitle("Pipit Lake") + coord_cartesian(ylim = c(-6, 6))
```

```
#Eagle
```

```
EagleAvg <- (Eagle$SWT + Eagle$PRISM.MJAT) / 2
```

```
EagleDif <- Eagle$SWT - Eagle$PRISM.MJAT
```

```
#Finally, code the plot and add the mean difference (blue line) and a 95% confidence interval (red lines)
```

```
#for predictions of a mean difference. This prediction interval gives the level of agreement (1.96 * SD).
```

```
Eaglepl <-ggplot(Eagle, aes(x = EagleAvg, y = EagleDif)) +  
  geom_point(alpha = 0.5) +  
  geom_hline(yintercept = mean(EagleDif), colour = "blue", size = 0.5) +  
  geom_hline(yintercept = mean(EagleDif) - (1.96 * sd(EagleDif)), colour = "red", size = 0.5)  
+  
  geom_hline(yintercept = mean(EagleDif) + (1.96 * sd(EagleDif)), colour = "red", size =  
0.5) +  
  ylab("Difference") +  
  xlab("Average Temperature") + ggtitle("Eagle Lake") + coord_cartesian(ylim = c(-6, 6))
```

```
#Box
```

```
BoxAvg <- (Box$SWT + Box$PRISM.MJAT) / 2
```

```
BoxDif <- Box$SWT - Box$PRISM.MJAT
```

```
#Finally, code the plot and add the mean difference (blue line) and a 95% confidence interval (red lines)
```

```
#for predictions of a mean difference. This prediction interval gives the level of agreement (1.96 * SD).
```

```
Boxpl <-ggplot(Box, aes(x = BoxAvg, y = BoxDif)) +
```

```

geom_point(alpha = 0.5) +
geom_hline(yintercept = mean(BoxDif), colour = "blue", size = 0.5) +
geom_hline(yintercept = mean(BoxDif) - (1.96 * sd(BoxDif)), colour = "red", size = 0.5) +
geom_hline(yintercept = mean(BoxDif) + (1.96 * sd(BoxDif)), colour = "red", size = 0.5) +
ylab("Difference") +
xlab("Average Temperature") + ggtitle("Box Lake") + coord_cartesian(ylim = c(-6, 6))

```

```
#Black
```

```
BlackAvg <- (Black$SWT + Black$PRISM.MJAT) / 2
```

```
BlackDif <- Black$SWT - Black$PRISM.MJAT
```

```
#Finally, code the plot and add the mean difference (blue line) and a 95% confidence interval (red lines)
```

```
#for predictions of a mean difference. This prediction interval gives the level of agreement (1.96 * SD).
```

```

Blackpl <-ggplot(Black, aes(x = BlackAvg, y = BlackDif)) +
  geom_point(alpha = 0.5) +
  geom_hline(yintercept = mean(BlackDif), colour = "blue", size = 0.5) +
  geom_hline(yintercept = mean(BlackDif) - (1.96 * sd(BlackDif)), colour = "red", size = 0.5)
+
  geom_hline(yintercept = mean(BlackDif) + (1.96 * sd(BlackDif)), colour = "red", size =
0.5) +
  ylab("Difference") +
  xlab("Average Temperature") + ggtitle("Black Lake") + coord_cartesian(ylim = c(-6, 6))

```

```
#Thunder
```

```
ThunderAvg <- (Thunder$SWT + Thunder$PRISM.MJAT) / 2
```

```
ThunderDif <- Thunder$SWT - Thunder$PRISM.MJAT
```

```
#Finally, code the plot and add the mean difference (blue line) and a 95% confidence interval (red lines)
```

```
#for predictions of a mean difference. This prediction interval gives the level of agreement (1.96 * SD).
```

```

Thunderpl <-ggplot(Thunder, aes(x = ThunderAvg, y = ThunderDif)) +
  geom_point(alpha = 0.5) +
  geom_hline(yintercept = mean(ThunderDif), colour = "blue", size = 0.5) +
  geom_hline(yintercept = mean(ThunderDif) - (1.96 * sd(ThunderDif)), colour = "red", size
= 0.5) +
  geom_hline(yintercept = mean(ThunderDif) + (1.96 * sd(ThunderDif)), colour = "red", size
= 0.5) +
  ylab("Difference") +
  xlab("Average Temperature") + ggtitle("Thunder Lake") + coord_cartesian(ylim = c(-6, 6))

```

```
grid.arrange(Conypl, Pipitpl, Eaglepl, Boxpl, Blackpl, Thunderpl, ncol=2, nrow=3, top="Bland-Altman Plot")
```

```
#####  
Bland-Altman Plots for differences btwn midge-MJAT and PRISM-MJAT #####
```

```
dev.new(height=8, width=10)  
#https://www.r-bloggers.com/bland-altmantukey-mean-difference-plots-using-ggplot2/
```

```
#Cony
```

```
ConyAvg <- (Cony$MJAT + Cony$PRISM.MJAT) / 2  
ConyDif <- Cony$MJAT - Cony$PRISM.MJAT
```

```
#Finally, code the plot and add the mean difference (blue line) and a 95% confidence interval  
(red lines)  
#for predictions of a mean difference. This prediction interval gives the level of agreement (1.96  
* SD).
```

```
Conypl <-ggplot(Cony, aes(x = ConyAvg, y = ConyDif)) +  
  geom_point(alpha = 0.5) +  
  geom_hline(yintercept = mean(ConyDif), colour = "blue", size = 0.5) +  
  geom_hline(yintercept = mean(ConyDif) - (1.96 * sd(ConyDif)), colour = "red", size = 0.5) +  
  geom_hline(yintercept = mean(ConyDif) + (1.96 * sd(ConyDif)), colour = "red", size = 0.5) +  
  ylab("Difference") +  
  xlab("Average Temperature") + ggtitle("Cony Lake") + coord_cartesian(ylim = c(-6, 6))
```

```
#Pipit
```

```
PipitAvg <- (Pipit$MJAT + Pipit$PRISM.MJAT) / 2  
PipitDif <- Pipit$MJAT - Pipit$PRISM.MJAT
```

```
#Finally, code the plot and add the mean difference (blue line) and a 95% confidence interval  
(red lines)  
#for predictions of a mean difference. This prediction interval gives the level of agreement (1.96  
* SD).
```

```
Pipitpl <-ggplot(Pipit, aes(x = PipitAvg, y = PipitDif)) +  
  geom_point(alpha = 0.5) +  
  geom_hline(yintercept = mean(PipitDif), colour = "blue", size = 0.5) +  
  geom_hline(yintercept = mean(PipitDif) - (1.96 * sd(PipitDif)), colour = "red", size = 0.5) +  
  geom_hline(yintercept = mean(PipitDif) + (1.96 * sd(PipitDif)), colour = "red", size = 0.5) +
```

```

ylab("Difference") +
xlab("Average Temperature") + ggtitle("Pipit Lake") + coord_cartesian(ylim = c(-6, 6))

#Eagle
EagleAvg <- (Eagle$MJAT + Eagle$PRISM.MJAT) / 2
EagleDif <- Eagle$MJAT - Eagle$PRISM.MJAT

#Finally, code the plot and add the mean difference (blue line) and a 95% confidence interval
(red lines)
#for predictions of a mean difference. This prediction interval gives the level of agreement (1.96
* SD).

Eaglepl <-ggplot(Eagle, aes(x = EagleAvg, y = EagleDif)) +
  geom_point(alpha = 0.5) +
  geom_hline(yintercept = mean(EagleDif), colour = "blue", size = 0.5) +
  geom_hline(yintercept = mean(EagleDif) - (1.96 * sd(EagleDif)), colour = "red", size = 0.5) +
  geom_hline(yintercept = mean(EagleDif) + (1.96 * sd(EagleDif)), colour = "red", size = 0.5) +
  ylab("Difference") +
  xlab("Average Temperature") + ggtitle("Eagle Lake") + coord_cartesian(ylim = c(-6, 6))

#Box
BoxAvg <- (Box$MJAT + Box$PRISM.MJAT) / 2
BoxDif <- Box$MJAT - Box$PRISM.MJAT

#Finally, code the plot and add the mean difference (blue line) and a 95% confidence interval
(red lines)
#for predictions of a mean difference. This prediction interval gives the level of agreement (1.96
* SD).

Boxpl <-ggplot(Box, aes(x = BoxAvg, y = BoxDif)) +
  geom_point(alpha = 0.5) +
  geom_hline(yintercept = mean(BoxDif), colour = "blue", size = 0.5) +
  geom_hline(yintercept = mean(BoxDif) - (1.96 * sd(BoxDif)), colour = "red", size = 0.5) +
  geom_hline(yintercept = mean(BoxDif) + (1.96 * sd(BoxDif)), colour = "red", size = 0.5) +
  ylab("Difference") +
  xlab("Average Temperature") + ggtitle("Box Lake") + coord_cartesian(ylim = c(-6, 6))

#Black
BlackAvg <- (Black$MJAT + Black$PRISM.MJAT) / 2
BlackDif <- Black$MJAT - Black$PRISM.MJAT

#Finally, code the plot and add the mean difference (blue line) and a 95% confidence interval
(red lines)

```

#for predictions of a mean difference. This prediction interval gives the level of agreement (1.96 * SD).

```
Blackpl <-ggplot(Black, aes(x = BlackAvg, y = BlackDif)) +  
  geom_point(alpha = 0.5) +  
  geom_hline(yintercept = mean(BlackDif), colour = "blue", size = 0.5) +  
  geom_hline(yintercept = mean(BlackDif) - (1.96 * sd(BlackDif)), colour = "red", size = 0.5) +  
  geom_hline(yintercept = mean(BlackDif) + (1.96 * sd(BlackDif)), colour = "red", size = 0.5) +  
  ylab("Difference") +  
  xlab("Average Temperature") + ggtitle("Black Lake") + coord_cartesian(ylim = c(-6, 6))
```

#Thunder

```
ThunderAvg <- (Thunder$MJAT + Thunder$PRISM.MJAT) / 2  
ThunderDif <- Thunder$MJAT - Thunder$PRISM.MJAT
```

#Finally, code the plot and add the mean difference (blue line) and a 95% confidence interval (red lines)

#for predictions of a mean difference. This prediction interval gives the level of agreement (1.96 * SD).

```
Thunderpl <-ggplot(Thunder, aes(x = ThunderAvg, y = ThunderDif)) +  
  geom_point(alpha = 0.5) +  
  geom_hline(yintercept = mean(ThunderDif), colour = "blue", size = 0.5) +  
  geom_hline(yintercept = mean(ThunderDif) - (1.96 * sd(ThunderDif)), colour = "red", size =  
0.5) +  
  geom_hline(yintercept = mean(ThunderDif) + (1.96 * sd(ThunderDif)), colour = "red", size =  
0.5) +  
  ylab("Difference") +  
  xlab("Average Temperature") + ggtitle("Thunder Lake") + coord_cartesian(ylim = c(-6, 6))
```

```
grid.arrange(Conypl, Pipitpl, Eaglepl, Boxpl, Blackpl, Thunderpl, ncol=2, nrow=3, top="Bland-  
Altman Plot")
```

#####Bland-Altman Plots for differences btwn midge-MJAT and midge-SWT ###

```
dev.new(height=8, width=10)
```

```
#https://www.r-bloggers.com/bland-altmantukey-mean-difference-plots-using-ggplot2/
```

#Cony

```
ConyAvg <- (Cony$MJAT + Cony$SWT) / 2  
ConyDif <- Cony$MJAT - Cony$SWT
```

```
#Finally, code the plot and add the mean difference (blue line) and a 95% confidence interval (red lines)
#for predictions of a mean difference. This prediction interval gives the level of agreement (1.96 * SD).
```

```
Conypl <-ggplot(Cony, aes(x = ConyAvg, y = ConyDif)) +
  geom_point(alpha = 0.5) +
  geom_hline(yintercept = mean(ConyDif), colour = "blue", size = 0.5) +
  geom_hline(yintercept = mean(ConyDif) - (1.96 * sd(ConyDif)), colour = "red", size = 0.5) +
  geom_hline(yintercept = mean(ConyDif) + (1.96 * sd(ConyDif)), colour = "red", size = 0.5) +
  ylab("Difference") +
  xlab("Average Temperature") + ggtitle("Cony Lake") + coord_cartesian(ylim = c(-6, 6))
```

```
#Pipit
PipitAvg <- (Pipit$MJAT + Pipit$SWT) / 2
PipitDif <- Pipit$MJAT - Pipit$SWT
```

```
#Finally, code the plot and add the mean difference (blue line) and a 95% confidence interval (red lines)
#for predictions of a mean difference. This prediction interval gives the level of agreement (1.96 * SD).
```

```
Pipitpl <-ggplot(Pipit, aes(x = PipitAvg, y = PipitDif)) +
  geom_point(alpha = 0.5) +
  geom_hline(yintercept = mean(PipitDif), colour = "blue", size = 0.5) +
  geom_hline(yintercept = mean(PipitDif) - (1.96 * sd(PipitDif)), colour = "red", size = 0.5) +
  geom_hline(yintercept = mean(PipitDif) + (1.96 * sd(PipitDif)), colour = "red", size = 0.5) +
  ylab("Difference") +
  xlab("Average Temperature") + ggtitle("Pipit Lake") + coord_cartesian(ylim = c(-6, 6))
```

```
#Eagle
EagleAvg <- (Eagle$MJAT + Eagle$SWT) / 2
EagleDif <- Eagle$MJAT - Eagle$SWT
```

```
#Finally, code the plot and add the mean difference (blue line) and a 95% confidence interval (red lines)
#for predictions of a mean difference. This prediction interval gives the level of agreement (1.96 * SD).
```

```
Eaglepl <-ggplot(Eagle, aes(x = EagleAvg, y = EagleDif)) +
  geom_point(alpha = 0.5) +
  geom_hline(yintercept = mean(EagleDif), colour = "blue", size = 0.5) +
  geom_hline(yintercept = mean(EagleDif) - (1.96 * sd(EagleDif)), colour = "red", size = 0.5) +
```

```
geom_hline(yintercept = mean(EagleDif) + (1.96 * sd(EagleDif)), colour = "red", size = 0.5) +
ylab("Difference") +
xlab("Average Temperature") + ggtitle("Eagle Lake") + coord_cartesian(ylim = c(-6, 6))
```

```
#Box
```

```
BoxAvg <- (Box$MJAT + Box$SWT) / 2
```

```
BoxDif <- Box$MJAT - Box$SWT
```

```
#Finally, code the plot and add the mean difference (blue line) and a 95% confidence interval (red lines)
```

```
#for predictions of a mean difference. This prediction interval gives the level of agreement (1.96 * SD).
```

```
Boxpl <-ggplot(Box, aes(x = BoxAvg, y = BoxDif)) +
  geom_point(alpha = 0.5) +
  geom_hline(yintercept = mean(BoxDif), colour = "blue", size = 0.5) +
  geom_hline(yintercept = mean(BoxDif) - (1.96 * sd(BoxDif)), colour = "red", size = 0.5) +
  geom_hline(yintercept = mean(BoxDif) + (1.96 * sd(BoxDif)), colour = "red", size = 0.5) +
  ylab("Difference") +
  xlab("Average Temperature") + ggtitle("Box Lake") + coord_cartesian(ylim = c(-6, 6))
```

```
#Black
```

```
BlackAvg <- (Black$MJAT + Black$SWT) / 2
```

```
BlackDif <- Black$MJAT - Black$SWT
```

```
#Finally, code the plot and add the mean difference (blue line) and a 95% confidence interval (red lines)
```

```
#for predictions of a mean difference. This prediction interval gives the level of agreement (1.96 * SD).
```

```
Blackpl <-ggplot(Black, aes(x = BlackAvg, y = BlackDif)) +
  geom_point(alpha = 0.5) +
  geom_hline(yintercept = mean(BlackDif), colour = "blue", size = 0.5) +
  geom_hline(yintercept = mean(BlackDif) - (1.96 * sd(BlackDif)), colour = "red", size = 0.5) +
  geom_hline(yintercept = mean(BlackDif) + (1.96 * sd(BlackDif)), colour = "red", size = 0.5) +
  ylab("Difference") +
  xlab("Average Temperature") + ggtitle("Black Lake") + coord_cartesian(ylim = c(-6, 6))
```

```
#Thunder
```

```
ThunderAvg <- (Thunder$MJAT + Thunder$SWT) / 2
```

```
ThunderDif <- Thunder$MJAT - Thunder$SWT
```

```
#Finally, code the plot and add the mean difference (blue line) and a 95% confidence interval (red lines)
```

#for predictions of a mean difference. This prediction interval gives the level of agreement (1.96 * SD).

```
Thunderpl <-ggplot(Thunder, aes(x = ThunderAvg, y = ThunderDif)) +  
  geom_point(alpha = 0.5) +  
  geom_hline(yintercept = mean(ThunderDif), colour = "blue", size = 0.5) +  
  geom_hline(yintercept = mean(ThunderDif) - (1.96 * sd(ThunderDif)), colour = "red", size =  
0.5) +  
  geom_hline(yintercept = mean(ThunderDif) + (1.96 * sd(ThunderDif)), colour = "red", size =  
0.5) +  
  ylab("Difference") +  
  xlab("Average Temperature") + ggtitle("Thunder Lake") + coord_cartesian(ylim = c(-6, 6))
```

```
grid.arrange(Conypl, Pipitpl, Eaglepl, Boxpl, Blackpl, Thunderpl, ncol=2, nrow=3, top="Bland-  
Altman Plot")
```

Commands from Analogue:

```
#Stratiplot(x, y, type = "l", ylab = NULL, xlab = "", pages = 1, rev = TRUE,  
# ylim, sort = c("none", "wa", "var"), svar = NULL, rev.sort = FALSE, strip = FALSE,  
# topPad =6, varTypes = "relative", absoluteSize = 0.5, zoneNames = NULL, drawLegend =  
TRUE,  
# na.action = "na.omit", labelAt = NULL, labelRot = 60, yticks, ...)
```

```
#####RELATIVE ABUNDANCE CURVES #####
```

```
#####Reads in R Packages needed for Code#####
```

```
library(analogue)  
library(palaeoSig)
```

```
###Training set data
```

```
Training_Set<-read.csv('Training Set Data.csv', header=TRUE)
```

```
#####Reads in Training Set Environment Data
```

```
Environment<-read.csv('Training set with temperatures.csv', header=TRUE)
```

```
#####Matches Training Set Data Frames and removes those that aren't in both sets
```

```
test<-merge(Training_Set, Environment)
```

```
Environment<-data.frame(cbind(test$CodeNum, test$FullName, test$MJAT, test$SWT))
```

```
colnames(Environment)<-c('CodeNum','FullName','MJAT', 'SWT')
```

```
Training_Set<-test[, c(4:77)]
```

```
Training_Set[is.na(Training_Set)]<-0
```

```
Training_Set<-Training_Set[,-c(18,39,42,50)]
```

```

##### WA Optima #####
## WA optima
(opt <- optima(Training_Set, Environment$SWT))

write.csv(opt, "wa optima.csv", row.names = TRUE)

## WA tolerances
(tol <- tolerance(Training_Set, Environment$SWT, useN2 = TRUE))

write.csv(tol, "tolerance.csv", row.names = TRUE)

dev.new(height=8, width=10)
par(mfrow=c(1,1))

## caterpillar plot
caterpillarPlot(opt, tol)

#####Black Lake#####
Black <- read.csv("Black Counts Age Depth.csv", header=TRUE, sep=",")

attach(Black)

Zones <- c(1957)
zone.labs <- c("Black-2", "Black-1")
dev.new(height=8, width=10)
par(mfrow=c(1,1))

(plt <- Stratiplot(Year ~ Diplind + Pseudo + Protan + TAA + Diamind + TAB + Heteind +
Euk.Tvet + Colivtyp + Synoind + Lim.Para +
                Doi.Pseu + Cric.Ort + Rheoind + Chirind + TAH + Cory.Th + Paratany + Tanyind
+ Richness + Concentration, data = Black,
                rev = FALSE, type = c(rep("h", "g", 19), rep("l", 2)), zones = Zones, zoneNames =
zone.labs,
                xlab = "% Relative Abundance", varTypes = c(rep("relative", 19), rep("absolute",
2)), col="gray48", pages = 1))
detach(Black)
#sort="wa"

#####Box Lake#####
Box <- read.csv("Box Loess Counts.csv", header=TRUE, sep=",")

attach(Box)

```

```
Zones <- c(1977)
zone.labs <- c("Box-2","Box-1")
dev.new(height=8, width=10)
par(mfrow=c(1,1))

(plt <- Stratiplot(Year ~ Chaeto + TAA + Smit.Ps + TAB + Sergind + Heteind + Euk.Tvet +
Colivtyp + Synoind +
      Cric.Ort + Corynamb + Chirind + TAH + Cory.Th + Paratany + Tanyind + Procind
+ Psecsemi +
      Pha eind + Richness + Concentration, data = Box,
      rev = FALSE, type = c(rep("h","g",19), rep("l", 2)), zones = Zones, zoneNames =
zone.labs,
      xlab = "% Relative Abundance", varTypes = c(rep("relative",19), rep("absolute", 2)),
col="gray48", pages = 1))
```

```
detach(Box)
```

```
##### Cony Relative Abundance #####
```

```
Cony <- read.csv("Cony Counts Age Depth.csv", header=TRUE, sep=",")
```

```
attach(Cony)
```

```
Zones <- c(1966)
zone.labs <- c("Cony-2","Cony-1")
dev.new(height=8, width=10)
par(mfrow=c(1,1))
```

```
(plt <- Stratiplot(Year ~ Diplind + Abisko + Pseudo + TAA + Diamind + TAB + Metrio +
Sergind + Heteind + Euk.Tvet + Colivtyp +
      Synoind + Cric.Ort + Chirind + TAH + Cory.Th + Paratany + Tanyind + Procind +
      Richness + Concentration, data = Cony,
      rev = FALSE, type = c(rep("h","g",19), rep("l", 2)), zones = Zones, zoneNames =
zone.labs,
      xlab = "% Relative Abundance", varTypes = c(rep("relative",19), rep("absolute", 2)),
col="gray48", pages = 1))
detach(Cony)
```

```
##### Eagle #####
```

```
Eagle <- read.csv("Eagle Counts Age Depth.csv", header=TRUE, sep=",")
```

```
attach(Eagle)
```

```
Zones <- c(1947)
zone.labs <- c("Eagle-2","Eagle-1")
```

```

dev.new(height=8, width=10)
par(mfrow=c(1,1))

(plt <- Stratplot(Year ~ Diplind + Pseudo + Hyd.Oliv + Protan + Smit.Ps + Diamind + TAB +
Heteind + Euk.Tvet + Colivtyp +
                Synoind + Lim.Para + Cric.Ort + Chirind + TAH + Cory.Th + Paratany + Tanyind
+ Procind +
                Micpsect + Psecsemi + Phaeind + Richness + Concentration, data = Eagle,
                rev = FALSE, type = c(rep("h","g",22), rep("l", 2)), zones = Zones, zoneNames =
zone.labs,
                xlab = "% Relative Abundance", varTypes = c(rep("relative",22), rep("absolute", 2)),
col="gray48", pages = 1))

detach(Eagle)

####Pipit#####

Pipit <- read.csv("Pipit Counts Age Depth.csv", header=TRUE, sep=",")

attach(Pipit)

Zones <- c(1991)
zone.labs <- c("Pipit-2","Pipit-1")
dev.new(height=8, width=10)
par(mfrow=c(1,1))

(plt <- Stratplot(Year ~ Abisko + Pseudo + Protan + TAA + Diamind + TAB + Sergind +
Heteind + Euk.Tvet + Colivtyp +
                Cric.Ort + Chirind + TAH + Cory.Th + Paratany + Tanyind + Procind +
                Micpsect + Pentind + Psecsemi + Phaeind + Richness + Concentration, data =
Pipit,
                rev = FALSE, type = c(rep("h","g",21), rep("l", 2)), zones = Zones, zoneNames =
zone.labs,
                xlab = "% Relative Abundance", varTypes = c(rep("relative",21), rep("absolute", 2)),
col="gray48", pages = 1))

detach(Pipit)

##### Thunder #####
Thunder <- read.csv("Thunder Counts Age Depth.csv", header=TRUE, sep=",")

attach(Thunder)

Zones <- c(2013,1932)
zone.labs <- c("Thunder-3", "Thunder-2","Thunder-1")

```

```
dev.new(height=8, width=10)
par(mfrow=c(1,1))
```

```
(plt <- Stratiplot(Year ~ Diplind + Brillia + Pseudo + Hyd.Oliv + Protan + Chaeto + TAA +
Diamind + TAB + Metrio +
      Sergind + Heteind + Euk.Tvet + Colivtyp + Synoind + Lim.Para + Cric.Ort +
Rheoind + Chirind +
      TAH + Cory.Th + Paratany + Tanyind + Procind + Micpsect + Pentind + Psecsemi
+ Phaeind +
      Polyind + Richness + Concentration, data = Thunder,
      rev = FALSE, type = c(rep("h","g",29), rep("l", 2)), zones = Zones, zoneNames =
zone.labs,
      xlab = "% Relative Abundance", varTypes = c(rep("relative",29), rep("absolute", 2)),
col="gray48", pages = 1))
```

APPENDIX B
ADDITIONAL MATERIALS

B.1 Western United States (WUS) Chironomid Training set data. SWT = surface water temperature;

MJAT = Mean July air temperature

Lake Name	Code	Location	Elevation (m)	Latitude (°N)	Longitude (°W)	Lake Depth (m)	SWT (°C)	MJAT (°C)
Hoover	01-UN-01	Uinta Mountains, UT	3003	40.68	110.87	8.1	16.9	12.5
Marshall	01-UN-02	Uinta Mountains, UT	3030	40.68	110.87	10.7	16.3	12.3
No name	01-UN-03	Uinta Mountains, UT	3115	40.67	110.89	1.8	16.2	11.2
No name	01-UN-04	Uinta Mountains, UT	3069	40.67	110.89	2	17	12.5
Echo	01-UN-05	Uinta Mountains, UT	2958	40.66	110.9	11.6	18.5	12.3
Taylor	01-UN-08	Uinta Mountains, UT	3394	40.79	110.09	9.7	13.5	9.1
Unnamed	01-UN-09	Uinta Mountains, UT	3212	40.78	110.02	1.1	16.4	9.9
No name	01-UN-10	Uinta Mountains, UT	2972	40.72	110.03	2.7	18.8	11.9
Big	01-UN-11	Uinta Mountains, UT	2636	40.7	109.54	1.5	19.1	14.4
Lilly Pad	01-UN-12	Uinta Mountains, UT	2921	40.74	109.73	1.6	21	12.3
Lilly	01-UN-13	Uinta Mountains, UT	2703	40.88	110.81	1.5	18.3	10.9
Bourbon	01-UN-15	Uinta Mountains, UT	2970	40.79	110.9	2.3	18.7	12.1
Beth	01-UN-16	Uinta Mountains, UT	2970	40.65	110.97	2.3	17.5	13.3
Buckeye	01-UN-17	Uinta Mountains, UT	2933	40.64	110.97	2.1	18	13
Quarter Corner	01-UN-21	Uinta Mountains, UT	2701	40.97	110.31	1.7	16.4	12.7
No name	01-UN-22	Uinta Mountains, UT	2721	40.98	110.32	2	17.2	12.8
Lofty	01-UN-23	Uinta Mountains, UT	3285	40.73	110.89	7.1	14.3	11
Kamas	01-UN-24	Uinta Mountains, UT	3179	40.73	110.9	4	15.7	11.3
Heart	02-UN-26	Uinta Mountains, UT	3188	40.59	110.81	4.1	18	11.3
Davis	02-UN-27	Uinta Mountains, UT	3356	40.81	110.22	1.7	13.7	10.8
Fehr	04-UN-30	Uinta Mountains, UT	3017	40.68	110.89	8	11.8	11
Pyramid	04-UN-31	Uinta Mountains, UT	2943	40.65	110.9	10.2	14.7	12.9
Elbow	04-UN-33	Uinta Mountains, UT	3335	40.79	110.03	10.7	10.1	10.4
Upper Rock	04-UN-34	Uinta Mountains, UT	3220	40.7	110.08	5.4	9.7	9.5
Larvae	04-UN-35	Uinta Mountains, UT	3055	40.68	110.04	8.2	13.2	11.2

Dead	04-UN-36	Uinta Mountains, UT	3053	40.67	109.91	6.5	13.9	11.8
Little Superior	04-UN-37	Uinta Mountains, UT	3396	40.73	110.47	6.9	11.9	10.1
No name	04-UN-39	Uinta Mountains, UT	3303	40.43	110.47	1.8	17.7	18.7
North Star	04-UN-40	Uinta Mountains, UT	3453	40.69	110.45	5.8	12.3	11.7
No name	04-UN-41	Uinta Mountains, UT	3531	40.76	110.46	3.1	11.3	9.4
No name	04-UN-42	Uinta Mountains, UT	3539	40.76	110.45	2.4	15.1	9.5
Tungsten	04-UN-43	Uinta Mountains, UT	3438	40.75	110.45	3.6	13.8	10
No name	04-UN-44	Uinta Mountains, UT	3426	40.75	110.43	4.5	14.6	10.1
Ruth	04-UN-45	Uinta Mountains, UT	3145	40.73	110.88	8.2	16.2	11.6
Bud	04-UN-46	Uinta Mountains, UT	3097	40.72	110.87	3.1	17.6	12
Little Lyman	04-UN-47	Uinta Mountains, UT	2811	40.94	110.62	7.3	19	12.1
Dave	04-UN-48	Uinta Mountains, UT	2795	40.92	110.54	1.1	20.8	12.8
No name	04-UN-51	Uinta Mountains, UT	2832	40.93	110.2	4.6	17.8	12.3
Summit	04-UN-52	Uinta Mountains, UT	3182	40.83	110	2.6	11.1	11.1
Gail	04-UN-53	Uinta Mountains, UT	3169	40.83	110.02	6.2	10	11
Upper Carrol	04-UN-55	Uinta Mountains, UT	3376	40.72	110.35	13.8	12.9	9.6
East Carrol	04-UN-56	Uinta Mountains, UT	3403	40.72	110.35	5.3	12.9	9.6
No name	04-UN-57	Uinta Mountains, UT	3336	40.71	110.38	5.2	13.6	8.7
No name	04-UN-58	Uinta Mountains, UT	3323	40.7	110.39	7.7	13.1	9
Twin	04-UN-59	Uinta Mountains, UT	3278	40.69	110.38	4.7	10	10.3
No name	04-UN-60	Uinta Mountains, UT	3000	40.75	109.74	6.4	15.4	11.9
No name	04-UN-61	Uinta Mountains, UT	2933	40.71	109.72	12.1	16	12.2
Hacking	04-UN-62	Uinta Mountains, UT	3220	40.77	109.81	4.9	12.7	10.5
Rainbow	04-UN-63	Uinta Mountains, UT	3373	40.81	110.24	7	12.8	9.5
No name	04-UN-64	Uinta Mountains, UT	3399	40.81	110.24	4.9	12.4	9.5
No name	04-UN-65	Uinta Mountains, UT	3436	40.82	110.25	3.6	12.9	8.5
Box	BL	Sierra Nevada, CA	3178	37.42	119.75	9.3	14.3	11.6
Big Pothole	BPL	Sierra Nevada, CA	3431	36.77	119.37	26	13.3	9.2
Barrett	BRL	Sierra Nevada, CA	2816	37.60	119.01	6.08	19.4	12.6
Bull	BUL	Sierra Nevada, CA	3268	37.15	119.56	5.9	15.1	10.2
Chocolate 1	CCL1	Sierra Nevada, CA	3355	37.15	119.54	8.5	14	9.2
Chocolate 2	CCL2	Sierra Nevada, CA	3355	37.15	119.55	6.3	14.3	9.2
Convict	CL	Sierra Nevada, CA	2309	37.59	119.86	40	16.1	13.4

Eastern Brook	EBL	Sierra Nevada, CA	3131	37.43	119.74	9	16.7	11.6
East Twin	ETL	Sierra Nevada, CA	3145	38.00	119.29	8.5	12.8	11.5
Funnel	FL	Sierra Nevada, CA	3180	37.20	119.51	10.2	15.4	11.1
Green	GL	Sierra Nevada, CA	3350	37.17	119.53	12.5	12.4	10.3
Gull	GLL	Sierra Nevada, CA	2303	37.78	119.08	19	18.9	15.3
Greenstone	GSL	Sierra Nevada, CA	3067	37.98	119.29	4.3	11.9	11.5
Golden Trout	GTL	Sierra Nevada, CA	3463	36.79	119.36	11.5	15.3	9.5
Golden Trout 3	GTL3	Sierra Nevada, CA	3440	36.79	119.36	6.5	17.2	10.6
Hummingbird	HBL	Sierra Nevada, CA	3105	37.99	119.29	5.9	15.4	11.5
Hidden	HDL	Sierra Nevada, CA	2379	38.26	119.54	9.7	19.1	13.9
Heart	HL	Sierra Nevada, CA	3160	37.42	119.75	4.3	14.2	11.6
Helen	HLL	Sierra Nevada, CA	3054	38.00	119.29	17.5	12.6	11.6
June	JL	Sierra Nevada, CA	2309	37.79	119.07	28	17.8	14.3
Koenig	KL	Sierra Nevada, CA	2905	38.28	119.63	2.9	12.3	11.3
Koenig	KL2	Sierra Nevada, CA	2897	38.28	119.63	3.5	15	11.3
Kirman	KRL	Sierra Nevada, CA	2174	38.34	119.50	3.8	18.4	14.5
Lower Conness	LCL	Sierra Nevada, CA	3220	37.97	119.31	6.3	11.7	11.4
Long	LL	Sierra Nevada, CA	3194	37.41	119.76	11.6	12.8	11.7
Long 2	LL2	Sierra Nevada, CA	3258	37.16	119.56	20.8	14.3	10.2
Lane	LLL	Sierra Nevada, CA	2213	38.29	119.54	11	20.4	13.6
Latopie	LPL	Sierra Nevada, CA	3145	38.29	119.64	6.5	10.8	10
Lower Sardine	LSL	Sierra Nevada, CA	2996	37.86	119.20	13.5	14	12.1
Leavitt	LVL	Sierra Nevada, CA	2896	38.27	119.62	24.5	11.4	11.5
Mack	ML	Sierra Nevada, CA	3155	37.43	119.57	6.2	15.9	11.6
Millie	MLL	Sierra Nevada, CA	2115	38.34	119.54	3.5	17.9	14.8
Mamie	MML	Sierra Nevada, CA	2694	37.61	119.01	5	16.1	13.7
Moat	MTL	Sierra Nevada, CA	3197	38.06	119.28	8.3	12.3	11.6
Mary	MYL	Sierra Nevada, CA	2714	37.60	119.00	16	15.8	12.6
Latopie	PL	Sierra Nevada, CA	3145	38.29	119.64	6.5	10.8	13.9
Rocky Bottom	RBL	Sierra Nevada, CA	3180	37.20	119.52	26.5	15.4	10.9
Rock Creek	RCL	Sierra Nevada, CA	2938	37.45	119.74	29.5	15	12.4
Red	RDL	Sierra Nevada, CA	2978	38.04	119.26	4.7	13.6	12.1
Ruwau	RL	Sierra Nevada, CA	3347	37.14	119.55	16	12.7	9.9

Roosevelt	RVL	Sierra Nevada, CA	2213	38.30	119.54	7.2	21.4	13.6
Sardine Adjacent	SAL	Sierra Nevada, CA	3170	37.86	119.21	2	18.7	12
Ski	SKL	Sierra Nevada, CA	2972	38.27	119.60	5.2	12.4	10
Serene	SL	Sierra Nevada, CA	3108	37.44	119.74	9.2	17.8	12
Satcher	SRL	Sierra Nevada, CA	2313	37.63	119.07	9.3	19.9	14.9
Silver	SVL	Sierra Nevada, CA	2186	37.78	119.12	14	15.4	14.1
Starkweather	SWL	Sierra Nevada, CA	2424	37.66	119.07	9.8	19	14.2
Trumbull	TBL	Sierra Nevada, CA	2921	38.05	119.26	6.7	16.3	12.8
Twin	TL1	Sierra Nevada, CA	2595	37.62	119.01	2	15.2	13.7
Twin	TL2	Sierra Nevada, CA	2595	37.62	119.01	2.3	15.7	13.7
Upper Conness 1	UCL1	Sierra Nevada, CA	3280	37.98	119.31	4.8	7.7	11.2
Upper Conness 2	UCL2	Sierra Nevada, CA	3251	37.98	119.31	4.6	13	11.2
Walker	WL	Sierra Nevada, CA	2405	37.87	119.17	3.1	15.2	13.6
West Twin	WTL	Sierra Nevada, CA	3152	38.00	119.29	8.1	13.1	11.5
Yost	YL	Sierra Nevada, CA	2756	37.74	119.10	2	15.4	13.3
American	AML	Sawatch Range, CO	3450	39.06	106.83	10.5	8.2	14.3
Anderson	AND	Sawatch Range, CO	3584	39.02	106.63	3.5	7.5	8.7
Bear	BER	Sawatch Range, CO	3351	39.30	106.42	4.6	15.2	14.8
Brady	BRD	Sawatch Range, CO	3353	39.37	106.50	2.1	15.1	11.1
Cathedral	CAT	Sawatch Range, CO	3598	39.03	106.84	6.7	5.4	13.5
Constantine	CNS	Sawatch Range, CO	3472	39.45	106.46	3.7	14.0	10.7
Crater	CRL	Sawatch Range, CO	3053	39.09	106.97	3.3	7.2	16.5
Cleveland	CVL	Sawatch Range, CO	3609	39.42	106.49	6.7	15.8	10.0
Diemer	DMR	Sawatch Range, CO	2869	39.33	106.61	2.6	20.3	13.7
Eagle	EGL	Sawatch Range, CO	3074	40.21	105.65	2.0	13.7	16.3
Galena South	GAL-S	Sawatch Range, CO	3364	39.30	106.42	3.1	15.6	14.7
Hunky Dory	HDY	Sawatch Range, CO	3452	39.42	106.48	2.5	16.2	14.3
Half Moon South	HFS	Sawatch Range, CO	3648	39.18	106.49	5.6	10.1	9.5
Hard Scrabble	HRD	Sawatch Range, CO	3070	39.23	107.10	4.1	14.8	16.4
Independence	IND	Sawatch Range, CO	3785	39.14	106.57	6.9	10.9	8.2
Linkin	LNK	Sawatch Range, CO	3639	39.13	106.59	9.0	5.6	13.2
Missouri Adjacent	MLA	Sawatch Range, CO	3524	39.40	106.52	2.5	14.6	10.0
Missouri Central	MLC	Sawatch Range, CO	3488	39.40	106.52	3.2	15.9	10.0

Missouri North	MLN	Sawatch Range, CO	3513	39.40	106.51	5.9	15.5	13.9
Missouri South	MLS	Sawatch Range, CO	3477	39.39	106.52	3.6	13.2	14.1
Maroon	MRL	Sawatch Range, CO	2903	39.10	106.95	3.1	5.8	17.3
Native	NTV	Sawatch Range, CO	3403	39.23	106.46	0.9	9.9	11.1
Savage	SAV	Sawatch Range, CO	3378	39.36	106.52	3.5	10.0	11.0
Seller	SLR	Sawatch Range, CO	3119	39.32	106.58	3.6	19.8	16.1
Sopris	SOP	Sawatch Range, CO	3364	39.37	106.50	5.4	16.6	9.6
Seven Sisters Central	SSC	Sawatch Range, CO	3755	39.44	106.48	5.8	15.2	11.0
Seven Sisters North	SSN	Sawatch Range, CO	3612	39.44	106.49	5.6	13.7	13.4
Seven Sisters South	SSS	Sawatch Range, CO	3708	39.44	106.48	1.2	12.6	12.9
Seven Sisters West	SSW	Sawatch Range, CO	3893	39.43	106.49	6.9	7.0	8.6
St. Kevin	STK	Sawatch Range, CO	3580	39.31	106.43	6.8	8.4	11.7
Tabor Creek	TCL	Sawatch Range, CO	3588	39.05	106.65	24.0	13.7	10.2
Tuhare East	TLE	Sawatch Range, CO	3691	39.45	106.47	11.0	14.1	9.2
Thomas North	TL-N	Sawatch Range, CO	3089	39.27	107.14	9.5	5.7	16.3
Thomas South	TL-S	Sawatch Range, CO	3114	39.27	107.14	5.7	15.2	16.1
Timberline	TMB	Sawatch Range, CO	3275	39.30	106.48	10.4	14.5	15.2
Whitney	WHT	Sawatch Range, CO	3321	39.43	106.45	7.8	15.2	15.0
Williams	WIL	Sawatch Range, CO	3277	39.22	107.12	3.6	7.5	13.3
Weller	WLL	Sawatch Range, CO	2894	39.12	106.72	8.7	8.1	13.9
Box	BOX	Front Range, CO	3274	40.21	105.65	11.0	13.9	12.2
Black	BLK	Front Range, CO	3237	40.40	105.96	21.2	10.9	14.3
Cony	CNY	Front Range, CO	3509	40.17	105.66	16.8	8.2	10.9
Eagle1	EGL1	Front Range, CO	3298	40.21	105.65	10.2	10.9	12.1
Falcon	FAL	Front Range, CO	3371	40.23	105.66	8.1	9.2	13.5
Hutcheson	HCH	Front Range, CO	3413	40.17	105.65	3.1	10.0	13.3
Odessa	ODS	Front Range, CO	3051	40.33	105.69	6.0	10.5	15.3
Pipit	PIP	Front Range, CO	3479	40.19	105.67	10.4	9.2	11.1
Thunder	THD	Front Range, CO	3225	40.22	105.65	7.05	13.1	14.3

B.2: Key for chironomid taxa

Taxa	Name	Taxa	Name
Diplind	<i>Diplocladius</i>	Corv.Th	<i>Corvnoneura/Thiensemanniella</i>
Brillia	<i>Brillia</i>	TAC	<i>Tanytarsus</i> type C
Abisko	<i>Abiskomyia</i>	Cladtany	<i>Cladotanytarsus</i>
Paraind	<i>Paracladius</i>	Apedind	<i>Apedilum</i>
Pseudo	<i>Pseudodiamesa</i>	Paratany	<i>Paratanytarsus</i>
Park A	<i>Parakiefferiella</i> type A	Tribind	<i>Tribelos</i>
Mes.Smit	<i>Mesosmittia</i>	Psecsept	<i>Psectrocladius septentionalis</i>
Hyd.Oliv	<i>Hydrobaenus/Oliveridia</i>	Tanyind	<i>Tanytarsus</i> indeterminable
Protan	<i>Protartypus</i>	Procind	<i>Procladius</i>
Chaeto	<i>Chaetocladius</i>	Zaluind	<i>Zaluschia</i>
TAA	<i>Tanytarsus</i> type A	Micpsect	<i>Micropectra</i>
Smit.Ps	<i>Smittia/Pseudosmittia</i>	unknown1	<i>Unknown</i>
Diamind	<i>Diamesa</i>	Pentind	<i>Pentaneurini</i>
TAB	<i>Tanytarsus</i> type B	Cladind	<i>Cladopelma</i>
Metrio	<i>Metricnemus</i>	TAE	<i>Tanytarsus</i> type E
Stilo	<i>Stilocladius</i>	Psecsemi	<i>Psectrocladius semi-sordidellus</i>
Sympind	<i>Symposiocladius</i>	Psecmono	<i>Psectrocladius monopsectrocladius</i>
Sergind	<i>Sergentia</i>	Nanoind	<i>Nanocladius</i>
Heteind	<i>Heterotrissocladius</i>	Mictind	<i>Microtendipes</i>
Parorth	<i>Parorthocladius</i>	unk.orth.MLC	<i>Unknown Orthocladius MLC</i>
unk.ortho.egl	<i>Unknown Orthocladius EGL</i>	Tany.chi	<i>Tanytarsus chinensis</i> group
Euk.Tvet	<i>Eukiefferiella/Tvetenia</i>	Psecall	<i>Psectrocladius allopectra</i>
Georth	<i>Georthocladius</i>	TAK	<i>Tanytarsus</i> type K
Colivtyp	<i>Corynocera oliveri</i> -type	Phaseind	<i>Phaenopsectra</i>
Synoind	<i>Synorthocladius</i>	PsecWalk	<i>Psectrocladius Walker</i> type
Lim.Para	<i>Limnophyes/Paralimnophyes</i>	Pagaind	<i>Pagastiella</i>
Endoch	<i>Endochironomus</i>	Polyind	<i>Polypedilum</i>
Einfel	<i>Einfeldia</i>	Labrind	<i>Labrundinia</i>
Doi.Pseu	<i>Doithrix/Pseudodoithrix</i>	Tany.A.C	<i>Tanytarsus</i> type A/C
Cric.Ort	<i>Cricotopus/Orthocladius</i>	Pseuchi	<i>Pseudochironomus</i>
Stemind	<i>Stempellina</i>	Sticind	<i>Stictochironomus</i>
Triss	<i>Trissocladius</i>	TAD	<i>Tanytarsus</i> type D
Rheoind	<i>Rheocricotopus</i>		
Corynamb	<i>Corynocera ambigua</i> -type		
Chirind	<i>Chironomus</i>		
TAH	<i>Tanytarsus</i> type H		
Chpherp	<i>Cryptochironomus</i>		
TAG	<i>Tanytarsus</i> type G		

B.3: Figure 3: Caterpillar plot for the WUS training set showing the optimal SWT for midge taxa (dot) with the tolerance range. Optima and tolerances were found by weighted averaging.

